Temporal distribution of physiological states within pure bacterial cultures producing isopropanol : understanding of microbial subpopulation to process optimization

Catherine Boy

Université Fédérale
Toulouse Midi-Pyrénées

THÈSE

En vue de l'obtention du

DOCTORAT DE L'UNIVERSITÉ DE TOULOUSE

Délivré par l'Institut National des Sciences Appliquées de Toulouse

---

Présentée et soutenue par

Catherine BOY

Le 18 décembre 2020

Distribution temporelle d'Etats Physiologiques au sein de Culture Pure Bactérienne Productrice d'Isopropanol: Prise en compte des sous-populations microbiennes pour une optimisation du procédé

Ecole doctorale : **SEVAB - Sciences Ecologiques, Vétérinaires, Agronomiques et Bioingenieries**

Spécialité : **Ingénieries microbienne et enzymatique**

Unité de recherche :
TBI - Toulouse Biotechnology Institute, Bio & Chemical Engineering

Thèse dirigée par
Stéphane GUILLOUET et Nathalie GORRET

Jury

Mme Catherine BéAL, Rapporteure
M. Stéphane DELAUNAY, Rapporteur
Mme Marielle BOUIX, Examinatrice
M. Jillian MARC, Examinateur
M. Stéphane GUILLOUET, Directeur de thèse
Mme Nathalie GORRET, Co-directrice de thèse
Mme Sandrine ALFENORE, Co-directrice de thèse

Nom: Boy **Prénom:** Catherine

Titre: Distribution temporelle d'Etats Physiologiques au sein de Culture Pure Bactérienne Productrice d'Isopropanol: Prise en compte des sous-populations microbiennes pour une optimisation du procédé

Année: 2020 **Nombre de pages:** 254
Spécialité: Ingénierie microbienne et enzymatique **Lieu :** INSA Toulouse

Résumé

Les cultures monoclonales de microorganismes en bioréacteur ont longtemps été considérées comme homogènes (*i.e.* toutes les cellules sont identiques). Cependant, des hétérogénéités de population peuvent survenir, dues à des modifications stochastiques de l'expression génétique, une instabilité plasmidique ou à des gradients de concentration. Cette hétérogénéité peut impacter négativement les performances des procédés en diminuant leur robustesse, notamment dans le cas de production de molécules recombinantes. L'objectif de ce travail est d'identifier les sous-populations provenant d'une culture pure en bioréacteur, de comprendre leurs effecteurs et de contrôler leur distribution. Le modèle d'étude choisi est la production d'isopropanol par une souche recombinante de *Cupriavidus necator*. Des outils doivent être développés pour suivre le comportement de ces sous-populations en cours de fermentation. Néanmoins, de tels outils ne sont, à ce jour, pas encore adaptés au suivi dynamique des cultures bactériennes. Ainsi pour répondre aux questions scientifiques, un biosenseur eGFP (codé sur un plasmide recombinant chez *C. necator*) a été construit afin de suivre dynamiquement des sous-populations par cytométrie en flux en cours de cultures en bioréacteurs. Différentes stratégies de stabilisation plasmidique, dans différentes conditions d'environnements contrôlées, ont été étudiées afin de caractériser leur réponse et efficacité. Deux méthodes différentes mais complémentaires pour le suivi de stabilité de l'expression plasmidique ont été mises en place : la numération sur boîte et la cytométrie en flux. Dans un premier temps, la production d'isopropanol par *C. necator* en culture discontinue alimentée a été étudiée avec différentes constructions plasmidiques. Les rendements et vitesses de production en isopropanol diminuent drastiquement lorsque l'instabilité de l'expression plasmidique augmente. Ce seuil peut être modulé en fonction du design plasmidique (système de stabilisation plasmidique ou non). Dans un second temps, une technique de suivi de l'expression plasmidique à l'échelle de la cellule unique a été développée. Le gène codant pour l'eGFP a été inséré sur le plasmide recombinant. L'impact de la force de différents promoteurs constitutifs a été quantifié afin de déterminer la construction présentant la charge métabolique la plus faible sur les cellules hôtes tout en garantissant une sensibilité satisfaisante des mesures de fluorescence. L'outil ainsi défini a ensuite été confronté à des conditions de cultures permettant de générer une hétérogénéité de population, afin de comprendre ses réponses en fonction des conditions opératoires. Ainsi, l'impact du taux de croissance sur le niveau d'expression plasmidique a pu être étudié en culture continue, dans des conditions stringentes de perte plasmidique. De plus, la robustesse de souches non productrices d'isopropanol, a été évaluée dans différentes conditions d'alimentation en substrat et de systèmes de stabilisation plasmidique. Dans un dernier temps, le système de suivi de l'expression plasmidique a été inséré dans un plasmide codant pour la production d'isopropanol. Son insertion a conduit à une diminution de la productivité en isopropanol, liée à une instabilité d'expression plasmidique par rapport à la souche non fluorescente. Des niveaux différents d'expression plasmidique ont pu être identifiés et quantifiés en cours de culture. Ces travaux ont permis, de par le développement d'un biosenseur, de mieux comprendre le lien entre les conditions opératoires imposées au cours des cultures bactériennes et l'apparition d'hétérogénéité de l'expression plasmidique sur la robustesse d'un procédé.

Mots-clés: *Cupriavidus necator*, cultures discontinues, discontinues alimentées et continues, isopropanol, eGFP, cytométrie en flux, hétérogénéité de population

Last-name: Boy **First-name:** Catherine
Title: Temporal distribution of physiological states within pure bacterial cultures producing isopropanol : understanding of microbial subpopulation to process optimization
Year: 2020 **Number of pages:** 254
Specialty : Ingénierie microbienne et enzymatique **Place :** INSA Toulouse

Abstract

Monoclonal cultures of microorganisms in bioreactors have long been considered homogeneous (*i.e.* all cells are identical). However, population heterogeneities may occur, due to stochastic changes in gene expression, plasmid instability or concentration gradients. This heterogeneity can negatively impact the performance of the processes by decreasing their robustness, especially in the case of recombinant molecule production. The objective of this work is to identify the sub-populations coming from a pure culture bioreactor, to understand their effectors and to control their distribution. The chosen study model is the production of isopropanol by a recombinant strain of *Cupriavidus necato*r. Tools need to be developed to monitor the behavior of these sub-populations during culture. However, such tools are not yet adapted to the dynamic monitoring of bacterial cultures. Thus, to answer the scientific questions, an eGFP biosensor (coded on a recombinant plasmid in *C. necator*) has been built to dynamically monitor sub-populations by flow cytometry during bioreactor cultures. Different plasmid stabilization strategies, under different controlled environment conditions, were studied in order to characterize their response and efficacy. Two different but complementary methods for monitoring the stability of plasmid expression have been implemented: plate count and flow cytometry. In a first step, isopropanol production by *C. necator* in fed batch culture was studied with different plasmid constructs. Isopropanol yields and production rates decreased drastically as the instability of plasmid expression increased. This threshold can be modulated according to the plasmid design (plasmid stabilization system or not). In a second step, a technique for plasmid expression monitoring at the single-cell level has been developed. The gene coding for eGFP was inserted into the recombinant plasmid. The impact of the strength of different constitutive promoters was quantified in order to determine the construct with the lowest metabolic load on host cells while ensuring satisfactory sensitivity of the fluorescence measurements. The tool defined was then confronted with culture conditions allowing the generation of population heterogeneity, in order to understand its responses according to the operating conditions. Thus, the impact of growth rate on plasmid expression level was studied in continuous culture, under stringent conditions of plasmid loss. In addition, the robustness of non-isopropanol-producing strains was evaluated under different conditions of substrate feeding and plasmid stabilization systems. Finally, the plasmid expression monitoring system was inserted into a plasmid coding for isopropanol production. Its insertion led to a decrease in isopropanol productivity, linked to instability of plasmid expression compared to the non-fluorescent strain. Different levels of plasmid expression could be identified and quantified during culture. This work has allowed, through the development of a biosensor, to better understand the link between the operating conditions imposed during bacterial cultures and the appearance of plasmid expression heterogeneity on the robustness of a process.

Keywords : *Cupriavidus necator,* batch, fed-batch, continuous culture, isopropanol, eGFP, flow cytometry, population heterogeneity

Remerciements

La première image de la thèse que l'on m'a donnée lorsque j'ai débuté, était qu'il s'agissait d'un marathon, et non d'un sprint. En tant que passionnée de course à pied, cette comparaison m'a tout de suite parlé. Ainsi, dans le cadre de ce marathon un peu particulier, j'ai bénéficié du soutien de nombreuses personnes. Je souhaite leur exprimer ici ma profonde gratitude.

Je souhaite remercier mes directeurs de thèse, Stéphane Guillouet (PR INSA), Natalie Gorret (CR INRA) et Sandrine Alfenore (MCF INSA) pour m'avoir donné l'opportunité d'effectuer ce travail de thèse au sein de l'équipe FAME à TBI. Je suis reconnaissante de leur supervision académique ainsi que de leurs conseils et expertises précieuses pour l'orientation scientifique de ma thèse. Enfin, je les remercie de leur engagement durant les expérimentations, nous ayant permis de mener des fermentations 24/24h durant plusieurs jours.

Je tiens à remercier Julie Lesage, pour son implication dans ma thèse. Son expertise et sa patience ont été précieuses pour la réalisation des constructions plasmidiques. Je la remercie également pour la construction du plasmide pJLCB2, alors que je n'avais pas eu le temps de le réaliser moi-même.

Je remercie mes rapporteurs de thèse, Catherine Béal (PR INRA, AgroParisTech) et Stéphane Delaunay (PR ENSAIA, Nancy), ainsi que mes examinateurs Marielle Bouix (PR INRA, AgroParisTech) et Jillian Marc (MCF Faculté de Pharmacie, Tours), pour l'intérêt qu'ils ont porté à mes travaux de thèse, pour leurs précieuses discussions, suggestions et commentaires lors de la soutenance ainsi que dans leurs rapports.

Je remercie sincèrement Claude Maranges, directeur de l'école doctorale SEVAB, pour la réactivité de ses réponses, ainsi que pour ses sages conseils et ses mots d'encouragements lors de ma dernière année de thèse.

Mes remerciements vont aussi à l'ensemble de l'équipe FAME, qui m'a accompagnée durant ces quatre années :

> Carine, Carole, César, Elodie, Éric, Julie L., Luc, Nathalie, Philippe, Sandrine, Stéphane, Stéphanie et Xavier, chez les personnels permanents.
>
> Angel, Arnaud, Asma, Bastien, Bérangère, Clémentine, Elise, Florence, François, Gemma, Julie T., Laure, Laurie, Léa, Louna, Lucie, Lucile, Marie Sarah, Marine C., Marine D., Ming, Nelly,

Oumarou, Pierre, Raphaël, Safa, Siwar, Susana, Wesley, William et Yassim, chez les personnels non-permanents.

Parmi eux, je tiens à remercier Éric Lombard pour son aide et sa réactivité lors de la mise en place de nouveaux dispositifs et de la gestion de problèmes techniques lors des fermentations.

De plus, je remercie Florence Leray pour son accompagnement bienveillant en chimie analytique, où elle m'a beaucoup appris.

Je remercie également Bérengère, Julie T. et Louna, grâce à qui les nuits et week-end de fermentations que nous avons effectuées ensemble m'ont paru moins longs.

Enfin, à mes camarades doctorants ; Arnaud, Asma, François, Lucile, Marine D., Siwar, Susana et Yassim, partager avec vous nos galères et nos réussites a été un plaisir.

Merci à Manon, Maher, Mounir et Arthur pour nos soirées-jeux, remplies de fous rires, trahisons et retournements de situations en tout genre. Au détour d'une partie, nos discussions sur nos différentes expériences de thèse m'ont permis de me sentir moins seule et mieux comprise.

Merci à ma chère bande d'Insaiens de la première heure, Violaine, Quentin, Nicolas et Alexandre. Je n'ai pas pu être aussi présente que je l'aurais souhaité, mais vous avez toujours répondu présents avec enthousiasme pour se raconter nos petites vies sur Skype. Nos escapades estivales ont été pour moi un formidable sas de décompression ces dernières années.

A Yassim, qui partage ma vie, ton soutien indéfectible et ton optimisme à toute épreuve m'ont donné de la force lorsque j'en manquais. Les deux marathons que nous avons courus ensemble ont été d'excellents exutoires et une grande source de fierté.

A ma marraine Christine et mon parrain Daniel, merci pour votre enthousiasme et vos mots d'encouragement lors de nos discussions par-dessus le grillage du jardin.

A ma famille, ma grand-mère Odette, mes tantes Geneviève et Hélène, mes oncles Daniel et Alain, mes cousin.e.s Nathalie, Camille et Mickaël, merci pour votre soutien et votre gentillesse. Nos réunions de famille ont été source de joie et de convivialité.

A ma sœur Elise, ma complice de toujours et meilleure amie, ton écoute sage et bienveillante m'ont aidé plus d'une fois à remettre les choses en perspectives et à y voir plus clair. Notre passion partagée de films et de séries m'a permis de m'évader lorsque j'en avais besoin.

A ma mère Marie-Cécile, la personne la plus forte que je connaisse, merci pour ta confiance sans faille et pour tout ce que tu as fait pour moi. Merci également d'avoir fait face à mes sautes d'humeur (presque) sans sourciller. Sans ton amour et ta résilience, je n'en serai pas là aujourd'hui.

Je dédie cette thèse à deux personnes chères à mon cœur, qui ont quitté ce monde à l'heure où j'écris ces lignes : mon père et mon grand-père.

A mon grand-père Jean, qui du haut de ses 99 printemps était un passionné de sciences, ton enthousiasme et ta curiosité m'ont vivement inspiré.

A mon père Jean, tu as été la première personne à me prédire que je ferai une thèse, il y a longtemps maintenant. Je ne l'envisageai pas à l'époque, mais tu as cru en moi, merci.

Publications and communications

International journals

Boy, C., J. Lesage, S. Alfenore, N. Gorret and S. E. Guillouet (2020). "Plasmid expression level heterogeneity monitoring via heterologous eGFP production at the single-cell level in *Cupriavidus necator*." Applied Microbiology and Biotechnology

National conferences

Oral presentations

Boy, C., S. Alfenore, N. Gorret and S. E. Guillouet. (2019) : Analyse des dynamiques de distribution de populations microbiennes au sein de cultures de bactéries génétiquement modifiées par cytométrie en flux : Cas de la production hétérologue d'isopropanol par *Cupriavidus necator*. *Congrès annuel de la Société Française de Microbiologie, Paris, France.*

Boy, C., S. Alfenore, N. Gorret and S. E. Guillouet. (2018) : Analyse des dynamiques de distribution de populations microbiennes au sein de cultures de bactéries génétiquement modifiées par cytométrie en flux : Cas de la production hétérologue d'isopropanol par *Cupriavidus necator*. *Congrès annuel de l'Agence Française de Cytométrie, Lyon, France.*

Poster presentation

Boy, C., S. Alfenore, N. Gorret and S. E. Guillouet. (2018) : Analyse des dynamiques de distribution de populations microbiennes au sein de cultures de bactéries génétiquement modifiées par cytométrie en flux : Cas de la production hétérologue d'isopropanol par *Cupriavidus necator*. *Congrès annuel de l'Agence Française de Cytométrie, Lyon, France.*

Table of content

List of figures

Introduction and context of the study

Part 1: Literature study

Part 2 : Material and methods

Part 3: Results and discussion

Chapter 1

Chapter 2 - Subchapter 2

Chapter 2 - Subchapter 3

Chapter 3

List of tables

Part 1 : Literature review

Part 2: Material and methods

Part 3: Results and discussion

Chapter 1

Chapter 2 - Subchapter 2

Chapter 2 - Subbchapter 3

Chapter 3

List of abbreviations

ADC	Acetoacetate decarboxylase
ADH	Isopropanol dehydrogenase
AFM	Atomic force microscopy
Ar	Molar fraction of argon (mol)
$Ar^{dry\ air}$	Molar fraction of argon in dry air (mol)
ATP	Adenosine Triphosphate
CO_2	Molar fraction of carbon dioxide (mol)
$CO_{2,in}$	Molar fraction of carbon dioxide in inflow (mol)
$CO_{2,out}$	Molar fraction of carbon dioxide in outflow (mol)
$[CO_{2,L}]$	Concentration of carbon dioxide in liquid (mol·L^{-1})
$[CO_{2,tot}]$	Total concentration of carbon dioxide (mol·L^{-1})
C_T	Threshold cycle
CTF	Acetoacetyl-CoA transferase
DNA	Desoxyribonucleic acid
e.g.	For example; "*exempli gratia*"
eGFP	Enhanced Green Fluorescent Protein
FACS	Fluorescence activated cell sorting
FCM	Flow cytometry measurement
FISH	Fluorescence *in situ* hybridization
FSC	Forward scatter
Gen	Gentamicin
GFP	Green Fluorescent Protein
GTP	Guanosine Triphosphate

H_{CO_2}	Henry's constant
$[HCO_{3,L}^{-}]$	Concentration of carbon bicarbonate in liquid (mol·L^{-1})
i.e.	That is; "id est"
IPA	Isopropanol
IPTG	isopropyl- β-D-thiogalactopyranoside
Kan	Kanamycin
kLa_{O_2}	Global oxygen transfer coefficient in the liquid phase
m	Maintenance factor (h^{-1})
MRS	Multimer resolution systems
N_2	Molar fraction of nitrogen (mol)
${N_2}^{dry\ air}$	Molar fraction of nitrogen in dry air (mol)
$N_{2,in}$	Molar fraction of nitrogen in inflow (mol)
$N_{2,out}$	Molar fraction of nitrogen in outflow (mol)
$N_{2,G}$	Molar fraction of nitrogen in gas (mol)
$N_{2,L}$	Molar fraction of nitrogen in liquid (mol)
N_{res} and N_{alim}	Nitrogen concentrations in the bioreactor and feeding solution, respectively (g·L^{-1})
0_2	Molar fraction of oxygen (mol)
$[O_{2,L}]$	Concentration of dioxygen in water (mg·L^{-1})
$[O_{2,L}]^*$	Maximal solubility of dioxygen in water (atmospheric pressure; 30°C) (mg·L^{-1})
OTR	Oxygen Transfer Rate
OUR	Oxygen Uptake Rate
PCK	Phosphoenolpyruvate carboxykinase
PCN	Plasmid copy number
p_{CO_2}	Partial pressure of carbon dioxide
PCR	Polymerase Chain Reaction
PEP	phosphoenolpyruvate

PHB	Poly(3-hydroxybutyric Acid) or poly-β-hydroxybutyrate
PI	Propidium Iodide
p_{O_2}	Partial pressure of dioxygen
$p_{O_2}{}^*$	Maximal partial pressure of dioxygen
PSK	Post segregational killing
$Q_{G,in}$	Inlet flow rate (mol·h^{-1}) (air)
$Q_{G,out}$	Outlet flow rate (mol·h^{-1}) (air)
Q_{in}	Inlet flow rate at instant t (L·h^{-1}) (fructose and ammonium)
qPCR	Quantitative PCR
$R_{A/B}$	Production of yield of the compound A from the compound B
$r_{CO_{2,G}}$	Consumption rate of carbon dioxide in gaseous phase (mol·L^{-1}·h^{-1})
$r_{CO_{2,L}}$	Consumption rate of carbon dioxide in liquid phase (mol·L^{-1}·h^{-1})
r_N	Global consumption rate of the nitrogen (g·L^{-1}·h^{-1})
r_{N_2}	Consumption rate of nitrogen (mol·L^{-1}·h^{-1})
$r_{O_{2,G}}$	Consumption rate of dioxygen in gaseous phase (mol·L^{-1}·h^{-1})
$r_{O_{2,L}}$	Consumption rate of dioxygen in liquid phase (mol·L^{-1}·h^{-1})
RQ	Respiratory quotient
r_X	Global production rate of the biomass (g·L^{-1}·h^{-1})
S_{res} and S_{alim}	Fructose concentrations in the bioreactor and feeding solution, respectively (g·L^{-1})
SSC	Side scatter
TCA cycle	Tricarboxylic acid cycle
THL	β-ketothiolase
V_0	Initial volume (L)
$V_{addition}$	Volume of inducer, antibiotics and / or macro-elements added (L)
V_{evap}	Difference between V_{ferm} and V_{real}(L)

V_{ferm}	Volume calculated in the reactor (L)
$V_{fructose}$	Volume of fructose added (L)
V_G	Volume of gas (L)
V_L	Volume of liquid (L)
V_{NH3}	Volume of nitrogen added (L)
V_{pH}	Volume of acid and base solutions added (L)
V_{real}	Volume measured at the end of fermentation (L)
V_{sample}	Volume of sample taken (L)
X and X_0	Biomass concentration at instant t and at the beginning of the fed-batch phase, respectively ($g \cdot L^{-1}$)
$Y_{N/X}$	Theoretical yield of biomass production from nitrogen (= 5.96 $g_X \cdot g_{NH3}^{-1}$)
$Y_{S/X}$	Theoretical yield of biomass production from fructose (= 0.46 $g_X \cdot g_{NH3}^{-1}$)
γ_A	Reduction degree values of the element A
μ	Specific growth rate (h^{-1})
$\phi_{O_{2,G}}$	Transfer flow of dioxygen in gas ($mol \cdot h^{-1}$)
$\phi_{O_{2,G/L}}$	Gas / Liquid transfer flow of dioxygen ($mol \cdot h^{-1}$)
$\phi_{O_{2,L}}$	Transfer flow of dioxygen in liquid ($mol \cdot h^{-1}$)
$\phi_{CO_{2,G}}$	Transfer flow of carbon dioxide in gas ($mol \cdot h^{-1}$)
$\phi_{CO_{2,G/L}}$	Gas / Liquid transfer flow of carbon dioxide ($mol \cdot h^{-1}$)
$\phi_{CO_{2,L}}$	Transfer flow of carbon dioxide in liquid ($mol \cdot h^{-1}$)

Introduction and context of the study

Introduction and context of the study

La consommation mondiale de pétrole en 2018 s'élevait à 99,7 millions de barils par jour (Mb/j). D'après les prévisions de l'Agence International de l'Énergie, la consommation pourrait augmenter de 5,7 Mb/j d'ici à 2024 [1],[2]. En 2016, le transport routier était responsable de 11,9 % des émissions mondiales de gaz à effet de serre, contre 15,9 % pour le secteur des transports dans sa globalité [3]. Les ressources fossiles venant à se raréfier, le secteur automobile a commencé à développer la production de biocarburants durables, afin aussi de diminuer son impact sur l'environnement [4].

Actuellement, les recherches concernant le développement de biocarburants alternatifs s'est largement concentré sur l'éthanol. Cependant, ce biocarburant est à l'origine de nombreux problèmes techniques : corrosion des métaux ferreux, dégradation des flexibles de transfert dans les moteurs, niveau d'énergie plus faible que l'essence et impossibilité de transport *via* pipelines (Bruno *et al.* 2009). Afin de surmonter les limitations liées à l'utilisation d'éthanol comme biocarburant, d'autres alcools sont considérés comme des alternatives intéressantes, tels que l'iso-butanol, le butanol, le propan-1-ol, le 3-méthyl-1-butanol, le 2-méthyl-1-butanol, l'iso-pentenol et l'isopropanol (Lee *et al.* 2008, Bruno *et al.* 2009, Connor *et al.* 2010). Parmi eux, l'isopropanol a un indice d'octane élevé (*i.e.* indice de résistance à la détonation) ; il est déjà utilisé comme additif dans l'essence et le diesel (Peralta-Yahya *et al.* 2010). Sa production par voie microbienne a déjà été réalisée chez *Escherichia coli* (Hanai *et al.* 2007), *Clostridium acetobutylicum* (Dusséaux *et al.* 2013, Jang *et al.* 2013), *Candida utilis* (Tamakawa *et al.* 2013) et *Cupriavidus necator* (Grousseau *et al.* 2014, Marc *et al.* 2017, Garrigues *et al.* 2020). *C. necator* présente deux intérêts majeurs pour la production de molécules recombinantes. Tout d'abord, elle présente un métabolisme versatile (*i.e.* chemolithoautotrophe) (Johnson *et al.* 1971, Friedrich *et al.* 1979, Tanaka *et al.* 1995, Budde *et al.* 2011, Grunwald *et al.* 2015, Crepin *et al.* 2016, Marc *et al.* 2017, Garrigues *et al.* 2020), permettant l'utilisation d'une grande variété de substrats. De plus, en conditions de limitation nutritionnelle, elle peut massivement stocker du carbone *via* la synthèse de poly(3-Hydroxybutyrate) (*abbr.* PHB) (Ryu *et al.* 1997, Pohlmann *et al.* 2006), ce qui suggère une capacité intéressante à dévier son flux de carbone. Ainsi, l'intérêt pour *C. necator* en tant que bio-plateforme de production de molécules d'intérêt économique s'est intensifié ces dernières années (Ewering *et al.* 2006, Hoefel *et al.* 2010, Muller *et al.* 2013, Grousseau *et al.* 2014, Crepin *et al.* 2016, Marc *et al.* 2017, Sydow *et al.* 2017, Black *et al.* 2018, Krieg *et al.* 2018, Garrigues *et al.* 2020).

Dans le cadre du développement d'un bioprocédé, la robustesse de celui-ci doit être maintenue afin d'assurer une performance suffisante et donc sa viabilité économique. Les populations microbiennes cultivées en milieux supposés homogènes sont souvent considérées comme constituées d'individus

identiques. Néanmoins, des hétérogénéités peuvent émerger, même dans le cas de cultures monoclonales (Carlquist *et al.* 2012, Delvigne *et al.* 2014, Gonzalez-Cabaleiro *et al.* 2017). Elles peuvent être dues à des modifications stochastiques de l'expression génétique (Elowitz *et al.* 2002), à des milieux et conditions de culture non homogènes (*i.e.* microenvironnements) (Delvigne *et al.* 2015) ou encore à une instabilité plasmidique (Brehm-Stecher *et al.* 2004, De Gelder *et al.* 2007). Les hétérogénéités d'expression génétique, notamment dans le cas de production de molécules recombinantes, semblent impliquées dans les diminutions des performances de production (*i.e.* diminution des rendements et des vitesses de production). Donc, étudier et comprendre le rôle des hétérogénéités de populations dans les procédés microbiens constitue un enjeu majeur pour la biologie synthétique et l'optimisation des procédés (Binder *et al.* 2017).

Des méthodes de suivi des sous-populations en cours de fermentation doivent être développées pour comprendre leurs mécanismes d'apparition et leurs effecteurs. Néanmoins, de tels outils ne sont, à ce jour, pas encore adaptés au suivi dynamique des cultures bactériennes (Gonzalez-Cabaleiro *et al.* 2017).

Lors de travaux antérieurs dans notre équipe de recherche, il a été suspecté que lors de la production d'isopropanol par *C. necator*, la diminution de performance en cours de culture, au-delà d'une certaine concentration produite, était en partie due à la perte du plasmide recombinant. De premières évaluations de cette perte par comptage sur boîte, basé sur la résistance à la kanamycine, ont confirmé cette hypothèse. La production d'isopropanol par *C. necator* a donc été choisi comme modèle d'étude dans ce travail.

Les travaux présentés dans ce manuscrit de thèse ont pour objectif de répondre aux questions suivantes :

- Comment identifier et discriminer, avec fiabilité, différentes sous-populations provenant d'une culture pure en bioréacteur, dynamiquement, en cours de fermentation ?
- Quels sont les effecteurs de l'apparition d'hétérogénéités dans des cultures monoclonales en bioréacteur ? Comment évolue le comportement des sous-populations en réponse à ces effecteurs ?
- Peut-on contrôler la distribution de sous-populations dans un bioprocédé en cours de fermentation ? A quel niveau ce contrôle peut-il être opéré, avec quelle efficacité ?

Les travaux portent donc sur l'étude de la stabilité du niveau d'expression d'un plasmide recombinant, mais aussi sur l'étude du lien entre stabilité d'expression et hétérogénéité de populations, au cours de

cultures contrôlées d'une souche recombinante de *Cupriavidus necator* avec ou sans production d'isopropanol.

Pour répondre à ces questions scientifiques, la stratégie expérimentale a été pensée de la manière suivante (**Figure 1**). Des outils (*i.e.* biosenseurs spécifiques eGFP) et des méthodologies (*i.e.* cytométrie en flux) permettant la caractérisation des dynamiques de réponse à l'échelle de la cellule unique ont été développés et optimisés. Des cultures en bioréacteurs en environnement contrôlé et quantifié ont été menées avec plusieurs souches recombinantes de *C. necator* portant des constructions plasmidiques différentes, dans des conditions de culture stringentes (fluctuation de l'environnement, température supra-optimale) ou optimales, et dans différents modes de cultures (batch, fed-batch, chémostat). Ainsi, la réponse du biocapteur (distribution d'intensité de fluorescence) et le comportement des souches recombinantes (cinétiques, rendements, métabolisme, viabilité, cultivabilité) ont pu être caractérisés en fonction des conditions opératoires et/ou des constructions plasmidiques étudiées.

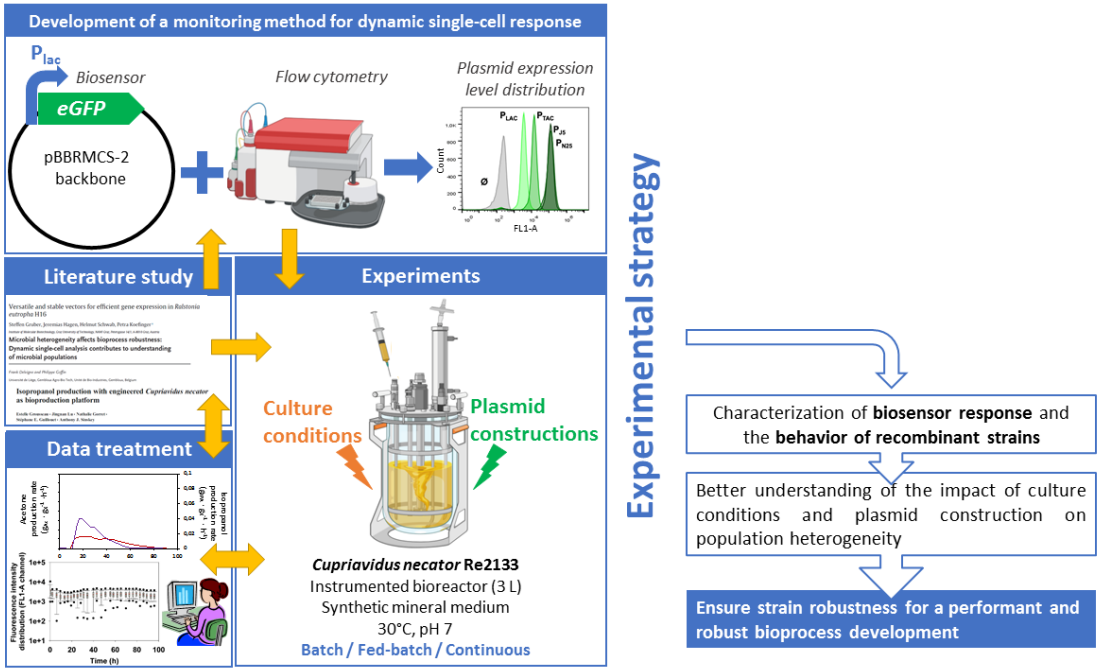

Figure 1: Stratégie expérimentale de la thèse

Le manuscrit de thèse est structuré en quatre parties, comme décrit ci-dessous :

La première partie du manuscrit se concentre sur l'état de l'art, ou un aperçu général de la littérature sur les hétérogénéités de populations dans les bioprocédés, les méthodes d'identification et de quantification de ces hétérogénéités et les stratégies de contrôle de l'hétérogénéité sont décrits. Le

métabolisme de la bactérie *Cupriavidus necator*, ainsi que les méthodes de stabilisation plasmidique déjà développées pour ce microorganisme, sont aussi décrits.

La seconde partie détaille le matériel et les méthodes utilisés au cours de ce travail.

La troisième partie présente et discute les résultats des travaux de recherche. Elle est organisée en trois chapitres :

Le chapitre 1 est consacré à l'étude des hétérogénéités de stabilité d'expression plasmidique lors de la production hétérologue d'isopropanol par *Cupriavidus necator* en mode discontinu alimenté. Deux constructions plasmidiques visant à augmenter la robustesse de la souche ont été comparées par rapport à un plasmide de référence. La stabilité de l'expression plasmidique a été évaluée par la méthode classique (étalement et comptage sur milieux gélosés sélectifs), méthode basée sur la résistance aux antibiotiques codée sur les plasmides recombinants. La robustesse des souches a aussi été étudiée en regard de leur dynamique de production d'isopropanol.

Le chapitre 2 est consacré au développement d'une souche fluorescente à visée biocapteur pour le suivi des sous-populations en dynamique sous différentes conditions de culture. Ce chapitre est composé en trois sous-parties.

Le *sous-chapitre 1* concerne la construction et la caractérisation de différents biocapteurs ainsi que l'analyse des sous-populations à l'échelle de la cellule unique par cytométrie en flux, basée sur l'expression d'un gène *eGFP* codé sur le plasmide recombinant. Plusieurs promoteurs constitutifs de différentes forces (faibles à fortes) ont été étudiés pour choisir celui permettant le meilleur compromis entre intensité de fluorescence des cellules et faible charge métabolique. Une fois la construction plasmidique validée, elle a été confrontée à des conditions de culture stringentes favorisant l'hétérogénéité d'expression plasmidique afin de confirmer sa fiabilité lors de cultures microbiennes. Les sous-populations obtenues ont été caractérisées après tri cellulaire par FACS (*abbr.* Fluorescence Activated Cell Sorting) puis repiquage en microplaques. Le biocapteur sélectionné est utilisé pour la suite des travaux afin de quantifier les distributions des niveaux d'expression plasmidique. Ce sous-chapitre a été publié en tant qu'article scientifique dans le journal « Applied Microbiology and Biotechnology ».

Le *sous-chapitre 2* concerne l'étude des hétérogénéités générées dans des conditions de perte d'expression plasmidique. Dans un premier temps, une stratégie d'induction de perte d'expression plasmidique sans inhibition de la croissance a été mise en œuvre en mode batch. Dans un second temps, cette stratégie a été appliquée au cours de cultures successives permettant de générer un grand nombre de générations, puis à différents taux de croissance en culture continue. Ces

expériences ont permis de quantifier par cytométrie en flux l'impact du taux de croissance sur le niveau de l'expression plasmidique.

Le *sous-chapitre 3* vise à quantifier la robustesse des cellules lors de cultures mettant en œuvre (1) deux stratégies d'alimentation en sucre (pulse, continu) et (2) des constructions plasmidiques visant à assurer la stabilisation du plasmide. Les données cinétiques (macroscopiques), physiologiques (perméabilité membranaire) et de distribution de niveau d'expression plasmidique ont été confrontées pour choisir les conditions de culture permettant d'atteindre une meilleure robustesse du procédé.

Le chapitre 3 concerne l'étude de l'hétérogénéité d'expression plasmidique par notre biocapteur eGFP lors de la production d'isopropanol avec *C. necator*. Trois souches recombinantes de *C. necator* ont été comparées pour le besoin de cette étude : une souche productrice d'isopropanol (Re2133/pEG7c), une souche fluorescente (Re2133/pCB1) et une souche couplant les deux (Re2133/pJLCB2). Les comportements de ces souches ont été quantifiés en mode fed-batch : L'étude de l'hétérogénéité d'expression plasmidique est basée sur les distributions d'intensité de fluorescence et comparée aux hétérogénéités de stabilité d'expression mesuré par comptage sur boîte, en lien avec la production d'isopropanol au cours des cultures.

La **dernière partie donne lieu à une discussion générale** des résultats par rapport à l'état de l'art et permet de donner des conclusions générales ainsi que des perspectives à ces travaux.

Part 1: Literature review

Part 1: Literature review

1 Population heterogeneity

Microbial populations cultivated in assumed homogeneous environments are by extension also considered homogeneous in terms of its individuals. However, this postulate is being discussed and more and more studies showing that population heterogeneity (*i.e.* uneven behavior of single-cells) can be observed among monoclonal cultures in homogeneous environments are being published (Carlquist *et al.* 2012, Delvigne *et al.* 2014, Gonzalez-Cabaleiro *et al.* 2017, Heins *et al.* 2018, Boy *et al.* 2020).

Population distribution within a culture can be observed as a Gaussian distribution among single-cells, or even a bimodal and multi-modal. So, population heterogeneity cannot be described accurately through mean values obtained by standard analytical techniques; indeed, it might lead to misinterpretation of phenomenon occurring in single-cells. Population heterogeneity study within a bioprocess is complex and requires being led over an extended amount of time and single-cells. Especially, it remains complicated to follow the precise path of cells during their presence in a bioreactor when environmental gradients appear during scale-up for instance (Lara *et al.* 2006, Delvigne *et al.* 2014, Delvigne *et al.* 2014, Martins *et al.* 2015, Lemoine *et al.* 2017, Heins *et al.* 2018). So, concerning population heterogeneity in bioprocesses, the mechanisms responsible for it and their control have to be investigated.

1.1 Form of heterogeneity

Subpopulations heterogeneities can be divided into four different main categories: genetic, biochemical, physiological and phenotypic (Brehm-Stecher *et al.* 2004). There are often connections between these categories (Martins *et al.* 2015).

Genetic heterogeneity

Genetic heterogeneity is characterized by differences in the DNA and RNA nucleotide sequences. For example, genetic heterogeneity can be caused by different factors, like: spontaneous point mutations, transcription errors, phage-related mechanism (*e.g.* transduction, lysogeny), or mobile genetic elements (*e.g.* plasmids, transposons) (Brehm-Stecher *et al.* 2004, Martins *et al.* 2015).

Biochemical or metabolic heterogeneity

This category is defined by differences in macromolecular composition between mother and daughter cells (*e.g.* asymmetric repartition of nucleic acids, proteins, storage compounds (*i.e.* carbohydrates, Poly(3-Hydroxybutyric Acid)) (Martins *et al.* 2015) or in activity levels between cellular subpopulations. It can be caused by genetic heterogeneity and variations in cell cycle-related processes like turnovers or cellular aging-related events (Brehm-Stecher *et al.* 2004, Martins *et al.* 2015).

Physiological heterogeneity

Physiological heterogeneity is defined by morphological differences between individuals: cell size, shape, volume, buoyant density (*i.e.* measure of the tendency of a substance to float in some other substance), nucleoid morphology or surface characteristics. Some explanations have been proposed in certain cases. For instance, physiological heterogeneity can be due to differences in the cell-cycle, especially in the case of microorganisms undergoing sporulation or formation of fruiting bodies. Another explanation for physiological heterogeneity can be found in the apparition of microenvironments where cells are not submitted to the same culture conditions due to mass transfer limitations mainly (*i.e.* colonies, biofilm, insufficient mixing) (Brehm-Stecher *et al.* 2004, Timoumi *et al.* 2017).

Phenotypic heterogeneity

Phenotypic heterogeneity, also called behavioral heterogeneity, is defined as the consequence of both biochemical and/or physiological heterogeneities (Brehm-Stecher *et al.* 2004). Phenotypic heterogeneity consists in variations (macromolecular composition, activity levels, morphological differences, antibiotic production, increased lag phase, SOS response) observed among cells in an isogenic population, that are not directly due to genetic mechanisms. On one hand, it is assumed to increase bacterial fitness in non-optimal environments (*i.e*. medium composition, culture conditions or fluctuations) (Grote *et al.* 2015). On the other, within a bioprocess where the aim lies in the production of a molecule of interest, it might decrease production yields and rates as all cells are not in an optimal production state (Delvigne *et al.* 2014).

1.2 Cause of heterogeneity

1.2.1 Gene expression stochasticity

Even monoclonal cultures grown in homogeneous environments can experience cellular heterogeneity. The number of proteins produced from a particular gene will vary among cells in a population and also through time for a single cell. Most of the time, this is due to heterogeneous gene expression (Swain *et al.* 2002, Brehm-Stecher *et al.* 2004, Cao *et al.* 2018). Noise in the gene expression

is a natural phenomenon arising in two ways: “intrinsic” and “extrinsic” noise (Elowitz *et al.* 2002, Nana *et al.* 2018, Mortier *et al.* 2019).

“Intrinsic” noise is caused by the biochemical processes of gene expression itself. Reactions leading to transcription and translation do not necessary occur simultaneously, nor in the same order, among cells. A gene might be expressed at different levels even within cells in the same state. Such stochastic behavior is defined locally by the particular gene sequence and the inherent properties of the encoded protein (Swain *et al.* 2002, Cao *et al.* 2018).

“Extrinsic” noise is due to fluctuations in the amount of crucial cellular components like regulatory proteins, ribosomes, RNA polymerase or even stage in the cell cycle stage. Indeed, these molecules are also gene products and therefore vary through time, and within cells. So, extrinsic noise appears independently of the expression of the gene of interest, but nevertheless has an effect on it (Swain *et al.* 2002, Cao *et al.* 2018).

1.2.2 Cell cycle

Generally, bacterial populations are considered to show little diversity. However, it has been demonstrated that some bacterial species present pleomorphic states. This heterogeneity may be caused by differences in cell cycle phases (Muller *et al.* 2010).

On one hand, the durations of DNA replication and cell division phases in a bacterial cell cycle occur in a specific time frame, depending on the bacteria specie, and are generally relatively independent of growth conditions. On the other, durations of the cell cycle steps before both replication and cell division are confronted to much more variations; for instance, when the growth rate is low due to carbon, energy or nutrient limitation. So, physiological changes may arise from the length variations of these stochastic steps and favors the apparition of cell heterogeneity (Muller *et al.* 2010).

In the case of optimal growth conditions, a new DNA replication round is initiated even before the previous one is completed. This phenomenon might cause accentuated heterogeneity concerning chromosome and plasmid copy number, and DNA contents (Muller *et al.* 2010).

1.2.3 Age distribution

Age distribution phenomena associated with the three following mechanisms cause population heterogeneity (Muller *et al.* 2010).

- Replicative aging: This state is defined as a cumulative cell fitness loss in a sibling-specific fashion with increasing age resulting in a less active mother-type lineage. Studies have shown that “age factors” (*i.e.* deleterious mutations, damaged proteins, lower reproductive capacity) might be

implicated. In one hand they could be directly transferred from the aged mother cell to the daughter cell. On the other, they could remain in the aged mother cell, causing the production of less active daughter cells (Muller *et al.* 2010).

- Asymmetric cell division: Smaller and larger cells are formed during cell division. Daughter cells differ on the base of their structure and molecular composition. The duration of the replication phase will be impacted and become a source of heterogeneity (Muller *et al.* 2010).
- Aged cell poles: Some long-lived cell components like nucleotides and membrane lipids tend to be deposited on cell poles (Nyström *et al.* 2007, Muller *et al.* 2010) and so, are not inherited equally between daughter cells.

So, cells running through manifold replication cycles during cultures monitored over long periods might show reduced capacities; for example: decreased reproduction capacity, lower single-cell growth rate and decreased metabolic efficiency (Muller *et al.* 2010).

1.2.4 Bet-hedging

Bet-hedging is a survival strategy hypothesized to set up in isogenic populations to minimize temporal variance of living offspring in order to maximize mean fitness of the whole population in numerous environments over several generations (Grimbergen *et al.* 2015, Heins *et al.* 2018). Subpopulations develop new phenotypes of reduced fitness toward the current environment, but that might be more appropriate to a future environment. This strategy has been shown to efficiently ensure cell survival of at least one part of the population when environmental conditions changed abruptly and unpredictably (Delvigne *et al.* 2014, Grimbergen *et al.* 2015, Heins *et al.* 2018). This strategy seems to act as protection against stress. In the case of fluctuations in nutrient availability, regrowth can be delayed to spread the risk. Plus, subpopulations that first froze their metabolism are also the first to regrow when nutrient availability is favorable, depending on the carbon source and intensity of endured stress (Heins *et al.* 2018). True bet-hedging by microorganisms should fulfill two conditions. First, the bet-hedging strategy should enhance cell fitness in a fluctuating environment, compared to conditions where it does not occur. Second, phenotype switching rates should be correlated with environmental fluctuation frequency, to increase cell fitness. Evidence for true bet-hedging have been difficult to find (Grimbergen *et al.* 2015).

1.2.5 Extracellular micro-environment

On one hand, in lab-scale and industrial bioreactors, concentration gradients (*e.g.* temperature, pH, nutrient concentrations) often arise, because of insufficient mixing capacities of the system (*e.g.* large volume, high viscosity). In these conditions, population heterogeneity is likely to occur and its intensity depends on the heterogeneous culture conditions met by cells in the bioreactor (Heins *et al.* 2018). In

this case, population heterogeneity might greatly disrupt process performances: reduction of production and biomass yields, decreased growth and production rates (Lara *et al.* 2006, Barkai *et al.* 2007, Hewitt *et al.* 2007, Masel *et al.* 2009, Delvigne *et al.* 2015, Limberg *et al.* 2017). As an example, a progressive loss of viability might occur under nutrient depletion conditions. This phenomenon starts when the two main regulatory systems responsible for damage protection stop working: stress defense regulon σ^S and heat shock regulon σ^{32}. Non-prolific microbial populations composed of starving cells appear under nutrient limitation. These cells are different from others because of their cellular components' deterioration. This particular state is attained stochastically and might be irreversible depending on damage extent (Muller *et al.* 2010).

On the other, in Nature, cell populations have to adapt to fluctuating growth conditions (*e.g.* temperature, pH, nutrient and toxin concentrations…). To do so, cell populations may improve their fitness thanks to individuals that evolve stochastically between several different phenotypes. Therefore, some cells might always be prepared to face sudden environmental fluctuation (Kussell *et al.* 2005, Acar *et al.* 2008). In this case, population heterogeneity allows the emergence of cells with a higher stress tolerance and cell fitness (Heins *et al.* 2018).

Another segregating mechanism linked to the extracellular environment has been described: bistability. In response to environmental stress, regulatory systems answer with an "either-or" verdict. Two different subpopulations arise directly from this "either-or" verdict or this metabolic state can possibly be transmitted to the next generation through epigenetic inheritance. In this condition, the obtained heterogeneous population might present higher fitness than homologous population (Muller *et al.* 2010).

1.3 Heterogeneity analysis at single-cell level

Single-cell analysis has become a key step to process control and optimization in recombinant molecule production (Zhang *et al.* 2015). Originally, the first tools used to study population heterogeneity were light microscopy and plate counting. Even if they are rather time consuming compared to new high throughput analysis methods, they are still commonly used in routine methods today for particular applications. Because of technological progresses these last few decades, new analyzing methods are available, like time-laps microcopy, flow-cytometry or single-cell RNA seq (Brehm-Stecher *et al.* 2004, Martins *et al.* 2015).

The possible bias that has to kept in mind concerning these analyzing methods is that they require fluorescent probes that are potentially toxic to the cell, intense light, electric or magnetic energy physical manipulation using mechanical optical or electrokinetic forces, or also carry genes like β-

galactosidase or GFP that modify their genome and increase metabolic load. So, the simple fact of observing cells might impact the response of the analysis method. However, these methods allow a direct and simple analysis of protein expression and therefore expression levels during culture. Plus, they allow a fast and direct answer, easily analyzed by high throughput methods. Their impact on cell metabolism / physiology can be controlled and minimized, as detailed below. (Brehm-Stecher *et al.* 2004, Avraham *et al.* 2015).

1.3.1 Single-cell isolation / individualization

The isolation / individualization of a significant number of cells is important in order to analyze each single-cell separately as a unique individual in order to build an image of the whole population. So, high throughput methods have been developed to isolate single cells from cell suspension (Zhang *et al.* 2015).

In all techniques, the first step to single-cell analysis is the isolation of cells. There are three main methods: serial dilutions, field-gradient traps and flow-driven single cell suspension.

First, serial dilution of cell suspensions is the easiest and most traditional method. Theoretically, the aim would be to reach one single cell (Gonzalez-Cabaleiro *et al.* 2017). Second, the most common approaches among field-gradient traps are optical, magnetic and dielectrophoretic tweezers. Optical tweezers are based on a highly focused laser beam producing an optical gradient, where microscopic and neutral objects get trapped (Zhang *et al.* 2008). Magnetic tweezers are based on electromagnetic field gradients and magnetic beads attached to single-cell surface (Laurent *et al.* 2002, Zhang *et al.* 2008). Dielectrophoretic tweezers are based on the interaction between a dielectrophoretic field and a single-cell, where the magnitude and the direction of the force might be controlled voltage frequency (Lee *et al.* 2007). Third, the method of flow-driven single suspension aims to flow a cell suspension into a narrow microchannel. So, single-cells are forced to cross the detection chamber or are confined for further analysis. The most common example of flow-driven single suspension is flow cytometry (Zhang *et al.* 2015).

1.3.2 Single-cell analysis

Once single-cell have been isolated, heterogeneity analysis can be performed on samples. Methods to monitor population heterogeneity could be classified into three different categories: Biophysical characterization, gene expression method and protein analysis (**Figure 1**).

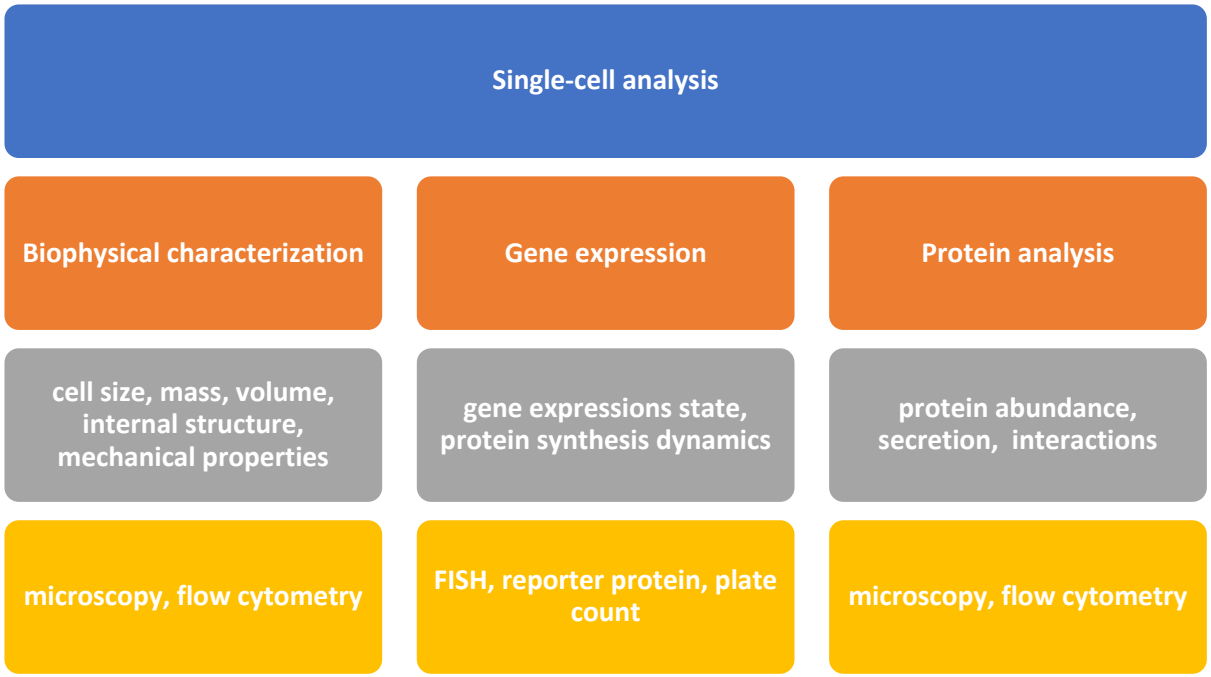

Figure 1: Overview of single-cell analysis methods

1.3.2.1 Plate count

The aim of this method is to determine the percentage of plasmid-containing cells based on selection pressure. Cell samples are cultivated on agar plates under selective pressure. For instance, plasmids can encode for antibiotic resistance or for the biosynthesis of an essential compound needed for growth in an auxotrophic strain. The ability of these cells to grow under this specific conditions is supposed to prove that plasmid encoded genes are expressed (Weber *et al.* 1988). Another possibility consists in a plasmid-encoded enzyme (*e.g.* β-galactosidase) lysing a specific substrate (*e.g.* X-gal), which under these conditions releases a fluorescent marker. Thus, plasmid-bearing cells are stained (e.*g.* blue with X-gal). Diluted samples are respectively plated on selective and not selective medium and the ratio of growing colonies between these plates determine plasmid stability (Friehs *et al.* 2004, Lau *et al.* 2013, Sato *et al.* 2013, Gruber *et al.* 2014).

There are many limitations in this method. First, the noise in gene expression might create noise in the phenotypic expression of the plasmid encoded genotype and so, underestimate the plasmid-containing fraction. Then, the main limitation of this method is its cultivability dependence, which means that a plasmid-bearing cell that is not cultivable is not counted as plasmid-containing cell, leading to an underestimation. Last, a specific problem linked to auxotrophic methods has been demonstrated. In fact, it has been proven that plasmid-free cells take advantage of the compound synthesized by plasmid-containing cells and consume it and be able to grow. In this case, plasmid stability results are overestimated (Gupta *et al.* 2001).

1.3.2.2 Reporter strains

Reporter strains (*i.e.* biosensors) are the most common tools used to study subpopulation behavior during bioprocess as they are fast and non-invasive (Heins *et al.* 2018). Reporter strains are composed of two components: an input and a transduction module. First, the input module is activated by the intracellular event of interest. It can be either promoter-based, transcription factor-based, FRET-based or riboswitch-based. Second, the transduction module (*i.e.* reporter molecules) transforms the input module into a measurable output signal, which is specific and proportional to the event of interest. If mechanism behind the event of interest is well-known, a correlation between output signal and its concentration must be made. The measurable output signal is often a fluorescent signal (Delvigne *et al.* 2014, Heins *et al.* 2018).

Induction mechanisms

The most common reporter strains in the literature for investigation of cell heterogeneity in bioprocesses are promoter-based. The promoter specifically controls the expression of the reporter protein in response to a cellular event of interest. Expression level can be used to measure promoter activity. Reporter strains can be selected to detect nutrient or dissolved oxygen limitation because of environmental fluctuations, intrinsic stress factors (*e.g.* redox metabolism imbalance, oxidative damage, unfolded protein accumulation) (Longo *et al.* 2006, Delvigne *et al.* 2014, Polizzi *et al.* 2015, Heins *et al.* 2018).

Transcription factor-based reporter strains are mainly used in studies for the detection of regulatory circuits and their corresponding intracellular metabolites (*e.g.* product formation, protein interaction). The synthesis of the reporter protein is induced by the interaction of a transcription factor with a metabolite of interest. Transcription factor-based biosensors can sense and control intracellular metabolite concentration, and so, might be used monitor their concentration. Several transcription factors control the promoters' transcriptional response, and transcription factor-based biosensors can be related to promoter-based biosensors (Mahr *et al.* 2016, Rogers *et al.* 2016, Heins *et al.* 2018).

FRET (Förster energy transfer)-based biosensors are based on energy transfer between two fluorophores (*i.e.* from a "donor" to an "acceptor") without photon emission. When both fluorophores are apart by more than 10 nm, donor emission is detected after its excitation. When "donor" and "acceptor" fluorophores are closer than 1 to 10 nm, they interact and acceptor emission is mostly detected (Zadran *et al.* 2012). These reporter strains are useful in real-time monitoring of concentration fluctuations of intracellular molecules (*e.g.* cAMP, ATP, amino acids) in single-cells and interaction between molecules (protein-protein, protein-DNA) (Delvigne *et al.* 2014, Heins *et al.* 2018).

A riboswitch is a specific regulatory region of mRNA modulating its own transcription or translation levels in response to the presence of ubiquitous metabolites (*e.g.* amino acids, vitamins) (Delvigne *et al.* 2015, Heins *et al.* 2018).

Fluorescent reporter molecules

Principle of fluorescence-based methods

The principle of fluorescence can be briefly explained as follows. First, photons from an incident beam of light increase the energy level of electrons in a fluorophore to reach a so-called "excited state". Then, when the molecules come back to a lower-energy state an emission of light occurs and is defined as fluorescence. The difference between the emission wavelength and the excitation wavelength is defined as "Stokes shift" (Brehm-Stecher *et al.* 2004, Fernandes *et al.* 2011).

Beyond the importance of fluorophore intrinsic properties, it is also necessary to consider the analysis environment because several factors might alter the outcome fluorescence. For example, parameters like pH, physical proximity to other molecules in solution and the presence of localized charge concentrations like DNA and its polarized backbone (Brehm-Stecher *et al.* 2004, Fernandes *et al.* 2011) might impact fluorescence characteristics. For instance, conjugation of fluorescent protein to nucleic acids might affect molar absorptivity, fluorescence quantum yields and fluorescence lifetimes. Plus, pH might favor the apparition of monomers or dimers of fluorophores, which should influence the molar absorptivity reached as well (Sjöback *et al.* 1998).

The advantages of fluorescence-based methods are rapidity and facility to stain cells within a complex mixture depending on their individual characteristics (*e.g.* biochemical, physiological, taxonomic) (Brehm-Stecher *et al.* 2004, Fernandes *et al.* 2011).

Examples of fluorescent proteins

Variety of fluorescent proteins are available in the whole visible spectrum from deep blue (*i.e.* ultra-violet) to deep red (*i.e*. infra-red), offering a large choice of genetically encoded biosensors for cell biology study (Shaner *et al.* 2007, Day *et al.* 2008). The most commonly used fluorescent reporter protein is the Green Fluorescent Protein (*abbr.* GFP), and is originated from the jellyfish *Aequorea victoria*. It is a fluorescent protein of 238 amino acids that does not require specific substrates or cofactor to be expressed. So, GFP can be used as reported protein by all cell types (Tsien *et al.* 1998, Fernandes *et al.* 2011). It has been shown that several other marine organisms also express fluorescent proteins like or similar to GFP (**Table 1**). For example, the first red fluorescence protein DsRed was isolated from the mushroom anemone *Discosoma striata*. After directed evolution and mutagenesis,

stable, bright and rapid maturing red fluorescence proteins were synthesized (*e.g.* mCherry, tdTomato). Plus, the coral *Clavularia* expresses a cyan fluorescent protein which was engineered to obtain the monomeric teal fluorescent protein mTFP. The mushroom coral *Fungia concinna* expresses a yellow-orange fluorescent protein which was engineered to the monomeric Kusabira orange mKO (Day *et al.* 2008).

Some points need to be considered before selecting a fluorescent protein (Shaner *et al.* 2005, Shaner *et al.* 2014, Rodriguez *et al.* 2017). Fluorescent protein should be bright enough for significant detection compared to auto-fluorescence. Cytotoxicity due to fluorescent protein should be minimal. Fluorescent proteins should be expressed as monomers unless they are expressed as fusion protein. However, the majority of wild type fluorescent proteins are dimers or tetramers. So, significant efforts were made to produce monomeric engineered fluorescent proteins. In experiments requiring multi-labelling, fluorescent proteins should be chosen with the least interference in terms of emission wavelengths. Environmental factors (*e.g.* O_2, pH) should not disrupt apparent brightness of fluorescent protein expression. Photostability of fluorescent proteins should be high enough to allow measurements all along experiments (Shaner *et al.* 2005, Day *et al.* 2008, Rodriguez *et al.* 2017).

Intrinsic fluorescent brightness is proportional to the product of the molecular extinction coefficient (ε) and of the fluorescence quantum yield (Φ). In most cases, engineered fluorescent proteins have been optimized at 37°C, but some may, however, fold more or less efficiently (Shaner *et al.* 2005, Rodriguez *et al.* 2017). So, mutational strategies developed these last past years aimed at enhancing gene expression through codon usage optimization, protein folding improvement, protein maturation enhancement and protein stability increase toward environment factors (Rodriguez *et al.* 2017).

Table 1 : Selection of fluorescent proteins used as biosensor in cell biology

Fluorescence protein	Color	Excitation (nm)	Emission (nm)	Intrinsic brightness $(mM \cdot cm)^{-1}$	Photo-stability	Reference
Aequorea-based color variants						
Enhanced GFP	Green	488	507	34	++++	(Shaner *et al.* 2005)
ECFP	Cyan	4433/445	475/503	13	++	(Shaner *et al.* 2007)
Enhanced YFP	Yellow	514	527	51	++	(Shaner *et al.* 2007)
EBFP2	Blue	383	448	18	++	(Day *et al.* 2008)
mCerulean	Cyan	433-445	475-503	27	++	(Day *et al.* 2008)
mEmerald	Green	487	509	39	++++	(Day *et al.* 2008)
mVenus	Yellow	515	528	53	+	(Day *et al.* 2008)
mRFP-based color variants						
tdTomato	Orange	554	581	95	+++	(Day *et al.* 2008)
mCherry	Red	587	610	17	+++	(Day *et al.* 2008)
Color variants from corals						
mTFP1	Cyan / green	462	492	54	+++	(Day *et al.* 2008)
mKO	Orange	548	559	31	+++	(Day *et al.* 2008)
mKate	Far-red	588	635	15	++++	(Day *et al.* 2008)

The greater interest in using GFP lies in the fact that it is a non-invasive probe allowing real-time analysis of dynamic events occurring in living cells. GFP is frequently used to study *in vivo* protein expression (*e.g.* localization, functionality) (Brehm-Stecher *et al.* 2004) or to monitor intracellular activities (*e.g.* pH in organelles) (Day *et al.* 2008). Many groups have studied and optimized GFP expression depending on their purpose. Most of the fluorescent proteins used today were optimized through mutagenesis depending on their application from the *Aequorea* GFP (Day *et al.* 2008): blue, cyan, green fluorescent proteins. For example, GFP has been optimized for fluorescence-activated cell sorting and fluorescent microscope. Plus, GFP-derived proteins have been developed which have emission peaks ranging from blue to yellow. Physical properties have also been studied such as folding efficiency (*e.g.* eGFP) and thermostability. It has also been shown that codon usage of heterologous gene in host organism has to be taken into consideration (Fernandes *et al.* 2011).

The only limiting aspect of the use of fluorescent protein in living organisms is that it cannot be expressed without oxygen. Dioxygen is required to dehydrogenate amino acids during chromophore formation (Shaner *et al.* 2005, Fernandes *et al.* 2011).

1.3.2.3 Fluorescent dyes

Fluorescent dyes are frequently applied to population heterogeneity studies because of their relevance with calibration procedures (Heins *et al.* 2018) (**Table 2**). The use of fluorescent dyes can either be complementary to fluorescent reporter strains or time-saving to avoid designing a new recombinant strain. Indeed, in industrial bioprocess, it might be impossible to genetically modify strains because of regulation (Fernandes *et al.* 2011, Heins *et al.* 2018). In the use of fluorescent dyes, output signal must be verified to be representative of single-cell characteristics, otherwise dyes might change stained cells characteristics and lead to artefacts or false-positives. For instance, membrane integrity dyes (*e.g.* Propidium Iodide *abbr.* PI, SYTO®) have been shown to affect cell viability in some cases (Davey *et al.* 2011), which might lead to an overestimation of cell mortality. Indeed, it has been shown that a small portion (*i.e.* > 10 % with *Saccharomyces cerevisiae*) of “fragile” cells was still able to grow even after being stained by PI (Davey *et al.* 2011, Delobel *et al.* 2012). These membrane potential stains should be used to compare viability between several strains, or for one strain through time.

Table 2 : Selection of most common fluorescence dyes in cell biology

Properties	Indicator	Techniques	Reference
Cell viability	Membrane integrity	SYTO® 9	(Fernandes *et al.* 2011)
		Propidium Iodide (PI)	(Fernandes *et al.* 2011, Heins *et al.* 2018)
		Ethidium Monoazide Bromide (EMA)	(Fernandes *et al.* 2011, Heins *et al.* 2018)
		bis-oxonol (BOX)	(Sträuber *et al.* 2010, Heins *et al.* 2018)
		Rhodamine 123 (RH123)	(Sträuber *et al.* 2010, Heins *et al.* 2018)
		5-cyano-2,3-ditolyltetrazolium chloride (CTC)	(Sträuber *et al.* 2010, Heins *et al.* 2018)
		SYBR® Green	(Sträuber *et al.* 2010, Heins *et al.* 2018)
		DNA stains	(Fernandes *et al.* 2011)
	+ Detection of membrane carbonylated proteins	Alexa Fluor hydrazide Fluorescent dyes	(Fernandes *et al.* 2011)
Cell Activity			
Respiratory activity	Reduction of formazan crystals by the cell electron transport system	5-cyano-2,3ditolyl tetrazolium chloride (CTC)	(Fernandes *et al.* 2011)
	Reductase activity in cell electron transport system	Redox Sensor Green (RSG)	(Fernandes *et al.* 2011)
	Reactive oxygen species	Dihydrorhodamine 123 (DHR)	(Sträuber *et al.* 2010, Heins *et al.* 2018)
Metabolic activity	Ribosome concentration	Fluorescent probes used in Fluorescence in Situ Hybridization (FISH)	(Fernandes *et al.* 2011)
	Esterase activity	Carboxyfluorescein diacetate (CFDA)	(Fernandes *et al.* 2011, Heins *et al.* 2018)
	Redox indicator	Methylene blue	(Heins *et al.* 2018)
Microbial surface properties	Cell surface hydrophobicity (CSH)	Fluorescent polystyrene microspheres designed for Microsphere	(Fernandes *et al.* 2011)
		Adhesion to Cells (MAC)	(Fernandes *et al.* 2011)
	Cell surface polysaccharides	Fluorescent lectin	(Fernandes *et al.* 2011)
	Amyloidic fibrils	Fluorescent antibodies	(Fernandes *et al.* 2011)
	Various exoenzymes	Fluorescent dye-labeled substrates	(Fernandes *et al.* 2011)
Internal storage compounds	Polyhydroalkanoates	Nile blue	(Fernandes *et al.* 2011)

1.3.2.4 Microscopy

Microscopy is one of the first equipment used to study single-cell properties and population heterogeneities. Light, atomic force and fluorescence microscopies are all adapted to analyze single-cell properties during fermentation at different levels. Cell suspensions are commonly diluted for microscope observation. Even if this method allows observing each cell individually (*e.g.* morphology, viability, fluorescence), microscopic analysis is limited concerning the amount of data collected (Fernandes *et al.* 2011, Zhang *et al.* 2015).

Light microscopy

Light microscopy is mostly used to observe population heterogeneity based on cell morphology (*i.e.* cell size and shape) (Fernandes *et al.* 2011).

Fluorescence microscopy

Some specific fluorescence related observations can only be made by fluorescence microscopy. Several fluorescent dyes developed for fluorescent microscopy are nowadays used in flow cytometry that offers the advantages of a high-throughput method. With fluorescent microscopy, it is possible to use multiple stains simultaneously which is a good strategy to obtain more data about single-cell physiological state, as long as the emission spectrum of the fluorescent dyes do not overlay. This method also allows observing fluorescent protein producing strains. On one hand, the main advantages of using fluorescent microscopy in single-cell analysis are its specificity, sensitivity, temporal and spatial resolution. On the other hand, the main drawbacks are the fading and photobleaching of the dye and fluorescence quenching (Fernandes *et al.* 2011).

1.3.2.5 Flow cytometry

General principle

Cytometry refers to the technologies used to characterize biological single-cells by counting, measuring or comparing them (Brehm-Stecher *et al.* 2004). Flow cytometry measurement (*abbr.* FCM) is used to measure the detailed properties of individuals in a whole population by sorting, counting and examining.

The first step of the analysis after sampling is based on hydrodynamics properties. Single cells are indeed focused in a fluid stream (*i.e.* sheath fluid). Then, this stream is intercepted by a beam of light which is most of the time a laser beam. The laser beam illuminates each cell to measure light scattering properties and to excite fluorescent molecules. Data concerning optical properties are collected in real-time and saved (Brehm-Stecher *et al.* 2004, Tracy *et al.* 2010, Fernandes *et al.* 2011).

This analysis relies on light scattering, excitation and emission properties. If the light deviation angle through the particles is small (0°-5°), it will be defined as forward scatter (*abbr.* FSC) which is related to cell size or volume. Otherwise, if the light deviation angle is big (90°) it will be defined as side scatter (*abbr.* SSC) and can be related to intracellular content called also granularity (Fernandes *et al.* 2011). Cell number, size and content can be measured simultaneously by this method as well as the fluorescent probe response of the cells (Brehm-Stecher *et al.* 2004). Analyzing at the single-cell level allows analyzing each individual in a cell population which enables to access distributions within a short time of analysis and large number of cells (**Figure 2**). Therefore, it gives a more precise information about cell populations behavior than mean-populations analysis (Fernandes *et al.* 2011).

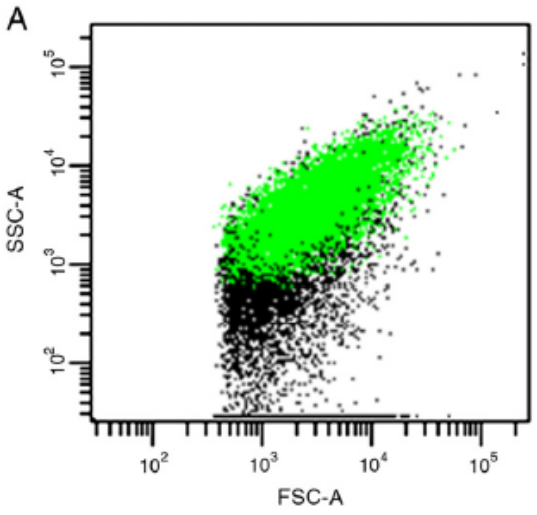

Figure 2: Results of a flow cytometry analysis of a heterogenic population of *E. coli* strain expressing GFP (SSC *vs.* FSC) (Fernandes *et al.* 2011)

Cell properties measurable by flow cytometry can be divided into two groups: intrinsic and extrinsic properties. On one hand, intrinsic properties (*e.g.* membrane composition, size) can simply be measured without cell labelling with the FSC and SSC channels. On the other hand, extrinsic properties (*e.g.* membrane integrity or potential) require fluorescent strains or probes to be characterized (Fernandes *et al.* 2011). So, flow cytometry provides information-rich data sets on cell populations at the single-cell level (Brehm-Stecher *et al.* 2004). As this analysis method allow visualizing single-cells from different subpopulations, flow cytometry is more and more used to study population heterogeneity in bioprocesses, especially with reporter strains and fluorescent dyes (Heins *et al.* 2018).

Even if flow cytometry has been mainly used to study mammalian cells, it is also possible to apply this method to bacteria. However, smaller cell size constitutes a real challenge (Brehm-Stecher *et al.* 2004). Accurate FCM analysis requires that the number of events counted in bacterial sample really corresponds to the number of cells of interest within the sample. In the work of Bahl *et al.* (2004) the

results obtained by FCM were compared to those obtained by plate counting from the same bacterial sample (Bahl *et al.* 2004).

Fluorescence-activated cell sorting

Fluorescence-activated cell sorting (*abbr.* FACS) is an interesting extension of flow cytometry principles as it enables to physically sort cells according to their light scattering and fluorescence. Cells are ordered in a sheath fluid and pass a laser beam where the fluorescent proteins are excited. Fluorescence emission signal of single-cells allows highly specific downstream cell sorting. The method set to capture cells consists in a vibrating mechanism to split the continuous flow into cell-containing droplets. These droplets are selectively charged and electrostatically diverted into a collecting container (Ma *et al.* 2017). Therefore, FACS permits to physically separate subpopulations of interest from a heterogenic population (Fernandes *et al.* 2011). FACS systems are efficient and accurate, but they also are expensive and bulky. Plus, the viability of cells might be disrupted because of the strong electric fields encountered during sorting (Ma *et al.* 2017).

As FACS is a rather common method among eucaryotic cell (*e.g.* isolation of cell type-specific apoptotic bodies from mice (Atkin-Smith *et al.* 2017), selective breeding of live oil-rich microalgua *Euglena gracilis* (Yamada *et al.* 2016). It is still less used in bacterial cells studies (*e.g.* selection of pyruvate variants of *Corynebacterium glutamicum* enabling improved lysine production from glucose (Kortmann *et al.* 2019) because of certain challenges (*i.e.* small cell size, lower protein content per cell) (Tracy *et al.* 2010).

1.3.2.6 Fluorescence in situ hybridization: FISH

Fluorescence *in situ* hybridization is a high throughput method using nucleotide probes tagged with a fluorescent stain to hybridize specific RNA or DNA sequences. So, this method allows the visualization of cell subpopulation. Historically, stained cells are then analyzed by microscopy. Few examples using flow cytometry or even sorted with fluorescence activated cell sorting (FACS) (Haroon *et al.* 2013) have been developed. Cells are fixated and permeabilized for the need of this technique (Brehm-Stecher *et al.* 2004).

Flow-FISH

For mammalian cells, this method has already been associated with flow cytometry and the newly created method is often referred as Flow-FISH (Tracy *et al.* 2010). Flow-FISH requires cell fixation, permeabilization and hybridization with a set of fluorescently labeled oligonucleotide probes. Samples are then analyzed by flow cytometry (Arrigucci *et al.* 2017).

rRNA-targeted FISH

Ribosomes are a privileged target because they are largely amplified in growing cells. So, fluorescent tagged oligonucleotides (about 15-20 bp long) which target rRNAs are hybridized to whole cells (Brehm-Stecher *et al.* 2004, Haroon *et al.* 2013). Other RNA targets can be used in FISH methods like mRNA or tmRNA, but in these cases an amplification step is often necessary. The abundance of these RNA is indeed lower than with rRNA so, amplifying the sequences of interest is a way to make the fluorescent signal significant and precisely detectable (Brehm-Stecher *et al.* 2004).

Ring-FISH

FISH-based analyzing methods can also be used to detect target DNA sequences on low-copy-number plasmids (10^1-10^3 copies per cell) or on chromosomes (< 10 copies per cell). In this case, polynucleotide probes are used and they are introduced in higher concentration (x 1000) and present higher hybridization times because of their increased length (50 to 1200 nucleotides). The name of the method Ring-FISH comes from the resulting fluorescent signal that forms a halo around the fluorescence-emitter cells (Brehm-Stecher *et al.* 2004).

Immunofluorescence

It has also been possible to used FISH-methods to detect antibodies and other characteristic diagnostic binding events like capsular, flagellar or cell-wall antigens. These are whole cell methods (Brehm-Stecher *et al.* 2004).

2 Plasmid stability

Plasmid instability is a major concern of industrial recombinant strains. Plasmid instability has three main causes. First, asymmetric segregation during cell division causes plasmid loss for a certain portion of cells. Then, instability of genome structure can change in certain cells when all of them have the plasmid. Last, compared to plasmid-free cells, plasmid-bearing cells present a growth disadvantage (Alhumaizi *et al.* 2006).

2.1 Causes and consequences of plasmid loss

2.1.1 Metabolic load of recombinant plasmids

The introduction of a recombinant plasmid in a host cell requires resources to be maintained, replicated and to produce recombinant proteins (De Gelder *et al.* 2007). So, two main biological mechanisms are competing in plasmid-bearing cells: plasmid replication and cell growth (Silva *et al.* 2012). The metabolic load is defined by the amount of host cell resources (*e.g.* raw material, energy)

derived from host metabolism to synthesize recombinant RNA or recombinant proteins (Glick *et al.* 1995). Plasmid stability and metabolic burden problematics are difficult to dissociate from each other. In fact, the introduction of a plasmid into the host might induce a metabolic burden.

Higher plasmid copy number or plasmid size increase metabolic load. Indeed, the amount of energy required to replicate the plasmid in host cells is higher in this case, causing lower growth rates and lower gene expression levels (Bentley *et al.* 1990, De Gelder *et al.* 2007, Million-Weaver *et al.* 2014). For instance, it was demonstrated for recombinant plasmids with RSF1050 and pFH118-backbone in *E. coli* HB101 (*i.e.* 1 copy, 0.92 h^{-1}; 34 copies, 0.77 h^{-1}) (Bailey et *al.* 1993), as well as for plasmid pGFPuv in *E. coli* JM101-derivatives (*i.e.* 129 copies, 0.76 h^{-1}; 537 copies, 0.59 h^{-1}) (Cunningham *et al.* 2009). Nevertheless, plasmid maintenance and replication have a lower impact on metabolic burden than recombinant protein expression itself (Silva *et al.* 2012). Indeed, protein biosynthesis requires energy. More precisely, several GTP (*abbr.* Guanosine Triphosphate) are consumed for every amino acid added to the protein chain and one ATP (*abbr.* Adenosine triphosphate) molecule is consumed per aminoacyl-tRNA (Glick *et al.* 1995). Plus, recombinant protein overproduction might also cause depletion of some aminoacyl-tRNA or amino acids (*i.e.* codon bias)(Glick *et al.* 1995).

Metabolic load may also lead to size and shape heterogeneity among isogenic host cells (Glick *et al.* 1995), as well as decrease in host viability (Silva *et al.* 2012). Problems in plasmid carriage in the host cell can occur when recombinant plasmid proteins are interfering with the actions of host natural proteins. Moreover, the presence of a recombinant plasmid in a host cell has been associated with drastic variations in concentration of cellular enzymes involved in carbon, amino acid, nucleotide metabolism, translation and also with ribosome content decrease (De Gelder *et al.* 2007).

So, the relative importance of metabolic load due to recombinant protein production depends on the amount of protein produced, the plasmid copy number and its size, the host cell metabolic state and the growth medium composition (Bentley *et al.* 1990, Glick *et al.* 1995). As a result, plasmid-free cells grow faster than plasmid-bearing cells because they are not submitted to metabolic load anymore (Glick *et al.* 1995). The resulting growth rate difference intensifies segregational instability (Bentley *et al.* 1990, De Gelder *et al.* 2007). As a result, plasmid loss causes decrease in encoded protein expression (Glick *et al.* 1995). Therefore, in the absence of selection pressure, recombinant plasmids are more likely to be lost during culture. It has been demonstrated that plasmid-induced metabolic load is the cause not only of physiological and metabolic alteration in the host cell, but also of several stress responses (Silva *et al.* 2012).

Most microorganisms possess a complex biochemical response mechanism to face diverse environmental stress (Glick *et al.* 1995). The presence of a heterogeneous plasmid might induce stress

responses in host cells. Such mechanisms might lead to disrupted cell growth, plasmid expression and to lower plasmid DNA yields, which might favor plasmid instability. First, heat-shock is a stress response mechanism characterized by the expression of so-called heat-shock proteins. They are encoded on the σ^{32} operon on *Escherichia coli* and a lot of them are either chaperones ensuring proper protein folding or proteases degrading proteins. Second, stringent response is induced by amino acid starvation and limitation (Silva *et al.* 2012) or aminoacyl-tRNA pool depletion because of recombinant protein overexpression. In case of aminoacyl-tRNA limitation because of recombinant protein overexpression, the probability to insert incorrect amino acids instead of limiting amino acids increases. Consequently, translational errors increase during foreign protein overexpression because of codon bias (Glick *et al.* 1995). Stringent response might either inhibit energy consuming synthesis (*e.g.* proteins, rRNA, tRNA, plasmid DNA synthesis), or activate synthesis of proteases or other proteins to manage the stress situation (Silva *et al.* 2012). Third, the SOS response consists in a network of reactions insuring DNA repair in *Escherichia coli*. One of the reactions related to the SOS response is the nucleotide excision repair (*abbr.* NER) ensuring the detection and removal of unusual DNA structures (Silva *et al.* 2012).

2.1.2 Segregational plasmid stability

Plasmid segregational instability is the main cause of plasmid loss in a growing culture (Mathur *et al.* 2009).

2.1.2.1 Active plasmid partitioning of low copy number plasmids

Partitioning systems insure the efficiency of plasmid copy distribution to daughter cells throughout cell division (Schwartz *et al.* 2003). They also ensure that no foreign plasmid is transmitted to daughter cells and that only pre-existing copies are properly segregated. Two types of active partitioning systems are found among low copy plasmids: type I and type II. Active partitioning systems like the ones described below have not been observed within high copy plasmid (Million-Weaver *et al.* 2014). Type I and type II *par* systems are both based on three main components (**Figure 3**): a DNA-binding protein serving as adaptor (*i.e.* SopB for F plasmid and ParR for R1 plasmid), a motor protein (*e.g.* SopA-ATP for F plasmid, ParM-ATP for R1 plasmid) and a *cis*-acting centromeric sequence element (*e.g. sopC* for F plasmid, *parC* for R1 plasmid). First, the DNA-binding protein serves as adaptor protein and binds to the centromere. Then, adaptor protein binding to the centromere nucleates the motor polarization. The formation of a filament occurs and pulls plasmids apart (*par* type I) or push plasmids to opposite poles of the cell (*par* type II). To polymerize the motor protein energy derives from hydrolysis of nucleotide triphosphate. *Par* systems are autoregulated by their own DNA-binding protein (Million-Weaver *et al.* 2014).

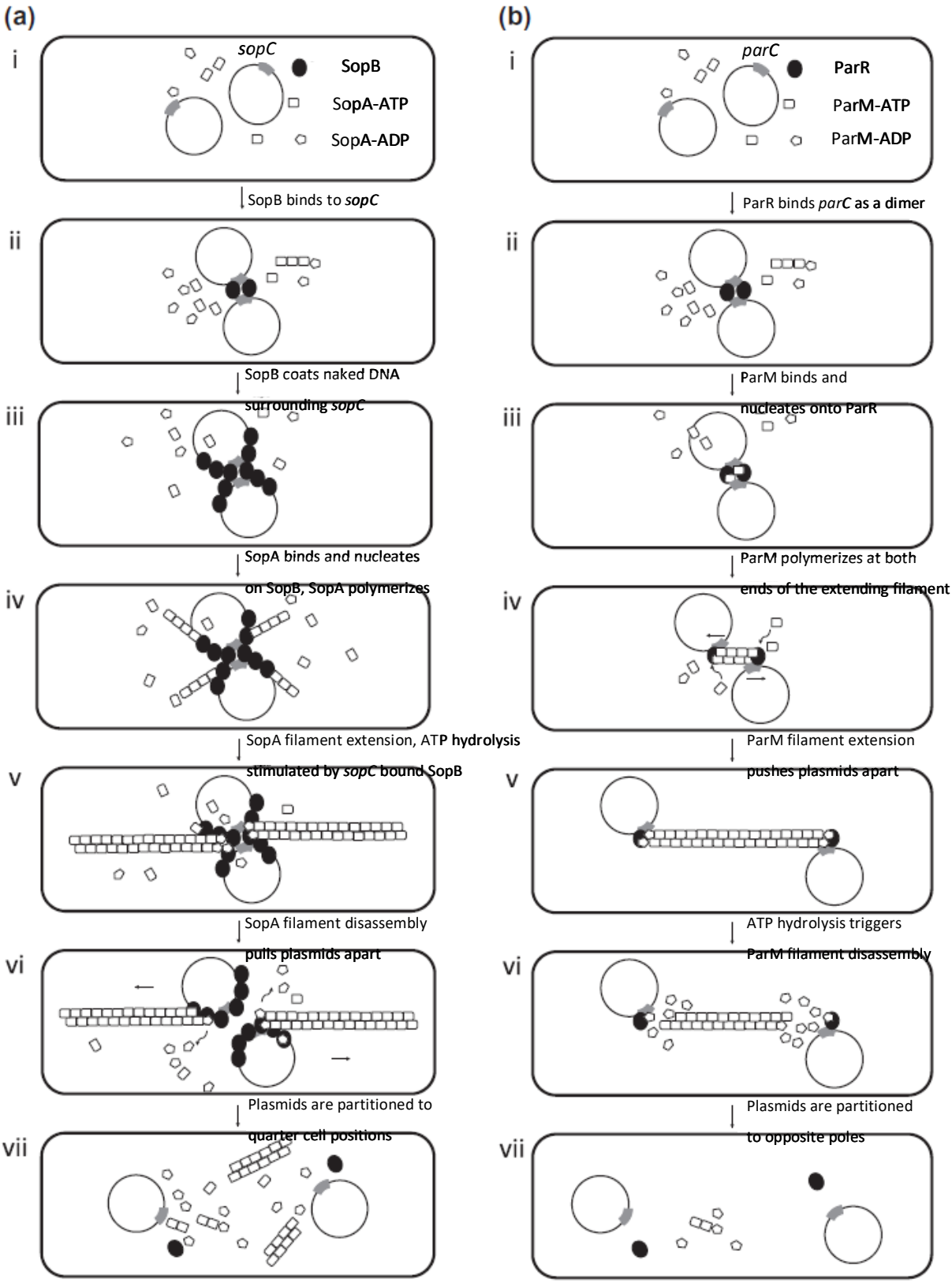

Figure 3 : Par-mediated plasmid segregation (a) type I *par* system like the *sopABC* locus from the conjugative plasmid F with *sopC*, the centromere; SopB, the adaptor protein and SopA, the motor protein (b) type II *par* system like *parRMC* locus from the *E.coli* multidrug resistance plasmid R1 with *parC*, the centromere; ParR, the adaptor protein; ParM, the motor protein (Million-Weaver *et al.* 2014)

2.1.2.2 Partitioning mechanisms for high copy plasmid segregation

Like explained above, no active partitioning system has been found among high copy plasmids yet. Plus, high copy plasmids segregational stability is negatively impacted by their higher metabolic burden (Mathur *et al.* 2009). Thus, plasmid-free cells stochastically arising from segregational instability will have a fitness advantage compared to plasmid-bearing cells and overwhelm them in whole cell population (Million-Weaver *et al.* 2014).

There are several hypotheses to explain plasmid segregation among high copy number plasmids.

- Random distribution hypothesis:

  During cell division, high copy number plasmids are partitioned among daughter cells by random plasmid diffusion and nucleoid exclusion. Therefore, daughter cells might not receive the same plasmid copies from the mother cell (Pogliano *et al.* 2002, Million-Weaver *et al.* 2014).

  Theoretically, because high copy number plasmids have a large plasmid copy number, they have low probability of plasmid-free cells to emerge and low plasmid loss frequency. However, several clues suggest that other phenomena might affect segregational stability of high copy number plasmids (Million-Weaver *et al.* 2014). In fact, there are proofs that not all plasmids diffuse freely through the membrane. For instance, ColE1 plasmids in *E. coli* have been shown to be excluded from the nucleoid region and are being localized at poles and mid-cell. In this case, the mid-cell region of the mother cell becomes a pole of one of the daughter cells (Pogliano *et al.* 2001).

  Plus, high copy number plasmids are more exposed to plasmid dimerization which is an increasing factor of plasmid instability. Based on these observations, the hypothesis of a normal distribution of the plasmid copy number is less than likely (Million-Weaver *et al.* 2014).

- Alternative hypothesis:

  Studies demonstrated that elements like clustering and plasmid loss dynamics as well as recombinant gene expression are not consistent with a randomly plasmid segregation, but rather with a regulated distribution mechanism like active partitioning. For high copy number plasmids, this mechanism might depend on chromosome-encoded proteins (Million-Weaver *et al.* 2014). But all of this is still at the hypothetical state and the existence of a regulating mechanism for high copy number plasmid still needs to be proven. But it is also possible that the host has a negative effect on the active partitioning system (De Gelder *et al.* 2007, Ponciano *et al.* 2007).

2.1.3 Structural plasmid stability

Structural plasmid instability is defined as the modification in the nucleotide sequence of the plasmid by any kind of mutations. In case of frame shift mutation, proteins with the wrong amino acid sequences might be synthesized (Friehs *et al.* 2004). Structural stability has a lower impact on plasmid stability than segregational stability and is commonly maintained at a low frequency (Silva *et al.* 2012).

There are various causes for structural instability like (Friehs *et al.* 2004, Silva *et al.* 2012):

- Plasmid size,
- PolyA sequences, inverted and direct repeats,
- Mutagenes or free oxygen radicals causing modifications in the nucleotide sequence,
- DNA polymerase mistakes or insufficient repair mechanism,
- Recombination events occurring between the plasmid and the chromosome,
- High expression of transposons and insertion sequences.

To increase structural plasmid stability, parameters that one can act on are growth conditions and the choice of the host strain (Friehs *et al.* 2004).

2.1.4 Mating

Conjugation (or mating) consists in the transfer of DNA by direct cell to cell contact by a conjugative plasmid (Harrison *et al.* 2012). It has been proven that plasmid re-uptake by segregants through conjugation with neighboring plasmid-bearing cells occurs and influences plasmid stability (De Gelder *et al.* 2007). Indeed, the insertion of a heterologous plasmid in a host cells through conjugation mechanisms might lead to metabolic load due to plasmid maintenance and the production of plasmid-encoded proteins, as detailed above (Harrison *et al.* 2012).

2.1.5 Importance of the plasmid-host interaction

The interaction between the bacterial host and the plasmid vector is of crucial importance, because it can influence the ability of the plasmid vector to colonize new hosts or simply to be maintained and transmitted. In fact, most plasmid vectors depend on the host replication machinery for their own expression. Plasmid stability of a particular plasmid vector can be highly variable within the same genus and even the same species. Patterns of plasmid loss can be different from one strain to another, suggesting that plasmid loss causes might be different (De Gelder *et al.* 2007).

All plasmids have a different host range. For instance, broad-host range plasmids can be replicated and transferred among phylogenetically distant organisms, whereas narrow-host range plasmids are only compatible with organisms from the same species. First, host range can be affected by replication and maintenance mechanisms. In a same host, the chromosome and the plasmid(s) share the replication

system of the host. So, plasmids with similar replication initiation systems are supposed to have similar host ranges. However, if two plasmids share comparable replication and / or partitioning systems, they have higher chances not to be stably propagated in host cells. This phenomenon is called plasmid incompatibility, and is a classical method for plasmid classification (Shintani *et al.* 2019).

The main cause of plasmid loss, for the same plasmid vector from one host to the other can be different (De Gelder *et al.* 2007, Ponciano *et al.* 2007). For instance, the plasmid pCAR1 encodes for degradation of carbazole to catechol. It has been shown that different growth rates were obtained with different hosts cells (*e.g*. *P. fluorescens* Pf0-1, *P. aeruginosa* PAO1, *P. putida* KT2440) with carbazole as the sole carbon source on minimal media. Plus, DNA re-arrangements (*i.e.* gene deletion) were found in the slower growing strains. Kinetic differences were due to cumulated catechol toxicity and to differences in catechol metabolism between host cells (Takahashi *et al.* 2009). Another example with the plasmid pB10 in 19 different hosts is given in De Gelder et *al.* (2007). It was shown that stability of pB10 was impacted by disrupted plasmid replication leading to lower plasmid copy numbers, higher segregation frequency causing less efficient active partitioning, important differential growth between plasmid bearing and free cells because of increased metabolic load and conjugative transfer allowing conjugative plasmid-reuptake by cells.

So, the main factors influencing plasmid persistence into a bacterial population are : segregational plasmid loss, conjugative plasmid transfer, plasmid cost (*i.e.* metabolic burden and differential growth rate between plasmid-free and plasmid-bearing cells) and selection pressure (De Gelder *et al.* 2007).

2.2 Segregational plasmid stability monitoring

2.2.1 Plate count

Two techniques of plate count based on antibiotic resistance of plasmid-bearing cells have been tested in the literature: parallel plate count (*i.e.* spread method) and serial plate count (*i.e.* replicate method) (**Table 3**). Parallel plate count consists in plating the same diluted sample on agar plates with and without antibiotics. Serial plate count generally consists in transferring colonies, either with sterile sticks or sterile velvets, from an agar plate without to one with antibiotics.

When the percentage of plasmid-bearing cell is important and majority, both methods tend to give comparable results. However, when the plasmid-free cell population increases, serial plate count tends to give higher results than parallel plate count (Weber *et al.* 1989). Indeed, as the serial plate count method presents a first step where cells are grown on non-selective medium before transferring to a selective one, only cultivable cells are selected. In the parallel plate count method, as the same sample

is plated on non-selective and selective medium, the lower results obtained might be due to the amount of non-cultivable cells taken into account in this method.

Over the years (**Table 3**), this methodology for segregational plasmid stability monitoring has been used as being an easy to set up and cheap technique. However, this is a rather time-consuming method and tedious, as results can only be obtained several hours after the sample was taken (12 to 48 h (Weber *et al.* 1989, Gruber *et al.* 2014) and in the case of serial plate count, 100 to 200 colonies (Weber *et al.* 1989, Sato *et al.* 2013, Sydow *et al.* 2017) have to be transferred to the selective medium.

Table 3: Examples of plate count for segregational plasmid stability monitoring

Antibiotic	Microorganism	Plasmid	Culture conditions	Results	Reference
Ampicillin resistance (100 $mg \cdot L^{-1}$): parallel and serial plate count	*E. coli* RR1 (K12 - derivative)	pBR322 (Amp^R)	In chemostat at 0.31 and 0.61 h^{-1} *Lysogeny Broth + 0.5 $g \cdot L^{-1}$ glucose*	100 % plasmid bearing cells for both methods until 60 h at 0.61 h^{-1} and 100 h at 0.31 h^{-1}. Decrease for both methods after that point. At 250 h for 0.31 h^{-1}, 15% for parallel method and 30 % for serial method. At 350 h for 0.61 h^{-1}, 10% for parallel method and 25 % for serial method.	(Weber *et al.* 1989)
Kanamycin resistance (50 $mg \cdot L^{-1}$): serial plate count	*C. necator* H16	pCUP2, pCUP3, pJRD215	In flasks with thrice 24 h subcultures *Basal (MBM) and N-limited (MBN) mineral medium*	Depending on plasmid construction and media: after 3 subcultures: 0 (MBN) or 20 (MBM) % for pCUP2, 100% for pCUP3, 30 (MN) or 85 (MBM) % pJRD215.	(Sato *et al.* 2013)
Kanamycin resistance (200 $mg \cdot L^{-1}$): serial plate count	*C. necator* H16	pKRSF1010, pKRP4 and pKSa backbone derivatives (Kan^R)	In flasks with four times 24 h subcultures *Tryptic Soy Broth*	For all plasmid constructions, over 95 % plasmid stability all along subcultures.	(Gruber *et al.* 2014)
Tetracyclin resistance (15 $mg \cdot L^{-1}$): serial plate count	*C. necator* H16 PHB-4	pKRTc_Plac_eGFP (Tc^R), pKRrha (Tc^R), pJeM1_Tc (Kan^R + Tc^R)	In flasks with four times 24 h subcultures *Lysogeny Broth and mineral medium (+/- tetracyclin)*	100 % stability for all plasmid constructions all along culture, except for pJeM1-Tc (5-20 %) without selection pressure (Tc^R).	(Sydow *et al.* 2017)

2.2.2 Reporter protein expression

The detection of plasmid-encoded recombinant proteins by flow cytometry has been more and more used to monitor plasmid stability within a pure culture. These methods depend on plasmid-encoded proteins, and consequently, might be affected by expression and maturation errors (Friehs *et al.* 2004). Several strategies exist; they could be separated into two categories that we could qualify as indirect and direct methods.

Indirect methods are based on the release of a fluorescent molecule by a substrate, after lysis by a plasmid-encoded enzyme. The so-obtained fluorescent molecule in single-cells can be detected by flow cytometry. This is the case in Miao et *al.* (1993) for instance (**Table 4**). In this work, the expression of a plasmid encoded-β-galactosidase in *E. coli* could be detected by flow cytometry (Miao *et al.* 1993). The expression of β-galactosidase was induced by the addition of isopropyl-β-D-thiogalactopyranoside (*abbr.* IPTG; 0.1 $g \cdot L^{-1}$). A substrate composed of, a *di*-β-galactopyranoside coupled to a lipophilic group with 12 carbons (C_{12}FDG) that can pass freely through cell membranes under normal conditions, was used. Once the lipophilic moiety is cleaved by β-galactosidase, FDG is retained within cells and the green fluorescent product made plasmid-bearing cells detectable by flow cytometry. So, it was possible to distinguish plasmid free (β-galactosidase negative, not fluorescent) from plasmid bearing-cells (β-galactosidase positive, fluorescent).

Direct methods are based on the detection of a plasmid-encoded fluorescent protein in single-cells (**Table 4**). Among these methods, two strategies can be found depending on the application: plasmid loss or plasmid stability determination.

First, plasmid loss determination has been described in Bahl et *al.* (2004). In this work, the expression of a chromosome encoded GFP was induced by the lac-promoter $p_{A1\text{-}04/03}$ in *E. coli* (Bahl *et al.* 2004). A functional *lacI* gene, encoding for a repressor protein, was integrated on the recombinant plasmid, thus preventing GFP expression initiation when plasmid is present in the cell. Inversely, GFP biosynthesis is induced after plasmid loss and plasmid-free cells were fluorescent. The accuracy of this method was confronted to traditional plate count measurements. In the work of Riber et *al.* (2016), they used the same approach to study plasmid loss in *E. coli* cultures exposed to the irgasan, an antimicrobial compound, which was delivered from interpenetrating polymer network (*abbr.* IPN) silicone hydrogels (Riber *et al.* 2016). These strategies allowed a quantitative measurement of plasmid loss in a cell population. The plasmid-free cell population corresponded to GFP expressing cells. Therefore, these methods allowed plasmid-free cell quantification at a very low detection limit.

Second, plasmid stability determination has been studied in Huguet et *al*. (2020). In this work, the mobilizable resistance island *Salmonella* genomic island 1 (*abbr.* SGI1) was inserted in the genome of an *E. coli* strain. The SGI1 requires an IncC plasmid to use its conjugation apparatus in order to be extracted from the chromosome and transferred to a new host. Nevertheless, SGI1 and IncC plasmid are incompatible, and IncC plasmid are lost in the presence of SGI1. So, in this work, the stability of SGI1 and pVCR94, a IncC plasmid, was studied by FACS, from fluorescent reporters (*i.e. mNeonGreen* for pVCR94^{GreenKn} and *mCherry* for SGI1^{RedKan}). Plasmid stability was also evaluated in Persad et *al.* (2017), through the expression of GFP by plasmid-bearing cells (Persad *et al.* 2017). In this work, quantification was achieved through plate count with fluorescence detection under UV illumination. The presence of the plasmid was verified on arbitrary chosen samples by agarose gel electrophoresis.

As for all biosensor-based approaches, bias has to be considered: (i) Half-life time of the molecules involved (*e.g.* GFP, LacI, mNeonGreen…) may lead to an underestimation of population heterogeneity; (ii) metabolic burden put on the host by the recombinant plasmid and / or the chromosomal insertion needs to be considered carefully in order to prevent phenotypic instability. Metabolic burden might be the cause of plasmid instability or methylation of recombinant gene on the host's chromosome (Heller *et al.* 1995). Biosensors are precious tools for *in vivo* and/or *in situ* monitoring. However, it is crucial to be aware of the drawbacks.

Table 4: Examples of plasmid stability monitoring techniques through plasmid-encoded reporters expression

Reporter	Microorganism	Plasmid	Culture conditions	Detection	Results	Reference
C_{12} Fluorescein *di* – β - galactopyranoside (C_{12}FDG) (2.5 – 5 µM)	*E. coli* BL21(DE3) and *E. coli* D1210	pBC26 (*lacZ* regulated by T_7 or P_{tac})	In flasks *Rich (LB) and mineral (M9) medium*	Flow cytometry	When hydrolyzed by β -galactosidase, C_{12}FDG generates a green fluorescent product. Optimal staining time at more than one hour. Comparison with plate count method, which greatly underestimated plasmid-bearing cells (< 10 % in all cases). The higher OD at which β -galactosidase production was induced, the higher the plasmid bearing cell fraction (90 % at 0.37 OD).	(Miao *et al.* 1993)
Repression of a chromosome-encoded *gfp* by plasmid encoded-*lacI*	*E. coli* MC4100 :: $p_{A1-04/03}$ – *gfpmut3*	pBBR322 :: $lacI^{q/}$ and pKJK5 :: $lacI^{q/}$ (Kan^R)	In flasks *Rich (LB) medium*	Flow cytometry	Plasmid-bearing cell fraction determined as the amount fluorescent cells on total cells. Optimal culture conditions (0.3 % plasmid loss) and plasmid curing by 5µg·mL^{-1} nalixidic acid addition (3 to 22 % plasmid loss) were tested. Comparison with plate count method, and 98% of flow cytometry counted cells were able to form colonies on plates.	(Bahl *et al.* 2004)
		pKJK5 :: $lacI^{q/}$ (Kan^R + Tet^R)	In flasks *Rich (LB) medium*	Flow cytometry	Cells exposed to the irgasan-impregnated IPNs for 24 h, presented 2.8 to 4.7 % plasmid loss, gradually increasing with increasing impregnation concentration. Repeated exposure to irgasan-impregnated IPNs drastically increased the plasmid loss of up to 83 %.	(Riber *et al.* 2016)
Expression of GFP by plasmid-bearing cells	*E. coli* O157:H7	pGFPuv	In flasks *Rich (LB) medium*	Plate count	Plasmid loss could be evaluated by comparing the concentrations of fluorescent and total cells on plates through time. The presence of the plasmid was verified in fluorescent cells by agarose gel electrophoresis.	(Persad *et al.* 2017)
Expression of mNeonGreen by plasmid bearing cells	E. coli K12 :: $SGI1^{RedKn}$	$pVCR94^{GreenK}$	In flasks *Rich (LB) medium*	FACS	Stability of SGI1 and the plasmid pVCR94, each expressing fluorescent reporters (*mNeonGreen* and *mCherry*), studied by FACS. Without selection pressure, cells were divided into three subpopulations, and after 54 generations: 15% $IncC^+$ (pVCR94) cells, 50% $SGI1^+$ (SGI1) and 35% empty cells. With selection pressure, 100% cells contained SGI1 and pVCR94.	(Huguet *et al.* 2020)

2.2.3 Plasmid copy number determination

Several methods for plasmid copy number (*abbr.* PCN) monitoring have been developed over the years, thanks to progresses in molecular biotechnology (**Table 5**). However, this method consists in a global determination of plasmid copy number on the whole cell population. PCNs can be determined by two different approaches: indirect and direct determination.

On one hand, indirect methods are based on the expression of a reporter gene (*e.g. lacZ* or *phoA* in *E. coli*) that are placed under the control of the same promoter as the gene of interest (Schendel *et al.* 1989).

On the other, direct methods are based on the quantification of both plasmid and chromosomal DNA, and on the calculation of the ratio between them (Silva *et al.* 2012). Such methods are mainly based on nucleic acid analysis and quantification, through measuring band density produced through a DNA hybridization method. Among those, agarose gel electrophoresis is the most frequently used method (Pushnova *et al.* 2000, Wu *et al.* 2010, Silva *et al.* 2012, Standley *et al.* 2019). This is a simple and low-cost technique. However, this method presents several drawbacks. Incomplete recovery and irreproducible extraction and precipitation might lead to biased PCN calculation. Plus, lysis and extraction procedures can make the entire process cumbersome. Finally, the use of hazardous products (*e.g.* ethidium bromide) presents safety issues (Pushnova *et al.* 2000).

Among direct methods, another approach based on real-time quantitative PCR (*abbr.* qPCR) has been developed to quantify PCN. This method is considered as a fast reliable quantification method for any gene of interest (Burgos *et al.* 2002). Quantification of PCN using qPCR can be achieved through two strategies: absolute and relative quantification. Both methods present the advantage to be fast (compared to DNA hybridization methods), cost-effective, safe and easy to perform. They might be applied to dynamic PCN monitoring (Lee *et al.* 2006).

- Absolute quantification allows determining the precise copy concentration of the plasmid-encoded gene by correlating the threshold cycle (*abbr.* C_T) value to a standard curve (Lee *et al.* 2006). This standard curve was constructed by amplifying standard dilutions of a calibration plasmid (*e.g.* pGEM-BD) containing a single copy of the gene of interest. So, C_T results are represented depending on the gene copy number. However, absolute quantification presents the disadvantage to not take into account the differences in amplification efficiencies between samples and standard curves (Skulj *et al.* 2008).

Table 5: Examples of plasmid copy number determination for segregational plasmid stability monitoring

Technique	Microorganism	Plasmid	Culture conditions	Principle	Reference
Alkaline phosphatase (*abbr.* AP) reporter	*E. coli* MZ9387 (Δ*phoA*)	pUC19 derivatives encoding for *phoA*	In flasks *Mineral medium*	A linear relation was found between AP's activity and PCN (expressed in mol plasmid DNA/dry cell weight) determined from dot-blot hybridization.	(Schendel *et al.* 1989)
DNA quantification by agarose gel electrophoresis	*E. coli*	pIL-2	In flasks (endpoint) *Rich medium*	Plasmid and genomic DNA isolation, purification and dilution prior to agarose gel electrophoresis, followed by ethidium bromide staining. Gel negative scans were used to quantify DNA. PCN was deduced from ratio and size of plasmid and genome DNA.	(Pushnova *et al.* 2000)
qPCR on purified DNA (absolute and relative quantification)	*E. coli* DH5α	pBR322	In flasks (endpoint) *Rich medium*	Quantification of plasmid β-lactamase gene (*bla*) and chromosomal D-1-deoxyxylulose 5-phosphate synthase gene (*dxs*). PCN is expressed as the copy ratio of *bla* / *dxs*. Comparable results with absolute (18.3-18.7) and relative (18.4-18.7) quantification method.	(Lee *et al.* 2006)
qPCR on whole cells (relative quantification)	*E. coli* BL21 (DE3)	pET3a-hG-CSF and pGEM-BD (calibrator for relative quantification)	In batch bioreactor (24 h) *Mineral medium*	Whole cells treated by heat (95°C, 20 min) allowed reaching lowest C_T. Different amplification efficiencies for both chromosome and plasmid amplicons were used. PCN is expressed as the copy ratio plasmid / chromosomal amplicons. PCN was shown to increase during fermentation until an optimum (100 without and 130 with ampicillin).	(Skulj *et al.* 2008)
qPCR on whole cells (combination of relative and absolute methods)	*E. coli* AF1000	pFM20 and pFM46 (used as their own calibrators)	In flasks (24h) *Mineral medium*	Whole cells lysed by heat (95°C, 10min). Same cell amount in each reaction. Standard curves for the quantification of plasmid-encoded *gfp* gene and chromosomal amplicon was prepared by spiking purified plasmid DNA with non-transformed cells. PCN was expressed based on the plasmid base pair number and the average molecular weight of a DNA base pair. During culture, an optimal PCN was reached by each plasmid (70 for pFM46 and 400 for pFM20)	(Carapuça *et al.* 2007)

- Relative quantification determines the amount of plasmid-encoded gene in a sample compared to a calibrator, which contains both plasmid-encoded and chromosomal-encoded genes with a constant ratio (*e.g.* pGEM-BD, 1:1) (Lee *et al.* 2006). The ratio of plasmid-encoded / chromosomal-encoded genes in a sample is normalized by the ratio of plasmid-encoded / chromosomal-encoded genes in the calibrator (Livak *et al.* 2001). So, PCN is expressed as a fold ratio of the normalized plasmid-encoded gene amount. Nevertheless, relative quantification ignores the differences in amplification efficiencies between plasmid and chromosomal encoded genes (Skulj *et al.* 2008).

The qPCR quantification methods for PCN developed in Lee et *al.* (2006) still requires DNA extraction. Thus, qPCR quantification has been developed on whole bacterial cells (Carapuça *et al.* 2007, Skulj *et al.* 2008, Anindyajati *et al.* 2016). In Skulj et *al.* (2008) lysis of whole cells was induced by heating (20 min at 90°C) followed by freezing at -20°C, instantly after sampling, prior to qPCR. This protocol was further used in Anindyajati et *al.* (2016) for the determination of the pCAD plasmid copy number in *E. coli*. The same procedure was applied by Carapuça et *al.* (2007), where they tested three different cell concentrations in order to determine if certain cell components released after cell lysis might inhibit amplification during PCR. However, no significant inhibition of amplification was detected.

2.3 Plasmid stabilization strategies

Plasmid stability can be defined as the probability that a plasmid will be inherited by daughter cells during cell division. It can be said that in the absence of any additional fitness cost, a plasmid stabilization strategy increases not only the frequency but also the number of plasmid-containing cells within a population (Cooper *et al.* 2000).

2.3.1 Recombinant plasmid genetic construction

2.3.1.1 Plasmid copy number

In order to decrease the metabolic load imposed to the host by recombinant plasmid expression, the use of a low-copy number plasmid instead of a high-copy number plasmid might be interesting. Indeed, a significant increase in plasmid copy number might lead to a decrease in the growth rate, but also to a decrease in the expression efficiency of recombinant genes (Carrier *et al.* 1998, Pushnova *et al.* 2000). For instance, Carrier et *al.* (1998) were able to increase plasmid encoded-β-galactosidase activity by increasing plasmid copy number (from 1 to 90). However, when the induction level of the promoter controlling β-galactosidase expression was increased, the increase in activity was lower (+ 6 – 16 %), than with lower expression levels (+ 20 %). Therefore, an optimal plasmid copy number must be determined in order to ensure optimal recombinant protein production. Indeed, a compromise must

be found between plasmid copy number enabling low metabolic load and significant recombinant expression level.

2.3.1.2 Promoter choice

The use of strong constitutive promoters is an important cause of metabolic load, so it could be positive to use inducible promoters instead. This approach can be interesting in the case of an uncoupled protein production (Glick *et al.* 1995). During growth phase, genes which are placed under the control of the inducible promoter are not expressed, resulting in a lower plasmid related metabolic burden and therefore a higher plasmid stability (Friehs *et al.* 2004). For instance, this was shown for the L-arabinose promoter controlling the human granulocyte colony stimulating factor (*abbr. h*G-CSF) in *E. coli* (Choi *et al.* 2000). Plasmid pGW2.0 stability was determined through plate count measurements based on plasmid-encoded ampicillin resistance. Under non-induced culture conditions, plasmid stability was maintained stably at 100 % during 170 generations in flasks cultures. However, under induced culture conditions in fed-batch culture, plasmid stability decreased regularly until reaching 0 %. This led to a decrease of *h*G-CSF production rates.

2.3.1.3 Plasmid size

It has been shown increasing plasmid size decrease segregational plasmid stability (Friehs *et al.* 2004). Smith et *al.* (1998), studied the impact of plasmid size on plasmid loss and growth rate of *E. coli* host cells (Smith *et al.* 2007). Three different plasmid sizes were studied 2.961, 3.661 and 11.961 kb, all derived from the pBluescript plasmid. They showed that the largest plasmid induced a longer lag phase during growth of host cells (in mineral medium: 12.6, 12.9 and 19.8 h, for increasing size). In addition, this same largest plasmid presented a higher plasmid loss during successive subcultures.

2.3.2 Mechanisms of plasmid stable maintenance

Different stabilizing mechanisms already exist in Nature and have been efficiently transposed to recombinant plasmids through stabilizing cassettes insertion. The main three known stabilizing mechanisms are:

- Plasmid addiction systems: Plasmid-free daughter cells are killed or their growth rate is reduced by plasmid addiction systems.
- Site-specific recombination systems: Plasmid multimers formed during replication and / or recombination can be resolved by a site-specific recombination system. So, every single monomer is independently transmitted to daughter cells. This system can also be referred as plasmid multimers resolution system.

- Active partitioning systems: Plasmid copies are efficiently vertically transmitted to every daughter cell (Zielenkiewicz *et al.* 2001).

2.3.2.1 Plasmid addiction systems

Antibiotic resistance

One of the simplest and most used techniques to select plasmid-bearing cells and enhance segregational plasmid stability is to apply antibiotic resistance selection pressure. In that end, an antibiotic is added to the culture medium. Resistance genes are located on the recombinant plasmid, so, only plasmid-bearing cells will develop an antibiotic resistance. Meanwhile, plasmid-free cells are killed or their growth is inhibited. However, this technique is not transposable at an industrial scale because of the expensive cost of antibiotics (Friehs *et al.* 2004) and the increasing amount of multidrug resistance bacteria (Buckner *et al.* 2018). For instance, the addition of 15 $mg \cdot L^{-1}$ tetracyclin improved plasmid stability of recombinant pJeM1_Tc plasmid in *C. necator* H16 PHB-4 from 20 % to 100 % in rich LB medium in flask cultures (Sydow *et al.* 2017).

In the particular case of ampicillin resistance, it should be verified that the recombinant plasmid does not bear the gene encoding for β-lactamase expression *(bla)*, because β-lactamase degrades ampicillin. This eventuality must be taken into account because for historical reasons, many plasmid encode for β-lactamase (Friehs *et al.* 2004). This issue was assessed in Kim et *al.* (1998), during the production of recombinant levansucrase controlled by a T7 promoter, encoded on the pELCHis24 plasmid (derived from the pET plasmid) (Kim *et al.* 1998). Even before the induction of levansucrase by IPTG addition, only 40 % of cells bore the plasmid in presence of ampicillin (100 $mg \cdot L^{-1}$). This proportion dropped to 13 %, 2 h after induction. As explained above, β-lactamase expression released in the medium led to the degradation of ampicillin, therefore decreasing selection pressure. To overcome this issue, methicillin, which is an inhibitor of β-lactamase, has been used. Methicillin belongs to the β-lactam antibiotic of the penicillin class. When methicillin (100 $mg \cdot L^{-1}$) was combined with ampicillin in recombinant ampicillin resistant cells cultures, it inhibited β-lactamase negative impact on plasmid stability. Indeed, after levansucrase induction, plasmid stability was maintained between 70 and 100 % for over 100 generations.

The main problem with antibiotic resistance is that the genes encoding for this characteristic are often expressed in a constitutive manner (*e.g.* except for the *tet*-operon encoding for tetracycline resistance) (De Gelder *et al.* 2007). Plus, the expression of the antibiotic resistance cassette itself represents a metabolic burden on the host and the segregational plasmid stability is also expression dependent.

Chromosomal mutation complementation

To be able to enhance segregational plasmid stability at an industrial scale, auxotrophy-based methods (or complementation of chromosomal mutations) have been developed. Strains are mutated in order to delete genes encoding for the biosynthesis of essential substances or proteins. A plasmid bearing the genes encoding for the production of this essential compound is designed. Cells are grown on a minimal (selective) medium lacking the essential compound for which the strain is auxotroph. So, plasmid-bearing cells will synthesize the essential compound and grow, whereas plasmid-free cells will not (Gupta *et al.* 2001, Friehs *et al.* 2004). However, plasmid-free cells might take advantage on the essential compound synthesized by plasmid-bearing cells, and so will be able to grow even without plasmid. So, this method presents a high error rate. But one way to overcome these issues is to create strains with defective transport system for the metabolite for which the strain is auxotroph. So, even if the metabolite is present in the media for any reason the plasmid-free cell will not be able to consume it (Gupta *et al.* 2001).

For instance, Fiedler et *al.* (2001) combined antibiotic resistance toward chloramphenicol and auxotrophy toward proline to ensure stable plasmid inheritance during the inducible production of partially humanized IN-1 antibody F_{ab} fragment (Fiedler *et al.* 2001). The gene encoding for proline production *proBA* was not present in the strain *E. coli* JMB83, and encoded on the pMF1 plasmid to ensure growth of only plasmid bearing cells. Plasmid stability was studied during culture in a 4 L-batch bioreactor for the production of the antibody, by plate count based on antibiotic resistance. Plasmid loss was equal to 10 % at induction and 15 % at antibody harvest when only 30 $mg \cdot L^{-1}$ chloramphenicol was added with a proline-producing strain *(E. coli* W3110). However, plasmid loss was equal to 0 % all along culture when 30 $mg \cdot L^{-1}$ chloramphenicol was added to the culture with the proline-auxotroph strain (*E. coli* JMB83).

Another example can be given for *C. necator* for the production of cyanophycin by a KDPG-aldolase-auxotrophic strain during growth on gluconate (Voss *et al.* 2006). The plasmid pBBR1MCS-2:*cphA/eda* encoding for cyanophycin production and KDPG-aldolase complementation was inserted in the strain *C. necator* H16-PHB-4-Δ*eda.* Plasmid stability was evaluated in 30 L and 500 L-batch bioreactors by plate count based on kanamycin resistance (50 $mg \cdot L^{-1}$). Plasmid stability was maintained all along culture and maximum only 7 % of cells had lost their plasmid. There was a 90 % increase in plasmid stability compared to cultures where selective pressure was only based on antibiotic resistance.

Finally, the small essential gene *infA* encoding for the translation initiation factor 1 (IF1) has been inserted in the plasmid pRK04 (Hägg *et al.* 2004). Host strain *E. coli* MG1655 was deleted toward *infA*. Plasmid stability was determined through plate count based on ampicillin resistance of plasmid bearing

cells during successive subcultures flasks. Plasmid stability was maintained at 100 % during 100 h with the *infA* deleted strain, whereas it decreased continuously until reaching 17 % at 120 h with the *E. coli* wild type strain.

Post-Segregational Killing system

Some natural plasmids have developed a particular segregational plasmid stability mechanism called Post-Segregational Killing (*abbr.* PSK) system. The aim is to kill plasmid free cells through intracellular mechanisms (Friehs *et al.* 2004) (**Table 6**).

Table 6: Post-segregational killing systems (Thisted *et al.* 1994, Friehs *et al.* 2004)

Plasmid	Killer gene	Toxin	Antitoxin
R1	*Hok*	Hok	Sok-antisense RNA
	parD (pem)	PemK	Protein PemI
F	*srnB'*	SrnB'	SrnC-antisense RNA
R583	*pndA*	PndA	PndB-antisense RNA
RP4	*parDE*	ParE	Protein ParD
pUM505	*pumAB*	PumA	Protein PumB

The main interest of integrating PSK systems on recombinant plasmid is to ensure their stable vertical inheritance to daughter cells (Cooper *et al.* 2000). This system is based on the production of a toxin and an antitoxin by plasmid-bearing cells. So, segregational plasmid stability is maintained by killing plasmid-free cells (Thisted *et al.* 1994). Two different mechanisms have been observed. Either the antitoxin (or antidote) is a protein, or it is an antisense RNA (Friehs *et al.* 2004). The toxin molecule has a long-life expectancy once produced. However, the antitoxin molecule has short-life expectancy once produced, which means that only plasmid-bearing cells will survive. Thus, plasmid-bearing cells have to produce the antitoxin continuously (Cooper *et al.* 2000).

More precisely, post-segregational killing systems encode highly stable mRNAs that can be translated into toxins or toxic proteins (Hok, SrnB' and PndA) able to kill the cell. The expression of these toxins is regulated by very unstable antisense RNAs (Sok-RNA, SrnC-RNA, and PndB-RNA) with very short half-lives. These antisense RNAs are complementary to reading frames (*mok*, *srnB* and *pndC*) overlapping the corresponding killer mRNAs (*hok*, *srnB'* and *pndA*). This kind of RNA-RNA binding is thermodynamically very stable and target RNA is irreversibly inactivated (Thisted *et al.* 1994, Friehs *et al.* 2004).

The *hok/sok* PSK mechanism is based on an antisense RNA (**Figure 4**). Promoters of toxin and antitoxin genes are both constitutive. But, *hok* constitutive promoter is weak whereas *sok* constitutive promoter is strong (Friehs *et al.* 2004). Translation of killer genes (*hok*, *srnB'* and *pndA*) is linked to translation of the overlapping reading frame (*mok*, *srnB* and *pndC*). So, when antisense RNAs hybridize with the open

reading frames they prevent the translation of both killer genes and their overlapping reading frames by avoiding ribosome fixation (Thisted *et al.* 1994).

The *parDE* PSK mechanism is based on a protein antitoxin expression (Thisted *et al.* 1994, Johnson *et al.* 1996, Friehs *et al.* 2004). It encodes for both a toxin ParE and an antitoxin ParD. The cellular target of the basic protein ParE has not yet been identified (Jensen *et al.* 1995, Oberer *et al.* 1999). In the meantime, the antitoxin ParD is an unstable acidic protein degraded by a protease that has not yet been identified (Oberer *et al.* 1999). It seems likely that ParD protects plasmid-bearing cells from the toxic effects of ParE. In order to do so, ParD needs to be constantly produced (Johnson *et al.* 1996). ParD and ParE form a tight complex, thus inactivating ParE toxic effects (Oberer *et al.* 1999).

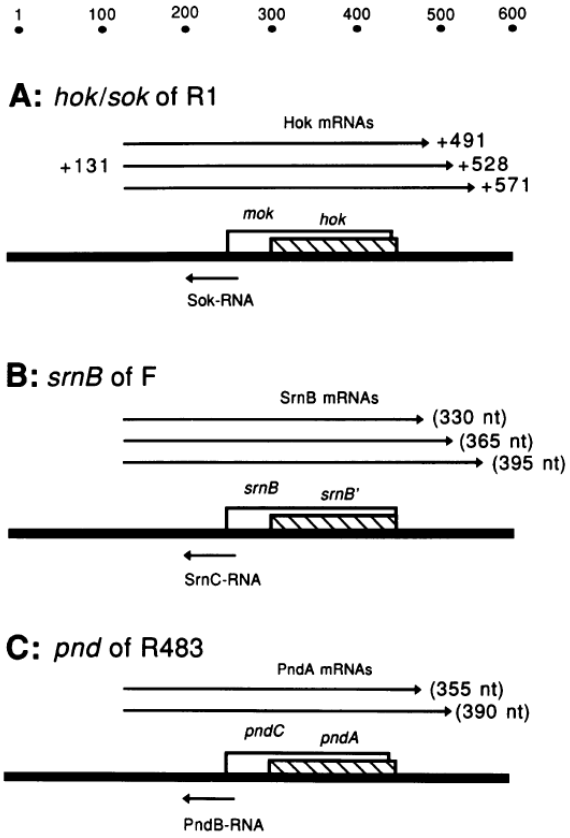

Figure 4 : Genetic organization of the post-segregational killing systems *hok/sok* from R1, *srnB* from F and *pnd* from R485. The encoded RNA related to the PSK system are designated by arrows. The toxin genes are represented by hatched boxes and the reading frames are represented by open boxes (Thisted *et al.* 1994)

Post-segregational killing systems are based on the differential decay rate between antisense RNAs and killer genes encoding mRNAs. As above-mentioned, antisense RNAs has a higher decay rate than killer genes encoding mRNAs (Thisted *et al.* 1994). During cell division if the plasmid is transmitted only to one of the two daughter cells, the plasmid-bearing cell will express the unstable antitoxin to block

toxin actions and remain viable whereas the plasmid-free cell is vulnerable to the stable toxin because the unstable antitoxin is degraded (Cooper *et al.* 2000, Friehs *et al.* 2004).

Plasmid stability of cell bearing the *parDE* PSK system has been tested in successive subcultures and measured by plate count (Cooper *et al.* 2000). The plasmid pTP100, encoding for *parDE* was inserted in *E. coli* RR1 cells. Higher plasmid stability was measured with PSK expressing strains (< 90 %) compared to PSK free cells (decrease until 20 % at 200 generations).

A similar protocol was used on *E. coli* pJM101 bearing a pJET1.2/blunt backbone-plasmid encoding for the *pumAB* PSK system from *Pseudomonas aeruginosa* (Hernández-Ramírez *et al.* 2017). Plasmid stability was determined by plate count based on ampicillin resistance. During six daily subcultures, plasmid-bearing cells encoding for *pumAB* were maintained in the culture around the same proportion, whereas plasmid-bearing cells without *pumAB* where regularly lost between subcultures until there was none left.

Successive subcultures were also used to study the plasmid stabilization efficiency of the *hok/sok* PSK system in the works of Wu et *al.* (1994), with the strain *E. coli* BK6 to study bearing the pMJKR15750 plasmid (Wu *et al.* 1994). Plasmid stability was determined by plate count. With the *hok/sok* PSK system, plasmid stability (100 %) was ensured for over 300 h, whereas without PSK system the plasmid started being lost at 19 h and was completely eliminated at 100 h.

Finally, Pecota and coworkers (1997) even combined PSK systems among them in *E. coli* BK6 to enhance plasmid stability of a pMJR1750-backbone plasmid: *hok/sok*, *parDE* and *pnd* (Pecota *et al.* 1997). The following combinations were made: *hok/sok* + *parDE* and *hok/sok* + *pnd*. Plasmid stability was evaluated by plate count during flask cultivations. Plasmid loss experiments were achieved by serial subcultures of 12 h. Without PSK systems, stability reached 90 % after less than 5 h of culture. To reach 90 % of plasmid stability, the most stable combinations were: 50 h for *hok/sok* + *parDE*, 37 h for *hok/sok* alone, 27 h for *hok/sok* + *pnd* and 18 h for *parDE* alone.

2.3.2.2 Multimer resolution systems

Plasmid multimerization leads to segregational instability. Some natural plasmids carry genes, whose expression leads to monomerization of plasmid multimers. A plasmid dimer is actually a catenate of two monomers (Friehs *et al.* 2004).

Multimer resolution systems (*abbr.* MRS) are based on a site-specific recombinase, also called resolvase, and a *res* sequence. Both of them are located on the plasmid. A recombinase resolves plasmid multimers by specific recombination between repeated *res* sequences. Either MRS are entirely

encoded on the plasmid, or the plasmid *res* site is combined with a host encoded recombinase (Zielenkiewicz *et al.* 2001).

For example, the broad-host range plasmid RK2, identical to plasmid RP4, encodes for *parCBA*, a multimer resolution system, which encodes for a resolvase ParA, a calcium-dependent nuclease ParB and a protein ParC whose function has not been determined yet. So, the *parCBA* operon encodes for a plasmid multimer resolution system which has been proven to enhance plasmid stability in several Gram-negative bacteria (*e.g. Escherichia coli*, *Pseudomonas aeruginosa, Cupriavidus necator*) (Easter *et al.* 1998, Friehs *et al.* 2004, Gruber *et al.* 2014). ParA and *res* site specific recombination system is the key of *parCBA* stabilizing activity. Even if ParB and ParC roles have not been precisely determined yet they might enhance ParA and *res* site-specific recombination system to monomerize multimers (Easter *et al.* 1998). In Easter et *al.* (1998), the impact of the multimer resolution system *parCBA* was studied in *E. coli* and *P. aeruginosa*, with the plasmid pCE61-2.3. Plasmid stability was determined by plate count depending on antibiotic resistance. With *P. aeruginosa*, plasmid stability depended on the strain used. With the strain *P. aeruginosa* PAO1161Rif^r, plasmid stability was better with *parCBA* (75 % at 50 cell generations) than without it (25 % at 50 cell generations). For *P. aeruginosa* PAC452Rif^r, plasmid stability decreased only until 80 % with *parCBA* after 100 cell generations, whereas it reached 30 % without it. For *E. coli* RR1 and MC1061K, plasmid stability was maintained close to 100 % when *parCBA* was encoded on the plasmid.

Another example can be given with the multimer resolution system from transposon Tn*1000* (*res* site and *tnpR* gene encoding for a resolvase) (Bellani *et al.* 1997). It was encoded in the pBR322 plasmid and inserted in the strains *E. coli* GT123 and HB101. Plasmid stability was determined in flask cultures by plate count based on antibiotic resistance. After 48 h, plasmid stability was equal to 100 % for the MRS-encoding strains, whereas it decreased to 64 % for *E. coli* GT123 and 1 % for *E. coli* HB101.

2.3.2.3 Active partitioning system

Proper plasmid segregation during vertical inheritance to daughter cells can be achieved by expression of *par*-regions (Friehs *et al.* 2004). This system is defined as “active” because it is energy consuming for the host cell (Zielenkiewicz *et al.* 2001).

The partition mechanism is achieved by two proteins often referred to as protein A and B (**Figure 5**). The genetic organizations of *par*-regions from different active partitioning systems are very similar; a *cis*-acting centromere-like DNA sequence is adjacent to two *trans*-acting proteins (*i.e.* protein A and B). The ParB protein binds to the centromere-like region. It is supposed that ParA role is to produce energy for the process (Zielenkiewicz *et al.* 2001, Friehs *et al.* 2004).

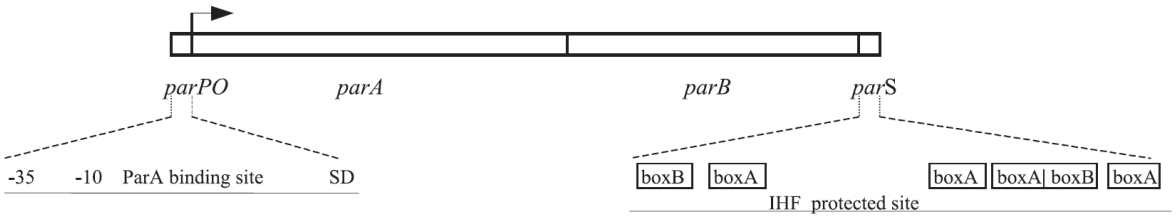

Figure 5: Schematic representation of P1 plasmid *par* operon organization (Zielenkiewicz *et al.* 2001)

The example of the active partitioning system of the plasmid P1 in *Escherichia coli* is given (**Table 7**). P1 partition system is composed of three main elements: the ATPase ParA, the centromere binding dimeric protein ParB and the centromere-like DNA sequence *parS*. The *E. coli* integration host factor (*abbr.* IHF) protein highly stimulates ParB binding to *parS*. Indeed, *parS* contains a IHF binding site which is framed by specific sequences named *boxA* and *boxB* which are recognized by ParB. Together, ParB and IHF form a high affinity nucleoprotein complex. So, ParB dimers are recruited which polymerize away from *parS*. ParA is an ATPase binding to the *par* operator protein, thus repressing *parA* and *parB* expression. This is important because an excess of ParB might destabilize the plasmid (Zielenkiewicz *et al.* 2001, Friehs *et al.* 2004).

Table 7: Different active partitioning systems (Friehs *et al.* 2004)

Plasmid/Phage	Par-region	Gene product/function
R1	*parA*	ParM : ATPase
		ParR : binding protein
		parC : binding region
P1	*par*	ParA : ATPase
		ParB : binding protein
		parS : binding region
P7	*par*	ParA : ATPase
		ParB : binding protein
		parS : binding region
F-factor	*sop*	SopA : ATPase
		SopB : binding protein
		opC : binding region

The operon *parMRC* of the R1 plasmid can also be integrated in recombinant plasmid as explained above in this. The mechanism involved is comparable to one from P1. ParM protein is an ATPase interacting with ParR protein which binds to the centromere-like region *parC* (Friehs *et al.* 2004).

Even if there are functional similarities between chromosomal and plasmid segregational systems, both of these mechanisms have to be distinguished (Zielenkiewicz *et al.* 2001). The main disadvantage of integrating active partitioning systems in recombinant plasmids is that it significantly increases

plasmid size. In this way, it might enhance plasmid structural and segregational instability (Friehs *et al.* 2004).

A concrete example of the application of this stabilization strategy was given in Sato et *al.* (2013) for *C. necator* H16. The partition locus (*parABS28*) of the megaplasmid pMOL28 and the origin of replication (oriV28) of *C. metallidurans* CH34 was inserted in a pCR-Blunt 2-TOPO plasmid backbone (pUC3) in order to enhance plasmid maintenance during poly(3-hydroxybutyrate-co-3-hydroxyhexanoate) recombinant production. Plasmid stability was determined by plate count based on kanamycin resistance during successive subcultures in flasks. In all media tested (rich and mineral medium), plasmid stability was maintained at 100 % for *parABS28*-encoding strains, whereas plasmid stability dropped to 0 % without it after four subcultures.

A synthesis of all plasmid stabilization strategies described in this subpart is given in **Table 8**.

Table 8: Examples of plasmid stabilization strategies

Plasmid addiction systems			Segregation optimization systems	
Antibiotic resistance	**Auxotrophy**	**PSK**	**Multimer resolution**	**Active partitioning**
Kanamycin (40 mg·L^{-1}) *C. necator* H16 100 % plasmid stability (Gruber *et al.* 2014)	**Proline (Δ*proBA*)** *E. coli* JM83 100 % plasmid stability (Fiedler *et al.* 2001)	***parDE*** *E. coli* RR1 90-100 % plasmid stability (Cooper *et al.* 2000)	***parCBA*** *E. coli* and *P.aeruginosa* enhanced plasmid stability *(Easter et al. 1998)*	***parABS28*** *C. necator H16* 100% plasmid stability *(Sato et al. 2013)*
Tetracyclin (15 mg·L^{-1}) *C. necator* H16-PHB-4 100% plasmid stability (Sydow *et al.* 2017)	**IF1 (Δ*infA*)** *E. coli MG1655* 100 % plasmid stability (Hägg *et al.* 2004)	***pumAB*** *E. coli* pJM101 100% plasmid stability (Hernández-Ramírez *et al.* 2017)	**Tn*1000*** *E. coli* GT123 and HB101 100% plasmid stability *(Bellani et al. 1997)*	
Ampicillin + Methicillin (100 mg·L^{-1} each) *E. coli BL21* 70-100% plasmid stability (Kim *et al.* 1998)	**KDPG-aldolase (Δ*eda*)** *C. necator H16*-PHB-4--Δ*eda* 93-100 % plasmid stability (Voss *et al.* 2006)	***hok/sok*** *E. coli* BK6 100% plasmid stability (Wu *et al.* 1994)		
		hok/sok, parDE, pnd *E. coli* BK6 90% plasmid stability (50h *hok/sok* + *parDE*, 37h *hok/sok*, 27h *hok/sok* + *pnd,* 18h *parDE)* (Pecota *et al.* 1997)		

3 Study model: isopropanol production by *Cupriavidus necator*

Cupriavidus necator H16 is a chemolithoautrophic Gram-negative bacterium that belongs to the beta-subclass of *Proteobacteria*. *C. necator* natural habitat is soil and water. This strain can grow either heterotrophically or autotrophically. One of *C. necator* particularities is its ability to synthesize and store large amount of poly(3-HydroxyButyricAcid) (PHB) (Pohlmann *et al.* 2006).

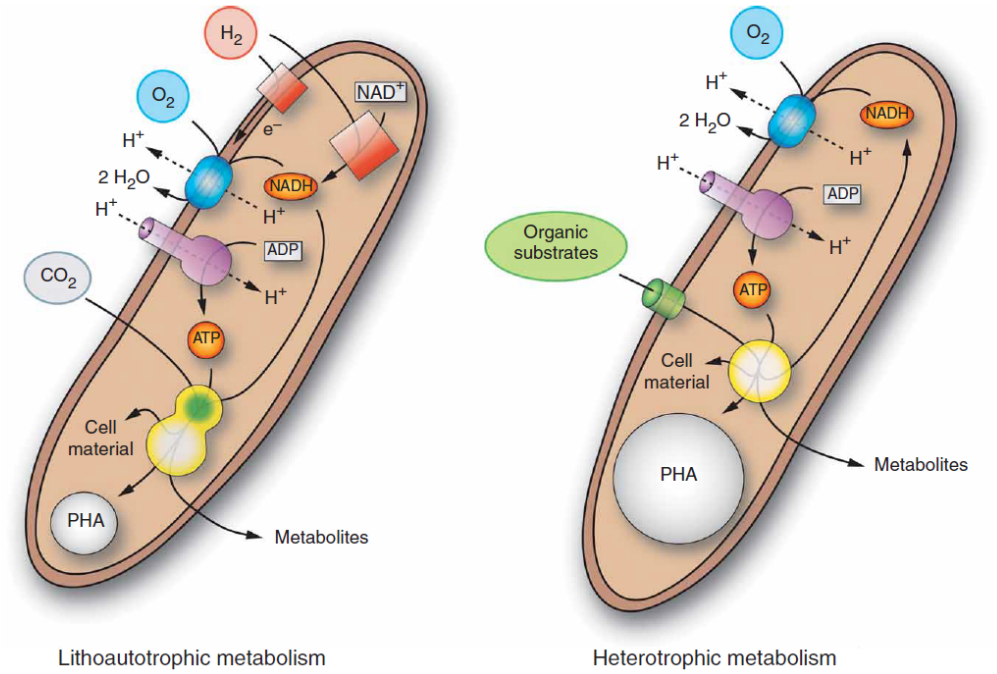

Figure 6 : Main aspects of lithoautotrophic and heterotrophic metabolism of *Cupriavidus necator* H16. Legend: Yellow circles: central metabolism; Yellow/green circle: Calvin-Benson-Bassham cycle; Red squares: energy-conserving hydrogenases; Gray circle: polyhydroxyalkanoate (PHA) storage granules (Pohlmann *et al.* 2006)

The taxonomy of *Cupriavidus necator* has evolved over the years. Its classification in chronological order are: *Alcaligenes eutrophus* (Vandamme *et al.* 2004), *Ralstonia eutropha* (Vandamme *et al.* 2004, Gruber *et al.* 2015), *Wautersia eutropha* (Vandamme *et al.* 2004) and *Cupriavidus necator*. Nowadays, *Cupriavidus necator* is a model organism for the study of CO_2 fixation, hydrogen oxidation and denitrification (Pohlmann *et al.* 2006, Gruber *et al.* 2015).

3.1 Genome description

Cupriavidus necator carries three circular replicons, composed of two chromosomes and a megaplasmid (Pohlmann *et al.* 2006, Gruber *et al.* 2015). The total size of the genome is 7, 416, 678 pb with 4, 052, 032 pb for the first chromosome, 2, 912, 490 pb for the second chromosome and 452, 156 pb for the megaplasmid (Pohlmann *et al.* 2006).

3.1.1 The two chromosomes

The chromosomes 1 and 2 present nearly the same G+C contents, respectively 66.4 % and 66.7 %. Chromosome 1 encodes the main functions of DNA replication, transcription and translation (*e.g.* ribosomal proteins). Chromosome 2 encodes genes dedicated to the central steps of 2-keto-3-deoxy-6-phosphogluconate (*abbr.* KDPG) sugar and sugar acid catabolism pathway, to decomposition of aromatic compounds and to utilization of nitrogen sources (Pohlmann *et al.* 2006).

3.1.2 The megaplasmid

In several *Cupriavidus necator* strains, functions leading to H_2 oxidation are encoded on large plasmids. In *C. necator* H16 strain, this large self-transmissible plasmid is designated as megaplasmid pHG1. This megaplasmid is composed of 429 potential genes representing a coding density of 79.7 %, with a G+C content of 62.3 %, slightly lower than the total genome G+C content (64.8 %). Most of them contribute to the lithoautotrophic metabolism of *C. necator*, including 41 genes encoding for the biosynthesis of four hydrogenases. A large cluster on pHG1 also encodes genes for denitrification pathways (Schwartz *et al.* 2003). The *cbb* operon encoding for the genes of the Calvin-Benson-Bassham cycle (*abbr*. CBB) is also present on pHG1 (Schwartz *et al.* 2003). The megaplasmid encodes the ability to produce polyhydroxybutyrate (*abbr.* PHB) and to perform denitrification (Gruber *et al.* 2015).

Replication and maintenance mechanisms

Megaplasmid pHG1 is equipped with genes for replication and stable vertical inheritance like any other natural plasmid. The plasmid maintenance systems encoded on pHG1 are: replication initiation, plasmid partitioning, multimer resolution, post-segregational killing and restriction/modification (Schwartz *et al.* 2003).

The restriction/modification cluster encodes RepA plasmid initiator protein. Rep A triggers replication by unwinding a stretch at DNA origin, alone or in collaboration with DnaA replication initiator. The plasmid partitioning protein RepB is encoded downstream *repA* gene on the opposite strand. Two open reading frames (*abbr.* ORF) named *parA* and *parB1* are adjacent to *rep* genes. Theses ORFs encode partitioning proteins (ParA and ParB) (Schwartz *et al.* 2003).

pHG1 also encodes multimer resolution systems, like for example an integrase / recombinase protein, that participates to plasmid stability by resolving multimers due to homologous recombination (Schwartz *et al.* 2003).

A putative type II restriction / modification system is located near the replication/maintenance region. These plasmid restriction / modification systems are useful to the cell to block foreign DNA, and also

participate to stable vertical plasmid inheritance by post-segregational killing (*abbr.* PSK) mechanisms (Schwartz *et al.* 2003).

Conjugation mechanism and pilus biosynthesis

The self-transmissible megaplasmid pHG1 bears a large region of 27 kb containing genes implicated in its conjugative transfer and to pilus biosynthesis. It has been shown that two kinds of pili are produced by *C. necator*: related type IV pili and RP4-type sex pili. Pilus main structural components encoded by the megaplasmid are pilins (*pilS1* and *pilS2* genes) (Schwartz *et al.* 2003).

3.2 Metabolism description

3.2.1 Heterotrophic metabolism

C*. necator* is able to use many different organic carbon sources, like intermediates of the tricarboxylic acid cycle, sugar acids (*e.g*. gluconic acid), certain fatty acids, amino acids, as well as some alcohols and polyols (Pohlmann *et al.* 2006). No evidence of the activity of key enzymes of glycolysis and pentose phosphate pathway, phosphofructokinase and 6-phosphogluconate dehydrogenase respectively, has been found in *C. necator* H16 (Pohlmann *et al.* 2006).

Wild type strains of *C. necator* (H16) are not able to consume glucose, mannose and ribose (Wilde 1962). However, the strain *C. necator* DSM 545 (spontaneous mutation) is able to consume glucose. Cells seems to be able to oxidize intracellular glucose but do not seem to possess a transport system (Raberg *et al.* 2011).

The only carbohydrates *C. necator* is able to metabolize are fructose, *N*-acetylglucosamin and glucose in certain strains. Fructose is imported by an ABC transporter and then metabolized through the Entner-Doudoroff (KDPG) pathway (Pohlmann *et al.* 2006, Gruber *et al.* 2015). *N*-acetylglucosamin is possibly imported by a phosphotransferase-type transport system (Pohlmann *et al.* 2006).

C. necator has the ability to use formate as a source of organo-autotrophic growth as at least four formate deshydrogenases are encoded in its genome (Schwartz *et al.* 2003, Grunwald *et al.* 2015).

3.2.2 Autotrophic metabolism

Carbon dioxide fixation in *C. necator* H16 is achieved through Calvin-Benson-Bassham (CBB) cycle (Pohlmann *et al.* 2006). Rubisco (Ribulose-1,5-bisphosphate carboxylase oxygenase) is the enzyme catalyzing CO_2 assimilation. The major enzymes of the pathway are encoded by the *cbb* operon, which is present in duplicate within the entire genome; one copy on the megaplasmid pHG1 (cbb_p) and the other on the chromosome 2 (cbb_c). The chromosome 2 bears the gene *cbbR* encoding a transcriptional activator, which is a LysR-type regulator (Schwartz *et al.* 2003). A defective copy of this regulatory gene

is present on the megaplasmid pHG1. So, the chromosomal-borne copy of *cbbR* controls the coordinated expression of both of the *cbb* operons (Pohlmann *et al.* 2006). The CbbR transcriptional regulator is activated when intracellular concentrations of phosphoenolpyruvate become low (Shimizu *et al.* 2013).

pHG1 bears the *cbb* operon encoding a red-type form I RubisCo and other enzymes of the CBB cycle: pentose-5-phosphate 3-epimerase (*cbbEp*), fructose-1,6-bisphosphatase/sedoheptulose-1,7-bisphosphatase (*cbbFp*), phosphoribulo-kinase (*cbbPp*), transketolase (*cbbTp*), 2-phosphoglycolate phosphatase(*cbbZp*), glyceraldehyde-3-phosphate dehydrogenase (*cbbGp*) and fructose-1,6-bisphosphate/sedoheptulose-1,7-bisphosphate aldolase (*cbbAp*) (Schwartz *et al.* 2003).

Carbonic anhydrases catalyze the interconversion between carbon dioxide and bicarbonate. These enzymes are implicated in CO_2 transport, carbonates transport and intracellular pH control. In *Cupriavidus necator*, four genes encoding for different carbonic anhydrases have been identified: *can, can2, caa and cag* (Gai *et al.* 2014).

3.2.3 Central carbon metabolism

The only C_3-carboxylating enzyme detected in *Cupriavidus necator* is the phosphoenolpyruvate (*abbr*. PEP) carboxykinase, also abbreviated PCK (**Figure 7**). *C. necator* also possesses a phosphoenolpyruvate carboxylase. As shown on the pathways of the central metabolism of *Cupriavidus necator* above, PCK requires GDP and inosine diphosphate for its activity. The activity of other CO_2-fixing enzymes (*i.e.* pyruvate carboxylase, phosphoenolpyruvate carboxylase) has not been detected in *C. necator* disregarding whether the growth is performed under heterotrophic or autotrophic conditions (Schobert *et al.* 1984). Two enzymes are able to mediate reactions between C_4 and C_3 intermediates: the malic enzyme MaeB and the phosphoenolpyruvate carboxykinase PCK. Expression of enzymes of the C_3 and C_4 metabolism in *Cupriavidus necator* is apparently constitutive (Schobert *et al.* 1984).

To use *Cupriavidus necator* as a bioplatform for metabolic engineering, it is important to understand the anaplerotic reactions mediating between the Entner-Doudoroff pathway and the tricarboxylic acid cycle (TCA cycle) as well as the reactions between the TCA and the gluconeogenesis (Bruland *et al.* 2010).

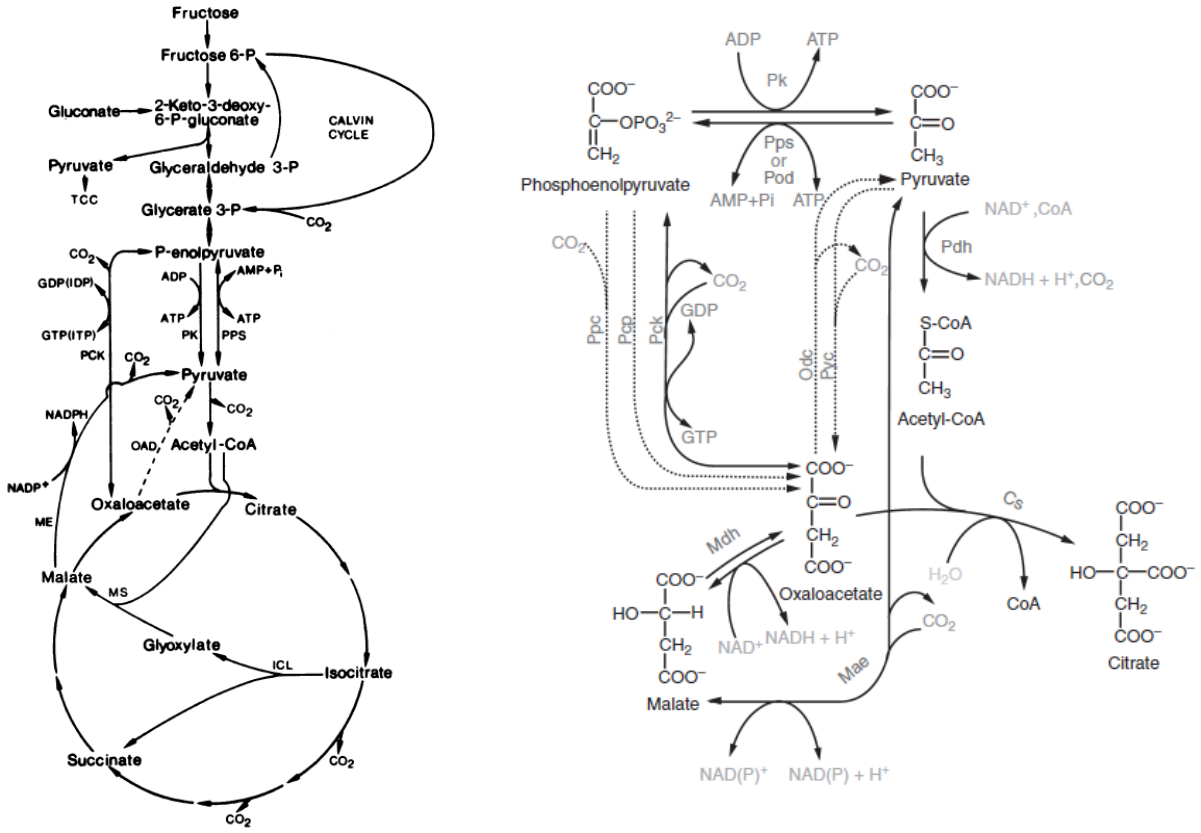

Figure 7 : (Left) Pathways of the central carbon metabolism of *Cupriavidus necator*. Extra attention is given to the enzymes involved in the interconversion of C_3 and C_4 intermediates and in the glyoxylate cycle (Schobert *et al.* 1984); (Right) Proposed pathways mediating between C_3 and C_4 intermediates of central metabolism in *Cupriavidus necator* (Bruland *et al.* 2010)

Abbreviations: Cs: citrate synthase; PCK: PEP carboxykinase; Ppc: phosphoenolpyruvate carboxylase; PK: pyruvate kinase; Pc: phosphoenolpyruvate carboxtransphosphorylase; PP: PEP synthetase; Pps: phosphoenolpyruvate synthase; Pod: pyruvate orthophosphate dikinase; Pdh: pyruvate dehydrogenase; Pyc: pyruvate carboxylase; ME or MAE: malic enzyme; Mdh: malate dehydrogenase; OAD or ODC: oxaloacetate decarboxylase; ICL: isocitrate lyase; MS: malate synthase; TCC: tricarboxylic acid cycle

3.2.4 Lithotrophic metabolism

C. necator is able to metabolize H_2 as energy and reductive power in the absence of organic substrates. *C. necator* possesses two energy conserving hydrogenases: a membrane-bound enzyme (*abbr.* MBH) and a cytoplasmic soluble hydrogenase (*abbr.* SH) (Burgdorf *et al.* 2005, Cramm 2009). These are [NiFe] metalloproteins catalyzing H_2 oxidation, thus providing energy and reductive power to *C. necator* (Schwartz *et al.* 2003, Pohlmann *et al.* 2006). Hydrogenases mediate the reversible catalysis of molecular hydrogen H_2 to $2H^+$ and $2e^-$.

First, the Membrane-Bound Hydrogenase is composed of three subunits. The catalytic subunit HoxG and the electron transfer unit HoxK face the periplasm. HoxZ is a di-heme cytochrome *b* anchored into

the membrane. So, MBH is linked to the respiratory chain. The H_2 oxidation energy is most likely recovered through vectorial proton transfer. Then, the Soluble Hydrogenase is located in the cytoplasm. It is composed of a heterodimer HoxH-HoxY hydrogenase moiety and a heterodimeric HoxF-HoxU flavin-containing NADH dehydrogenase moiety. Finally, *C. necator* possesses a third non-energy-conserving hydrogenase that is also called Regulatory Hydrogenase (RH). It acts as an environmental H_2 sensor and then transmits the signal via phosphorylation / dephosphorylation to a hydrogen-response regulator triggering MBH and SH gene expression (Burgdorf *et al.* 2005, Cramm *et al.* 2009).

3.2.5 Respiratory mechanism

Cupriavidus necator performs oxidative phosphorylation coupled to various substrates depending on their availability and is able to adapt to changing environments.

Dioxygen as electron acceptor

Growth can occur lithoautrophically or heterotrophically with similar H^+/O ratios of respectively 6-7 or 8. So, for each electron used to form water, three to four electrons are translocated across cytoplasmic membrane. Therefore, there are a maximum of four coupling sites with an H^+/e^- ratio of 1. *Cupriavidus necator* respiratory chain is composed of: a NADH dehydrogenase, a succinate dehydrogenase, a *bc1* complex and at least three terminal oxidases. Terminal oxidases catalyze reduction of dioxygen to water (Schwartz *et al.* 2003, Pohlmann *et al.* 2006).

The NADH dehydrogenase (complex I, NADH : quinone oxidoreductase, NDH-1) is a membrane-bound protein, whose function is to couple NADH oxidation with protons translocation across cytoplasmic membrane. The gene encoding for the NADH dehydrogenase of *C. necator* is located on chromosome 1 (Cramm *et al.* 2009).

The succinate dehydrogenase (complex II, succinate : quinone reductase, SQR) catalyzes the two-electron oxidation of succinate to fumarate. The genes encoding for the succinate dehydrogenase are located on chromosome (Cramm *et al.* 2009).

Nitrate as electron acceptor

Under environmental anaerobic or anoxic conditions, *C. necator* is able to shift to anaerobic respiration and oxidize nitrate compounds, as alternative electron acceptors through a complete denitrification pathway (Schwartz *et al.* 2003, Pohlmann *et al.* 2006, Gruber *et al.* 2015) at a growth rate of 0.021 h^{-1} (Tiemeyer *et al.* 2007).

Nitrate reduction is catalyzed by four terminal oxidoreductases:

- Nitrate reductase (NAR) catalyzes nitrate reduction,
- Nitrite reductase (NIR) catalyzes nitrite reduction,
- Nitric oxide reductase (NOR) catalyzes nitric oxide reduction,
- Nitrous oxide reductase (NOS) catalyzes nitrous oxide reduction (Cramm *et al.* 2009).

The genes encoding for the different functions of anaerobic metabolism within *C. necator* are present on the megaplasmid pHG1 and on the chromosomes (Schwartz *et al.* 2003).

3.2.6 PHB biosynthesis

Cupriavidus necator has the natural ability to produce and store poly-β-hydroxybutyrate (*abbr.* PHB) in specialized storage granules, under limitation conditions (Pohlmann *et al.* 2006, Gruber *et al.* 2015). This capacity is an adaptation to fluctuating availability of growth-limiting nutrients like O_2, phosphate or azote in presence of abundant carbon availability (Pohlmann *et al.* 2006, Koller *et al.* 2010). *Cupriavidus necator* can produce about 80 % of its dry weight mass in PHB under starvation or limitation conditions (Ryu *et al.* 1997, Grousseau *et al.* 2014).

Cupriavidus necator has become a model organism for the study of PHB bioproduction. The main genes involved in PHB biosynthesis are: PHB synthase (*phaC1*), β-ketothiolase (*phaA*) and NADPH-dependent acetoacetyl-CoA reductase (*phaB1, phaB2, phaB3*) (Pohlmann *et al.* 2006) (**Figure 8**). Lately, PHB production has also been improved by metabolic engineering (Cruz *et al.* 2019, Nangle *et al.* 2020, Tang *et al.* 2020).

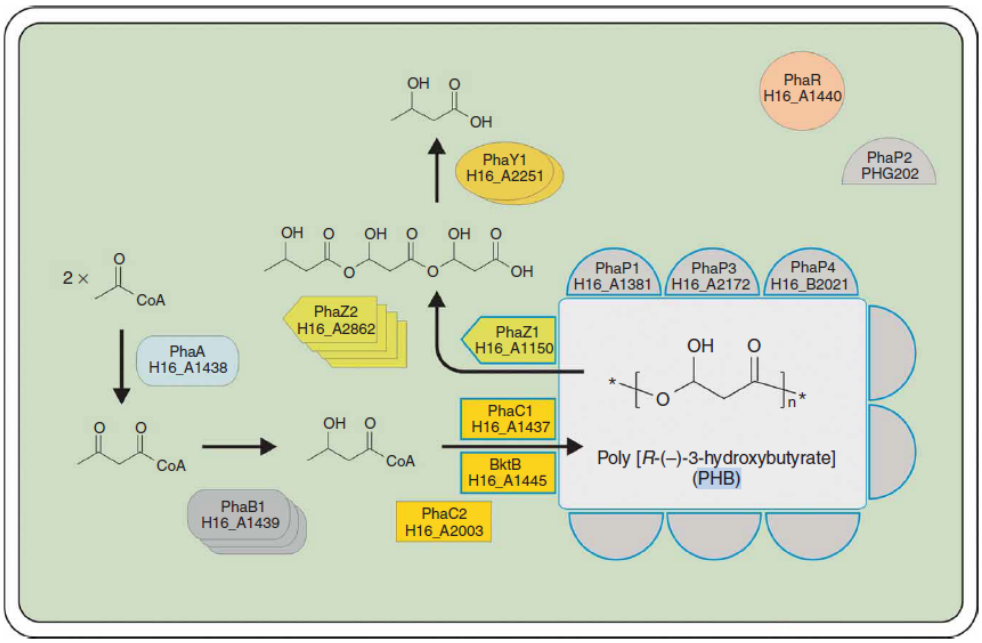

Figure 8: Representation of the PHB biosynthesis pathway in *C. necator* H16 (Pohlmann *et al.* 2006), at the scale of a PHB storage granule in a cell

Legend: Light gray field, PHB storage granule inside a bacterial cell; Arrows, major enzymatic reactions; Boxes/circles/other shapes, enzymes / proteins of PHB metabolism; Stacked symbols, multiple alleles in the genome. Blue outline highlights proteins associated with the PHB granule

3.3 *C. necator* as a recombinant bioproduction platform

The natural capacity of *C. necator* to produce large amount of PHB in conditions of nutrient limitation presents a major interest, since several biosynthesis pathways for chemicals of economic interest also utilize acetyl-coA as precursor. Therefore, lighter genetic modifications would be required to deflect carbon flow after acetyl-coA, from the synthesis of PHB toward an industrial molecule of interest.

Lately, *C. necator* has been engineered into a bioproduction platform toward the biosynthesis of isopropanol (Grousseau *et al.* 2014, Marc *et al.* 2017, Garrigues *et al.* 2020), isobutanol (Black *et al.* 2018), alka(e)ne (Crepin *et al.* 2016), carboxylic acids (Ewering *et al.* 2006, Hoefel *et al.* 2010), α-humulene (Krieg *et al.* 2018) and methyl ketones (Muller *et al.* 2013), both heterotrophically and autotrophically (**Table 9**).

Table 9: Examples of *C. necator* engineering for recombinant molecule production

Molecules	Culture conditions	Substrates	Titer max	References
2-hydroxyisobutyric acid	N-limited Fed-batch	Fructose	6.4 $g \cdot L^{-1}$	(Hoefel *et al.* 2010)
2-methylcitric acid	Flasks	Fructose	19.2 $g \cdot L^{-1}$	(Ewering *et al.* 2006)
α-humulene	Septum flasks	CO_2	6 $mg \cdot L^{-1}$	(Krieg *et al.* 2018)
Alka(e)ne	N-limited Fed-batch	Fructose	1.48 $g \cdot L^{-1}$	(Crépin *et al.* 2018)
		CO_2	4.4 $mg \cdot L^{-1}$	
Isobutanol	Rubber-Capped test tubes	Fructose	30 $mg \cdot L^{-1}$	(Black *et al.* 2018)
Isopropanol	N-limited Fed-batch	Fructose	9.1 $g \cdot L^{-1}$	(Marc *et al.* 2017)
		CO_2	3.5 $g \cdot L^{-1}$	(Garrigues *et al.* 2020)
Methyl ketones	Batch	Fructose	65 $mg \cdot L^{-1}$	(Muller *et al.* 2013)
		CO_2	180 $mg \cdot L^{-1}$	

3.4 Population heterogeneity in *Cupriavidus necator*

One study has been focusing specifically on population heterogeneity in *Cupriavidus necator* as a study model to develop a coupled flow cytometry and proteomics strategy (Wiacek *et al.* 2006). Population heterogeneity was generated through higher concentration of phenol, as a carbon and energy source. Even if *C. necator* was able to consume phenol, high concentrations were toxic for cells. Three subpopulations were obtained in the most drastic culture conditions: two growing subpopulations with different metabolic activity levels and one dormant subpopulation. This dormant population appeared in response to toxic phenol concentrations. On one hand, this subpopulation is less metabolically active, with smaller size and lower DNA content. One the other, translational proteins are upregulated. So, dormant cells might be preparing to re-enter cell cycle in case environmental growth conditions

become favorable again (Wiacek *et al.* 2006). So, in the case of toxic phenol concentrations, population heterogeneity among *C. necator* cells allows increasing cell fitness and stress resistance.

3.5 Plasmid stability strategies in *Cupriavidus necator*

To ensure the design of a robust recombinant strain it is necessary to develop a broad-host synthetic biology toolbox adapted to *Cupriavidus necator*, with for example plasmids and promoters compatible with an expression and maintenance in host cells (Bi *et al.* 2013, Gruber *et al.* 2014).

The plasmid stabilization strategies that have already been applied to *C. necator* can be sorted in the three following categories: plasmid addiction system, site-specific recombination systems and active partitioning.

Plasmid addiction systems consist in the killing of plasmid-free cells, or the reduction of their growth rate (Friehs *et al.* 2004). Three of them have been already adapted to *C. necator*: antibiotic resistance (*e.g.* kanamycin (Grousseau *et al.* 2014, Gruber *et al.* 2014), chloramphenicol (Sydow *et al.* 2017)), chromosomal mutation complementation (*e.g.* single-cell auxotrophy through KDPG-aldolase (Voss *et al.* 2006), proline (Budde *et al.* 2011)) and the PSK system *parDE* (Gruber et *al.* 2014).

Site-specific recombination systems ensure that plasmid multimers formed during replication and / or recombination can be resolved by a site-specific recombination system. Each monomer is transmitted independently to daughter cells. This system can also be referred as plasmid multimer resolution system (Zielenkiewicz *et al.* 2001). The *parCBA* operon encoding for the multimer resolution system of the plasmid RK2 (or RP4) (Easter *et al.* 1998) from *Escherichia coli* has been tested in *Cupriavidus necator* (Gruber *et al.* 2014).

Active partitioning systems ensures that the plasmid copies are vertically transmitted efficiently to every daughter cell (Zielenkiewicz *et al.* 2001, Schwartz *et al.* 2003, Million-Weaver *et al.* 2014). The partition locus of the megaplasmid pMOL28 from *Cupriavidus metallidurans* CH34 has been successfully applied in *Cupriavidus necator* H16 (Sato *et al.* 2013).

As described above (**Table 8)**, all these plasmid stabilization systems allowed maintaining plasmid stability above 90 % all along culture. The efficiency of most of these systems were evaluated during successive flask subcultures by the means of plate count based on antibiotic resistance.

3.6 Isopropanol production by recombinant *Cupriavidus necator* strains

Isopropanol (or propan-2-ol) can chemically be synthesized by three different commercial processes (Papa *et al.* 2000): Indirect or direct hydration of propene and catalytic hydrogenation of acetone.

3.6.1 Natural biological production

Producing species and strains

Microbial production of isopropanol has been discovered at the beginning of the twentieth century. The major isopropanol producing specie is *Clostridium*. Clostridium ABE (Acetone-Butanol-Ethanol) fermentations used to be one of the most important biotechnological processes, especially during the first oil crisis in 1973. The interests in this bioprocess led to the study of *Clostridium*'s genome, metabolism and new innovative fermentation conducts (Dürre *et al.* 1998).

Clostridium beijerinckii is considered as the model organism to study bacterial isopropanol production (Dürre *et al.* 1998). *Clostridium butyricum* and *Clostridium aurantibutyricum* have been shown to produce isopropanol as well (Dürre *et al.* 2008). However, not all *C. beijerinckii* strains are able to synthesize isopropanol in significant amounts (Dürre *et al.* 1998). For example, on yeast extract medium with glucose as substrate, *Clostridium beijerinckii* 2968 reached an isopropanol concentration of 9.8 $g \cdot L^{-1}$, 8 $g \cdot L^{-1}$ for *C. butylicum* 13437, and 10 $g \cdot L^{-1}$ for *C. aurantibutyricum* 10789 (**Table 10**).

Biosynthetic pathway in Clostridium beijerinckii

Synthetic pathways leading to isopropanol synthesis in *C. beijerinckii* is described below (**Figure 9**).

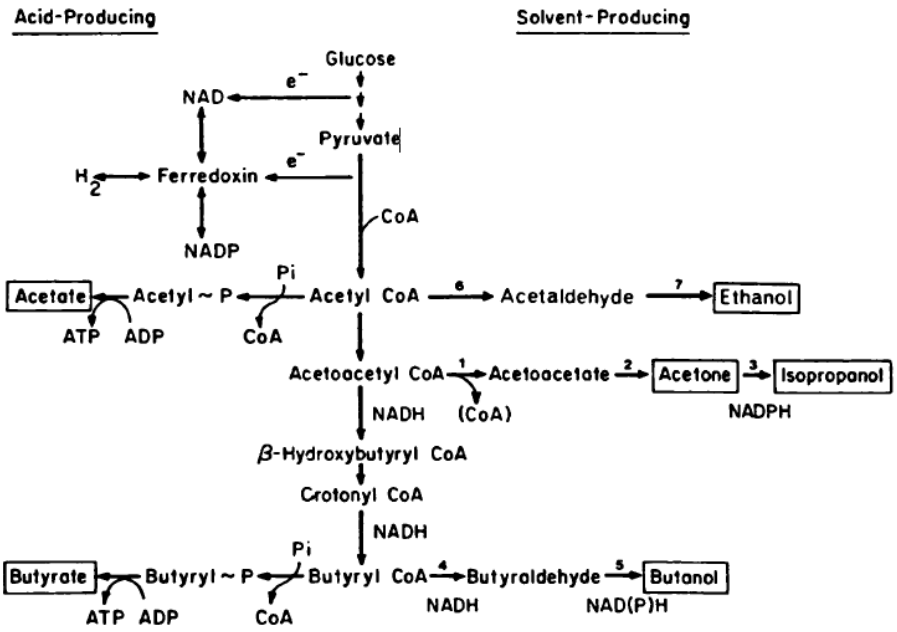

Figure 9 : Synthesis pathway of acetone-butanol-isopropanol-ethanol fermentation in *Clostridium beijerinckii* (Yan *et al.* 1988)

Key enzymes: ① acetoacetyl-CoA:acetate/butyrate-CoA transferase or acetoacetyl-CoA hydrolase or both; ② acetoacetate decarboxylase; ③ isopropanol dehydrogenase; ④butyraldehyde dehydrogenase; ⑤ butanol dehydrogenase; ⑥ acetaldehyde dehydrogenase; ⑦ ethanol dehydrogenase

In these strains, isopropanol production is associated with acetate and butanol productions. From acetyl-CoA, four enzymes are required to synthesize isopropanol. First, a β-ketothiolase (THL) catalyzes the reaction for acetyl-CoA to acetoacetyl-CoA. Then, acetoacetyl-CoA is metabolized to acetone by the action of acetoacetyl-CoA transferase (CTF) and acetoacetate decarboxylase (ADC). The last step is catalyzed by isopropanol dehydrogenase (ADH) that metabolizes acetone into isopropanol.

3.6.2 Recombinant biological production

Cupriavidus necator is naturally able to produce the equivalent of 80 % of its dry weight mass in polyhydroxybutyrate (PHB) under starvation or limitation conditions (Ryu *et al.* 1997). Therefore, *Cupriavidus necator* is able to divert its carbon flux toward the production of a carbonated metabolite, after acetyl-CoA (Grousseau *et al.* 2014). Moreover, *Cupriavidus necator* is a host of interest to study the production of recombinant metabolites and proteins under autotrophic and heterotrophic conditions (Gruber *et al.* 2015).

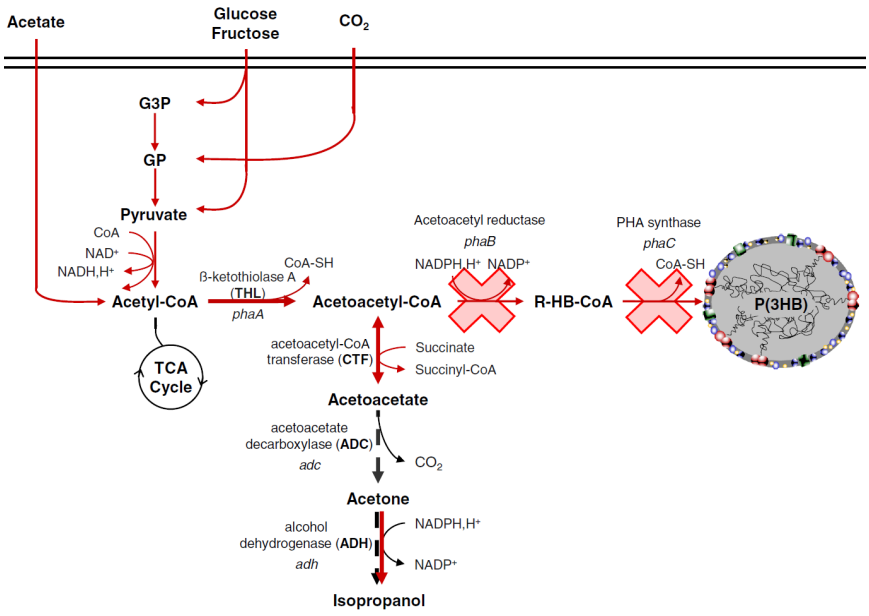

Figure 10 : Isopropanol production pathway in an engineered *Cupriavidus necator* strain. Construction in (Grousseau *et al.* 2014)

In our lab, strains of *Cupriavidus necator* have already been engineered to produce isopropanol by deleting its PHB biosynthesis pathway, and inserting a recombinant plasmid bearing the isopropanol synthesis pathway. In more details, the PHB biosynthesis pathway have been deleted from the wildtype strain *C. necator* H16 to engineer the strain *C. necator* Re2133 (**Figure 10**). More precisely, genes encoding for both acetoacetyl-CoA reductases (*phaB*$_1$*B*$_2$*B*$_3$) and PHA synthase (*phaC*) were deleted. Heterologous isopropanol production was based on the addition of a recombinant plasmid bearing an isopropanol operon composed of genes encoding for acetoacetyl-CoA transferase (CTF) acetoacetate decarboxylase (ADC) and alcohol dehydrogenase (ADH) from *Clostridium* species

(Grousseau *et al.* 2014). So, in conditions of nutrient limitation or depletion, the carbon flow could be diverted from PHB biosynthesis toward isopropanol production.

A first study by Grousseau et *al.* (2014) aimed at developing an efficient plasmid design to ensure high isopropanol production. The design of the isopropanol production operon has been optimized by testing different gene configurations (**Figure 11**). First, one or two copies of the same genes (*thl* or *adh*) have been tested on the plasmid. Then, *adc* and *adh* have either been directly incorporated with their sequence unchanged like in *Clostridium* species, or they have been codon-optimized to fit in the high G+C content genome of *C. necator*. Finally, inducible and constitutive promoters with different strength have been evaluated. Translation was secured in all isopropanol production pathways by the insertion of ribosome binding sites between every recombinant gene. The best strain was *C. necator* Re2133/pEG7c, where isopropanol was controlled by an inducible promoter P_{BAD} with 1 $g \cdot L^{-1}$ arabinose. In flasks, an isopropanol concentration of 3.44 $g \cdot L^{-1}$ and an overall yield of 0.24 $Cmoles \cdot Cmoles^{-1}$ were reached (Grousseau *et al.* 2014) (**Table 10**).

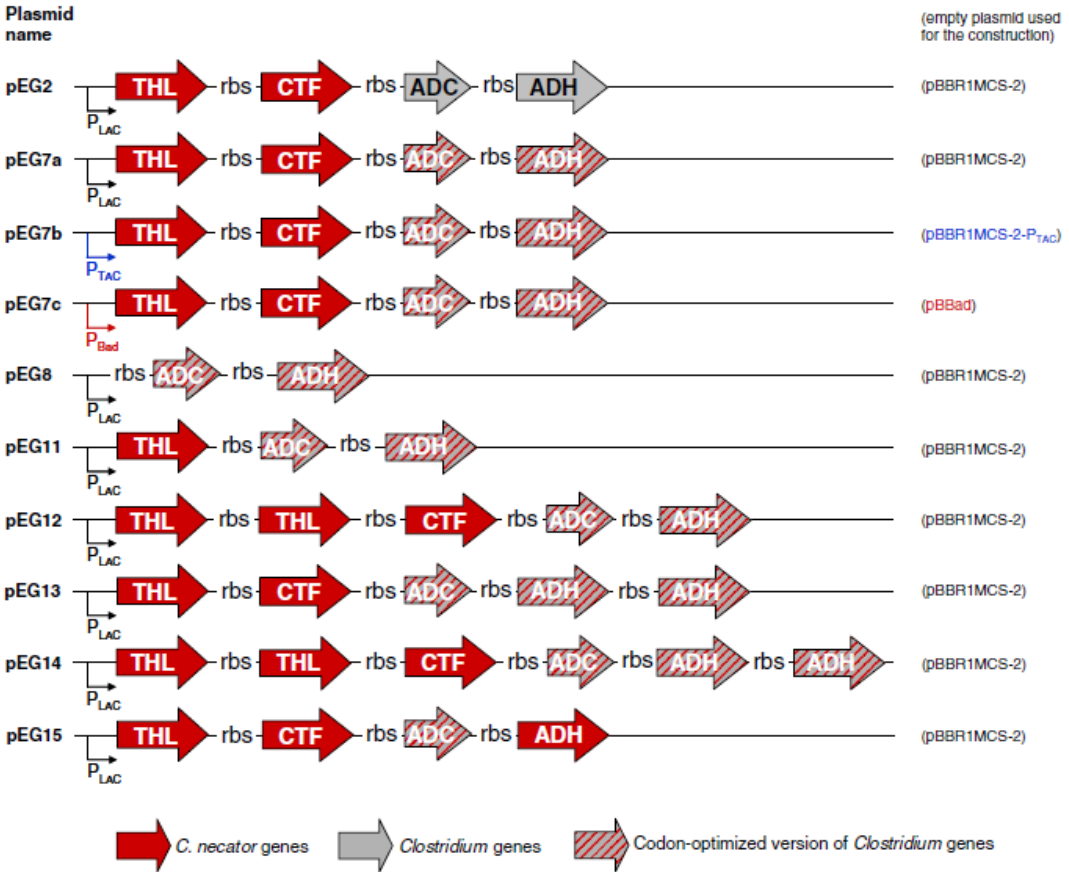

Figure 11: Isopropanol production pathway design and backbone plasmids used. The host strain used was *C. necator* Re2133 (Grousseau *et al.* 2014)

For the production of isopropanol in bioreactor from *Cupriavidus necator*, a fed-batch strategy was used and led in two phases (Marc *et al.* 2017). During the first phase, optimum biomass growth occurred without nutrient limitation. An arabinose pulse was applied when 75 % of the maximum biomass concentration was reached to induce isopropanol recombinant production. The second phase started when nitrogen depletion occurred and growth rate was limited through nitrogen feeding. Growth rate was monitored around 0.04 h^{-1}, as it was shown that the PHB production rate was the highest when growth was maintained at this rate (Grousseau *et al.* 2013).

In Marc et *al*. (2014), isopropanol production reached a concentration at 8.5 ± 0.1 $g{\cdot}L^{-1}$ in the liquid phase with the reference strain Re2133/pEG7c in fed-batch conduct in nitrogen limiting conditions (Marc *et al.* 2017) (**Table 10**). However, it has been demonstrated that production titers reached by engineered strains might be limited by alcohol toxicity on host strains (Chakravarty *et al.* 2018). Indeed, high solvent hydrophobicity increases its toxic impact on host cells, leading to solvent accumulation in the cytoplasmic membrane, causing higher cell permeability (ATP, ions, phospholipids, RNA, proteins leaking), higher membrane fluidity (cell membrane stability, structure disruption), energy transduction decrease and membrane protein function disruption (nutrient transport disruption) (Nicolaou *et al.* 2010, Dunlop *et al.* 2011, Mukhopadhyay *et al.* 2015). Plus, solvents might also denature biological molecules and lead to proteins unfolding, DNA and lipid damages, RNA unfolding or degradation (Nicolaou *et al.* 2010). Consequently, cell growth is inhibited which might lead to cell death. Mechanisms behind the induction or regulation of physiological changes in bacteria because of alcohol are not fully understood yet (Ingram *et al.* 1984, Jia *et al.* 2010). So, the overexpression of GroESL chaperones (*i.e.* heat shock protein family) from *Escherichia coli* in *Cupriavidus necator* proved to be efficient to enhance isopropanol production in fed-batch mode (Marc *et al.* 2017). The final concentration of isopropanol produced was increased (up to 9.1 $g{\cdot}L^{-1}$), as well as its production yield, compared to a reference strain not expressing the GroESL chaperones.

Table 10 : Examples of isopropanol production by natural and recombinant producers; Abbreviations: N/P, natural producer; N/R, not reported

Strain	Plasmid	Substrate	Culture conditions	Titer max.($g \cdot L^{-1}$)	Overall yield ($g \cdot g^{-1}$)	Co-products	References
C. beijerinckii 2968	N/P	Glucose	N/R	9.8	N/R	Acetone, *n*-butanol	(George *et al.* 1983)
C. butylicum 13437	N/P	Glucose	N/R	8	N/R	Acetone, *n*-butanol	
C. aurantibutyricum 10789	N/P	Glucose	N/R	10	N/R	Acetone, *n*-butanol	
***C. acetobutylicum* ATCC824**	pFC007	Glucose	Batch	8.8	N/R	Ethanol, butanol, acetate, butyrate, acetoïn, acetone, 2,3 butanediol	(Collas *et al.* 2012)
***C. acetobutylicum* ATCC824**	pCLF952	Glucose	Batch	6	N/R	Ethanol, butanol, acetate, butyrate, acetoin	(Dusséaux *et al.* 2013)
***C. acetobutylicum* BKM19**	pIPA100	Glucose	Batch	3.5	N/R	Ethanol, butanol, acetate, butyrate	(Jang *et al.* 2013)
***E. coli* ATCC11303**	pSA140	Glucose	Flasks	4.9	N/R	Ethanol, acetone	(Hanai *et al.* 2007)
***C. utilis* TMS272**	pCU155-acs2-erg10	Glucose	Flasks	9.5	N/R	Ethanol, acetate	(Tamakawa *et al.* 2013)
***C. necator* Re2133**	pEG7c	Fructose	Flasks	3.44	0.16	Acetone	(Grousseau *et al.* 2014)
	pEG7c	Fructose	Fed-batch	8.5	0.159	Acetone	(Marc *et al.* 2017)
	pEG23	Fructose	Fed-batch	9.1	0.187	Acetone	
	pEG23	CO_2	Fed-batch	0.25	0.093	Acetone	
	pEG7b	CO_2	Fed-batch	3.5	0.059	Acetone	(Garrigues *et al.* 2020)

4 Conclusion and objective of the study

Population heterogeneity plays a major role in the robustness of a bioprocess in order to achieve high productivity and / or yields. Most recombinant productions are based on the expression of heterogenous plasmid vectors. Plasmid instability has been shown to occur quite frequently in recombinant bioprocesses without selection pressure to favor plasmid-bearing cells maintenance.

The general context of population heterogeneity was presented, its main causes and the quantification strategies available up to date. Population heterogeneity is increasingly studied and the fact that bioprocesses are not constituted of identical individuals is more and more taken into account during their design. Several tools for single-cell study have been developed over the years. One of the most common strategy is based on the expression of a fluorescent reporter protein, generally GFP, controlled by a promoter. This technique allows non-invasive probe for real-time analysis of dynamic events occurring in living cells. Flow cytometry seems like an interesting technology to analyze individuals from a population, which gives access to distributions within a short time of analysis. However, this method is more frequently used in mammalian cells applications, even if progresses have been made with bacterial cell cultures.

Plasmid stability is a major concern of cultures with industrial recombinant strains. Plasmid segregational instability is the main cause of plasmid loss in a growing culture. Plasmid stability monitoring techniques such as plate count, reporter protein expression (detection by flow cytometry or microscopy) and plasmid copy number measurements (based on qPCR) have efficiently been used to evaluate plasmid maintenance. Plate count and PCN measurements have been both used to evaluate plasmid stability in flasks and bioreactors. However, the use of reporter proteins is more documented in flask cultures. The drawback of plate count and PCN measurements lies in their bulky and time-consuming set-up during cultures. Plus, PCN measurements are achieved on the global cell population. Strategies to enhance plasmid stability consist: *(i)* in minimizing the impact of plasmid design and / or *(ii)* in using plasmid stabilization systems; and have efficiently been applied during culture, as detailed in this literature review. However, PSK, MRS systems and active partitioning efficiency have only been evaluated in flasks and have not often been confronted to bioreactor procedures. Some negative aspects have also been identified: antibiotic resistance relies on the presence of an expensive toxic molecule in the medium and MRS' efficiency highly depends on strain-host compatibility. Mostly, efficiency of these systems has been assessed through plate count, which might not allow detecting several subpopulations with different expression levels. Therefore, it might be beneficial to implement these plasmid stabilization strategies in bioreactor cultures, and to evaluate

their efficiency through the expression of a reporter protein by flow cytometry, which might allow fast and easy plasmid expression stability evaluation.

The study model chosen for this work was isopropanol production with *C. necator*. First, *C. necator* was described through its metabolism and growing use as bioproduction platform. Plasmid stabilization strategies constructed for this bacterium were all efficiently implemented, but were only evaluated in successive flasks subcultures by plate count. We observed that population heterogeneity mechanisms in *C. necator* have not been really studied yet. Second, the bacterial production of isopropanol by natural and recombinant strains was described, especially with *C. necator*. Production of isopropanol from *C. necator* is a well-documented recombinant bioprocess concerning plasmid design and culture monitoring in bioreactors. Nevertheless, the impact of plasmid instability on bioprocess robustness, considering that isopropanol might potentially be toxic for cells, has not been intensively studied yet.

Considering its impact on recombinant molecule production, the dynamic identification and characterization of plasmid segregational instability during bioreactor cultures of recombinant *C. necator* has to be achieved. Indeed, the conditions and mechanisms of plasmid stability during culture are key in optimizing isopropanol production by recombinant *C. necator*. To this end, the following scientific questions have to be investigated:

- How to dynamically identify and discriminate different subpopulations from a pure culture in a bioreactor during fermentation?
- What are the effectors of the appearance of heterogeneities in monoclonal bioreactor cultures? How does the behavior of subpopulations evolve in response to these effectors?
- Is it possible to control the distribution of subpopulations in a bioprocess during fermentation? At what level can this control be performed, and how effective is it?

Part 2: Material and methods

Part 2: Material and methods

This chapter describes the materials and methods used to achieve the objectives of the PhD work. It includes a presentation of the strain, the culture media employed and the culture conditions adopted. In addition, the analytical methods used to characterize the dynamics of growth; metabolism and morphology of *C. necator* were described in detail. Finally, the methodology employed for the treatment of the kinetic data (rates, yields, carbon and generalized reduction rate balances…), as well as smoothing and reconciliation of the experimental results are detailed.

1 Strains, plasmids and media

1.1 Strains

The main strain used in this study was *Cupriavidus necator* Re2133 (Budde *et al.* 2011). This strain was obtained by deleting genes encoding for acetoacetyl-CoA reductases (*phaB1B2B3*) and for PHA synthase (*phaC1*) from the wildtype strain *C. necator* H16 / ATCC17699, which is gentamicin resistant (Gen^R). Most commonly, the optimal growth conditions of the *C. necator* Re2133 strain on minimum medium are a temperature of 30 °C and a pH 7 (Grousseau *et al.* 2014, Crepin *et al.* 2016, Marc *et al.* 2017). The strains *Escherichia coli* S17-1 and Top10 were used during plasmid construction. All strains are summarized in **Table 1**.

Table 1: Strains used in the PhD work

Strains	Characteristics	Reference
Cupriavidus necator Re2133	*C.necator* H16/ATCC17699 Δ*phaB1B2B3* and Δ*phaC1*, Gentamicin resistant.	(Budde *et al.* 2011)
Escherichia coli S17-1	Highly efficient conjugative donor strain	(Strand *et al.* 2014)
Escherichia coli Top10	Competent strain for plasmid amplification	Thermo Fischer

1.2 Media

Two types of growth media were used for *C. necator* and *E. coli* cell cultures: rich (TSB, LB) and mineral media. All reagents used for medium preparation were of the highest grade commercially available.

1.2.1 Rich media

The composition of the Tryptic Soy Broth (TSB) used for colony isolation (in solid form by the addition of agar) and for cell revivication (in liquid form) is described in **Table 2**. It was prepared with osmosis water and sterilized by autoclaving at 121 °C for 20 min.

Table 2: Composition of the TSB and TSA rich media

Compound	Composition ($g \cdot L^{-1}$)	
	TSB	**TSA**
Tryptic Soy Broth	27.5	27.5
Agar	0	20
Gentamicin sulfate	0.01	0.01
Kanamycin sulfate *(for plasmid conservation)*	0.2	0.2

1.2.2 Mineral media

1.2.2.1 For flask cultures: MIT mineral medium

The MIT defined mineral medium (MM MIT) used for all flask cultures was prepared as described in **Table 3**. It is a mineral medium with an optimized composition adapted to *C. necator* cell needs in flasks. Concentrated stock solutions of each oligo-element were prepared separately and sterilized by autoclaving at 121 °C for 20 min. However, antibiotics and Na_2HPO_4 stock solutions were sterilized by filtering through a 0.22 µm syringe-fitted filter. Fructose was also prepared as a stock solution (500 $g \cdot L^{-1}$) and autoclaved separately.

Stock solutions were mixed in a sterile Schott flask containing sterile osmosis water according to the composition presented in **Table 3**. After mixing the components, pH reached a value of 6.8, due to phosphate buffer used (Na_2HPO_4 / NaH_2PO_4). A biomass concentration of 2 $g_{CDW} \cdot L^{-1}$ can be reached, based on the amount of nitrogen in this medium.

Table 3: Composition of the MIT mineral medium

	Compounds	Concentration ($g \cdot L^{-1}$)
Oligo-elements	NaH_2PO_4, 2 H_2O	5.2
One of each	Na_2HPO_4, 12 H_2O	11.6
	K_2SO_4	0.45
	NaOH	0.04
	$MgSO_4$, 7 H_2O	0.8
	$CaCl_2$, 2 H_2O	0.08
Trace solution	$FeSO_4 \cdot 7H_2O$	0.015
In one solution	$MnSO_4 \cdot H_2O$	0.0024
	$ZnSO_4 \cdot 7H_2O$	0.0024
	$CuSO_4 \cdot 5H_2O$	0.00048
Antibiotics	Gentamicin sulfate	0.01
One of each	Kanamycin sulfate	0.2
Carbon source	D-Fructose	20
Nitrogen source	NH_4Cl	1

1.2.2.2 For Bioreactor cultures: FAME mineral medium

The FAME defined mineral medium (MM FAME) used for all bioreactor fermentations was prepared as described in **Table 4**. It is a mineral medium with an optimized composition adapted to *C. necator* cell needs in bioreactors. Concentrated stock solutions of each oligo-element were prepared separately and sterilized by autoclaving at 121 °C for 20 min. However, antibiotics and rich phosphate stock solutions were sterilized by filtering through a 0.22 µm syringe-fitted filter. Fructose was also prepared as a stock solution (500 $g \cdot L^{-1}$) and autoclaved separately.

First, macro-elements were mixed in osmosis water according to the composition presented in **Table 4**. After mixing the components, the pH was adjusted to 7 by addition of 4 M potassium hydroxide solution and the mixture was sterilized for 20 min at 121 °C. After cooling, oligo-elements, antibiotics and glucose stock solutions were added sterilely, from their respective stock solutions, to the medium mixture at the target concentrations. A biomass concentration of 4 $g_{CDW} \cdot L^{-1}$ can be reached due to the amount of nitrogen in this medium.

Table 4: Composition of the FAME minimum medium

	Compounds	Concentration ($g \cdot L^{-1}$)
Macro-elements	$(NH_4)_2SO_4$	2.8
One of each	$MgSO_4 \cdot 7H_2O$	0.75
	Nitrilotriacetic Acid	0.285
Oligo-elements	$CaCl_2 \cdot 2H_2O$	0.015
Rich phosphate solution	$Na_2HPO_4 \cdot 12H_2O$	1.568
In one solution	KH_2PO_4	0.263
Element solution	H_3BO_3	4.50E-04
In one solution	$CoCl_2 \cdot 6H_2O$	3.00E-04
	$ZnSO_4 \cdot 7H_2O$	1.50E-04
	$MnCl_2 \cdot 4H_2O$	4.50E-05
	$Na_2MoO_4 \cdot 2H_2O$	4.50E-05
	$CuSO_4 \cdot 5H_2O$	1.50E-05
	$NiCl_2 \cdot 6H_2O$	3.30E-05
	Ammonium Iron (III) Citrate (28%)	0.09
Carbon source	D-Fructose	30
Antibiotics	Gentamicin sulfate	0.01
One of each	Kanamycin sulfate	0.2

1.3 Plasmids

1.3.1 Description of plasmids

The plasmids pKRSF1010-P_{lac}-egfp, pKRSF1010-P_{tac}-egfp, pKRSF1010-P_{n25}-egfp and pKRSF1010-P_{j5}-egfp were used to screen the impact of promoter strength on host cell physiology. Their design was detailed in Gruber et *al.* (2014). They all encoded kanamycin resistance (Kan^R) as well as eGFP expression (enhanced Green Fluorescent Protein, *egfp*). Plasmid stability was ensured by a post-segregational killing system (*abbr*. PSK, *parDE*) and a multimer resolution site (*parCBA*), from the RP4 plasmid (Friehs *et al.* 2004). The only difference between these four plasmids was the nature of the promoter upstream *egfp*.

1.3.2 Plasmid construction

Plasmids pCB1, pCB3 and pJLCB2 were designed and constructed in the team. Their construction consisted in the insertion by Gibson isothermal assembly of the *P_{lac}-egfp* cassette of the plasmid pKRSF1010-P_{lac}-egfp into the plasmid pBBad (Budde *et al.* 2011), the plasmid pBBad-Par and pEG7c (Grousseau *et al.* 2014), respectively. So, all these plasmids encode for kanamycin resistance (Kan^R) as well as eGFP expression (enhanced Green Fluorescent Protein, *egfp*); pCB3 encodes in addition for the post-segregational killing system *hok/sok* and pJLCB2 for the isopropanol operon. The backbone pBBAD was chosen because it is the plasmid backbone used in our team for the construction of recombinant strains toward the production of heterologous molecules of interest. An example of

plasmid construction was shown in **Figure 1** and the complete list of plasmids used in this work is given in **Table 5**.

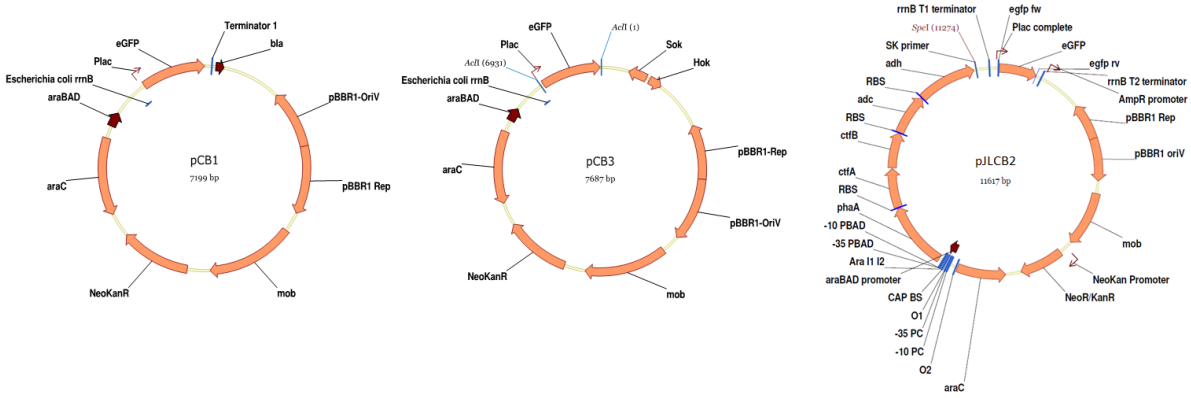

Figure 1: Plasmid construction design for pCB1 and pCB3

Table 5: Plasmids used in this work

Plasmids	Characteristics	References
pBBad	Kan^R; PBad; pBBR1MCS-2 derivative	(Fukui *et al.* 2009)
pBBad-Par	Kan^R; PBad; *hok/sok* operon; pBBR1MCS-2 derivative	(Fukui *et al.* 2009)
pEG7c	pBBad with phaA-RBS-ctfAB-RBS-adc*- RBS-adh* sequence inserted into the multiple cloning site (MCS), Kan^R, PBad	(Grousseau *et al.* 2014)
pKRSF1010-P_{lac}-egfp	Kan^R; P_{lac}; egfp; par; RSF1010 mob and oriV	(Gruber *et al.* 2014)
pKRSF1010-P_{tac}-egfp	Kan^R; P_{tac}; egfp; par; RSF1010 mob and oriV	(Gruber *et al.* 2014)
pKRSF1010-P_{n25}-egfp	Kan^R; P_{n25}; egfp; par; RSF1010 mob and oriV	(Gruber *et al.* 2014)
pKRSF1010-P_{j5}-egfp	Kan^R; P_{j5}; egfp; par; RSF1010 mob and oriV	(Gruber *et al.* 2014)
pCB1	Kan^R; P_{lac}-egfp; PBad; pBBRMCS-2 derivative	This work
pCB3	Kan^R; P_{lac}-egfp; PBad-Par; pBBRMCS-2 derivative	This work
pJLCB2	Kan^R; P_{lac}-egfp; pEG7c	This work

1.3.2.1 DNA amplification by PCR

DNA primers were ordered from Eurofins Genomics. Their sequences were designed as described in **Table 6**.

Table 6: Sequences of the primers used to construct the recombinant plasmids

Primers	Sequence 5' → 3'	Tm (°C) *complete*	Tm (°C) *without overlaps*	
pBBAD_eGFP_acl1_rv_long	CCTCCGGGCCGTTGCTTCGCAACGTT TTACTTGTACAGCTCGTCCATGC	85	53.8	Amplification of the P_{lac}-eGFP cassette
pCB3_Plac_acl1_fw_long	ATCCGCCGGGAGCGGATTTGAACGTT TTTACACTTTATGCTTCCGGCTC	82.7	54.5	
Plac_EGFP_pBBad_fw	GGATGATCCTCCAGCGCGGGGATTTACA CTTTATGCTTCCGGCTC	70	70	
Plac_EGFP_pBBad_rv	GGGGTGGGCGAAGAACTCCAGTTACTTG TACAGCTCGTCCATGC	70	70	Amplification of the pEG7c plasmid
pBBad_Plac_EGFP_fw	GCATGGACGAGCTGTACAAGTAACTGGA GTTCTTCGCCCACCCC	70	70	
pBBad_Plac_EGFP_rv	GAGCCGGAAGCATAAAGTGTAAATCCCC GCGCTGGAGGATCATCC	70	70	

Upon reception of the primers, the tubes were centrifuged at 13,400 rpm during 3 min. Then, they were resuspended in Milli-Q grade water (18.2 mΩ-cm resistance) filtered with a 0.22 µm syringe-fitted filter to reach a stock concentration of 100 µM. Tubes were vortexed and heated during 15 to 20 min at 40°C to help dissolve the primers. After that, tubes were vortexed again and centrifuged at 13,400 rpm during 3 min. Finally, the tubes were stored at -20°C.

To prepare the working solution, primers stock solutions were diluted in Milli-Q water to reach a concentration of 10 µM. The tubes were stored at -20°C.

All samples for PCR amplification were prepared with Phusion enzyme High-Fidelity PCR Master Mix (GC Buffer) (NEB, USA) as described in **Tables 7 and 8**.

Table 7: Sample preparation for PCR amplification of eGFP

	µL
Each primer (10µM)	2.5
DNA	1
DMSO	1.5
Phusion enzyme High-Fidelity PCR Master Mix (GC Buffer)	12.5
q.s. Filtered Milli-Q water	50

Table 8: Sample preparation for PCR amplification of pEG7c

	µL
Each primer (10µM)	2.5
DNA	1
DMSO	1.5
Phusion enzyme High-Fidelity PCR Master Mix (GC Buffer)	25
q.s. Filtered Milli-Q water	50

The *P_{lac}-egfp* cassette was amplified from the plasmid pKRSF1010-Plac-eGFP (Gruber *et al.* 2014) and its sequence was given in **Figure 2**. The plasmid pEG7c was also amplified by PCR for pJLCB2 construction (**Tables 6 & 8**).

5'TTACACTTTATGCTTCCGGCTCGTATGTTGGTGAGCAAGGGCGAGGAGCTGTTCACCGGGGTGGTGCCCA
TCCTGGTCGAGCTGGACGGCGACGTAAACGGCCACAAGTTCAGCGTGTCCGGCGAGGGCGAGGGCGATGC
CACCTACGGCAAGCTGACCCTGAAGTTCATCTGCACCACCGGCAAGCTGCCCGTGCCCTGGCCCACCCTCGT
GACCACCCTGACCTACGGCGTGCAGTGCTTCAGCCGCTACCCCGACCACATGAAGCAGCACGACTTCTTCAA
GTCCGCCATGCCCGAAGGCTACGTCCAGGAGCGCACCATCTTCTTCAAGGACGACGGCAACTACAAGACCC
GCGCCGAGGTGAAGTTCGAGGGCGACACCCTGGTGAACCGCATCGAGCTGAAGGGCATCGACTTCAAGGA
GGACGGCAACATCCTGGGGCACAAGCTGGAGTACAACTACAACAGCCACAACGTCTATATCATGGCCGACA
AGCAGAAGAACGGCATCAAGGTGAACTTCAAGATCCGCCACAACATCGAGGACGGCAGCGTGCAGCTCGC
CGACCACTACCAGCAGAACACCCCCATCGGCGACGGCCCCGTGCTGCTGCCCGACAACCACTACCTGAGCA
CCCAGTCCGCCCTGAGCAAAGACCCCAACGAGAAGCGCGATCACATGGTCCTGCTGGAGTTCGTGACCGCC
GCCGGGATCACTCTCGGCATGGACGAGCTGTACAAGTAA 3'

Figure 2: Sequence of the fluorescence cassette P_{lac}-eGFP from the plasmid pKRSF1010-P_{lac}-egfp

The PCR amplification was executed on an Mx3005P QPCR System (Agilent Technologies, USA) and the program was encoded on the MxP10 software (Agilent Technologies, USA). The PCR program was elaborated to allow both the amplification of sequence of interest and to add the overlaps necessary for Gibson isothermal assembly as presented in the **Figure 3** below.

Cycle n°1: DNA amplification

↺ Repeat 10 times

- 1 min at 98 °C (cell lysis)
- 10 s at 98 °C (separation of the strands)
- 30 s at 54 °C, (annealing at hybridization temperature of the gene sequence primers)
- 30 s at 72 °C (elongation)

Cycle n°2: Overlaps addition

↺ Repeat 30 times

- 10 s at 98 °C (separation of the strands)
- 30 s at 81 °C, (annealing at hybridization temperature of the primers)
- 30 s at 72 °C (elongation)

➔ 5 min at 72 °C

➔ Store at -20 °C

Figure 3: PCR amplification cycle for cassette and overlaps amplification

1.3.2.2 Plasmid linearization by restriction enzymes

The pBBad-backbone derived plasmids were linearized prior to insertion of the fluorescence cassette *P_{lac}-egfp*. A unique AclI restriction site was present on the backbone pBBad. This restriction enzyme was used to linearize the plasmid vector following the recommendation of the producer of the enzyme, NEB (New England Biotechnology, USA).

1.3.2.3 Purification PCR product

For the construction of the plasmid pJLCB2, the PCR products were purified by gel agarose electrophoreses 0.8 % with SyberSafe diluted at 1/10,000 and cleaned with the QIAquick Gel Extraction Kit (Qiagen, USA). The concentrations of DNA fragments were measured with the spectrophotometer NanoDrop UV visible spectrophotometer (Thermoscientific, USA) and used for the Gibson assembly method.

1.3.2.4 Gel electrophoresis

The sizes of the DNA fragments were estimated through electrophoresis. To do so, a 0.8% (m/V) agarose gel was prepared with TAE 1x buffer. First, the TAE 1x buffer was prepared following the composition described in **Table 9**.

Table 9: Composition of the TAE 50x and TAE 1x buffers for gel electrophoresis

Compounds	50x		1x	
Tris Base	2 M	242.2 $g \cdot L^{-1}$	40 mM	4.844 $g \cdot L^{-1}$
Glacial Acetic Acid	1 M	60.5 $mL \cdot L^{-1}$	20 mM	1.21 $mL \cdot L^{-1}$
EDTA Sodium salt dihydrate (pH 8)	50 mM	18.612 $g \cdot L^{-1}$	1 mM	0.372 $g \cdot L^{-1}$

To perform gel electrophoresis, the Mupid®-One (Eurogentex, Belgium) electrophoresis cell was used. TAE 1x buffer was added in the gel electrophoresis tank until the agarose gel was completely covered. For every different PCR product, 2.5 µL of Purple Gel Loading Dye 6x (NEB, USA) was mixed with 15 µL of PCR product. 5 µL of this mix were taken to fill the agarose gel wells. 5 µL of 1kb DNA Ladder (NEB, USA) was added in the first well. Voltage was set at 100 V during 30 min.

For revelation, the gel was placed in an EtbR (Ethidium Bromide) bath and incubated 10 min. The gel was rinsed with distilled water and observed with the ChemiDoc system (Bio-Rad, Hercules, CA, USA).

The linearized plasmid vector was supposed to have a size of 6,442 bp for pBBad and 6,930 bp for pBBad-Par. The fluorescence cassette was supposed to have a size of 791 bp (**Figure 4**).

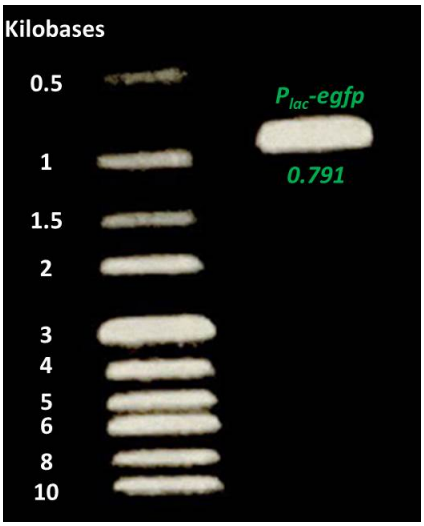

Figure 4: Gel electrophoresis for the fluorescent cassette P_{lac}-eGFP

1.3.2.5 Cloning by Gibson isothermal assembly

Gibson isothermal assembly (Gibson *et al.* 2009) is a method allowing assembling several overlapping DNA fragments within a single-reaction involving at the same time a 5' exonuclease, a DNA polymerase and a DNA ligase. The *P_{lac}-egfp* cassette was inserted in the plasmids of interest by this cloning method.

Reagents preparation

First, a 5x isothermal assembly reaction buffer was assembled on ice: 3 mL of 1M Tris-HCl at pH 7.5**;** 300 µL of 1M $MgCl_2$**;** 600 µL of 10 mM each dNTP (Nucleoside triphosphate: A, T, C, G)**;** 300 µL of 1M Dithiothreitol (DTT) solution**.** Second, one aliquot of 320 µL 5x isothermal assembly reaction buffer was added to the following mix: 1.2 µL of T5 Exonuclease (NEB M0363S, USA); 20 µL of Phusion HF polymerase (NOT HOTSTART) (NEB, USA); 160 µL of Taq ligase (NEB M0208L, USA); 700 µL of Milli-Q Water**.** 80 Isothermal Assembly reaction aliquots of 15 µL were prepared on ice in PCR tubes and stored at -20°C.

Isothermal Assembly reaction

First, the fragments of choice (vector and insert) with overlapping regions were purified with the Monarch® PCR & DNA Cleanup Kit or gel agarose extraction. Then, not exceeding a total volume of 5 µL, fragments were combined in PCR tubes and for gel extraction many PCR tube were used to have enough at the end of the extraction method. The ratios insert:vector applied were 5:1 and 10:1 (w:w) except for the pJLCB2, the ratio used was 1:74. The combined fragments were added to 1 Isothermal Assembly reaction aliquot and mixed by pipetting. Then, reaction took place at 50°C for 30 min in the Mx3005P QPCR System (Agilent Technologies, USA). The whole volume (20 µL) of assembly product was transformed in *E. coli* Top 10 following the protocol described above.

1.3.2.6 Transformation in E. coli Top 10

Preparation of high efficiency competent cells

First, an LB agar plate was inoculated with *E. coli* Top 10 (NEB 10-beta, USA) and incubated at 37 °C during 12 to 16 h. A single colony was transfer in 5 mL of LB and incubated at 37 °C with vigorous shaking during 12 to 16 h. 2.5 mL of subculture were used to inoculate 250 mL of LB (flask of 1L) and incubated at 37 °C and 200 RPM, until OD_{600nm} = 0.4.

Then, the whole broth volume was transferred in 5 cold Falcon tubes and incubated on ice for 20 min. After incubation, the 5 Falcon tubes were centrifuged at 3000 g during 10 min at 4 °C and the supernatant was removed. Pellets were individually re-suspended in 3 mL of cold 0.1 M $CaCl_2$ before being transferred in one Falcon tube, which was incubated on ice during 30 min. The so-prepared cell suspension was centrifuged at 3000 g during 10 min at 4 °C and the supernatant was removed. The pellet was re-suspended in 4 mL cold 0.1 M $CaCl_2$ with 15 % Glycerol.

Finally, aliquots of 100 µL were transferred in cold Eppendorf tubes, and frozen in liquid nitrogen before being stored at -80 °C.

Transformation of High Efficiency Competent Cells

First, a tube of thermo-competent *E. coli* Top 10 (NEB 10-beta, USA) was thawed on ice for 10 min. The 100 µL of cell suspension was split in 2 aliquots of 50 µL. For plasmid insertion, 1 to 5 µL containing 1 pg to 100 ng of plasmid DNA were added to the cell mixture. For Gibson assembly product, the whole Gibson product was added. The tube was carefully flipped 4 to 5 times in order to mix cells and DNA and then, the mixture was placed on ice for 30 min without mixing. Heat shock was led at exactly 42°C for exactly 45 seconds without mixing. Then, the tube was placed on ice again for 5 minutes without mixing. 450 µL of room temperature SOC (Super Optimal broth with Catabolite repression,(Lessard 2013)) was added into the mixture and the cells were incubated at 37°C for 60 min. Finally, the cell suspension was stripped on LB plates with kanamycin 50 $mg \cdot L^{-1}$ and incubated overnight at 37 °C

1.3.2.7 Colony PCR screening

To check if the insertion of the cassette of interest was led accurately, colonies were screened by PCR with primers allowing the amplification of the fragment of interest when inserted in the plasmid vector. For simplicity, green fluorescence of colonies was also chosen as screening target for eGFP successful insertion. The characteristics of the primers used and the obtained amplified fragments are enlisted in **Table 10**.

Table 10: List of the primers used to amplify the P_{lac}-egfp florescence cassette and the isopropanol operon

Primers	Sequence	Tm	Amplified fragment
pBBAD_eGFP_acl1_rv_long	CCTCCGGGCCGTTGCTTCGCAACGTT TTACTTGTACAGCTCGTCCATGC	85	*P_{lac}-egfp* **791 bp**
pCB3_Plac_acl1_fw_long	ATCCGCCGGGAGCGGATTTGAACGTT TTTACACTTTATGCTTCCGGCTC	82.7	
Seq-pBBad_1	CTCTCTACTGTTTCTCCATAC	59	*Isopropanol operon* **4,555 bp**
Seq-pBBad_2	GGCTGAAAATCTTCTCTCATC	60	

Two strategies were led for verification of correct fragment insertion:

- PCR on colonies: First, colonies were numbered and annotated on the plates. Then, PCR screening mix was prepared on ice (quantities given for one PCR screening tube) with 0.25 µL of both primers (10mM), 6.25 µL of OneTaq® 2X Master Mix with GC Buffer (NEB, USA) and

5.75µL of Milli-Q water. Aliquots of 12.5µL were transferred in PCR tubes. One colony was picked with a sterile toothpick and dipped into the corresponding annotated tube.

- PCR on purified plasmids: First, fluorescent colonies were used to inoculate 5 mL of LB medium with appropriate antibiotics (usually 50 mg·L^{-1} kanamycin) and grown 12 h at 37°C and 130 rpm. Second, the so-obtained culture broth was used for plasmid DNA purification, as detailed just below.

From there, the following PCR screening programs were run on the Mx3005P QPCR System (Agilent Technologies, USA) and the programs were encoded on the MxP10 software (Agilent Technologies, USA). The one described in **Table 7** was designed to verify the presence of the *P_{lac}-egfp* cassette in the Gibson Assembly products. The one described in **Table 8** was designed to verify the presence of the isopropanol operon in the Gibson Assembly products. An agarose diagnostic gel was ran to check if the fragment of interest was amplified and presented the appropriate size.

1.3.2.8 Plasmid DNA purification from cell pellets

A single colony from a LB plate with 50 mg·L^{-1} kanamycin was used to inoculate a culture of 5 mL LB medium with 50 mg·L^{-1} kanamycin. The flask was incubated for 12 h at 37 °C with vigorous shaking (140 rpm). Cells were harvested by centrifugation at 5400 g for 10 min at 4 °C and the supernatant was removed.

Plasmid extraction was led with the QIAprep® Spin Miniprep Kit (QIAGEN, Germany). The different buffers used during plasmid purification are described below. The purified plasmids were stored at -20°C.

1.3.2.9 Electroporation in E. coli S17-1 strains

Preparation of electro-competent cells

First, a LB-plate was inoculated with *E. coli* S17-1 and incubated overnight at 37°C. A single colony was picked and transferred in 3 mL of LB in a 10 mL tube and incubate overnight at 37°C with vigorous shaking (150 rpm). Then, 1 mL of the overnight culture was transferred to 500 mL aliquots of LB in 2 L flasks. The culture was incubated at 37°C with vigorous agitation (150 rpm) for 2-6 hours. The optical density (600 nm) was followed every 30 min, after the first hour of incubation, until it reached 1. Flasks were removed from the incubator and chilled on ice for at least 30 minutes.

Then, cells were centrifuged at 5000 g for 15 min and the supernatant was removed. Cell pellets were transferred to cold 50 mL falcon tubes and re-suspended in 25-30 mL of sterile ice-cold water. Cells were centrifuged again, and the supernatant was removed. The two last steps were done a second

time. Then, cells pellets were re-suspended in 20 mL ice-cold sterile 10 % glycerol. Centrifugation was led as before and supernatant was removed. Cells were re-suspended in a final volume of 3 ml sterile water with 10 % glycerol. Last, cells were divided into 150 µl aliquots in Eppendorf tubes and stored at -80°C.

Transformation of electro-competent Cells

All plasmids were transformed into *Escherichia coli* S17-1 (ATCC 47055) by electroporation. First, 1 to 3 µL of plasmid DNA were added to electrocompetent cells and the whole incubated on ice for 5 min. The mix was transferred to a chilled 2 mm electroporation cuvette (Cell projects, Sutton Valence, GB). Electroporation was performed in the Gene Pulser® II Electroporation System (Bio-Rad, Hercules, CA, USA) with the following settings: voltage, 2.5 kV; capacity, 25 µF, external resistance 200 Ω. After the pulse, 850 µl of Super Optimal broth with Catabolite repression (*abbr.* SOC) were added to the cuvette. The cells were incubated at 37 °C for 1 h to recover. Cells were plated on LB agar plates containing 50 $mg \cdot L^{-1}$ kanamycin.

1.3.2.10 Mating of E. coli S17 to C. necator Re2133

E. coli S17-1 plasmid bearing cells were used to insert the plasmid into *C. necator* Re2133 by conjugative transfer. *E. coli* S17-1 plasmid bearing cells and *C. necator* Re2133 were grown to stationary phase in LB with 50 $mg \cdot L^{-1}$ kanamycin for 24 h and in Tryptic Soy Broth *abbr.* TSB (Becton Dickinson, Sparks, MD, USA) with 10 mg/L gentamicin for 48 h respectively. Optical density at 600 nm (OD_{600nm}) was measured for both strains using a visible spectrophotometer (DR3900, Hachlange, Loveland, Colorado, USA). Cells were washed twice with 0.85% saline buffer. Cell suspension volumes were combined to reach equal OD units for *C. necator* 2133 and *E. coli* S17-1 plasmid bearing cells in a total volume of 50 µL. The cell mixture was spotted in the middle of LB plates supplemented with 0.2 % fructose (w/v). Plates were incubated at 30 °C for 48 h. Half of the cell's colony was scraped off the plate and resuspended in 100 µL saline solution. 10 µL of this cell suspension was plated on LB + 0.2 % (w/v) fructose with 10 $mg \cdot L^{-1}$ gentamicin and 200 $mg \cdot L^{-1}$ kanamycin. Plates were incubated at 30 °C for 48 h. One colony was used to inoculate 3 mL of TSB with addition of 10 $mg \cdot L^{-1}$ gentamicin and 200 $mg \cdot L^{-1}$ kanamycin. Cells were grown in flasks for 24 h at 30 °C and 110 rpm in an incubation shaker (Multitron standard, Infors, Massy, France). Glycerol stocks were prepared by adding 30 % (v/v) glycerol to the cell suspension and then, stored at -80 °C in 1.5 mL aliquots.

2 Culture conditions

2.1 Glycerol stock preparation

C. necator cell frozen stocks were prepared as follows: From a TSA plate of the desired *C. necator* strain, a single colony was picked and transferred into a 50 mL sterile baffled erlenmeyer containing 5 mL of TSB medium with appropriate antibiotics. After incubation for 24 h at 30 °C and 130 rpm, the culture (5 mL) was mixed with 2.1 mL of pure sterile glycerol solution to reach a final concentration of 30 % (v/v). Finally, the prepared stock culture was aliquoted into sterile cryotubes (1 mL each) and stored at -80 °C. Sterilization of glycerol and TSB medium was carried out by autoclaving at 121 °C for 20 min.

2.2 Preculture scheme and flask cultivation on fructose

2.2.1 Preculture scheme

For every culture, one glycerol stock kept at -80 °C was plated on TSA plates and incubated for 72 h at 30 °C. Well-isolated single colony from TSA plate was used for inoculum preparation. One colony was used to inoculate a 50 mL flask culture containing 5 mL of TSB medium, which was grown for 24 h at 30 °C and 130 rpm. Then, a second subculture at 10 % (v/v) was carried out on 30 mL MIT mineral medium, which was incubated 12 h at 30 °C and 130 rpm. Finally, cells from this second subculture were used to inoculate a last subculture at 10 % (v/v) culture flask containing 300 mL of the MIT mineral medium, which was also incubated 12 h at 30 °C and 130 rpm (**Figure 5**).

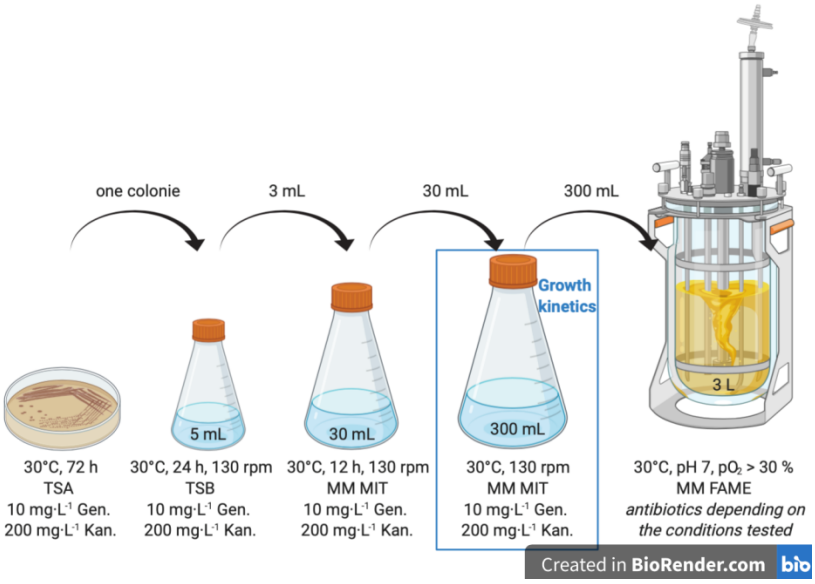

Figure 5: Precultures scheme on fructose for bioreactor cultures

2.2.2 Flask cultivations on fructose

For preliminary experiments in flasks, broth samples were taken regularly during the last subculture step consisting in a 2 L-culture flask inoculated at 10 % (v/v) and containing 300 mL of the MIT mineral medium, which was incubated at 30 °C and 130 rpm (**Figure 5**).

For the induction of isopropanol production, arabinose was added at 75 % of the targeted maximal OD, which was 1 in our culture conditions with the MM MIT, with a 1 $g \cdot L^{-1}$ pulse of arabinose.

2.2.3 Plasmid curing subcultures in flasks

The last subculture step was considered as the positive control for reference fluorescence intensity distribution (**Figure 6**). The next subculture, and all the others that followed, were started by a tenfold dilution in flask mineral medium without any antibiotics and grown at 37 °C and 110 rpm until an OD_{600nm} of 0.5 was reached.

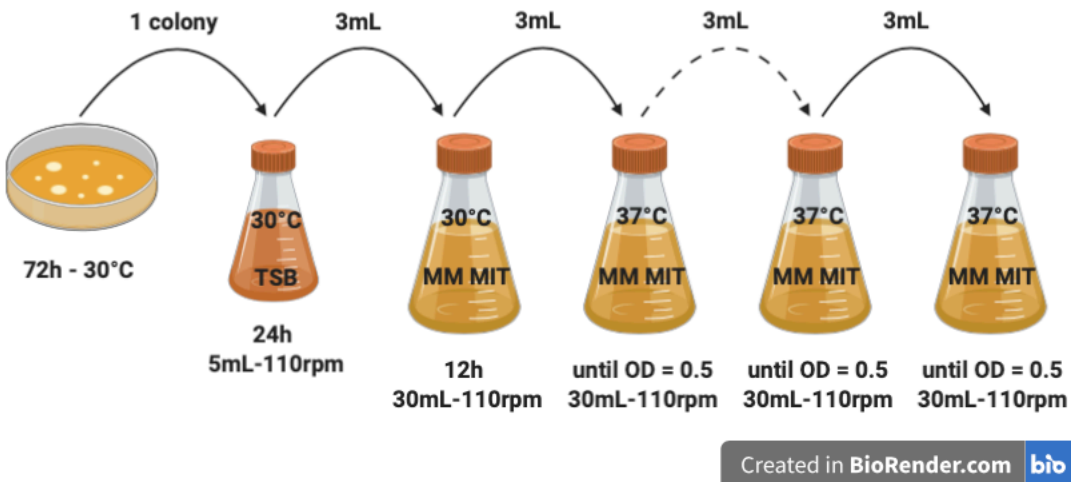

Figure 6: Preculture scheme for supra-optimal plasmid curing

2.2.4 Bioreactor inoculation

For bioreactor inoculation, a 300 mL inoculum from the last preculture step (**Figure 5**), was used to inoculate the bioreactor at an initial biomass concentration close to 0.1 $g_{CDW} \cdot L^{-1}$. The three successive subcultures of the pre-culture were incubated in these same conditions for all fermentations to obtain well-standardized inoculums.

2.3 Bioreactor fermentations

2.3.1 Experimental set-up

Batch and fed-batch cultures were led in a 5 L stainless-steel stirred tank bioreactor (BIOSTAT® Bplus, Sartorius, Germany) (3 L working volume). Continuous bioreactor cultures were carried out in 1.6 L stainless-steel stirred tank bioreactor (BIOSTAT® Bplus, Sartorius, Germany) (1 L working volume). Both stirred tank types were fitted with two six-bladed Rushton impellers and four equally spaced baffles. The system is equipped with control systems of pH (pressurized gel-filled pH electrode, Mettler Toledo, Columbus, OH, USA), temperature, partial pressure of dioxygen (pO_2) (optical oxygen sensor InPro 6860i, Mettler Toledo, Columbus, OH, USA), agitation speed and air flow rate. Regulation, monitoring and data acquisition were done using MFCS/win 2.1 software package (Sartorius, Göttingen, Germany). Each culture was operated and automatically controlled with the BIOSTAT® Bplus control tower.

2.3.2 Process control and regulation

Temperature was regulated at 30 °C by fluid circulation in the jacket surrounding the reactor. A pH 7 was maintained by automatic addition of a 4 M potassium hydroxide solution and a diluted twofold commercial solution of 85 % H_3PO_4 (about 7.3 M). Temperature and pH regulation systems consist of probes and electrodes linked to PID controller modules managed by the MFCS/win 2.1 software.

Strict aerobic conditions throughout the batch cultures were ensured by maintaining partial oxygen pressure (pO_2) higher than 30 % of saturation. During batch and fed-batch fermentations, agitation and aeration rates were increased manually from 300 to 1400 rpm and 0.3 to 2 $L \cdot min^{-1}$ respectively (depending on culture conditions). During continuous fermentation, pO_2 was stabilized around 30% of saturation by maintaining agitation and aeration rates at constant levels.

Antifoam (Polypropylene Glycol, PPG) was periodically added by means of a peristaltic pump (controlled pulse-based addition), one pulse every 30 min.

Incoming gas crossed a PTFE membrane filter of 0.2 µm pore size (Midisart®, Sartorius). The pH probe was calibrated before sterilization using standard buffer solutions at pH4 and 7. Calibration of the dissolved oxygen probe was carried out after sterilization at a pO_2 of 100 % in the bioreactor. The culture vessel was inoculated with 300 mL of exponentially growing pre-culture, by means of a stainless-steel cannula.

2.3.3 Gas analysis

During fermentation cultures, inlet and outlet gas compositions were measured by a fermentation gas monitor system (LumaSense Technologies Europe). This device is composed of a multipoint sampler 1309 (INNOVA 1309) combined with a gas analyzer (INNOVA 1313). Regular and precise measurements of both oxygen (O_2) and carbon dioxide (CO_2) molar fractions are achieved by magneto-acoustic and photo-acoustic spectroscopic methods. Gas analysis data were recorded every minute throughout fermentations with the BZ 6003 software. The gas analyzer was calibrated before each experiment to ensure accuracy of measurements using a standard gas mixture composed of 5% CO_2 and 10% O_2.

When isopropanol was produced, an "isopropanol trap" was placed between the output of the condenser and the entrance of the INNOVA gas analyzer. Two hermetic Schott flasks in a series, filled with osmosis water and kept on ice, allowed re-dissolving isopropanol and acetone in water. Plus, this assembly allowed diluting the output airflow with gaseous nitrogen before analysis by the INNOVA gas analyzer.

2.3.4 Batch cultivations

The mineral medium FAME composed only of the macro-elements was sterilized in the bioreactor by autoclaving for 20 min at 121 °C. After cooling, pre-sterilized stock solutions of oligo-elements, antibiotics (if necessary) and glucose (500 $g \cdot L^{-1}$) were injected into the bioreactor, via a septum using sterile syringes, according to their concentrations presented in **Table 4**.

2.3.5 Fed-Batch cultivations

When nitrogen exhaustion was reached in the MM FAME (corresponding to 4 $g_{CDW} \cdot L^{-1}$ biomass), nitrogen (ammonium, NH_3) was fed in the bioreactor through calibrated peristaltic pump with an exponential flow rate set at 0.04 h^{-1}. This growth rate corresponded to the one set for previous isopropanol producing conditions (Grousseau *et al.* 2014, Marc *et al.* 2017). Nitrogen was the limiting substrate in the fed-batch phase.

Two strategies were developed for fructose feeding during the fed-batch cultures:

1) **Fructose pulse strategy**: when fructose concentration reached 20 $g \cdot L^{-1}$, a pulse to reach 50 $g \cdot L^{-1}$ of fructose was led.

2) **Continuous feeding strategy**: when fructose concentration reached 20 g·L^{-1}, fructose was fed in the bioreactor through calibrated peristaltic pumps to maintain a concentration of 20 g·L^{-1}. The feeding flow rate was calculated as follows.

$$\Rightarrow Q_{fructose,in} = \frac{\mu \cdot X_0 \cdot V_0 \cdot e^{\mu \cdot t}}{Y_{\frac{S}{X}} \cdot (S_{alim} - S_{res})} \quad \textbf{(Eq. 1)}$$

The limiting substrate controlling the evolution of the growth rate was nitrogen, which was added through an ammonium feeding solution. In fed-batch phase, the residual nitrogen concentration in the bioreactor and the maintenance factor are null and both the yield and the growth rate are constant. So, to calculate the feeding flow rate to reach the desired growth rate, the following equations are used:

$$\Rightarrow Q_{NH_3,in} = \frac{\mu \cdot X_0 \cdot V_0 \cdot e^{\mu \cdot t}}{Y_{\frac{N}{X}} \cdot (N_{alim} - N_{res})} \quad \textbf{(Eq. 2)}$$

2.3.6 Continuous cultures

Fructose-limited chemostat culture was carried out by feeding the bioreactor with fresh medium (MM FAME supplemented with 10 g·L^{-1} fructose) through a calibrated peristaltic pump at a defined constant flow rate. The working volume was kept constant at 1 L by removing the overflow medium by means of a stainless-steel cannula placed at the upper level of the culture. The outflow cannula was connected to a peristaltic pump operating at a slightly higher rate than the inflow pump. Steady state conditions were reached after at least five residence times. The steady state phase was assessed through constant measurements of biomass and residual fructose concentrations, as well as stable compositions of the exhaust gases. Dilution rate was set at either at 0.05 h^{-1} or 0.1 h^{-1}.

2.3.7 Sampling procedure description

Offline analyses were achieved on culture samples as detailed on **Figure 7**.

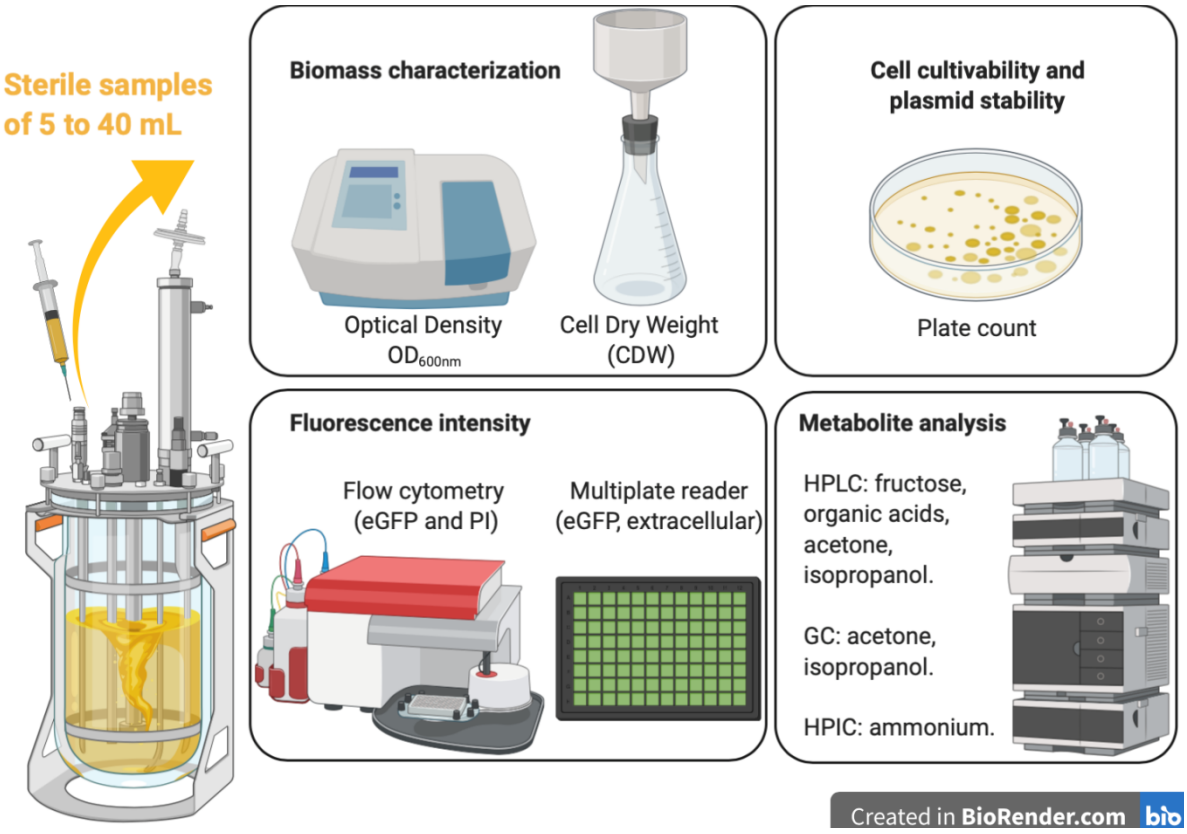

Figure 7: Off-line analysis during bioreactors cultures

For each mode of culture (batch, fed-batch or continuous), a different sampling procedure was adopted:

- *Batch*: samples were taken at approximately 2 – 3 h intervals all along the culture (**Figure 7**).
- *Fed-batch*: samples were taken at approximately 3 – 4 h intervals all along the culture (**Figure 7**).
- *Chemostat*: Steady state establishment was verified after at least five residence time and by stabilization of the state variables concentrations and off-gas composition. Steady state phase was characterized by taking-up one to three samples per day (approximatively every 8 h) during at least five residence times. For the deccelerostat experiment, samples were taken every 2 h. Samples of 5 mL were taken and characterized using the same measurements as described in **Figure 7**.

3 Analytical procedure

3.1 Biomass characterization

3.1.1 Optical density

Biomass growth was monitored by measuring optical density at 600 nm (OD_{600nm}) using a visible spectrophotometer (DR3900, Hachlange, Loveland, Colorado, USA) with a 2 mm path length absorption cell (Hellma). Culture samples were diluted so that the absorbance reading was within the linear working range of the spectrophotometer (between 0.1 and 0.5 absorbance unit).

3.1.2 Cell Dry Weight

Dry Cellular weight (DCW), expressed in $g \cdot L^{-1}$, was determined by gravimetry. A defined volume of culture medium was harvested and filtrated through a 0.2 µm pore-size pre-dried and pre-weighed polyamide membrane (Sartorius, Göttingen, Germany) with a vacuum pump. The membrane was then washed twice with deionized water in order to remove traces of salts, and then dried to a constant weight at 60 °C under partial vacuum (200 mmHg) for 72 h. The dry biomass concentration ($g.L^{-1}$) was calculated by dividing the difference in the weight of the filter over the sample volume. For each sample, the measured biomass was superior to 10 mg in order to meet the precision range scales. OD_{600nm} was calibrated against cell dry weight (CDW) measurements: 2 $g_{CDW} \cdot L^{-1}$ corresponds to 1 unit of OD_{600nm}.

3.1.3 Optical microscopy

Cell broth observations were performed under an Olympus BH-2 microscope (Olympus optical Co., Ltd, Tokyo, Japan). The device allowed several magnifications (x10, x20, x40 and x100) and observations in direct light and contrast phase under oil. This microscope is equipped with a color digital camera (Nikon's Digital System DS-Ri1, Surrey, UK) enabling digital images production of 1280 x 1024 pixels (dimensions: 2200 x 1760 µm² without magnification); the resolution of the instrument allowed observing details in the size of 0.2 µm.

3.2 Plate count

The numeration of cells resistant to gentamicin (Gen^R) and cells resistant to both gentamicin and kanamycin (Gen^RKan^R) was determined by serial and parallel plate count. Serial dilutions were carried out in 9 mL physiological water (0.85 % NaCl) tubes (bioMérieux, Marcy-l'Étoile, France). For every sample, three different dilutions were tested depending on the biomass concentration (generally between 10^{-5} and 10^{-9}). 100 µL of the suitable diluted sample were plated in triplicate using Whitley Automated Spiral Plater *abbr.* WASP (Don Whitley Scientific, Shipley, UK). Two kinds of plates were

used: TSA with only 10 $mg \cdot L^{-1}$ gentamicin and TSA with both 10 $mg \cdot L^{-1}$ gentamicin and 200 $mg \cdot L^{-1}$ kanamycin. Plate count method is based on the ability of plasmid bearing-cells to grow on a selective medium. In our case, *Cupriavidus necator* is resistant to gentamycin intrinsically. As said beforehand, kanamycin resistance is encoded on the pKRSF1010 backbone and on the pBBAD backbone. So, all plasmid-bearing cells are resistant to kanamycin. As a result, we consider that cells that are able to grow under selective pressure of both gentamycin and kanamycin are *C. necator* plasmid-bearing cells.

For **parallel plate count**, the same cell sample was plated on both kinds of antibiotic conditions. Parallel plate count quantification gives access to cell cultivability of the whole population (Gen^R) and the plasmid-bearing population (Gen^R + Kan^R) in the bioreactor.

For **serial plate count,** the cell sample was plated only on TSA with gentamicin plates. After growth, for every cell sample considered, 50 colony forming units (CFU) were stung with sterile toothpicks on TSA plates with both gentamicin and kanamycin.

The plates were then incubated at 30 °C during 72 h and CFU were counted manually. Serial plate count quantification gives access to cultivability of total cells in the bioreactor and evaluates the number of plasmid-expressing cells among the cultivable population.

3.3 Flow Cytometry

During fermentation, cell permeability after staining cells with fluorescent dyes and eGFP fluorescence was monitored by flow cytometry measurements.

3.3.1 Working principle of the flow cytometer

Flow cytometry is a laser-based device enabling the characterization of single-cells from light scattering and fluorescence analysis. Individual cells pass in single-file through a focused fluid stream. Scattered light and fluorescence emissions generated by every single-cell are collected by excitation lasers and detectors and transmitted to a computer for data analysis by suitable software.

In general, a flow cytometer is composed of the following main units: the light source, the flow cell, the hydraulic fluidic system, several optical filters, a group of detectors and a data processing unit (Chapman *et al.* 2000, Givan *et al.* 2001, Shapiro *et al.* 2003, Robinson *et al.* 2004, Bergquist *et al.* 2009, Diaz *et al.* 2010) (**Figure 8**).

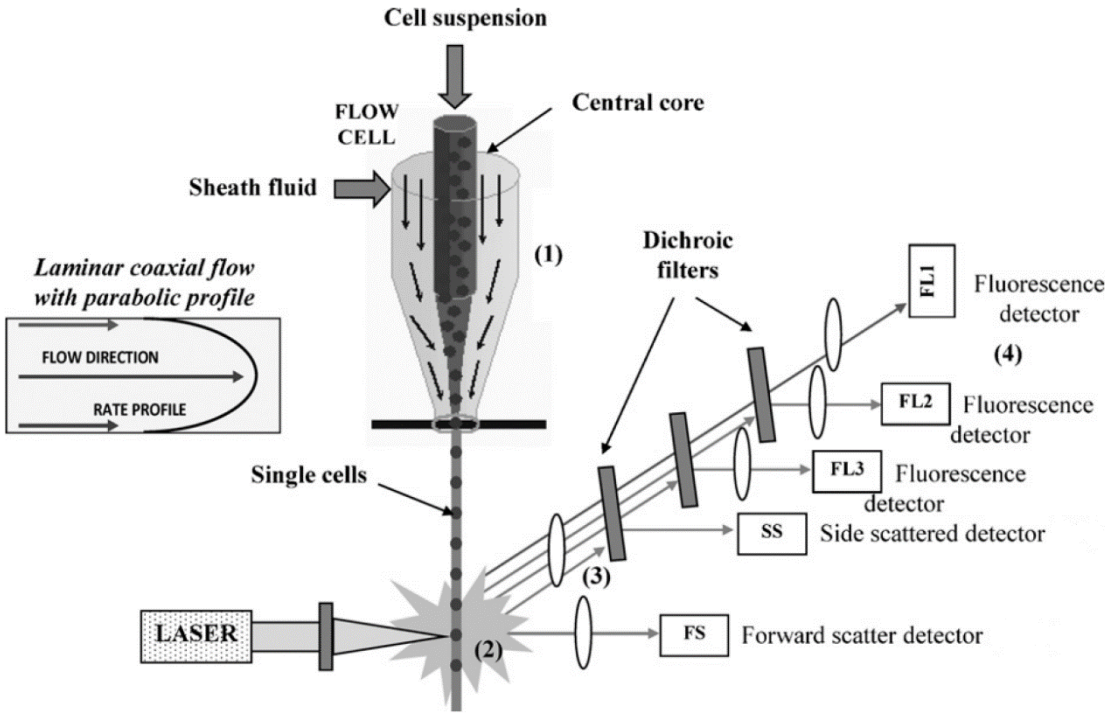

Figure 8: Simplified representation of a common flow cytometer setup (Diaz *et al.* 2010)

The device used during the PhD work was the BD Accuri C6® flow cytometer (BD Biosciences BD Biosciences, Franklin Lakes, NJ, USA). The device was equipped with blue (488 nm) and red (640 nm) excitation lasers. Light scatter was collected from two angles: forward (FSC: 0° ± 13) and side (SSC: 90° ± 13) scatter. FSC and SSC signals are respectively correlated to cell size and granularity. Fluorescence intensity was measured by four detectors (Photomultipliers/PMT): FL1 (533 ± 30 nm), FL2 (585 ± 40 nm), FL3 (>670 nm), and FL4 (675 ± 25 nm) bandpass/long pass optical filter/photomultiplier detector systems. The optical bench of the BD Accuri C6® flow cytometer is shown in **Figure 9**.

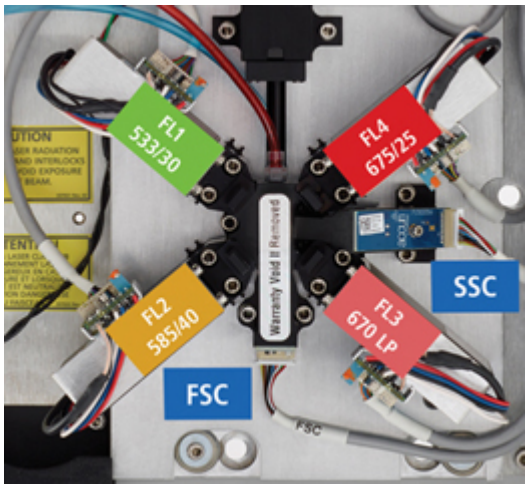

Figure 9: BD Accuri C6® optical configuration

3.3.2 Experimental protocol for population heterogeneity assessment

The use of fluorescent dyes provides additional information about the physiological status of cells. The fluorescent probes propidium iodide (PI) (Molecular probes, Invitrogen, USA) was used. The red fluorescence of the PI signal was collected in the FL3 channel. The reporter protein eGFP was encoded on the heterologous plasmid and so, expressed by plasmid bearing-cells. The green fluorescence of the eGFP signal was collected in the FL1 channel. Spectral properties of the fluorescent molecules studied are summarized in **Table 11**.

Table 11: Characteristics of the fluorescent molecules studied

Dye	Excitation wavelength (λ_{max}) (nm)	Emission wavelength (λ_{max}) (nm)	Emission detector	Cell substrate	Applications
Propidium Iodide (PI)	490	635	FL3	DNA,RNA	Membrane permeability
eGFP (Shaner *et al.* 2005)	488	507	FL1	N/A	Plasmid encoded reporter protein

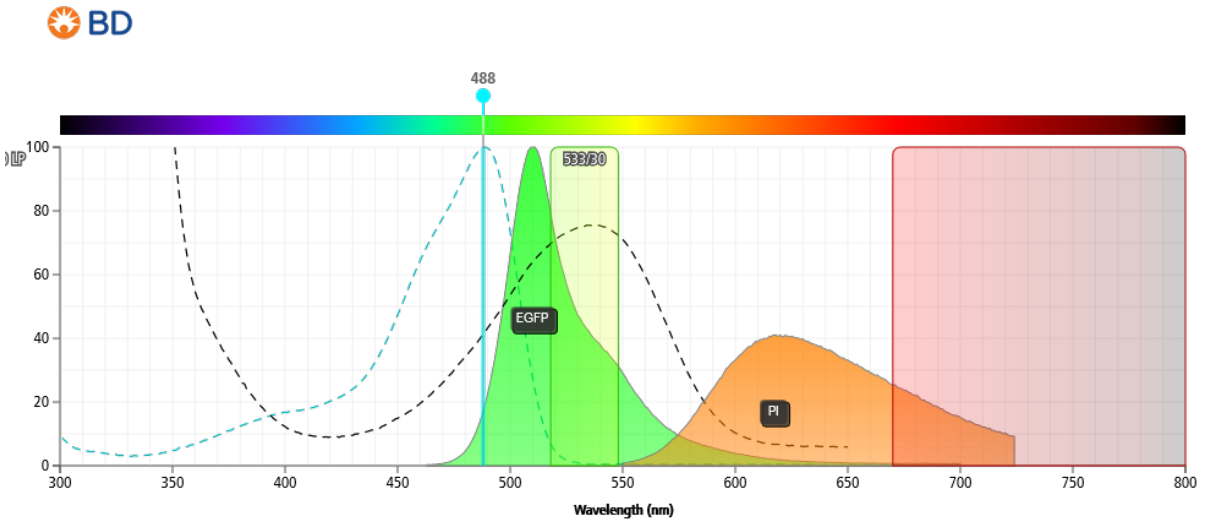

Figure 10 : Excitation and emission spectrum of eGFP and PI, as enabled by the flow cytometry Accuri C6 with excitation by the blue laser. Green curve, eGFP emission spectra; blue dotted curve, eGFP exctitation spectra; green rectangle, FL1 emission filter range; orange curve, PI emission spectra; black dotted curve, PI excitation spectra; red rectangle, FL3 emission filter range (from BD Spectrum Viewer)

Propidium iodide *abbr.* PI (Ref. P3566, Molecular probes, Invitrogen, USA) was used to evaluate membrane permeability as cell viability indicator. Commercial solution was used directly and was composed of 1 $mg \cdot mL^{-1}$ PI in water.

N.B. In this work, the expression “cell permeability” is used through misuse of language to describe that cells are permeable to propidium iodide.

First, culture samples were diluted in NaCl 0.9 % to reach approximately a cell concentration of 10^6 cells·mL^{-1}. Then, cells were stained by 20 µL of PI working solution and incubated for 20 min at room temperature in the dark. A 100 % dead–cell control was prepared by incubating cells in 70 % isopropanol for 1 h at room temperature. Sample runs were performed (until 20, 000 events were counted) at the slow flow-rate setting (14 µL·min^{-1}) using Milli-Q grade water (18.2 mΩ-cm resistance) as sheath fluid. For all sample analysis, the FSC signal (threshold: 12, 000) and SSC signal (threshold: 2, 000) were used as trigger channels. Green fluorescence of eGFP was collected in the FL1 channel and red fluorescence of PI in the FL3 channel. Data acquisition was performed with BD Accuri CFlow® software. Data processing was achieved with FlowJo software (Becton Dickinson, Sparks, MD, USA).

3.4 Fluorescence Activated Cell Sorting (FACS)

Cell sorting experiments were led on the MoFlo Astrios EQ cell sorter using the Summit v6.3 software (Beckman Coulter, Brea, CA, USA). Cell sorting was conducted with a 70 µm nozzle and 60 psi operating pressure. The sorting speed was set around 30, 000 events per second. The single cell mode for the sort mode and 0.5 drop for the droplet envelope were chosen. Cell samples were diluted in NaCl 0.9 % prior to the sorting experiment.

Based on the FSC-Height vs FSC-Area (488 nm laser) plot and the SSC-Height vs SSC-Area (488 nm laser) plot, single cells (singulet) with similar cell size and granularity were first selected. Then, based on the histogram of the eGFP fluorescence (488 nm laser, 526/52 filter), single cells were sorted depending on their fluorescence intensity.

Black and transparent Nunclon® 96-well plates (ThermoFisher, Waltham, MA, USA) were used for single-cell cultivations on plates after cell sorting. Every single cell was dropped in a well in 96-well plates. For each cell subpopulation, a total amount of six 96-well plates were generated, as described in the following figure (**Figure 11**).

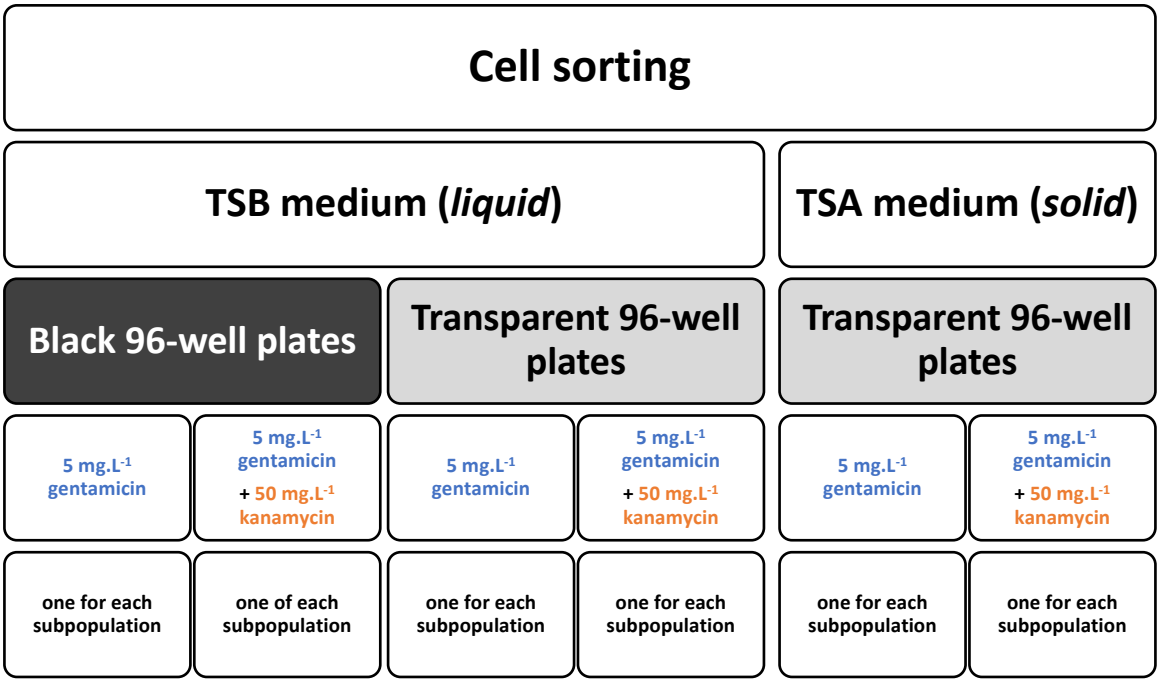

Figure 11: Plates repartition after cell sorting of subpopulations depending on medium, antibiotic composition and plate color

The TSB liquid plates were incubated at 30 °C and 40 rpm. Measurements of optical density and fluorescence unit were achieved every 8 h. For every TSB liquid plate, when the exponential phase was reached and around 7 cell generations, the fluorescence intensity distribution was determined in every well, by flow cytometry.

The TSA solid plates were incubated at 30°C. After growth, CFU were counted and observed under blue light with a Blue Light Transilluminator (ThermoFisher, Waltham, MA, USA) to reveal the green fluorescent colonies.

3.5 Fluorescence measurement in the medium

The extracellular fluorescence intensity in the medium was also measured. Broth samples were centrifuged 3 min at 13000 rpm with a MiniSpin® table-top microcentrifuge (Eppendorf, Hamburg, Germany). Then, 200µL of raw supernatant were poured in Black Nunclon® 96-well plates (ThermoFisher, Waltham, MA, USA). Fluorescence unit measurements were achieved with the Synergy™ HT (Biotek®, Winooski, VT, USA) at excitation wavelength 485 ± 20 nm and emission wavelength 525 ± 20 nm; the sensitivity of the device was set at 75. The control sample was constituted of osmosis water.

3.6 Determination of fructose, organic acids and ammonium concentrations

First, 1 mL broth samples were centrifuged (MiniSpin, Eppendorf, USA) in Eppendorf tubes at 13,400 rpm for 3 min. Then, supernatants were filtered on Minisart filters with 0.2 µm pore diameter polyamide membranes (Sartorius, Germany). Finally, supernatant samples were diluted (when required) with Milli-Q grade water (18.2 mΩ-cm resistance). In all chromatographic analysis, samples were processed following this protocol.

3.6.1 High-performance liquid chromatography (HPLC)

During fermentation and flask cultures, fructose, organic acids (acetate, acetoacetate, citrate, pyruvate and succinate), acetone and isopropanol concentrations were quantified by high performance liquid chromatography (HPLC).

Equipment description and operating conditions

The device used was a Dionex UltiMate 3000 HPLC system (California, USA) and was instrumented with: an autosampler (Dionex Ultimate Autosampler UHPLC+ focused), a pump (Ultimate 3000 Pump), a pre-column (Micro-Guard IG Cation H, BIO-RAD), a column Aminex HPX-87H$^+$ (Bio-RAd, US), an UV detector (Ultimate 3000 Photodiode Array Detector), a refractometer (Shodex RI-101) and a software system for data acquisition and processing (Chromeleon, Chromatography Management System version 6.80).

Separation of compounds of interest on the Aminex HPX-87H$^+$ column was performed using a 2.5 mM sulfuric acid (H_2SO_4) eluent under isocratic conditions. The flow rate of the mobile phase was set at 0.5 mL/min. The column temperature was set at 50 °C and the processed samples were kept in the HPLC autosampler at 8 °C. The injected sample volume was 20 µL and the running time of the chromatographic method was 35 min. Organic acid detection was performed using dual UV and refractive index (RI) detectors. Fructose, acetone and isopropanol concentrations were quantified employing the refractive index (RI) detector.

Experimental protocol

A standard stock solution containing the molecules studied at precise concentration was prepared with Milli-Q grade water in a gauged flask. The standards used for metabolite detection and quantification were fructose, acetate, acetoacetate, pyruvate, citrate, succinate, citrate, acetone and isopropanol. The stock solution was composed of 40 g·L^{-1} of glucose, 5 g·L^{-1} of each organic acid, 4 g·L^{-1} acetone and 30 g·L^{-1} isopropanol. From this stock solution, 1:2, 1:4, 1:8, 1:16 and 1:32 (v/v) dilutions were made in order to establish a 6-point calibration curve. The retention time, the concentration range and the appropriate detector for each compound are shown in **Table 12**.

Table 12: Retention times and concentration ranges of the compounds quantified by HPLC

Compound	Retention time (min)		Concentration range ($g \cdot L^{-1}$)
	UV	RI	
Citrate	9.4	9.7	0.16 - 2.5
Pyruvate	11	10.9	0.16 - 2.5
Fructose	X	12	1.25 - 20
Succinate	13.9	14.3	0.16 - 2.5
Acetoacetate	16.6	17	0.16 - 2.5
Acetate	18	18.4	0.16 - 2.5
Acetone	X	27.8	0.13 – 2.0
Isopropanol	X	28.5	0.94-15.0

To check for system stability and quality of analysis, calibration standards were injected at the beginning and at the end of the sequence analysis. In addition, one standard solution was analyzed after every 15 samples of the sequence.

3.6.2 Gas chromatography (GC)

The concentrations of the volatile compounds, acetone and isopropanol, were quantified by gas chromatography. Samples were prepared by mixing 1 volume of internal standard with 4 volumes of supernatant sample. The internal standard was composed of 5 $g \cdot L^{-1}$ propionic acid diluted in sulfuric acid (H_2SO_4) at 0.2 N.

Equipment description and operating conditions

The device used was a GC system 6890A Series (Hewlett Packard®, USA) and was instrumented with: an autosampler, a pump, an oven, a column SupelQ-Plot 30 x 0.53mm (ID), a flame ionization detector (FID), an injector 6890 Series Injector (Agilent Technologies, USA), a software system for data acquisition and processing (Chromeleon, Chromatography Management System version 6.80).

Separation of studied molecules on the SupelQ-Plot 30 x 0.53mm (ID) column was performed using nitrogen as gas vector at 3 $mL \cdot min^{-1}$. The carrier flow was composed of 300 $mL \cdot min^{-1}$ air and 30 $mL \cdot min^{-1}$ H_2. The injector and detector temperature were both set at 250 °C. The oven temperature gradient during sample analysis (total of about 15 min) was programmed as follows:

120 °C (1 min) → 210 °C (10 °C/min) → 240 °C (40°C/min) → 120 °C

The running time of the chromatographic method was set at 12 min. The remaining 3 min were mean to prepare the device for the analysis of the next sample.

Experimental protocol

Standard stock solutions were prepared as described above. The stock solution was composed of 4 $g \cdot L^{-1}$ acetone and 30 $g \cdot L^{-1}$ isopropanol. From this stock solution, 1:4, 1:8, 1:16, 1:32 and 1:64 (v/v) dilutions were made in order to establish a 6-point calibration curve. 4 volumes of standards solution were mixed with 1 volume of internal standard leading to a concentration of 1 $g \cdot L^{-1}$ of propionic acid in the final standard sample. The retention time and the concentration range for each compound are shown in **Table 13**.

Table 13: Retention times and concentration range of the compounds quantified by GC

Compound	Retention time (min)	Concentration range
Acetone *in standard solution*	6.42	0.08 - 1
Isopropanol *in standard solution*	6.72	0.52-8

To check for system stability and quality of analysis, calibration standards were injected at the beginning and at the end of the sequence analysis. In addition, one standard solution was analyzed after every 15 samples of the sequence. Plus, a blank sample was analyzed before every 5 samples analyzed.

3.6.3 High Pressure Ionic Chromatography (HPIC)

The concentration of ammonium in the culture medium was quantified through ionic chromatography by conductimetry. Supernatant samples were diluted (from 1:100 to 1:10,000) with Milli-Q grade water (18.2 mΩ-cm resistance). This high dilution aims to reduce the number of ions coming from salts in the medium that could interfere with the sensitivity of the analysis.

Equipment description and operating conditions

The device used was Dionex ICS-2100 RFIC (Dionex, USA) and was instrumented with: an autosampler (AS autosampler, Dionex), a pump (SP, Dionex), a pre column IonPac™ CG16, RFIC™ (3x250mm), a column IonPac™ CS16 (RFIC™, 3x50mm), an ion suppressor CERS 500 (2 mm, Thermo Scientific, USA), a heated conductivity cell detector DS (Dionex, USA), and a software system for data acquisition and processing (Chromeleon, Chromatography Management System version 6.80).

Separation of studied molecules on the IonPac™ VS16 column was performed using a 30 mM metanesulfonic acid (MSA) eluent under isocratic conditions. The flow rate of the mobile phase was set at 0.36 $mL \cdot min^{-1}$. The column temperature was set at 40 °C and the processed samples were kept

in the HPIC autosampler at 8 °C. The injected sample volume was 20 µL and the running time of the chromatographic method was 25 min. The current in the ion suppressor was set at 40 mA.

Experimental protocol

A standard stock solution containing ammonium through NH_4Cl at a concentration of 1 $g \cdot L^{-1}$ was added to a nitrogen-depleted-FAME mineral medium. From this stock solution, 1:10, 1:20, 1:40, 1:50 and 1:100 (v/v) dilutions were made in order to establish a 6-point calibration curve (*i.e.* second-degree polynomial). The retention time and the concentration range for each compound are shown in **Table 14**.

Table 14: Retention times and concentration range of the compounds quantified by HPIC

Compound	Retention time (min)	Concentration range ($mg \cdot L^{-1}$)
NH_4^+	9.37	0.1-100

To check for system stability and quality of analysis, calibration standards were injected at the beginning and at the end of the sequence analysis. In addition, one standard solution was analyzed after every 15 samples of the sequence.

4 Methodologies for data treatment

4.1 Rate expression for gas-phase reactions

Oxygen consumption rate r_{O2} and carbon dioxide production rate r_{CO2} were calculated from the mass balances in the gas and liquid phases. For this purpose, the following parameters were taken into account: inlet and outlet molar gas compositions, temperature, pH, salinity, and liquid volume in the bioreactor. The reactor system illustrated in the **Figure 12** is considered for gas balance calculations.

Plan of the system

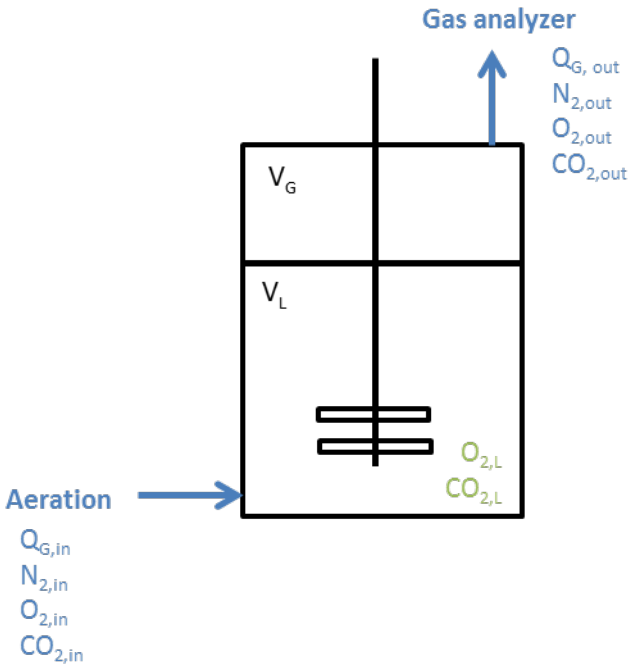

Figure 12: Reactor system and corresponding annotations for balances on gas-phase

4.1.1 Nitrogen balance

Nitrogen (N_2) is an inert gas, meaning that N_2 is not consumed nor produced by microorganism. So, in the liquid phase N_2 is only implicated in transfer phenomenon without any conversion. Knowing that nitrogen is only slightly soluble in the liquid phase, the term $\frac{dN_{2,L}}{dt}$ can be neglected. So, the global nitrogen transfer flow term can be neglected as well. Therefore, the nitrogen balance allows estimating the outlet gas flow rate $Q_{G,out}$ from the measurements of the inlet gas flow rate $Q_{G,in}$, nitrogen fractions in the inlet $N_{2,in}$ and outlet $N_{2,out}$ gas streams.

Calculation of the azote fraction in the inlet and outlet gas

The gas analyzer INNOVA 1313 does not quantify argon and azote in gas from fermentation. So, the molar fraction of nitrogen in the inlet and outlet gas throughout the fermentation can be expressed with the following system, from molar fractions of oxygen, carbon dioxide and argon:

$$\begin{cases} \mathbf{1} = \boldsymbol{O_2} + \boldsymbol{CO_2} + \boldsymbol{Ar} + \boldsymbol{N_2} \\ \dfrac{\boldsymbol{Ar}^{\boldsymbol{dry\ air}}}{\boldsymbol{N_2}^{\boldsymbol{dry\ air}}} = \dfrac{\boldsymbol{Ar}}{\boldsymbol{N_2}} \end{cases} \Rightarrow \boldsymbol{x_{N_2}} = \frac{\mathbf{1} - \boldsymbol{O_2} + \boldsymbol{CO_2}}{\mathbf{1} + \dfrac{\boldsymbol{Ar}^{\boldsymbol{dry\ air}}}{\boldsymbol{N_2}^{\boldsymbol{dry\ air}}}} \qquad \textbf{(Eq. 3)}$$

With: $\frac{Ar^{dry\ air}}{N_2{}^{dry\ air}} 1.19 \cdot 10^{-2}$

Calculation of the outlet gas flow

The mass conservation equation of nitrogen in the bioreactor can be written like:

Accumulation = Exchange flow + Reaction **(Eq. 4)**

⇨ Accumulation = [Inlet – Outlet] + [Production – Consumption]

When replacing the terms of the equation and taking into account the liquid and gaseous phases:

$$\frac{d}{dt}(N_{2,L} \cdot V_L) + \frac{d}{dt}(N_{2,G} \cdot V_G) = Q_{G,in} \cdot N_{2,in} - Q_{G,out} \cdot N_{2,out} + r_{N_2} \cdot V_L \quad \textbf{(Eq. 5)}$$

As written above, nitrogen is barely soluble in liquid phase, so: $r_{N_2} \cdot V_L = \frac{d}{dt}(N_{2,L} \cdot V_L) = 0$

$$\frac{d}{dt}(N_{2,G} \cdot V_G) = Q_{G,in} \cdot N_{2,in} - Q_{G,out} \cdot N_{2,out} \quad \textbf{(Eq. 6)}$$

$$\Rightarrow Q_{G,out} = \frac{Q_{G,in} \cdot N_{2,in} - \frac{d}{dt}(N_{2,G} \cdot V_G)}{N_{2,out}}$$

An approximation can be made:

$$\frac{d}{dt}(N_{2,G} \cdot V_G) = \frac{{N_{2,out}}^{t_{n+1}} \cdot {V_G}^{t_{n+1}} - {N_{2,out}}^{t_n} \cdot {V_G}^{t_n}}{t_{n+1} - t_n} \quad \textbf{(Eq. 7)}$$

4.1.2 Dioxygen balance

Dioxygen is present under dissolved form in the culture medium. Dissolved oxygen measurements are given by the value of oxygen partial pressure, pO_2.

Calculation of dissolved oxygen

At atmospheric pressure P_{atm} and 30°C, the maximal solubility of dioxygen in water is equal to: $[O_{2,L}]^* = 7.7 mg \cdot L^{-1}$ and $pO_2{}^* = 100\ \%$.

So, the dioxygen concentration in the medium during fermentation can be expressed (in $mg \cdot L^{-1}$) as follows:

$$\frac{pO_2}{pO_2^*} = \frac{[O_{2,L}]}{[O_{2,L}]^*} \Rightarrow [\boldsymbol{O_{2,L}}] = \frac{\boldsymbol{pO_2}}{\boldsymbol{pO_2^*}} \cdot [\boldsymbol{O_{2,L}}]^* \quad \textbf{(Eq. 8)}$$

Mass balance

The mass balance equation on dioxygen in the liquid and gaseous phase can be expressed as follows:

<u>In the liquid phase</u>:

$$\frac{d}{dt}(O_{2,L} \cdot V_L) = r_{O_{2,L}} \cdot V_L + \phi_{O_{2,L}} \quad \textbf{(Eq. 9)}$$

<u>In the gaseous phase</u>:

$$\frac{d}{dt}(O_{2,G} \cdot V_G) = r_{O_{2,G}} \cdot V_G + \phi_{O_{2,G}} \quad \textbf{(Eq. 10)}$$

As dioxygen is not consumed, nor produced in the gaseous phase:

$$r_{O_{2,G}} \cdot V_G = 0\ mol \cdot h^{-1} \quad \textbf{(Eq. 11)}$$

So, the mass balance equation on dioxygen in the gaseous phase becomes:

$$\frac{d}{dt}(O_{2,G} \cdot V_G) = \phi_{O_{2,G/L}} + Q_{G,in} \cdot O_{2,in} - Q_{G,out} \cdot O_{2,out} \quad \textbf{(Eq. 12)}$$

The gas-liquid transfer flow is presumed to be equal in both of these equations:

$$-\phi_{O_{2,L}} = \phi_{O_{2,G/L}} \quad \textbf{(Eq. 13)}$$

So:

$$r_{O_{2,L}} \cdot V_L - \frac{d}{dt}(O_{2,L} \cdot V_L) = -Q_{G,in} \cdot O_{2,in} + Q_{G,out} \cdot O_{2,out} + \frac{d}{dt}(O_{2,G} \cdot V_G) \quad \textbf{(Eq. 14)}$$

$$\Rightarrow r_{O_{2,L}} = \frac{Q_{G,out} \cdot O_{2,out} - Q_{G,in} \cdot O_{2,in} + \frac{d}{dt}(O_{2,G} \cdot V_G) + \frac{d}{dt}(O_{2,L} \cdot V_L)}{V_L}$$

$k_L a(O_2)$

The global oxygen transfer coefficient in the liquid phase can be calculated as follows:

OTR: Oxygen Transfer Rate = $k_L a_{O_2} \cdot \left([O_{2,L}]^* - [O_{2,L}]\right)$

OUR: Oxygen Uptake Rate = $-r_{O_{2,L}}$

So:

$$\frac{d}{dt}\left(O_{2,L} \cdot V_L\right) = (OTR - OUR) \cdot V_L \quad \textbf{(Eq. 15)}$$

$$\Rightarrow \frac{d}{dt}\left(O_{2,L} \cdot V_L\right) = \left[kLa_{O_2} \cdot \left([O_{2,L}]^* - [O_{2,L}]\right) + r_{O_{2,L}}\right] \cdot V_L$$

4.1.3 Carbon dioxide balance

Calculation of dissolved carbon dioxide

Dissolved CO_2 was not directly measured in the liquid phase. So, it was necessary to deduce its value from the other measured data. In the liquid phase, carbon dioxide is found under various forms depending on the pH and the salinity of the medium: carbon dioxide CO_2, carbonic acid H_2CO_3, bicarbonate ion HCO_3^- and carbonate ion CO_3^{2-}. In the FAME medium, the salinity is supposed to be low enough to be neglected. The hydration equilibrium constant K_h and the dissociation constants pKa_1 and pKa_2 for a null ionic force were found in Chemistry of the Elements (2nd ed., 1997) by Alan Earnshaw. The form of CO_2 in solution is thermodynamically controlled by the equilibria shown in the **Table 15**.

Table 15: Chemical Equilibria of carbon dioxide in solution (Millero *et al.* 1995)

Chemical equation	Associated constants (values at 25°C)	
$\boldsymbol{H_2O + CO_2 \overset{K_h}{\Leftrightarrow} H_2CO_3}$	$K_h = \frac{[H_2CO_3]}{[CO_2]}$; $K_h \approx 10^{-3}$	**(Eq.16)**
$\boldsymbol{H_2CO_3 + H_2O \overset{K_{a,1}}{\Longleftrightarrow} HCO_3^- + H_3O^+}$	$K_{a,1} = \frac{[HCO_3^-]\cdot[H_3O^+]}{[H_2CO_3]}$; $pKa_1=6.4$	**(Eq.17)**
$\boldsymbol{HCO_3^- + H_2O \overset{K_{a,2}}{\Longleftrightarrow} CO_3^{2-} + H_3O^+}$	$K_{a,2} = \frac{[CO_3^{2-}]\cdot[H_3O^+]}{[HCO_3^-]}$; $pKa_2=10.3$	**(Eq.18)**
$\boldsymbol{H_3O^+ + HO^- \overset{K_e}{\Leftrightarrow} 2H_2O}$	$K_e = 10^{-14}$	**(Eq.19)**

In conclusion:

$$CO_2 + H_2O \overset{K_h}{\leftrightarrow} H_2CO_3 \overset{K_{a,1}}{\longleftrightarrow} HCO_3^- + H^+ \overset{Ka,_2}{\longleftrightarrow} CO_3^{2-} + 2H^+ \quad \textbf{(Eq.20)}$$

The hydration equilibrium constant K_h is close to 10^{-3}, so most of undissociated dissolved CO_2 is in the dissolved CO_2 form (Millero 1995). So the form H_2CO_3 is present in minor proportions compared to the other forms. The pH has been precisely regulated at 7 during fermentations, so the compound CO_3^{2-} is

present in minor proportions (because pH>pKa_2-2) compared to the other forms. As a result, CO_2 is present under two different forms in the medium: dissolved CO_2 and bicarbonate ion HCO_3^-.

Therefore, the system can be simplified:

$$CO_2 + H_2O \overset{K_{a,1}}{\longleftrightarrow} HCO_3^- + H_3O^+ \quad \textbf{(Eq. 21)}$$

And:

$$K_{a,1} = \frac{[HCO_3^-] \cdot [H_3O^+]}{[CO_2]} \quad \textbf{(Eq. 22)}$$

$$\Rightarrow [\boldsymbol{HCO_3^-}] = \frac{[\boldsymbol{CO_2}] \cdot \boldsymbol{K_{a,1}}}{[\boldsymbol{H_3O^+}]}$$

Assuming Henry's law can be used, the concentration of dissolved CO_2 in the medium is proportional to the partial pressure of CO_2, pCO_2, in the gas above the liquid, so:

$$[\boldsymbol{CO_{2,L}}] = \boldsymbol{p_{CO_2}} \cdot \boldsymbol{H_{CO_2}} \quad \textbf{(Eq. 23)}$$

At 25°C, Henry's constant for carbon dioxide is: $H_{CO_2} = 0.034\ mol \cdot L^{-1} \cdot atm^{-1}$

As previously shown:

$$[CO_{2,tot}] = [CO_{2,L}] + [HCO_{3,L}^-] \quad \textbf{(Eq. 24)}$$

And:

$$[H_3O^+] = 10^{-pH} \quad \textbf{(Eq. 25)}$$

So:

$$[CO_{2,tot}] = [CO_{2,L}] + \frac{[CO_{2,L}] \cdot K_{a,1}}{10^{-pH}} \quad \textbf{(Eq. 26)}$$

$$\Rightarrow [\boldsymbol{CO_{2,tot}}] = \boldsymbol{p_{CO_2}} \cdot \boldsymbol{H_{CO_2}} \cdot \left(\mathbf{1} + \frac{\boldsymbol{K_{a,1}}}{\mathbf{10^{-pH}}}\right)$$

Mass balance

The mass balance equation on carbon dioxide in the liquid and gaseous phase can be expressed as follows:

In the liquid phase:

$$\frac{d}{dt}(CO_{2,L} \cdot V_L) = r_{CO_{2,L}} \cdot V_L + \phi_{CO_{2,L}} \quad \textbf{(Eq. 27)}$$

In the gaseous phase:

$$\frac{d}{dt}(CO_{2,out} \cdot V_G) = r_{CO_{2,G}} \cdot V_G + \phi_{CO_{2,G}} \quad \textbf{(Eq. 28)}$$

As CO_2 is not consumed, nor produced in the gaseous phase: $r_{CO_{2,G}} \cdot V_G = 0\ mol \cdot h^{-1}$

$$\Rightarrow \frac{d}{dt}(CO_{2,out} \cdot V_G) = \phi_{CO_{2,G/L}} + Q_{G,in} \cdot CO_{2,in} - Q_{G,out} \cdot CO_{2,out} \quad \textbf{(Eq. 29)}$$

The gas-liquid transfer flow is presumed to be equal in both of these equations:

$$-\phi_{CO_{2,L}} = \phi_{CO_{2,G/L}} \quad \textbf{(Eq. 30)}$$

So:

$$r_{CO_{2,L}} \cdot V_L - \frac{d}{dt}(CO_{2,L} \cdot V_L) = -Q_{G,in} \cdot CO_{2,in} + Q_{G,out} \cdot CO_{2,out} + \frac{d}{dt}(CO_{2,out} \cdot V_G) \quad \textbf{(Eq. 31)}$$

$$\Rightarrow \boldsymbol{r_{CO_{2,L}} = \frac{Q_{G,out} \cdot O_{2,out} - Q_{G,in} \cdot O_{2,in} + \frac{d}{dt}(CO_{2,out} \cdot V_G) + \frac{d}{dt}(CO_{2,L} \cdot V_L)}{V_L}}$$

From this point, the respiratory quotient (molar ratio) can be calculated:

$$\boldsymbol{RQ = \frac{r_{CO_{2,L}}}{r_{O_{2,L}}}} \quad \textbf{(Eq. 32)}$$

4.2 Volume determination during fed-batch cultures

To process fermentation data from fed-batch bioreactor cultures, special attention must be paid to the variation of the reaction volume. The variations in the volume are due to the adding of substrate solutions, pH correcting solutions and also to broth sample volumes and water evaporation due to the working temperature in the bioreactor. To evaluate the reaction volume throughout fermentation, the

following volumes have to be taken into account: initial, fructose addition, nitrogen addition, pH addition, stock solution addition and sampling. So, the fermentation reaction volume is calculated by supposing that volumes can be added or substracted as described below:

$$V_{ferm} = V_0 + V_{fructose} + V_{NH3} + V_{pH} + V_{addition} - V_{sample} \quad \textbf{(Eq. 33)}$$

Evaporation is calculated from the difference between the volume measured at the end of the experiment and the volume calculated above. The difference calculated is considered as corresponding to the volume of water evaporated all along culture. As a simplified view, the total volume evaporated is then equally shared all along culture.

$$V_{real} = V_{ferm} - V_{evap} \quad \textbf{(Eq. 34)}$$

Experimental values determined with the measured volume during fermentation (Vf_{erm}) can be corrected in comparison to the theoretical fermentation volume (V_{real}) with the volume of liquid evaporated between the beginning and the end of the culture.

4.3 Rate expressions for liquid-phase reactions

Substrate consumption as well as metabolite and recombinant molecules production rates were determined based on their experimental measurements and their respective mass balance equations. Calculations were adapted to the mode of fermentation (batch, fed-batch, chemostat). The general mass conservation equation of the component in the bioreactor can be written as previously described in **Eq. 4**.

When replacing the terms of the equation and taking into account the liquid phase:

Table 16: Mass conservation equation depending of the fermentation conduct

Fermentation Mode	Mass conservation equation	
Chemostat	$\frac{d}{dt}(A \cdot V_L) = r_A \cdot V_L + Q_{A,in} \cdot A_{alim} - Q_{A,out} \cdot A_{res} - Q_{sampling} \cdot A_{res}$	**(Eq. 35)**
Fed-batch	$\frac{d}{dt}(A \cdot V_L) = r_A \cdot V_L + Q_{in} \cdot A_{alim}$	**(Eq. 36)**
Batch	$\frac{d}{dt}(A) = r_A$	**(Eq. 37)**

Where:

- $Q_{A,in}$, $Q_{A,out}$ and $Q_{sampling}$ represent the inlet, outlet and sampling flow rates of compound A, respectively (L/h),

- A_{alim} and A_{res} represent the concentrations of compound A in the feed medium and in the bioreactor, respectively (g/L),
- V_L represents the volume of the liquid phase in the bioreactor (L),
- r_A represents the global reaction rate of compound A (g/L/h).

In batch fermentation mode, the reaction rate of the compound A can directly be determined by the equation: $r_A = \frac{d}{dt}(A)$

In chemostat fermentation mode, a continuous mode was set to reach a steady state phase. So, the concentration of compound A and the volume of the bioreactor are constants $\frac{d}{dt}(A) = 0$ and $\frac{d}{dt}(V_L) = 0$, and the sampling flow rate is null. The inlet and outlet liquid flow rates are equal ($Q_{A,in} = Q_{A,out}$). The reaction rate of compound A can be therefore determined according to the equation:

$$r_A = \frac{Q_{A,out} \cdot A_{res} - Q_{A,in} \cdot A_{alim}}{V_L} = D \cdot (A_{res} - A_{alim}) \quad \textbf{(Eq. 38)}$$

With: D the dilution rate (h^{-1}), expressed as:

$$D = \frac{Q_{A,out}}{V_L} = \frac{Q_{A,in}}{V_L} \quad \textbf{(Eq. 39)}$$

The specific reaction rate of the component A was defined as:

$$q_A = \frac{r_A}{X} \quad \textbf{(Eq. 40)}$$

If the compound A is a substrate, r_A is a global consumption rate and q_A is specific consumption rate. If A is a product, r_A is a global production rate and q_A is specific production rate. In the particular case of biomass, the specific growth rate is expressed as:

$$\mu = \frac{r_X}{X} \quad \textbf{(Eq. 41)}$$

4.4 Determination of instantaneous and overall yields

The yields on the carbon source (fructose) and nitrogen source (ammonium) are determined according to the following equations for biomass, CO_2, isopropanol and acetone:

$$R_{\frac{X}{S},instataneous} = \frac{r_X}{r_S} \; or \; R_{\frac{X}{S},overall} = \frac{\Delta X}{\Delta S} \;\; in \; Cmol_X/Cmol_S \; or \; g_X/g_S \qquad \textbf{(Eq. 42)}$$

$$R_{\frac{X}{NH_3},instantaneous} = \frac{r_X}{r_{NH_3}} \; or \; R_{\frac{X}{NH_3},overall} \frac{\Delta X}{\Delta NH_3} \;\; in \; Cmol_X/Cmol_{NH_3} \; or \; g_X/g_{NH_3} \qquad \textbf{(Eq. 43)}$$

$$R_{\frac{CO_2}{S},instantaneous} = \frac{r_{CO_2}}{r_S} \; or \; R_{\frac{CO_2}{S},overall} = \frac{\Delta CO_2}{\Delta S} \;\; in \; Cmol_{CO_2}/Cmol_S \; or \; g_{CO_2}/g_S \qquad \textbf{(Eq. 44)}$$

$$R_{\frac{IPA}{S},instantaneous} = \frac{r_{IPA}}{r_S} \; or \; R_{\frac{IPA}{S},overall} = \frac{\Delta IPA}{\Delta S} \;\; in \; Cmol_{IPA}/Cmol_S \; or \;\; g_{IPA}/g_S \qquad \textbf{(Eq. 45)}$$

$$R_{\frac{Ac}{S},instantaneous} = \frac{r_{Ac}}{r_S} \; or \; R_{\frac{Ac}{S},overall} = \frac{\Delta Ac}{\Delta S} \;\; in \; Cmol_{Ac}/Cmol_S \;\; or \; in \;\; g_{Ac}/g_S \qquad \textbf{(Eq. 46)}$$

4.5 Carbon and elemental balances

In order to validate experimental data, carbon, nitrogen and degree of reduction balances were calculated for every sample and at the whole fermentation scale, for each experiment. These balances allow verifying that no gross errors occurred in the measurement and no compound was omitted during data interpretation.

4.5.1 Carbon balance

This balance ensures that carbon is conserved, and that no carbonated compound was forgotten. The verification of the carbon balance consists in a compound balance in which every carbonated compound is expressed in Cmol. The formula in Cmol of a carbonated compound corresponds to the raw formula reduced to one carbon atom.

Generally speaking, the global reaction occurring in a bioreactor is written as follows:

$$a \cdot S + b \cdot O_2 + c \cdot NH_3 \;\rightarrow\; X + d \cdot CO_2 + e \cdot H_2O + f \cdot P \qquad \textbf{(Eq. 47)}$$

With: S = substrate; X = biomass; P = product(s) and a, b, c, d, e, f = stoichiometric coefficients of the reaction

In this work, under isopropanol producing conditions the reaction taking into account the carbonated compounds is written:

$$Fructose \rightarrow X + Organic\ Acids + Acetone + Isopropanol + CO_2 \quad \textbf{(Eq. 48)}$$

It is necessary to verify that the inlet carbon brought is equal to the carbon accumulated in the bioreactor (or found under gaseous form) as written as follows in Cmol·L^{-1}·h^{-1} (batch) or Cmol·h^{-1} (fed-batch):

$$r_{Fructose} = r_X + r_{Organic\ Acids} + r_{Acetone} + r_{Isopropanol} + r_{CO_2} \quad \textbf{(Eq. 49)}$$

When integrating this equation on a specific time interval, quantities can be express as concentrations (in batch) or mass (in fed-batch) that have been consumed / produced on this time period.

$$C_{Fructose} = C_X + C_{Organic\ Acids} + C_{Acetone} + C_{Isopropanol} + C_{CO_2} \quad \textbf{(Eq. 50)}$$

The percentage of verification of the carbon balance is given by the following equation:

$$\%Carbon\ balance = \frac{C_X + C_{Organic\ Acids} + C_{Acetone} + C_{Isopropanol} + C_{CO_2} + C_{residual\ fructose}}{C_{Fructose}} \cdot 100 \quad \textbf{(Eq. 51)}$$

4.5.2 Nitrogen balance

An elementary balance can also be made on nitrogen according to the following equation:

$$NH_3 \rightarrow X + eGFP \quad \textbf{(Eq. 52)}$$

As said above for carbon, inlet nitrogen brought is equal to the nitrogen accumulated in the bioreactor as written as follows in Nmol.

$$r_{NH_3} = r_X + r_{eGFP} \quad \textbf{(Eq. 53)}$$

On a specific time interval, quantities can be express as concentrations (in batch) or mass (in fed-batch) that have been consumed / produced on this time period.

$$N_{NH_3} = N_X + N_{eGFP} \quad \textbf{(Eq. 54)}$$

The verification percentage of the nitrogen balance is given by the following equation. These quantities express the concentrations / mass that have been consumed / produced.

$$\%Nitrogen\ balance = \frac{N_X\ +\ N_{NH_3\ residual} + N_{eGFP}}{N_{NH_3}} \quad \textbf{(Eq. 55)}$$

So:

$$\%Nitrogen\ balance = \frac{X \cdot \varepsilon_{C_X}^N + eGFP \cdot \varepsilon_{C_{eGFP}}^N}{N_{NH_3}} \cdot 100 \quad \textbf{(Eq. 56)}$$

4.5.3 Elemental balance

The reduction degree of a compound j with raw formula $CH_{\varepsilon_{C_j}^H} O_{\varepsilon_{C_j}^O} N_{\varepsilon_{C_j}^N}$ is given by the following formula:

$$\gamma_i = \sum_{i=1}^{j} \left(\gamma_i \cdot \varepsilon_{C_j}^i\right) = \gamma_C + \gamma_H \cdot \varepsilon_{C_j}^H + \gamma_O \cdot \varepsilon_{C_j}^O + \gamma_N \cdot \varepsilon_{C_j}^N \quad \textbf{(Eq. 57)}$$

The reduction degree values of the different elements in our system (ammoniac as N source) are the following:

$$\gamma_C = 4$$

$$\gamma_H = 1$$

$$\gamma_O = -2$$

$$\gamma_N = -3$$

To solve this system, the reduction degrees of CO_2, NH_3 and H_2O are fixed at zero.

Instantaneous elemental balance can be expressed as follows, in $Cmol \cdot L^{-1} \cdot h^{-1}$ (batch) or $Cmol \cdot h^{-1}$ (fed-batch):

$$\gamma_{O_2} \cdot r_{O_2} + \gamma_S \cdot r_S = \gamma_X \cdot r_X + \gamma_P \cdot r_P \quad \textbf{(Eq. 58)}$$

By integration on a specific time interval, quantities can be express as concentrations (in batch) or mass (in fed-batch) that have been consumed / produced on this time period.

$$\gamma_X \cdot X + \gamma_P \cdot P = \gamma_S \cdot S + \gamma_{O_2} \cdot O_2 \quad \textbf{(Eq. 59)}$$

The verification percentage of the elemental balance is given by the following equation. These quantities express the concentrations / mass that have been consumed / produced.

$$\%\, Elemental\ balance = \frac{\gamma_X \cdot X + \gamma_P \cdot P}{\gamma_S \cdot S + \gamma_{O_2} \cdot O_2} \cdot 100 \quad \textbf{(Eq. 60)}$$

Where:

- S is for substrate (fructose) concentration in Cmol
- P is for the products (isopropanol, acetone, organic acids) concentrations in Cmol

4.6 Smoothing of experimental data

Smoothing procedure is a data treatment obtained throughout the culture and that presents several aims: to free ourselves from experimental uncertainties and to calculate interpolated, derivative and integral values of the process variables, which would give access to the global reaction rates, specific reaction rates and overall yields characterizing the biological reactions.

For the smoothing, raw fermentation data were converted in amount of substance (expressed in g, mol, Cmol, Nmol depending on the considered substance) in order to free ourselves from volume variations and dilutions due to feeding and sampling. Results were processed using the LIREC software developed in the team. A polynomial regression in a moving window allows the fitting of experimental recorded data to continuous smoothed curves describing the evolution of the data considered during fermentation. The curves describe the evolution of production and consumption rates (first derivative) of the considered compounds.

Reconciliation is a statistical technique that evaluates the data accuracy and attempts to reduce experimental errors in measured variables by checking balances. Smoothed data were reconciled also through the LIREC software. Mass and elemental balances verification allows detecting gross errors in measured data or estimating missing values, and then evaluating the reaction rates that would close these balances. The amount of eGFP produced was thus estimated from reconciled data.

4.7 Statistical analysis: Normality of distribution functions by BoxPlot representation

Boxplots are graphical tools used to represent an empirical distribution through some simple localization parameters: the median (50th percentile), the first (25th percentile) and third quartile (75th percentile). The first and third quartiles respectively represent the bottom and top of the boxplot. The median, or second quartile, is represented by the line inside the box. The interquartile range (IQR) is situated between the first and third quartile and represents the length of the box. The whiskers represent the minimum and maximum values when they are within 1.5 x IQR from both extremities of the box. Values above 1.5 x IQR are considered as outliers and are represented by points. A symmetric boxplot with its median in the middle of the box and same length whiskers might be expected to be normally distributed (Rakotomalala *et al.* 2011).

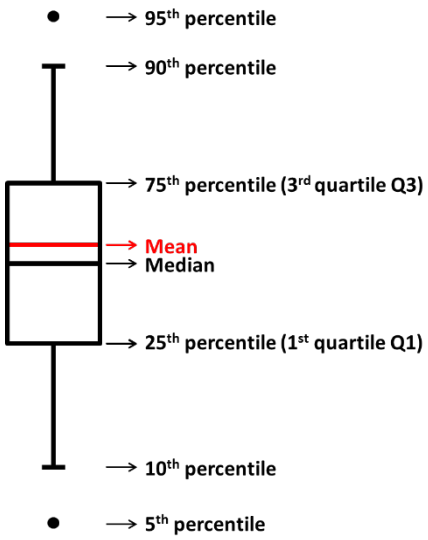

Figure 13: Definition of boxplot representation: The boundary of the box closest to zero indicates the 25th percentile, a black line within the box marks the median, a red line within the box marks the mean, and the boundary of the box farthest from zero indicates the 75th percentile. Whiskers above and below the box indicate the 90th and 10th percentiles. The black dot indicates the 95th and 5th percentiles

Part 3: Results and discussion

Part 3 : Results and discussion

Chapter 1: Plasmid expression stability during heterologous isopropanol production in fed-batch bioreactor

1.1 Abstract

Strain robustness during production of recombinant molecules is of major interest to ensure bioprocess profitability. Population heterogeneity was shown in the literature to be source of bioprocess instability. Thus, population heterogeneity was studied through plasmid stability variations during fermentation. Within the framework of microbial production of chemical molecules, isopropanol was produced by recombinant strains of *Cupriavidus necator*. Plasmid stability was followed by plate count method to evaluate the impact of isopropanol production on plasmid stability, depending on plasmid stabilization systems used for the strain engineering designs. With the reference strain Re233/pEG7c, an isopropanol titer of 15.1 $g{\cdot}L^{-1}$ could be reached. When isopropanol concentration increased, cell permeability increased and plasmid stability significantly decrease leading to a decrease in isopropanol production rates. Bioprocess robustness under isopropanol producing conditions was studied with two plasmid construction strategies (1) Post Segregational Killing *hok/sok* (in Re2133/pEG20) and (2) expression of chaperon proteins *GroESL* (in Re2133/pEG23). Surprisingly, the Re2133/pEG20 strain did not allow a significant improvement of plasmid stability compared to the reference strain. However, a higher proportion of the carbon flow was diverted toward isopropanol (instead of acetone by-product). The strain Re2133/pEG23 allowed minimizing cell permeability and enhancing growth capacities in response to increased isopropanol concentrations. Nevertheless, isopropanol production remained more efficient with the reference strain Re2133/pEG7c. Comparison with literature on the strains Re2133/pEG7c and pEG23 showed that the absence of antibiotic (*i.e.* kanamycin) and a homogeneous environment allowed increasing Re2133/pEG7c production efficiency, whereas pEG23 behavior seemed to be less impacted by culture conditions. Maximal isopropanol specific production rate was equal to 0.09 $g_{IPA}.g_X^{-1}.h^{-1}$ for pEG7C and only 0.05 $g_{IPA}.g_X^{-1}.h^{-1}$ for pEG20 and 0.04 $g_{IPA}.g_X^{-1}.h^{-1}$ for pEG23. This decrease in isopropanol production in the strains Re2133/pEG23 and pEG20 might be due to a metabolic load, linked to chaperones *GroESL* and PSK system *hok/sok* expression, respectively.

Keywords

Cupriavidus necator, isopropanol, plasmid stability, PSK *hok/sok*, chaperon proteins *GroESL*, strain robustness

1.2 Introduction

In the face of collective ecological awareness, the interest in developing alternative fuels increased over the years. These alternatives to fossil-based fuels are based on microbial production of biofuels and chemical synthons from renewable sources. Isopropanol was identified as an interesting substitute for biofuel production (Grousseau *et al.* 2014) and has already been produced in bioreactors from recombinant plasmid-bearing strains of *Cupriavidus necator* (Marc *et al.* 2017, Garrigues *et al.* 2020). The main goal of such bioprocesses is to maintain strain robustness all along culture. The appearance of multiple phenotypes even in isogenic populations is suspected to lower yields, and thus bioprocess robustness, because cells are not all at the maximum production state (Gonzalez-Cabaleiro *et al.* 2017, Heins *et al.* 2018). Therefore, homogeneous populations may be favored to enhance bioprocess robustness (Binder *et al.* 2017). Nevertheless, mechanisms behind the impact of population heterogeneity on bioprocess are still not fully understood (Delvigne *et al.* 2014).

Cupriavidus necator H16 (also known at *Ralstonia eutropha*) has a versatile metabolism and is naturally able to consume oils (Budde *et al.* 2011), carboxylic acids (Johnson *et al.* 1971, Friedrich *et al.* 1979, Grunwald *et al.* 2015), carbohydrates (Johnson 1971, Grousseau *et al.* 2014) and CO_2 (Tanaka *et al.* 1995, Crepin *et al.* 2016, Marc *et al.* 2017, Garrigues *et al.* 2020). One of its most remarkable characteristics is its ability to synthesize and store up to 80 % of its dry cell weight of poly-β-hydroxybutyrate (*abbr.* PHB) (Ryu *et al.* 1997). Under nutrient limitation conditions (*e.g.* oxygen, nitrogen, phosphorus) and with excess of carbon, *C. necator* is able to massively divert its carbon flow toward PHB biosynthesis (Koller *et al.* 2010). This natural capacity presents a major interest, since several biosynthesis pathways for chemicals of economic interest also comprise acetyl-coA as precursor. Therefore, less genetic modifications would be required to deflect carbon flow after acetyl-coA, from the synthesis of PHB towards an industrial molecule of interest (Crepin *et al.* 2016, Marc *et al.* 2017, Garrigues *et al.* 2020). Indeed, *C. necator* has been engineered into a bioproduction platform towards the biosynthesis of isopropanol (Grousseau *et al.* 2014, Marc *et al.* 2017, Garrigues *et al.* 2020), isobutanol (Black *et al.* 2018), alka(e)ne (Crepin *et al.* 2016), carboxylic acids (Ewering *et al.* 2006, Hoefel *et al.* 2010), α-humulene (Krieg *et al.* 2018) and methyl ketones (Muller *et al.* 2013), both heterotrophically and autotrophically. For the heterologous production of isopropanol from fructose by *C. necator* Re2133 (**Figure 1**), the PHB biosynthesis pathway had been removed from the wildtype strain *C. necator* H16 by deleting both acetoacetyl-CoA reductases (*phaB*$_1$*B*$_2$*B*$_3$) and PHA synthase

(*phaC*) (Budde *et al.* 2011). A recombinant plasmid has been added which is bearing an isopropanol operon composed of genes encoding for acetoacetyl-CoA transferase (CTF) acetoacetate decarboxylase (ADC) and alcohol dehydrogenase (ADH) from *Clostridium* species (Grousseau *et al.* 2014). In Marc et *al*. (2017), isopropanol production reached an isopropanol concentration of 8.5 ± 0.1 $g \cdot L^{-1}$ with the reference strain Re2133/pEG7c (arabinose inducible P_{Bad}; *thl and ctf* genes from *C. necator*; *adc and adh* codon optimized gene from *Clostridium*) under nitrogen limiting conditions and fructose pulses.

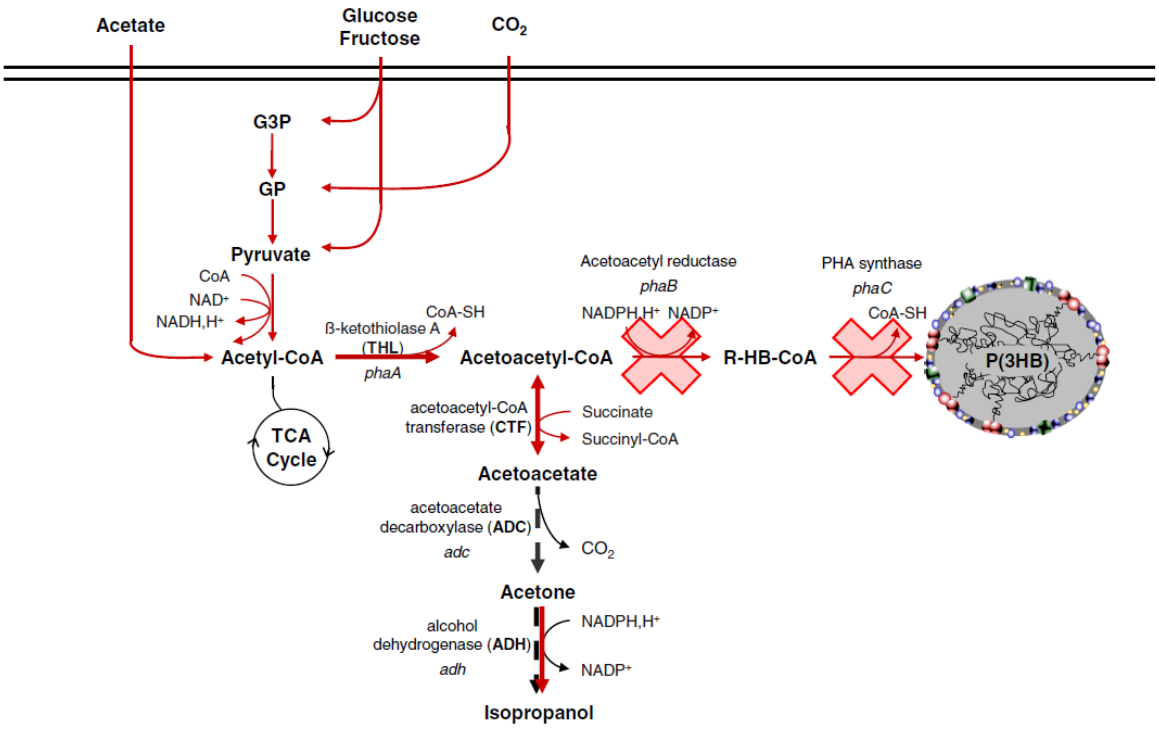

Figure 1 : Isopropanol production pathway in engineered *Cupriavidus necator* Re2133 (Grousseau *et al.* 2014)

Two plasmid constructions were studied regarding their impact on bioprocess robustness: (1) Post Segregational Killing system *hok/sok* (pEG20) and (2) chaperon protein GroEL/S expression (pEG23). Using plasmid expression stabilization systems, that are not based on antibiotic resistance, is interesting for bioprocess at an industrial scale in order to reduce production economic costs and fight against multidrug resistance.

The first strategy, based on PSK system *hok/sok*, aimed at increasing plasmid expression stability in isopropanol producing conditions. The post-segregational killing system *hok/sok* from the R1 plasmid of *Escherichia coli* ensures plasmid stabilization by the killing of plasmid-free cells; it encodes for two RNAs: *hok* mRNA and Sok antisense RNA. The *hok* gene encodes for a toxin protein Hok. The *sok* gene encodes for a Sok antisense RNA that regulates post-transcriptionally the expression of *hok* (Gerdes *et al.* 1990, Thisted *et al.* 1994). Plasmid stabilization mechanism of the PSK system *hok/sok* is based on

the differential decay rate between Sok antisense RNA and Hok toxin. Indeed, Sok antisense RNA has a higher decay rate than Hok toxin (Thisted *et al.* 1994). So, during cell division, if the plasmid is transmitted only to one of the two daughter cells, plasmid-bearing cells will express the Sok antisense RNA to block Hok toxin actions and remain viable, whereas plasmid-free cells are vulnerable to the stable Hok toxin because the unstable Sok antisense RNA antitoxin was degraded (Cooper *et al.* 2000, Friehs *et al.* 2004).

The second strategy is based on chaperon protein *GroESL* expression. This system aimed at diminishing the negative impact of isopropanol toxicity on the behavior of engineered cells. Indeed, solvents, like isopropanol, are often toxic for strains. A higher solvent hydrophobicity increases its toxic impact on cells, leading to solvent accumulation in the cytoplasmic membrane. This solvent accumulation causes higher cell permeability (ATP, ions, phospholipids, RNA, proteins leaking), higher membrane fluidity (cell membrane stability, structure disruption), energy transduction decrease and membrane protein function disruption (nutrient transport disruption) (Nicolaou *et al.* 2010, Dunlop *et al.* 2011, Mukhopadhyay *et al.* 2015). Plus, solvents might also denature biological molecules and lead to proteins unfolding, DNA and lipid damage, RNA unfolding or degradation (Nicolaou *et al.* 2010). Host's tolerance toward the solvent might be the main bottleneck to reach optimal production (Dunlop *et al.* 2011, Mukhopadhyay *et al.* 2015). It is commonly presumed that enhancing cell's tolerance might improve production yields (Dunlop *et al.* 2011, Mukhopadhyay *et al.* 2015). So, tolerance mechanisms are transferred to solvent-producing strains to increase production efficiency (Dunlop *et al.* 2011). Most studies about solvent toxicity have been led on extracellular addition mainly (Dunlop *et al.* 2011). Several mechanisms for tolerance improvement have already been identified, such as efflux pumps, heat shock proteins, modifications in membrane proteins and activation of stress response genes (Nicolaou *et al.* 2010, Dunlop *et al.* 2011, Mukhopadhyay *et al.* 2015, Shah *et al.* 2019). Among these strategies, up-regulation of *GroESL* chaperone expression (*i.e.* heat shock protein family) is often observed in response to protein misfolding, especially against short-chained alcohols (Mukhopadhyay *et al.* 2015) like isopropanol. The main role of *GroESL* consist in ensuring proper protein folding and even repair misfolded proteins (Masters *et al.* 2009, Zingaro *et al.* 2013). In Marc et *al.* (2017), a co-chaperonin GroES (H16_A0705) and two chaperonins GroEL (H16_A0706 and H16_A1997) were identified in *C. necator* H16. The chaperonins presenting the highest similarity to *C. acetobutylicum* and *E. coli* systems were selected. Thus, the overexpression of native *groEL* and *groES* genes from *C. necator* was shown to increase cell tolerance during isopropanol biosynthesis (Marc *et al.* 2017). Consequently, the final concentration of isopropanol produced was slightly increased (9.1 ± 0.1 $g \cdot L^{-1}$), as well as its maximal isopropanol production yield (0.187 ± 0.005 $g_{IPA} \cdot g_S^{-1}$), compared to a reference strain not expressing the *GroESL* chaperones (pEG7c: 8.5 ± 0.1 $g \cdot L^{-1}$ and 0.159 ± 0.005 $g_{IPA} \cdot g_S^{-1}$).

The aim of this work was to assess the impact of plasmid stabilization system (PSK system hok/sok) and a Chaperone protein (*GroESL*) overexpression in order to improve the strain robustness toward the heterologous isopropanol production by *C. necator*. This study was supported by kinetic data, isopropanol production performances, cell permeability measurements and plasmid stability analysis. As said above, the interest of using other plasmid expression stabilization systems than antibiotic resistance is based on the necessity to reduce production economic costs and fight against multidrug resistance in bioprocess at an industrial scale.

1.3 Material and method

1.3.1 Strains

C. necator Re2133 (Budde *et al.* 2011) was used as expression strain. This strain was obtained by deleting genes encoding for acetoacetyl-CoA reductases (*phaB1B2B3*) and for PHA synthase (*phaC1*) from the wildtype strain *C. necator* H16 / ATCC1769 which is gentamicin resistant (Gen^R). The strains *Escherichia coli* S17-1 and Top10 were used during plasmid construction.

1.3.2 Plasmids

The plasmids pEG7c, pEG20 and pEG23 were used in this work (**Table 1**). The design and associated molecular biology protocols for the construction of these plasmids were explained in more details in Grousseau et *al.* (2014) and in Marc et *al.* (2017).

Table 1: Strains and plasmids used in this study

Strains	**Relevant characteristics**	**References**
Re2133	*Cupriavidus necator* H16 *ΔphaB₁B₂B₃C₁* (Gen^R)	(Budde *et al.* 2011)
Plasmids		
pEG7c	pBBad with phaA-RBS-ctfAB-RBS-adc*- RBS-adh* sequence inserted into the multiple cloning site (MCS), Kan^R, P_{Bad}	(Grousseau *et al.* 2014)
pEG20	pEG7c and Plac-*hok/sok* cassette inserted after the MCS	This work
pEG23	pEG7c and Plac-RBS-groESL inserted after the MCS	(Marc *et al.* 2017)

1.3.3 Media

The rich medium for precultures was composed of 27.5 $g \cdot L^{-1}$ Tryptic Soy Broth (TSB, Becton Dickinson, Sparks, MD, USA) with addition of 10 $mg \cdot L^{-1}$ gentamicin and 200 $mg \cdot L^{-1}$ kanamycin as final concentration. For Tryptic Soy Agar (*abbr.* TSA) plates, 20 $g \cdot L^{-1}$ agar was added to the TSB medium.

For molecular biology, the rich Lysogeny broth medium (*abbr.* LB) was used and composed of 10 $g \cdot L^{-1}$ of peptone, 5 $g \cdot L^{-1}$ of yeast extract and 10 $g \cdot L^{-1}$ of NaCl. For LB agar plates, 20 $g.L^{-1}$ agar was added to the LB medium.

The mineral medium used for flask cultivations was previously described in Lu et *al.* (Lu *et al.* 2013). Gentamicin (10 mg·L^{-1}) and kanamycin (200 mg·L^{-1}) were added to this medium. Fructose (20 g·L^{-1}) and NH_4Cl (0.5 g·L^{-1}) were respectively used as carbon and nitrogen sources.

The mineral medium used for bioreactor cultivation was composed as follows (per liter): $(NH_4)_2SO_4$, 2.8 g; $MgSO_4$-$7H_2O$, 0.75 g; phosphorus (Na_2HPO_4-$12H_2O$, 1.5 g; KH_2PO_4, 0.25 g); nitrilotriacetic acid, 0.285 g; ammonium iron(III) citrate (28%), 0.09 g; $CaCl_2$, 0.015 g; trace elements (H_3BO_3, 0.45 mg; $CoCl_2$-$6H_2O$, 0.3 mg; $ZnSO_4$,$7H_2O$, 0.15 mg; $MnCl_2$-$4H_2O$, 0.045 mg; Na_2MoO4-$2H_2O$, 0.045 mg; $NiCl_2$-$6H_2O$, 0.03 mg; $CuSO_4$, 0.015 mg). Fructose was used as sole carbon source with an initial concentration at 30 g·L^{-1}. No antibiotics were added in the medium during bioreactor fermentations.

1.3.4 Precultures on fructose

One glycerol stock was plated on TSA plates containing 10 mg·L^{-1} gentamicin and 200 mg·L^{-1} kanamycin. The plates were incubated for 72 h at 30 °C. One colony was used to inoculate a rich medium flask culture (3 mL), which was grown for 48 h at 30 °C and 110 rpm. Then, the whole broth volume was used to inoculate a 30 mL mineral medium culture flask, which was incubated at 30 °C and 110 rpm during 24 h. Finally, the whole broth volume was used to inoculate a 300 mL mineral medium culture flask. The baffled flasks were incubated at 30 °C and 110 rpm during 10 h. This flask was used to inoculate the bioreactor culture.

1.3.5 Fed-batch cultivations on fructose

Batch cultivations consisted in non-limited growth on fructose. The cultures were led in a 5 L bioreactor Biostat®B-DCU (Sartorius, Germany) with a working volume of 3 L. Regulation and monitoring were done using MFCS/win 2.1 software package (Sartorius, Germany). Partial pressure of dioxygen (pO2) in the medium was measured with the optical oxygen sensor InPro 6860i (Mettler Toledo, USA) and pH was measured with a pressurized gel-filled pH electrode (Mettler Toledo, USA). Temperature was regulated at 30 °C and pH at 7.0 by addition of a 4 M KOH solution. Fermentation was carried out in aerobic conditions (*i.e.* air flow and stirring rates were regulated to maintain pO2 above 30 %). Two guard flasks, kept in ice, at reactor's outlet allows the re-solubilization of both gaseous acetone and isopropanol, in order to quantify their total production.

The medium was designed to reached 4 g·L^{-1} of biomass at the end of the batch phase. When 75 % of the maximum biomass concentration (*i.e.* 3 g·L^{-1}) was reached, isopropanol production was induced by an arabinose pulse (1 g·L^{-1}).

The fed-batch phase was initiated when nitrogen depletion was reached in mineral medium (corresponding to 4 g_{CDW}·L^{-1} biomass). Then ammonium, as nitrogen source, was fed in the bioreactor

through calibrated peristaltic pump with an exponential flow rate set at 0.04 h^{-1}. This growth rate corresponded to the optimum isopropanol producing conditions (Aragao *et al.* 1996, Grousseau *et al.* 2013). Nitrogen was the limiting substrate in the fed-batch phase. When fructose concentration reached 20 $g \cdot L^{-1}$, fructose was fed exponentially in the bioreactor through a calibrated peristaltic pump to maintain a concentration around 20 $g \cdot L^{-1}$. To prevent nutrient limitation, both rich phosphate solution (7 $mL \cdot L^{-1}$) and trace elements solution (2 $mL \cdot L^{-1}$) were added every 10 $g \cdot L^{-1}$ of biomass produced.

1.3.6 Analytical procedures

Biomass characterization

Biomass concentration was measured by optical density (OD) at 600 nm using a visible spectrophotometer (DR3900, Hachlange, Loveland, Colorado, USA) with a 0.2 cm path length absorption cell (Hellma). OD was correlated to cell dry weight (CDW) measurements (*i.e.* 2 $g_{CDW} \cdot L^{-1}$ = 1 OD unit). For cell dry weight measurements, 0.2 µm pore-size polyamide membranes (Sartorius, Göttingen, Germany), were beforehand dried (60°C, 200mmHg, 72 h) and weighted. Culture medium was sampled and filtrated on dried membranes, which were dried again in the same conditions.

Metabolite quantification

Cells samples were centrifuged, and supernatants were filtrated (0.2 µm PTFE syringe filters, VWR) before being used for substrate and products determination. Concentrations of residual fructose and organic acids were quantified by high-performance liquid chromatography (HPLC). The HPLC instrument (Series 1100, Agilent) was equipped with an ion-exchange column (Aminex HPX-87H, 300×7.8 mm, Bio-Rad, Hercules, CA, USA) protected with a guard column (Cation H+ cartridge, 30×4.6 mm, Bio-Rad) and coupled to a RI detector and an UV detector (λ=210 nm). The column was eluted with 2.5 mM H_2SO_4 as a mobile phase at 50 °C at a flow rate of 0.5 $mL \cdot min^{-1}$. Residual nitrogen concentration was quantified by higher-pressure ionic chromatography (HPIC). The HPIC instrument (ICS-2100 RFIC, Dionex) was equipped with an IonPac™ CS16 column (RFIC™, 3x50mm, BioRad) and an ion suppressor CERS 500 (2 mm, Thermo Scientific). The column was eluted with 30 mM Metanesulfonic Acid as a mobile phase at 40 °C and a 40 mA ion suppressor current, at a flow rate of 0.36 $mL \cdot min^{-1}$. Isopropanol and acetone concentrations were also determined by gas chromatography (GC), with a GC system 6890A Series (Hewlett Packard®, USA) and a column SupelQ-Plot 30 x 0.53mm (ID). Internal standard was 1 $g \cdot L^{-1}$ propionic acid.

Plate count

Plasmid stability was quantified by parallel plate count on antibiotic selective TSB Petri dishes (10 mg·L^{-1} Gentamicin and 10 mg·L^{-1} Gentamicin + 200 mg·L^{-1} Kanamycin). Serial dilutions were performed in physiological water (0.85 % NaCl) tubes (BioMérieux, Marcy-l'Étoile, France). For every sample, three dilutions were tested, between 10^{-5} and 10^{-9}. The diluted sample were plated in triplicate with the Whitley Automated Spiral Plater (Don Whitley Scientific, Shipley, UK). Decimal reduction rate from plate count measurements was calculated as: $N = log\left(\frac{Gen^R cells}{Gen^R Kan^r cells}\right)$.

Flow Cytometry

Cell permeability was accessed with propidium iodide staining (FL3 channel) and eGFP-fluorescence of plasmid-expressing cells (FL1 channel) by the BD Accuri C6® flow cytometer (BD Biosciences, Franklin Lakes, NJ, USA). Cell samples were diluted in physiological solution at 10^6 cells·mL^{-1} and then, were stained with 20 µL of a solution at 20 µM propidium iodide (*abbr.* PI) (Molecular Probes, Invitrogen, USA) and incubated 20 min at room temperature in the dark. A 100 % dead–cell control was prepared by incubating cells in 70 % isopropanol for 1 h at room temperature. Samples were run until 20, 000 events were counted at 14 µL·min^{-1} using milli-Q water as sheath fluid. The Forward Scatter Signal (threshold: 12, 000) and Side Scatter Signal (threshold: 2, 000) were used as trigger channels. Data acquisition was performed with BD Accuri CFlow® software and data processing was achieved with FlowJo software (Becton Dickinson, Sparks, MD, USA). Decimal reduction rate was calculated as described above from plasmid-expressing cells (eGFP-positive cells, FL1-A > $8 \cdot 10^2$) and total cells (Single cells, bisectors of both FCS-A *vs* FSC-H and SSC-A *vs* SSC-H): $N = log\left(\frac{Single-cells}{eGFP-cells}\right)$.

1.3.7 Data analysis

Specific substrate consumption (fructose q_S, ammonium q_N) and biomass production (μ) rates were calculated from experimental data and mass balances (carbon, nitrogen and elemental). Specific growth rate was determined as: $ln(X\ g_{CDW} \cdot L^{-1}) = f(t)$, and its error was calculated as the standard deviation of the slope. Determination of specific oxygen consumption (q_{O_2}) and specific carbon dioxide production (q_{CO_2}) was based on mass balance calculations in both liquid and gaseous phase, from inlet/outlet gas composition, temperature, pH, stirring, oxygen partial pressure (pO_2), and liquid volume. For overall production/consumption yield calculation, concentrations were plotted pairwise in a scatter plot. A linear regression was used to determine the considered yields and the error was calculated by the standard deviation of the slope.

1.4 Results

Among several plasmid constructions for isopropanol production, the strain Re2133/pEG23 (Marc *et al.* 2017) was the most efficient strain presenting the highest isopropanol production in terms of concentration (9.1 ± 0.1 $g \cdot L^{-1}$), yield (0.187 ± 0.005 $g_{IPA} \cdot g_X^{-1}$) and specific production rate (0.0047 $g_{IPA} \cdot g_X^{-1} \cdot h^{-1}$). The plasmid pEG23 was derived from the plasmid pEG7c (Grousseau *et al.* 2014), which did not encode for chaperone proteins *GroESL* expression. The strain Re2133/pEG7c was considered as reference for isopropanol overproducing strains.

In this work, the results concerning isopropanol production given by the reference strain Re2133/pEG7c and the best producer Re2133/pEG23 (chaperon *GroESL*) were confronted to the strain Re2133/pEG20, which encoded a PSK system *hok/sok*. To our knowledge, this plasmid stabilization strategy has never been applied to *Cupriavidus necator*. So, the impact of the PSK system *hok/sok* was compared to the *GroESL* over-expressing strategy, on isopropanol production.

Characterization of the strains Re2133/pEG7c, pEG23 and pEG20 in bioreactors was led in fed-batch cultures.

1.4.1 Macroscopic study

During batch phase, the maximum specific growth rate (calculated based on ln method calculation) reached by the three strains were close with 0.23 ± 0.02 h^{-1} for Re2133/pEG7c, 0.21 ± 0.01 h^{-1} for Re2133/pEG23 and 0.19 ± 0.01 h^{-1} for Re2133/pEG20 (**Table 2**). Growth rates were not significantly affected by the expression of the PSK *hok/sok* system (pEG20) or by chaperones *GroESL* (pEG23), compared to the reference strain pEG7c.

After arabinose induction (*i.e.* at 75% of the maximal biomass production), all strain started producing isopropanol and acetone in nitrogen limited fed-batch cultures and growth rate were maintained at 0.03 ± 0.01 h^{-1} (until the end), 0.04 ± 0.01 h^{-1} (until 90 h), 0.02 ± 0.01 h^{-1} (until 70 h) for Re2133/pEG7c, pEG23 and pEG20 respectively (**Figure 3 & Table 2**).

The carbon and degree of reduction balances were calculated for all strains and were at least equal to 90 %. The maximum isopropanol concentration reached in the liquid phase during fed-batch was 15.1 $g \cdot L^{-1}$ (76 h after induction) for pEG7c, 11 $g \cdot L^{-1}$ (46 h after induction) for pEG23 and 12.4 $g \cdot L^{-1}$ (62 h after induction) for pEG20 (**Table 2**). This metabolite was produced at a maximum production yield of 0.27 ± 0.01 $g_{IPA} \cdot g_S^{-1}$ for pEG7c, 0.12 ± 0.01 $g_{IPA} \cdot g_S^{-1}$ for pEG23 and 0.15 ± 0.01 $g_{IPA} \cdot g_S^{-1}$ for pEG20, at the beginning of the fed-batch phase, before decreasing for all strains (**Table 2**). Kinetics of the isopropanol specific production rate presented the same profile for all strains (**Figure 3**). First after arabinose induction, isopropanol production rate increased up to a maximum, which was equal to 0.09 $g_{IPA} \cdot g_X^{-1} \cdot h^{-}$

[1] for pEG7c, 0.04 $g_{IPA} \cdot g_X^{-1} \cdot h^{-1}$ for pEG23 and 0.05 $g_{IPA} \cdot g_X^{-1} \cdot h^{-1}$ for pEG20, before decreasing. The maximum isopropanol yield was reached during this phase. Second, isopropanol production rate was low until the end of culture.

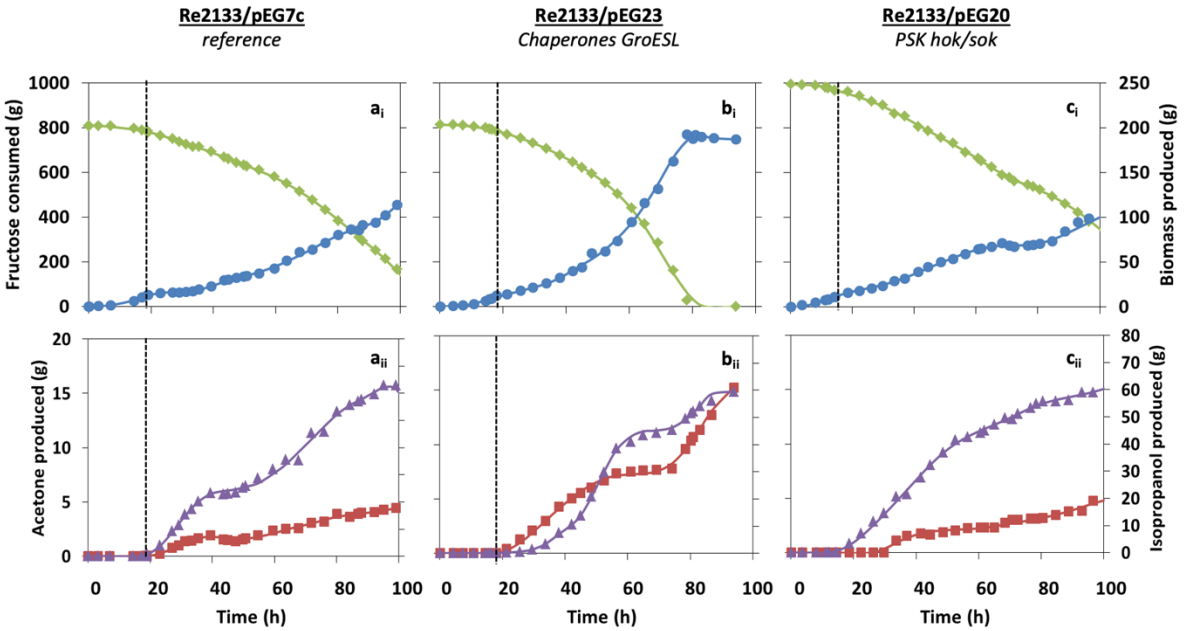

Figure 2: Kinetic macroscopic data: Evolution of cumulated masses (biomass (●), fructose (◆), isopropanol (▲), acetone (■)) through time during fed-batch cultivations on fructose of the strains Re2133/pEG7c (a), Re2133/pEG23 (b) and Re2133/pEG20 (c) The vertical dotted line represents the beginning of the fed-batch phase

Acetone is an intermediate in the isopropanol production pathway. It is produced simultaneously with isopropanol all along fed-batch for all strains (**Figure 2)**. Regarding the ratio Isopropanol / Acetone, for the strain Re2133/pEG7c, 14.6 g of isopropanol were produced for 1 g of acetone, all along culture. For the strain Re2133/pEG23, 18.9 g of isopropanol were produced for 1 g of acetone until isopropanol specific production rate reached 0 $g_{IPA} \cdot g^{-1}_X \cdot h^{-1}$ at 60 h. After that, the Isopropanol / Acetone ratio kept on decreasing until reaching 4 g of isopropanol produced for 1 g of acetone at the end of culture, meaning that acetone was accumulated at the expense of isopropanol. For the strain Re2133/pEG20, 11.7 g of isopropanol was produced for 1 g of acetone all along production phase (**Figure 2**). Maximum acetone production yield was equal to 0.024 ± 0.001 $g_{Ac} \cdot g_S^{-1}$ for pEG7c, 0.034 ± 0.001 $g_{Ac} \cdot g_S^{-1}$ for pEG23 and 0.017 ± 0.001 $g_{Ac} \cdot g_S^{-1}$ for pEG20 (**Table 2**). The curve for specific acetone production rate followed the same behavior as for the specific isopropanol production rate. The maximal acetone production rates reached were equal to 0.009 $g_{IPA} \cdot g^{-1}_X \cdot h^{-1}$ for pEG7c, 0.012 $g_{IPA} \cdot g^{-1}_X \cdot h^{-1}$ for pEG23 and 0.005 $g_{IPA} \cdot g^{-1}_X \cdot h^{-1}$ for pEG20 (**Figure 3**).

A slight peak of pyruvic acid production was observed after arabinose induction, but it was re-consumed shortly after for the strain Re2133/pEG7c. None was measured for pEG20 or for pEG23.

Oxygen consumption rate was rather stable during fed-batch for all strains, at 2.2 ± 0.2 mmol·g_X^{-1}·h^{-1} for pEG7c, 2.6 ± 0.3 mmol·g_X^{-1}·h^{-1} for pEG23 and 2.0 ± 0.2 mmol·g_X^{-1}·h^{-1} for pEG20 (**Figure 3**). Its value dropped for Re2133/pEG23 at 70 h. Likewise, carbon dioxide production rate was comprised around 2.9 ± 0.2 mmol·g_X^{-1}·h^{-1} for pEG7c, 3.6 ± 0.2 mmol·g_X^{-1}·h^{-1} for pEG23 and 2.2 ± 0.2 mmol·g_X^{-1}·h^{-1} for pEG20 (**Figure 3**). Its value dropped for Re2133/pEG23 at 70 h.

The respiratory quotient reached a maximum a few hours after arabinose induction (**Figure 3**), at 1.96 (30 h) for pEG7c, 1.96 (30 h) for pEG23 and 1.82 (22 h) for pEG20. After that, it decreased for all strains. For pEG7c and pEG20, its value stabilized until the end of culture at respectively 1.30 ± 0.07 and 1.13 ± 0.01. For pEG23, its value decreased continuously until reaching 1.

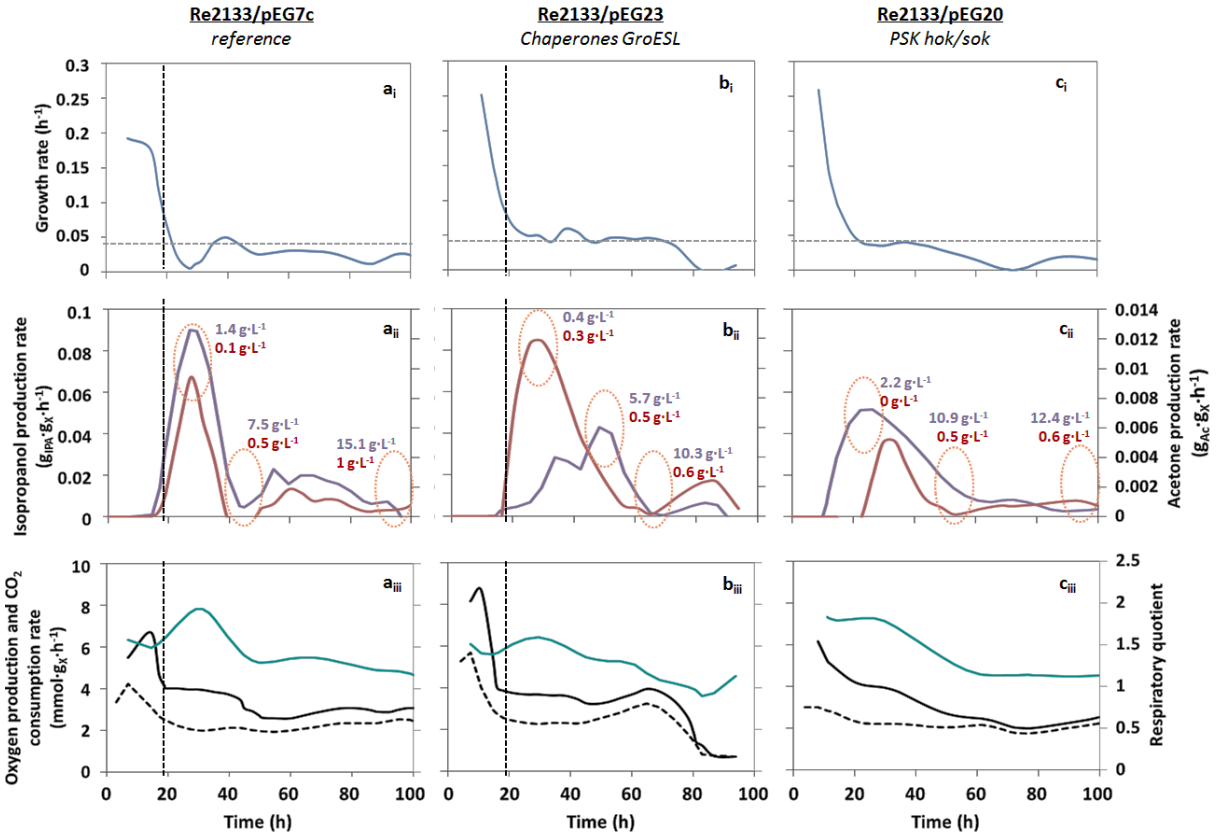

Figure 3: Growth rate (■), isopropanol (■) and acetone (■) production rates, oxygen consumption (■■) and carbon dioxide (■) production rates, and respiratory quotient (■) through time during fed-batch cultivations on fructose of the strains Re2133/pEG7c (a), Re2133/pEG23 (b) and Re2133/pEG20 (c) The vertical dotted line represents the beginning of the fed-batch phase

There was no difference in terms of overall carbon repartition between the strains Re2133/pEG7c and Re2133/pEG20, except a slightly higher carbon dioxide production at the expense of isopropanol for pEG20. Concerning the strain Re2133/pEG23, a slightly higher biomass and acetone production at the expense of isopropanol and carbon dioxide could be observed (**Figure 4 & Table 2**).

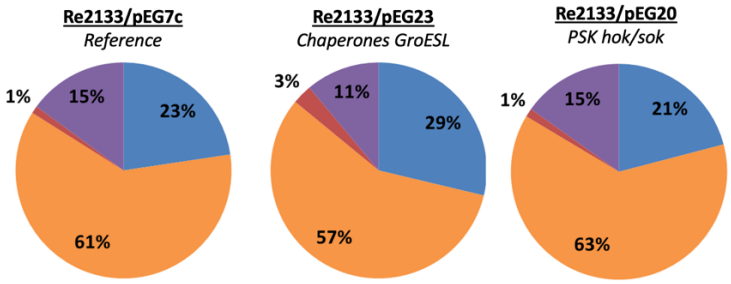

Figure 4: Overall carbon repartition (% Cmol) between biomass (■), carbon dioxide (■), acetone (■) and isopropanol (■)

1.4.2 Inhibition from isopropanol production

After the induction of isopropanol production, the specific isopropanol production rate increased up to a maximum, at 1.4 $g \cdot L^{-1}$ of isopropanol produced for Re2133/pEG7c, 5.7 $g \cdot L^{-1}$ for pEG23 and 2.2 $g \cdot L^{-1}$ for pEG20 (**Figure 3**). Then, isopropanol specific production rate decreased until getting close to 0 at 7.5 $g \cdot L^{-1}$ for Re2133/pEG7c, 10.3 $g \cdot L^{-1}$ for pEG23 and 12.4 $g \cdot L^{-1}$ for pEG20. For pEG7c, after reaching a low value, the isopropanol specific production rate remained low and constant, before getting close to zero again, at 15.1 $g \cdot L^{-1}$. A first critical acetone concentration was reached (pEG7c: 0.5 $g \cdot L^{-1}$; pEG23: 0.6 $g \cdot L^{-1}$; pEG20: 0.5 $g \cdot L^{-1}$) for all strains, where acetone specific production rate approached zero. For the strain Re2133/pEG7c, the acetone specific production rate was maintained low, before dropping again to zero at 1 $g \cdot L^{-1}$.

1.4.3 Cell permeability

The impact of isopropanol and acetone productions on cell membrane permeabilization was studied by propidium iodide staining (**Figure 5**).

The evolution of the percentage of permeabilized cells (*i.e.* propidium-iodide positive cells) presented two phases for Re2133/pEG7c (**Figure 5**). First, its value remained low until 9 $g \cdot L^{-1}$ of isopropanol (0.6 $g \cdot L^{-1}$ of acetone) was produced. Then, above that point, the percentage of permeabilized cells increased continuously to reach 23 % of permeabilized cells. For Re2133/pEG20, permeabilized cells increased as soon as isopropanol is produced, but rather slowly until the critical isopropanol value of 8 $g \cdot L^{-1}$ (0.5 $g \cdot L^{-1}$ of acetone) was reached. After that critical isopropanol concentration value, the permeabilized cell percentage increase faster up until 25 %. For the same isopropanol amount

produced, the percentage of permeabilized cells was slightly higher for pEG20 than for pEG7c.The percentage of permeabilized cells for pEG23 (**Figure 5)** increased up to 10 % at 10 g·L^{-1}of isopropanol, which was comparable to the values obtained with pEG7c, and then, remained stable all along fed-batch phase. The strain Re2133/pEG23 was significantly more resistant to permeabilization than Re2133/pEG7c and pEG20 when facing increasing concentrations of isopropanol (when above 10 g·L^{-1}) and acetone (when above 0.5 g·L^{-1}).

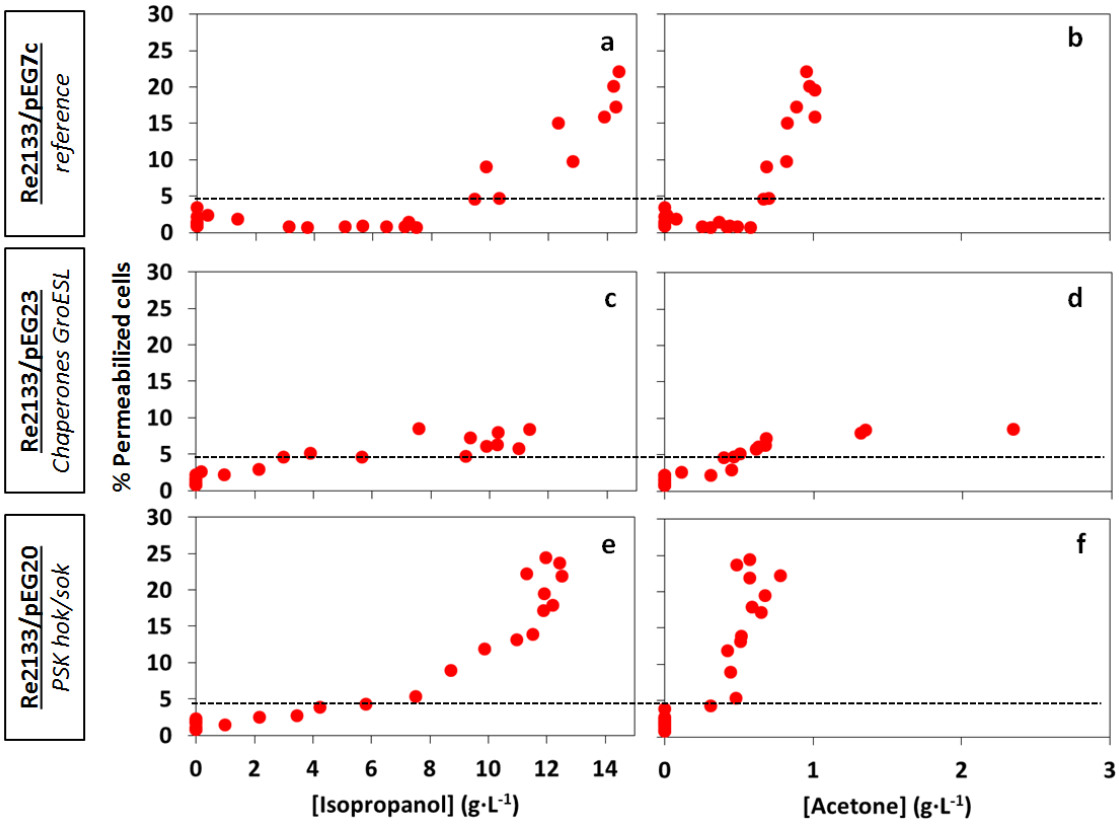

Figure 5 : Percentage of permeabilized cells, depending on acetone and isopropanol concentrations

1.4.4 Plasmid expression stability

Plasmid expression stability was evaluated by plate count, during isopropanol production (**Figure 6**).

For Re2133/pEG7c, the decimal reduction rate calculated from plate count increased up to 0.5 at 9 g.L^{-1} of isopropanol (0.5 g·L^{-1} of acetone) (**Figures 6a & b)**. From 9 to 14 g·L^{-1} of isopropanol, the decimal reduction rate was maintained at 0.7. After that threshold, the decimal reduction rate abruptly increased up to 1.3 at the end of culture, where maximum isopropanol concentration was reached. For the strain Re2133/pEG23, the decimal reduction rate was low (< 0.2) until 3 g·L^{-1} of isopropanol were produced (0.4 g·L^{-1} of acetone) (**Figures 6c & d**). After that threshold, decimal reduction rate increased with increasing isopropanol concentration. At the end of culture, pEG23 reached a 2 decimal reduction rate at 11.4 g·L^{-1} isopropanol (1.3 g·L^{-1} of acetone). Regarding **Figure 6c**, the points (9;2) and

(7;2) corresponded to the last points of the culture when isopropanol concentration decreased due to evaporation, whereas the decimal reduction rate value was still 2. Meanwhile, acetone increased but did not affect the decimal reduction rate, which did not vary.

For the strain Re2133/pEG20, the decimal reduction rate remained low until 10 $g.L^{-1}$ of isopropanol (0.4 $g{\cdot}L^{-1}$ acetone) were produced (**Figures 6e & f**). After that threshold, decimal reduction rate increased quickly up to 1.4 for 12.4 $g{\cdot}L^{-1}$ isopropanol (0.7 $g{\cdot}L^{-1}$ of acetone).

For the same isopropanol concentration reached, the decimal reduction rate reached was higher for Re2133/pEG23 (= 2) than for pEG7c (= 1.3) and pEG20 (= 1.4). In addition, the concentration of isopropanol at which decimal reduction rate started increasing was lower for Re2133/pEG23 (= 3 $g{\cdot}L^{-1}$) than for pEG7c (= 9 $g{\cdot}L^{-1}$) and pEG20 (= 10 $g{\cdot}L^{-1}$). So, the strain Re2133/pEG7c, allowed plasmid expression stability to be maintained longer than the strain Re2133/pEG23. However, there was only a slight difference between the decimal reduction rates reached for Re2133/pEG7c and pEG20.

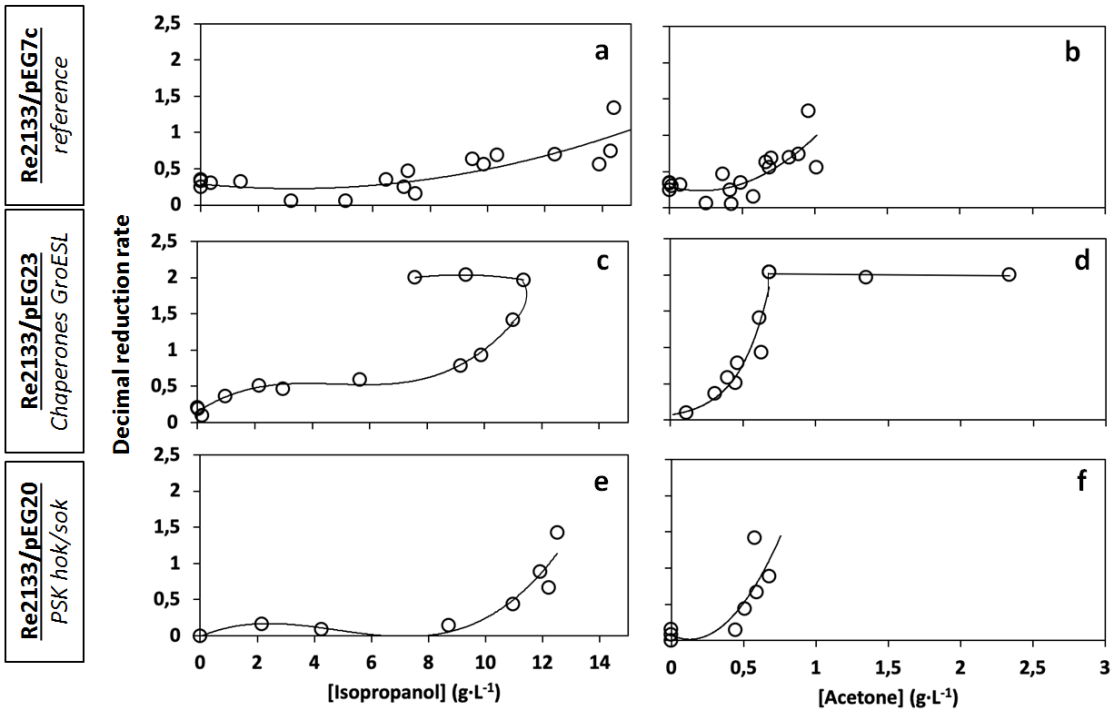

Figure 6: Decimal reduction rate, depending on acetone and isopropanol concentrations

Table 2 : Fed-batch cultivations parameters of the strains Re2133/pEG7c, pEG20 and pEG23. The critical isopropanol concentration corresponded to the isopropanol titer at which the specific isopropanol production rate reached 0 $g_{IPA} \cdot g_X^{-1} \cdot h^{-1}$ (a) Concentration measured in the liquid phase; (b) Maximal concentration calculated considering evaporation

	μ_{max}	μ_{prod}	[isopropanol] max	Yield biomass	Yield CO_2	Yield isopropanol	Yield acetone	$[Isopropanol]_{critique}$
	h^{-1}	h^{-1}	$g \cdot L^{-1}$	$g \cdot g^{-1}$	$g \cdot g^{-1}$	$g \cdot g^{-1}$	$g \cdot g^{-1}$	$g \cdot L^{-1}$
pEG7c	0.23 ± 0.02	0.03 ± 0.01	15.1 (a) 16.4 (b)	0.44 ± 0.02 (batch) 0.09 ± 0.01 (19-35h) 0.17± 0.01 (47-92h)	0.54 ± 0.03 (batch) 0.65 ± 0.01 (19-35h) 0.90± 0.01 (47-92h)	**0.27 ± 0.01** (19-35h) 0.098 ± 0.003 (47-92h)	**0.024 ± 0.001** (19-35h) 0.007 ± 0.003 (47-92h)	7.5 and 15.1
pEG23	0.21 ± 0.01	0.02 ± 0.01	11 (a) 13.5 (b)	0.41 ± 0.02 (batch) 0.25 ± 0.01 (25-74h) 0.10± 0.02 (78-83h)	0.47 ± 0.01 (batch) 0.70 ± 0.01 (25-48h) 0.88± 0.01 (48-83h)	**0.12 ± 0.01** (25-48h) 0.02 ± 0.01 (48-74h) 0.09 ± 0.01 (78-83h)	**0.034 ± 0.001** (25-48h) 0.003 ± 0.001 (48-74h) 0.03 ± 0.01 (78-83h)	10.3
pEG20	0.19 ± 0.01	0.04 ± 0.01	12.4 (a) 12.5 (b)	0.55 ± 0.05 (batch) 0.17 ± 0.01 (14-61h) 0.12 ± 0.01 (62-100h)	0.66 ± 0.03 (batch) 0.73 ± 0.01 (14-61h) 0.97 ± 0.01 (62-100h)	**0.15± 0.01** (14-61h) 0.05± 0.01 (62-100h)	**0.017 ± 0.01** (14-61h) 0.009 ± 0.001 (62-100h)	12.4

1.5 Discussion

This work aimed at characterizing the impact of the plasmid stabilization system PSK *hok/sok* (pEG20) and of the chaperone protein *GroESL* overexpression (pEG23) on strain robustness during heterologous production of isopropanol by *C. necator*. The behavior of the strain Re2133/pEG20 was compared to the already characterized strain Re2133/pEG7c (reference strain) and pEG23 (Marc *et al.* 2017). The increasing interest in using plasmid expression stabilization systems than are not base on antibiotic resistance is due to a growing interest in decreasing production costs and fight against multidrug resistance.

During batch phase, the growth rate reached were rather close between the three strains studied, 0.23 ± 0.02 h^{-1} for Re2133/pEG7c, 0.21 ± 0.01 h^{-1} for Re2133/pEG23 and 0.19 ± 0.01 h^{-1} for Re2133/pEG20. On one hand, the expression of *GroESL* did not enhance the growth capacity, because of more efficient protein folding, in absence of isopropanol production (Masters *et al.* 2009, Zingaro *et al.* 2013). This was also observed in the work of Marc et *al.* (2017), with the obtention of a comparable growth rate (0.22 h^{-1}). On the other hand, the constitutive expression of the PSK system *hok/sok* did not slow down growth, because of metabolic load due to the expression of the stabilization cassette. Compared to the growth rate obtained in flask for Re2133/pEG7c (0.17 h^{-1}) (Grousseau *et al.* 2014), there was a significant increase (+ 24 % in mean) during the batch phase for all strains, as cultivation mode allowed better controlling the cell environment (*e.g.* aeration, stirring, pH, temperature).

As shown in Marc et *al.* (2017), cell permeability of a non-isopropanol producing culture (Re2133/pBBRMCS-2) remains stable at 5 %, whereas cell permeability increased up to 20 % when isopropanol concentration was the highest (8.5 $g{\cdot}L^{-1}$) with the Re2133/pEG7c producing strain. Indeed, as isopropanol is produced intracellularly and accumulated in the cytoplasmic membrane, it might cause higher cell permeability, higher membrane fluidity, biological molecules denaturation and membrane protein function disruption (Nicolaou *et al.* 2010, Dunlop 2011, Mukhopadhyay 2015). In our culture conditions, the strain Re2133/pEG7c seemed to exhibit lower cell permeabilization toward an identical isopropanol concentration. Indeed, when we reached 8.5 $g{\cdot}L^{-1}$ of isopropanol (maximum isopropanol titer in Marc et *al.,* 2017), our cell permeabilization was only equal to 5 %, instead of 20 %. This might be due to differences in the fermentation strategy implemented: (1) no kanamycin was added in our medium and (2) fructose was fed continuously in this work instead of pulses. So, in our case of study, fructose continuous feeding and the absence of antibiotics contributed to have a positive impact on Re2133/pEG7c tolerance toward isopropanol. For the strain Re2133/pEG23, the culture conditions seemed to have no impact on cell permeability and so, the expression of the chaperone proteins *GroESL* seemed to have alone a positive impact on alcohol tolerance. After reaching the threshold isopropanol concentration, the percentage of permeabilized cells increased regularly and

continuously for the strains Re2133/pEG7c and Re2133/pEG20, whereas it stabilizes at 10 % for Re2133/pEG23. The same observations for the strains Re2133/pEG7c and pEG23 were made in Marc et *al.* (2017). The expression of chaperon *GroESL* in Re2133/pEG23, might have helped maintaining growth capacities and decreasing cell permeabilization (Marc *et al.* 2017) in response to increasing isopropanol concentrations, as the mode of action of *GroESL* consists in ensuring proper protein folding (Masters *et al.* 2009, Zingaro *et al.* 2013). When exposed to the same isopropanol concentration, the strain Re2133/pEG20 presented the highest cell permeability. Thus, the constitutive expression of the PSK system *hok/sok* seemed to have a negative impact on the strain's tolerance toward isopropanol.

The evolution of plasmid stability depending on isopropanol concentration was similar for the strains Re2133/pEG7c and Re2133/pEG20. Decimal reduction rates remained low until a certain isopropanol threshold (9 $g \cdot L^{-1}$ for Re2133/pEG7c; 8 $g.L^{-1}$ for Re2133/pEG20) was reached, and then increased abruptly to a similar maximum value (1.3 for Re2133/pEG7c; 1.4 for Re2133/pEG20). Therefore, the PSK system *hok/sok* did not significantly improve plasmid stability under the presence of isopropanol, compared to the reference strain Re2133/pEG7c. The expression of chaperon proteins *GroESL* had a negative impact on plasmid stability, as the critical isopropanol concentration was lower (3 $g.L^{-1}$) with a stronger decimal reduction of plasmid-bearing cells (= 2).

The critical inhibitory concentration of isopropanol was evaluated at 20 $g \cdot L^{-1}$ (Marc *et al.* 2017) when adding exogeneous isopropanol. This critical inhibitory concentration corresponded to the isopropanol concentration at which growth rate dropped to zero. In our work, a critical inhibitory isopropanol concentration was determined at 10.3 $g \cdot L^{-1}$ for Re2133/pEG23, 12.4 $g \cdot L^{-1}$ for and 15.1 $g \cdot L^{-1}$ for pEG7c. For Re2133/pEG23, this lower critical inhibitory isopropanol concentration might be due to higher plasmid expression loss for comparable isopropanol concentrations in Re2133/pEG7c and pEG23.

Maximum production yields varied depending on plasmid construction. The maximum isopropanol production yield was observed for Re2133/pEG7c (0.27 ± 0.01 $g_{IPA} \cdot g_S^{-1}$), which was higher than those obtained by Marc et *al*. (2017) (0.159 ± 0.005 $g_{IPA} \cdot g_S^{-1}$; - 41 % compared to our work). With the strain Re2133/pEG23 (0.12 ± 0.01 $g_{IPA} \cdot g_S^{-1}$), isopropanol production yield was lower than those obtained by Marc et *al.* (2017) (0.187 ± 0.005 $g_{IPA} \cdot g_S^{-1}$; + 56 % compared to our work). In our culture conditions, lower isopropanol production yields were measured for the strains Re2133/pEG20 (0.12 ± 0.01 $g_{IPA} \cdot g_S^{-1}$, - 44 %) and pEG23 (- 56 %), compared to our reference strain Re2133/pEG7c. All these values were lower than the theoretical isopropanol production yield, which was estimated through stoichiometric metabolic modelling at 0.33 $g_{IPA} \cdot g_S^{-1}$ (Marc *et al.* 2017), even if our result with the strain Re2133/pEG7c was the highest reached yet. In our culture conditions, carbon flow was globally diverted in higher

proportions toward isopropanol for the strain Re2133/pEG7c compared to pEG23 and pEG20. This was consistent with an increasing plasmid expression stability for this strain in response to higher isopropanol concentrations.

Acetone was produced as by-product of isopropanol biosynthesis. The highest maximum acetone production yield in our work was determined for Re2133/pEG23 at 0.034 ± 0.001 $g_{Ac} \cdot g_S^{-1}$ (*i.e.* 0.029 ± 0.002 $g_{Ac} \cdot g_S^{-1}$; -15 % in Marc et *al.* (2017)). There was a significant decrease for the reference strain Re2133/pEG7c at 0.024 ± 0.001 $g_{Ac} \cdot g_S^{-1}$ (*i.e.* 0.038 ± 0.002 $g_{Ac} \cdot g_S^{-1}$; + 58 % in Marc et *al.* (2017)). Maximum acetone production yield was the lowest for the strain Re2133/pEG20 at 0.017 ± 0.001 $g_{Ac} \cdot g_S^{-1}$. So, carbon flow was more efficiently drawn from acetone toward isopropanol production for the strain Re2133/pEG20, compared to pEG7c and pEG23.

As a result, maximum titer reached was significantly higher for the reference strain Re2133/pEG7c (15.1 $g \cdot L^{-1}$), compared to Re2133/pEG20 (*hok/sok*, 11 $g \cdot L^{-1}$, -18%) and pEG23 (*GroESL*, 12.4 $g \cdot L^{-1}$, -27%). In Marc et *al.* (2017), a higher titer with *GroESL* (9.1 $g \cdot L^{-1}$) in comparison with the reference strain Re2133/pEG7c (8.5 $g \cdot L^{-1}$) was obtained. In this work, maximum titer in the liquid phase reached with Re2133/pEG7c and pEG23 corresponded to an increase of +78 % and + 36 %, respectively compared to those obtained by Marc et *al.* (2017).

In Marc et *al.* (2017), the positive effect of *GroESL* over-expression by Re2133/pEG23 consisted in an increase heterologous enzymes activity (ADC and ADH), compared to the reference strain Re2133/pEG7c. As a result, carbon flow was pulled further toward isopropanol production, instead of toward undesired by-products like acetone. However, in our case of study, plasmid expression stability for Re2133/pEG23 was considerably lower and decreased way sooner than for Re2133/pEG7c and pEG20. These differences between our studies might be due to the fact that in Marc et *al.* (2017) the medium was supplemented with kanamycin, while no antibiotic was added in our bioreactors. Thus, overexpression of *GroESL* chaperon proteins during isopropanol production, by the plasmid pEG23, without selection pressure (+ 100 $mg \cdot L^{-1}$ kanamycin) might lead to a large drop in plasmid expression stability. This led to decreased isopropanol titers, yields and production rates. This response shows the interest of the PSK system encoded on the plasmid pEG20, which allowed, at least, the same response as the reference pEG7c, in terms of plasmid stability and cell permeability when facing increasing isopropanol concentrations.

In conclusion, a strain expressing the PSK system *hok/sok* (pEG20) was compared to a reference strain (pEG7c) and a *GroESL* chaperon expressing strain (pEG23), on the basis of their isopropanol production capacities. The reference strain Re2133/pEG7c presented the highest isopropanol production titer, yield and rate. However, the two recombinant strains succeeded in improving strain robustness on

precise phenomena. The over-expression of *GroESL* allowed improving cell tolerance toward isopropanol (permeabilization + growth) and the expression of the PSK system *hok/sok* allowed decreasing acetone production. Thus, both constructions allowed re-directing the carbon flow toward isopropanol production. Nevertheless, certain drawbacks limited their isopropanol production. The Re2133/pEG23 strain had a poor plasmid stability without selection pressure during the production phase, and Re2133/pEG20 had a lower isopropanol tolerance in terms of membrane permeability.

1.6 Results synthesis

➔ ***GroESL* allowed improving cell tolerance toward isopropanol and PSK system *hok/sok* allowed decreasing acetone production. But, *GroESL* induced poor plasmid stability during the production phase, and PSK system *hok/sok* caused a lower isopropanol tolerance.**

➔ During batch phase, maximum growth rate 0.23 ± 0.02 h^{-1} for Re2133/pEG7c, 0.21 ± 0.01 h^{-1} for Re2133/pEG23 and 0.19 ± 0.01 h^{-1} for Re2133/pEG20. Growth rate was not significantly affected by the expression of the PSK *hok/sok* system (pEG20) or by chaperones *GroESL* (pEG23), compared to the reference strain pEG7c.

➔ Maximum isopropanol concentration reached in the liquid phase during fed-batch was 15.1 $g{\cdot}L^{-1}$ for pEG7c, 11 $g{\cdot}L^{-1}$ for pEG23 and 12.4 $g{\cdot}L^{-1}$ for pEG20. Maximum isopropanol production yields reached were 0.27 ± 0.01 $g_{IPA}{\cdot}g_S^{-1}$ for pEG7c, 0.12 ± 0.01 $g_{IPA}{\cdot}g_S^{-1}$ for pEG23 and 0.15 ± 0.01 $g_{IPA}{\cdot}g_S^{-1}$ for pEG20. Maximum acetone production yield was equal to 0.024 ± 0.001 $g_{Ac}{\cdot}g_S^{-1}$ for pEG7c, 0.034 ± 0.001 $g_{Ac}{\cdot}g_S^{-1}$ for pEG23 and 0.017 ± 0.001 $g_{Ac}{\cdot}g_S^{-1}$ for pEG20.

➔ No difference on overall carbon repartition between the strains Re2133/pEG7c and Re2133/pEG20, except a higher carbon dioxide production at the expense of isopropanol for pEG20. For Re2133/pEG23, higher biomass and acetone production at the expense of isopropanol and carbon dioxide could be observed.

➔ For Re2133/pEG7c, %PI-cells was low until 9 $g{\cdot}L^{-1}$ of isopropanol (0.6 $g{\cdot}L^{-1}$ of acetone) and then, increased up to 23 %. For Re2133/pEG20, %PI-cells increased slowly as soon as isopropanol is produced until 8 $g{\cdot}L^{-1}$ of isopropanol (0.5 $g{\cdot}L^{-1}$ of acetone) and then, increase faster up to 25 %. For the same isopropanol amount produced, the %PI- cells was higher for pEG20 than for pEG7c. For Re2133/pEG23, %PI-cells increased up to 10 % at 10 $g{\cdot}L^{-1}$ and then, remained stable all along fed-batch phase.

➔ For the same isopropanol production, the decimal reduction rate reached was higher for Re2133/pEG23 (= 2) than for pEG7c (= 1.3) and pEG20 (= 1.4). Plus, the concentration of isopropanol at which decimal reduction rate started increasing was lower for Re2133/pEG23 (= 3 $g{\cdot}L^{-1}$) than for pEG7c (= 9 $g{\cdot}L^{-1}$) and pEG20 (= 10 $g{\cdot}L^{-1}$). So, the strain Re2133/pEG7c, allowed plasmid expression stability to be maintained longer than the strain Re2133/pEG23. However, there was only a slight difference between the performances of Re2133/pEG7c and pEG20.

Part 3 : Results and discussion

Chapter 2: Identification of heterologous subpopulations from a pure culture in a bioreactor

In previous work in our research team, different plasmid construction strategies were designed and studied to enable efficient isopropanol production with *Cupriavidus necator* (Grousseau *et al.* 2014, Marc *et al.* 2017).

In the previous chapter, a maximum isopropanol concentration in fed-batch was reached at 15.1 $g \cdot L^{-1}$ with the plasmid pEG7c, 12.1 $g \cdot L^{-1}$ with pEG20 and 11 $g \cdot L^{-1}$ with pEG23. We observed that production dynamics slowed down over time when isopropanol concentration increased in the medium, until completely stopping.

The most probable hypotheses to explain that production slowdown might be related to *(i)* isopropanol cytotoxicity, as this recombinant molecule is produced intracellularly, and to *(ii)* segregational plasmid loss, as isopropanol production imposes a metabolic load on host cells. Both phenomena may interfere with isopropanol production dynamics. The raises in both cell permeability and plasmid loss when isopropanol concentration increased were confirmed by PI-staining and plate count (Gen^R + Kan^R) in the previous chapter.

Thus, to improve strain robustness during isopropanol production, it would be beneficial to better understand the phenomena behind plasmid loss and cell tolerance disruption by single-cell analyses. Therefore, we developed an eGFP biosensor encoded on the recombinant plasmid. This new tool allowed monitoring plasmid expression level distributions through time by flow cytometry in response to diverse culture conditions and plasmid construction strategies, as shown in the following chapter.

So, a better understanding of the phenomena behind the apparition of population heterogeneity during recombinant isopropanol production might allow increasing strain robustness.

Part 3 : Results and discussion

Chapter 2: Identification of heterologous subpopulations from a pure culture in a bioreactor

Subchapter 1: Plasmid expression level heterogeneity monitoring via heterologeous eGFP production at the single-cell level in *Cupriavidus necator*

Applied Microbiology and Biotechnology
https://doi.org/10.1007/s00253-020-10616-w

APPLIED MICROBIAL AND CELL PHYSIOLOGY

Plasmid expression level heterogeneity monitoring via heterologous eGFP production at the single-cell level in *Cupriavidus necator*

Catherine Boy[1] · Julie Lesage[1] · Sandrine Alfenore[1] · Nathalie Gorret[1] · Stéphane E. Guillouet[1]

Received: 28 January 2020 / Revised: 2 April 2020 / Accepted: 6 April 2020

Abstract

A methodology for plasmid expression level monitoring of eGFP expression suitable for dynamic processes was assessed during fermentation. This technique was based on the expression of a fluorescent biosensor (eGFP) encoded on a recombinant plasmid coupled to single-cell analysis. Fluorescence intensity at single-cell level was measured by flow cytometry. We demonstrated that promoter evaluation based on single-cell analysis versus classic global analysis brings valuable insights. Single-cell analysis pointed out the fact that intrinsic fluorescence increased with the strength of the promoter up to a threshold. Beyond that, cell permeability increases to excrete the fluorescent protein in the medium. The metabolic load due to the increase in the eGFP production in the case of strong constitutive promoters leads to slower growth kinetics compared with plasmid-free cells. With the strain *Cupriavidus necator* Re2133, growth rate losses were measured from 3% with the weak constitutive promoter P_{lac} to 56% with the strong constitutive promoter P_{j5}. Through this work, it seems crucial to find a compromise between the fluorescence intensity in single cells and the metabolic load; in our conditions, the best compromise found was the weak promoter P_{lac}. The plasmid expression level monitoring method was tested in the presence of a heterogeneous population induced by plasmid-curing methods. For all the identified subpopulations, the plasmid expression level heterogeneity was significantly detected at the level of fluorescence intensity in single cells. After cell sorting, growth rate and cultivability were assessed for each subpopulation. In conclusion, this eGFP biosensor makes it possible to follow the variations in the level of plasmid expression under conditions of population heterogeneity.

Key Points

- *Development of a plasmid expression level monitoring method at the single-cell level by flow cytometry.*
- *Promoter evaluation by single-cell analysis: cell heterogeneity and strain robustness.*
- *Reporter system optimization for efficient subpopulation detection in pure cultures.*

Keywords Plasmid stability · Expression level · Biosensor · Flow cytometry · Cell sorting · *Cupriavidus necator* H16

Introduction

Microbial populations grown in supposedly homogeneous environments are often still considered as being composed of identical individuals. Several studies have proven the opposite even in the case of cultures derived from monoclonal colonies (Carlquist et al. 2012; Delvigne and Goffin 2014; Muller et al. 2010; Zielenkiewicz and Ceglowski 2001). Subpopulation heterogeneities can be divided into four main categories: genetic, biochemical, physiological, and phenotypic (Brehm-Stecher and Johnson 2004). There are often connections between these categories (Martins and Locke 2015). Genetic heterogeneity can be caused by spontaneous point mutations, transcription errors, or mobile genetic elements (Brehm-Stecher and Johnson 2004; Elowitz et al. 2002; Martins and Locke 2015). Biochemical heterogeneity is defined by differences in macromolecular composition (Martins and Locke 2015) or activity levels. It can be caused by genetic heterogeneity and variations in cell cycle–related processes (Brehm-Stecher and Johnson 2004; Martins and Locke 2015). Physiological heterogeneity shows morphological

Electronic supplementary material The online version of this article (https://doi.org/10.1007/s00253-020-10616-w) contains supplementary material, which is available to authorized users.

✉ Nathalie Gorret
ngorret@insa-toulouse.fr

[1] TBI, Université de Toulouse, CNRS, INRAE, INSA, Toulouse, France

heterogeneities between cell subpopulations. It can be explained by antibiotic presence or by nutrient availability, and also by variations in the cell cycle. Phenotypic heterogeneity is defined as the consequence of genetic, biochemical, and/or physiological heterogeneities (Brehm-Stecher and Johnson 2004).

In large-scale bioreactors, population heterogeneity is presumed to reduce production yields and increase process instability. So, ensuring phenotypic homogeneity of engineered microbial populations is of major interest for synthetic biology and bioprocess optimization (Binder et al. 2017).

On the one hand, phenotypic variation between clonal populations is a natural phenomenon that arises from stochastic gene expression and/or fluctuations in the cell cycle. Therefore, this noise in the phenotypic behavior of the cell can originate from the biochemical process of gene expression itself (Elowitz et al. 2002; Mortier et al. 2019; Nana et al. 2018).

On the other hand, maintenance and expression of heterologous genes add a metabolic burden on host cells. Some of these metabolic burdens are due to specific roles of the recombinant genes in the engineered strains (e.g., metabolite consumption by a heterologous enzyme). However, the majority of metabolic burdens observed are due to the consumption of cellular transcriptional resources during recombinant gene expression (Ceroni et al. 2018). So, two major biological mechanisms are competing within engineered strains: recombinant gene maintenance and cell growth (Silva et al. 2012). In this context, this resource reassignment will have a major impact on translation, especially if numerous mRNA expressed from the recombinant sequence encode for strong RBS (i.e., ribosome binding sites) sequences and require an increased number of ribosomes that will no longer be available for the host gene expression. Metabolic burden due to recombinant molecule expression has a stronger impact at the level of protein translation. The consequences of metabolic load are often a decrease of the growth rate and global physiological modifications, all of this leading to a decrease in the engineered microorganism performances toward the production of the recombinant molecule (Ceroni et al. 2018).

Numerous expression systems are based on plasmid vectors for recombinant molecule production, both in research and industry. However, many cases of expression instability have been reported and the causes are still often misunderstood. First, plasmid replication frequency must be high enough to ensure equal partition between daughter cells, but also reasonable to prevent host cell exhaustion because of plasmid-induced metabolic load (Wegrzyn and Wegrzyn 2002). The relative importance of metabolic load due to recombinant protein production depends on various parameters like the amount of protein produced, plasmid copy number and size, host cell metabolic state, or growth medium composition (Bentley and Quiroga 1993; Glick 1995). Then, plasmid partitioning should be efficiently performed between daughter cells. Finally, because of their decreased metabolic load, plasmid-less cells have a higher growth rate than plasmid-bearing cells; the resulting growth rate difference intensifies segregational instability (Bentley et al. 1990; De Gelder et al. 2007).

Various tools have been developed to study population heterogeneity in single cells regarding expression level heterogeneity, like single-cell RT-PCR and RNA-seq or FISH (fluorescence in situ hybridization) (Haroon et al. 2013; Lee et al. 2006; Loftie-Eaton et al. 2014; Skulj et al. 2008; Tal and Paulsson 2012). Nevertheless, most of them are time consuming and not adapted to the constraints of fermentation processes which require a suitable monitoring method under dynamic conditions. Plus, they were designed on eukaryotic cells and will require further development to be suitable to smaller cells like prokaryotes (Gonzalez-Cabaleiro et al. 2017).

Cupriavidus necator H16 is a chemolithoautotrophic Gram-negative bacterium which belongs to the beta-subclass of *Proteobacteria*. *C. necator* has a versatile metabolism and is naturally able to consume oils (Budde et al. 2011), carboxylic acids (Friedrich et al. 1979; Grunwald et al. 2015; Johnson 1971), carbohydrates (Grousseau et al. 2014; Johnson 1971), and carbon dioxide (Crepin et al. 2016; Marc et al. 2017). Lately, *C. necator* has been engineered as a bioproduction platform for the biosynthesis of alcohols (Gruber et al. 2014; Marc et al. 2017), alka(e)ne (Crepin et al. 2016), carboxylic acids (Ewering et al. 2006; Hoefel et al. 2010), and methyl ketones (Muller et al. 2013). Two main strategies for the introduction of heterologous genes in *C. necator* have been developed: plasmids (Bi et al. 2013; Grousseau et al. 2014; Gruber et al. 2014, 2015, 2016; Sato et al. 2013; Sydow et al. 2017) and chromosomal insertion (Budde et al. 2011; Mifune et al. 2010; Wong et al. 2012). Developing and improving tools for the molecular engineering of *C. necator* H16 would open up to new possibilities in terms of synthetic biology of the strain.

Our aim consisted in being able to monitor expression heterogeneity throughout fermentation processes as efficiently and accurately as possible. So, it was necessary to develop a fast and reliable method to follow the expression of plasmid-encoded genes under dynamic conditions. The favored methodology was the expression of a plasmid-encoded reporter protein: enhanced green fluorescent protein (eGFP) (Cinelli et al. 2000; Shaner et al. 2005). This approach allows the use of flow cytometry, which has been reviewed in many studies as being a relevant method to monitor single-cell variability under dynamic conditions (Delvigne and Goffin 2014; Muller and Nebe-von-Caron 2010; Tracy et al. 2010). The first objective was to characterize a constitutive promoter driving *egfp* expression with the lowest impact as possible on host metabolism in terms of growth and physiology. The second objective was to ensure significant single-cell fluorescence

intensity levels. Consequently, a compromise needed to be reached between these two issues. The work was supported by kinetic data and viability measurements to determine the most suitable constitutive promoter to induce eGFP production within the framework of plasmid stability monitoring. The third objective was to verify that our plasmid expression level biosensor successfully allowed monitoring expression heterogeneity in experimental conditions where population heterogeneity had been induced artificially. For that purpose, the designed strain bearing the plasmid encoding for the expression level reporter was exposed to plasmid-curing-like conditions.

Material and methods

Strains, plasmids, and media

Strains

C. necator Re2133 (Budde et al. 2011) was used as expression strain. This strain was obtained by deleting genes encoding for acetoacetyl-CoA reductases (*phaB1B2B3*) and for PHA synthase (*phaC1*) from the wild-type strain *C. necator* H16/ATCC17699 which was gentamicin resistant (Gen^R). The strains *Escherichia coli* S17-1 and Top10 were used during plasmid construction.

Media

The rich medium for precultures was composed of 27.5 $g{\cdot}L^{-1}$ tryptic soy broth (TSB, Becton Dickinson, Sparks, MD, USA) with addition of 10 $mg{\cdot}L^{-1}$ gentamicin and 200 $mg{\cdot}L^{-1}$ kanamycin as final concentration. For tryptic soy agar (abbr. TSA) plates, 20 $g{\cdot}L^{-1}$ agar was added to the TSB medium.

For molecular biology, the rich lysogeny broth (abbr. LB) medium was used and composed of 10 $g{\cdot}L^{-1}$ of peptone, 5 $g{\cdot}L^{-1}$ of yeast extract, and 10 $g{\cdot}L^{-1}$ of NaCl (i.e., sodium chloride). For LB agar plates, 20 $g{\cdot}L^{-1}$ agar was added to the LB medium.

The mineral medium used for flask cultivation was previously described in Lu et al. (2013). Gentamicin (10 $mg{\cdot}L^{-1}$) and kanamycin (200 $mg{\cdot}L^{-1}$) were added to this medium. Fructose (20 $g{\cdot}L^{-1}$) and NH_4Cl (0.5 $g{\cdot}L^{-1}$) were respectively used as carbon and nitrogen sources. The mineral medium used for bioreactor cultivation was previously described in Marc et al. (2017). Fructose (50 $g{\cdot}L^{-1}$) was used as carbon source.

Plasmids

The plasmids used in this work are enlisted in Table 1. The design of the pKRSF1010 plasmids was detailed in Gruber et al. (2014). The plasmid pCB1 was designed and constructed in the team. The plasmid backbone pBBad (Fukui et al. 2009, 2011) was chosen; pBBad had previously been used in our team for the construction of *C. necator* recombinant strains toward the production of heterologous molecules of interest.

The sequence of interest P_{lac}-egfp was amplified from the plasmid pKRSF1010-P_{lac}-egfp using the forward primer pBBAD_Plac_acl1_fw and the reverse primer pBBAD_egfp_acl1_rv listed in Supplementary Data 1. Primers were obtained from Eurogentec (Angers, France). DNA sequence amplification was achieved using Phusion High-Fidelity PCR Master Mix with GC Buffer (New England Biolabs, France) and led on the Mx3005P QPCR System (Agilent Technologies, USA). PCR products were purified with the Monarch® PCR & DNA Cleanup Kit (New England Biolabs, USA).

The plasmid pBBad was linearized by the restriction enzyme *AclI* (New England Biolabs, USA) using NEB protocol recommendations and then purified by gel agarose extraction with the QIAquick gel extraction kit of Qiagen ® (Qiagen, Germany).

The cloning of the P_{lac}-egfp cassette into the plasmid vector pBBad was achieved through Gibson Isothermal Assembly®. The insert to vector ratio applied was 10:1 (w:w). Reaction took place at 50 °C for 30 min. Assembly products were transformed into high-efficiency *E. coli* Top 10 (Invitrogen, USA) chemical competent cells by heat shock. After growth, green colonies of *E. coli* Top10 were selected for plasmid purification with the QIAprep Spin Miniprep Kit (Qiagen, Germany). Screen PCR with OneTaq Hot Start 2X Master Mix with GC Buffer (New England Biolabs, USA) was used to verify the correct gene insertion. Plasmid constructions were confirmed by sequencing. Then, all constructed plasmids were transformed into electrocompetent *E. coli* S17-1 (ATCC 47055) by electroporation like that described in Crépin et al. (Crepin et al. 2016). Finally, conjugative transfer of plasmids from *E. coli* S17-1 to *C. necator* Re2133 was achieved like that in Slater et al. (1998).

Precultures and flask cultivations on fructose

One glycerol stock was plated on TSA plates (tryptic soy agar, TSB with 20 $g{\cdot}L^{-1}$ agar) containing 10 $mg{\cdot}L^{-1}$ gentamicin and 200 $mg{\cdot}L^{-1}$ kanamycin. The plates were incubated for 72 h at 30 °C. One colony was used to inoculate a rich medium flask culture (3 mL), which was grown for 48 h at 30 °C and 110 rpm. Then, the whole broth volume was used to inoculate a 30-mL mineral medium culture flask, which was incubated at 30 °C and 110 rpm for 24 h. Finally, the whole broth volume was used to inoculate a 300-mL mineral medium culture flask. The baffled flasks were incubated at 30 °C and 110 rpm for 10 h. Broth samples were taken regularly during this step.

Table 1 List and characteristics of the plasmids used in this work

Plasmid	Description	Reference
pKRSF1010-P_{lac}-eGFP	Kan^R, P_{lac}, egfp, par, RSF1010 mob, and oriV	(Gruber et al. 2014)
pKRSF1010-P_{tac}-eGFP	Kan^R, P_{tac}, egfp, par, RSF1010 mob, and oriV	(Gruber et al. 2014)
pKRSF1010-P_{n25}-eGFP	Kan^R, P_{n25}, egfp, par, RSF1010 mob, and oriV	(Gruber et al. 2014)
pKRSF1010-P_{j5}-eGFP	Kan^R, P_{j5}, egfp, par, RSF1010 mob, and oriV	(Gruber et al. 2014)
pBBad	Kan^R; PBad; pBBR1MCS-2 derivative	(Fukui et al. 2009)
pCB1	Kan^R, P_{lac}-eGFP; PBad; pBBR1MCS-2 derivative	This work

Batch cultivations on fructose

Batch cultivations consisted in non-limited growth on fructose. The cultures were led in a 5-L bioreactor Biostat®B-DCU (Sartorius, Germany) with a working volume of 3 L. Regulation and monitoring were done using MFCS/win 2.1 software package (Sartorius, Germany). Partial pressure of dioxygen (pO_2) in the medium was measured with the optical oxygen sensor InPro 6860i (Mettler Toledo, USA) and pH value was measured with a pressurized gel-filled pH electrode (Mettler Toledo, USA).

Temperature was regulated at 30 °C and pH level at 7.0 by addition of a 4 M KOH solution. Fermentation was carried out in aerobic conditions (i.e., air flow and stirring rates were regulated to maintain pO_2 above 30%). The initial fructose concentration in the medium was 50 $g{\cdot}L^{-1}$. To prevent nutrient limitation, pulses of rich phosphate solution (7 $mL{\cdot}L^{-1}$) and trace element solution (2 $mL{\cdot}L^{-1}$) were carried out every 10 $g{\cdot}L^{-1}$ of biomass produced.

Plasmid-curing subcultures

One glycerol stock was plated on a TSA plate with addition of 10 $mg{\cdot}L^{-1}$ gentamicin and 200 $mg{\cdot}L^{-1}$ kanamycin. The plate was incubated for 72 h at 30 °C. A single colony was used to inoculate 10 mL TSB with 10 $mg{\cdot}L^{-1}$ gentamicin and 200 $mg{\cdot}L^{-1}$ kanamycin in a flask. The flasks were incubated 24 h at 30 °C and 110 rpm. Then, this culture was used to inoculate 30 mL of flask mineral medium with 10 $mg{\cdot}L^{-1}$ gentamicin and 200 $mg{\cdot}L^{-1}$ kanamycin at 0.1 $g{\cdot}L^{-1}$of biomass. This step was considered as the positive control for reference fluorescence intensity distribution. The next subcultures, and all the others that followed, were started by a tenfold dilution in flask mineral medium without any antibiotics and grown at 37 °C and 110 rpm until a concentration of 1 $g{\cdot}L^{-1}$ biomass was reached. At every subculture starting point and endpoint, the optical density (600 nm) was measured and the samples were analyzed by flow cytometry.

Analytical procedure

Biomass characterization

Biomass growth was monitored by measuring optical density (OD) at 600 nm using a visible spectrophotometer (DR3900, Hachlange, Loveland, CO, USA) with a 0.2-cm path length absorption cell (Hellma). OD was calibrated against cell dry weight (CDW) measurements: 2 $g_{CDW}{\cdot}L^{-1}$ corresponds to 1 OD unit. Beforehand, 0.2-μm pore-size polyamide membranes (Sartorius, Göttingen, Germany) were dried to a constant weight at 60 °C under partial vacuum (200 mmHg) in an oven (HERAEUS, France) for 72 h and weighted. For dry weight measurements, culture medium was harvested and filtrated on the before-mentioned membranes which were then dried again to a constant weight at 60 °C under partial vacuum (200 mmHg) for 72 h.

Plate count

Plate count method was based on the ability of plasmid-bearing cells to grow on a selective medium. In our case, *C. necator* is naturally resistant to gentamycin. Kanamycin resistance is encoded on all plasmids. As a result, we consider that *C. necator* plasmid–bearing cells are those able to grow under the double antibiotic selective pressure.

Two series of plates were used: TSA with only 10 $mg{\cdot}L^{-1}$ gentamicin and TSA with both 10 $mg{\cdot}L^{-1}$ gentamicin and 200 $mg{\cdot}L^{-1}$ kanamycin. Serial dilutions were carried out in 9-mL physiological water (0.85% NaCl) tubes (BioMérieux, Marcy-l'Étoile, France). For every sample, three different dilutions were tested depending on the biomass concentration (generally between 10^{-5} and 10^{-9}). One hundred microliters of the diluted sample was plated in triplicate using the Whitley Automated Spiral Plater (WASP, Don Whitley Scientific, Shipley, UK).

Flow cytometry

eGFP fluorescence and cell viability were monitored with a BD Accuri C6® flow cytometer (BD Biosciences, Franklin

Lakes, NJ, USA). The device is equipped with blue (488 nm) and red (640 nm) excitation lasers. Light scatter is collected from two angles: forward (FSC, 0° ± 13) and side (SSC, 90° ± 13) scatter. Fluorescence intensity is measured by four detectors: FL1 (533 ± 30 nm), FL2 (585 ± 40 nm), FL3 (> 670 nm), and FL4 (675 ± 25 nm).

Propidium iodide (PI, Molecular Probes, Invitrogen, USA) was used to evaluate membrane permeability as a cell viability indicator. Commercial solution is composed of 20 mM PI in anhydrous dimethyl sulfoxide (*abbr.* DMSO) solvent and was diluted at a concentration of 20 μM before use. First, culture samples were diluted in 0.9% NaCl to reach approximately a cell concentration of 10^6 cells mL^{-1}. Then, the cells were stained by 20 μL of PI working solution and incubated for 20 min at room temperature in the dark. A 100% dead-cell control was prepared by incubating cells in 70% isopropanol for 1 h at room temperature.

Sample runs were performed (until 20,000 events were counted) at the slow flow rate setting (14 μL $\cdot min^{-1}$) using milli-Q water as sheath fluid. The FSC signal (threshold, 12,000) and SSC signal (threshold, 2000) were used as trigger channels.

Green fluorescence of eGFP was collected in the FL1 channel and red fluorescence of PI in the FL3 channel. Data acquisition was performed with BD Accuri CFlow® software. Data processing was achieved with FlowJo software (Becton Dickinson, Sparks, MD, USA).

Fluorescence measurement in the medium

Broth samples were centrifuged for 3 min at 13,000 rpm with a MiniSpin® table-top microcentrifuge (Eppendorf, Germany) and supernatants were used for fluorescence measurement.

Fluorescence unit measurements were achieved with the Synergy™ HT (Biotek®, USA) at excitation wavelength of 485 ± 20 nm and emission wavelength of 525 ± 20 nm. The sensitivity of the device was set at 50. Black Nunclon® 96-well plates (Thermo Fisher, USA) were used.

Fluorescence-activated cell sorting

Cell sorting experiments were led on the MoFlo Astrios EQ cell sorter using the Summit v6.3 software (Beckman Coulter, USA). Cell sorting was conducted with a 70-μm nozzle and 60-psi operating pressure. The sorting speed was set around 30,000 events per second. The single-cell mode for the sort mode and 0.5 drop for the droplet envelope were chosen. Cell samples were diluted in 0.9% NaCl prior to the sorting experiment.

Based on the FSC-Area vs SSC-Area (488 nm laser) plot and the FSC-Height vs FSC-Area (488-nm laser) plot, single cells with similar cell size and granularity were first selected. Then, based on the histogram of the eGFP fluorescence (488-nm laser, 526/52 filter), single cells were sorted depending on their fluorescence intensity.

Black and transparent Nunclon® 96-well plates (Thermo Fisher, USA) were used. Every single cell was dropped in a well from a 96-well plate. For each cell subpopulation, a total amount of six 96-well plates was generated. Two series of two 96-well plates were generated for each subpopulation: one set in transparent plates and one set in black plates; one plate of each serial contained TSB + 5 $mg \cdot L^{-1}$ gentamicin and one plate of each serial contained TSB + 5 $mg \cdot L^{-1}$ gentamicin + 50 $mg \cdot L^{-1}$ kanamycin. For every subpopulation, two transparent 96-well plates were generated to evaluate growth on solid medium. One plate contained TSA + 5 $mg \cdot L^{-1}$ gentamicin and one with TSA + 5 $mg \cdot L^{-1}$ gentamicin + 50 $mg \cdot L^{-1}$ kanamycin.

The TSB liquid plates were incubated at 30 °C and 40 rpm. Measurements of optical density and fluorescence unit were achieved every 8 h. For every TSB liquid plate, when the exponential phase was reached and around 7 cell generations, the fluorescence intensity distribution was determined in every well by flow cytometry.

The TSA solid plates were incubated at 30 °C and after growth, CFU was counted and observed under blue light with a blue light transilluminator (Thermo Fisher, USA) to reveal green fluorescent colonies.

Statistical analysis: Normality of distribution functions by boxplot representation

Boxplots are graphical tools used to represent an empirical distribution through some simple localization parameters: the median (50th percentile, red line), the first quartile (25th percentile), and the third quartile (75th percentile). The first and third quartiles respectively represent the bottom and top of the boxplot (Fig. 1d). The median, or second quartile, was represented by the line inside the box. The interquartile range (IQR) was situated between the first and third quartiles and represents the length of the box. The whiskers represent the minimum and maximum values when they are within 1.5 × IQR from both extremities of the box. Values above 1.5 × IQR were considered as outliers and are represented by points. A symmetric boxplot with its median in the middle of the box and same length whiskers might be expected to be normally distributed (Rakotomalala 2011).

Results

Our aim was to develop a quick and reliable plasmid expression level monitoring technique suitable for

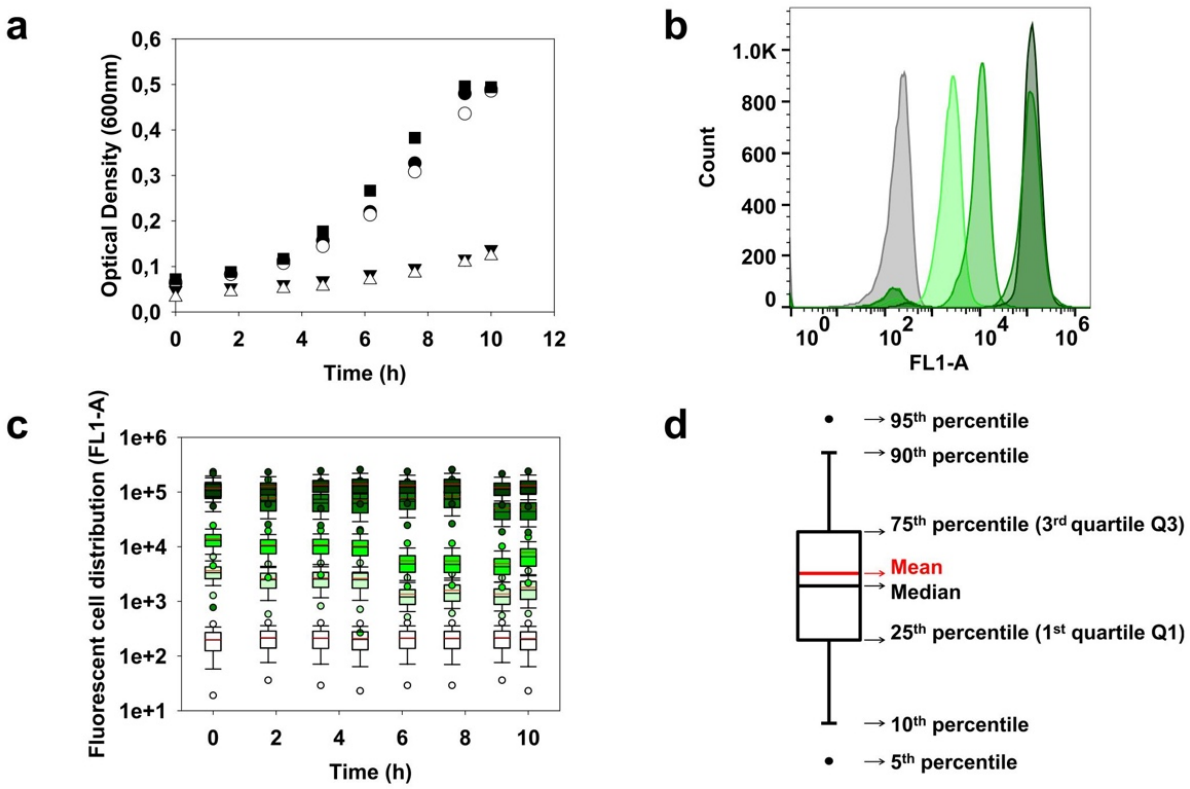

Fig. 1 **a** Growth kinetic in flasks of *Cupriavidus necator* Re2133 strains, harboring plasmids encoding for eGFP production with different constitutive promoters: Re2133/pKRSF1010-P_{j5}-eGFP (white-filled up-pointing triangle), Re2133/pKRSF1010-P_{n25}-eGFP (black-filled down-pointing triangle), Re2133/pKRSF1010-P_{tac}-eGFP (white-filled circle), Re2133/pKRSF1010-P_{lac}-eGFP (black-filled circle), and Re2133 (black-filled square). Data obtained by optical density measurements at 600 nm. **b** Fluorescence intensity distribution of *Cupriavidus necator* Re2133 strains bearing different plasmids based on various promoters. Gray: *C. necator* Re2133; from light to darker shades of green: *C. necator* Re2133 pKRSF1010-P_{lac}-egfp, pKRSF1010-P_{tac}-egfp, pKRSF1010-P_{n25}-egfp, and pKRSF1010-P_{j5}-egfp. Data obtained by flow cytometry in FL1 channel. **c** Boxplot comparing the fluorescence intensity distribution of the different *Cupriavidus necator* Re2133 strains, harboring plasmids encoding for eGFP production with different constitutive promoters (Re2133/pKRSF1010-P_{lac}-egfp, pKRSF1010-P_{tac}-egfp, pKRSF1010-P_{n25}-egfp, pKRSF1010-P_{j5}-egfp) during growth. White: *C. necator* Re2133; from light to darker shades of green: *C. necator* Re2133 pKRSF1010-P_{lac}-egfp, pKRSF1010-P_{tac}-egfp, and pKRSF1010-P_{n25}-egfp. Data obtained by flow cytometry in FL1 channel. **d** Definition of boxplot representation: The boundary of the box closest to zero indicates the 25th percentile, a black line within the box marks the median, a red line within the box marks the mean, and the boundary of the box farthest from zero indicates the 75th percentile. Whiskers above and below the box indicate the 90th and 10th percentiles. The black dot indicates the 95th and 5th percentiles

fermentation processes; this technique was based on the constitutive expression of the recombinant biosensor eGFP by plasmid-bearing cells. Flow cytometry was used as a fast, sensitive, statistically reliable method for fluorescence intensity measurements at the single-cell level which could be implemented for bioreactor on-line monitoring (Bahl et al. 2004). Four constitutive promoters inducing eGFP expression of increasing strength, respectively, P_{lac}, P_{tac}, P_{n25}, and P_{j5}, were evaluated regarding their impact on host cell physiology.

C. necator Re2133 was used as reference strain due to its increasing interest as a cell factory for different biomolecule production, like isopropanol and alkane (Crepin et al. 2016; Grousseau et al. 2014; Marc et al. 2017) under heterotrophic and autotrophic conditions.

Impact of the strength of promoters inducing eGFP production on *C. necator* physiology in flask cultures

Erlenmeyer flask cultures on mineral medium were carried out with *C. necator* Re2133 strains bearing plasmids encoding for eGFP production under the control of P_{j5}, P_{n25}, P_{tac}, and P_{lac} constitutive promoters. These promoters were designed by Gruber et al. (2014) and their strength was measured at the whole population level (Gruber et al. 2014). The plasmid-free strain *C. necator* Re2133 was used as reference.

Impact on growth kinetics

As expected, the growth rate of the plasmid-free strain *C. necator* Re2133 was the highest at 0.26 ± 0.01 h^{-1} (Fig. 1a). The highest maximum growth rate among plasmid-bearing strains Re2133/pKRSF1010-P_{lac}-egfp and *C. necator* Re2133/pKRSF1010-P_{tac}-egfp was 0.25 ± 0.01 h^{-1}, corresponding to a non-significant loss of 3% compared with the plasmid-free strain. The lowest maximum growth rates were reached by Re2133/pKRSF1010-P_{n25}-egfp and Re2133/pKRSF1010-P_{j5}-egfp with 0.12 ± 0.01 h^{-1} and 0.11 ± 0.01 h^{-1}, respectively, corresponding to a loss of about 56% and 54% compared with the reference strain.

Fluorescence intensity at the single-cell level

Samples from flask cultures were analyzed by flow cytometry to determine fluorescence intensity distribution at the single-cell level within the whole population. As expected, *C. necator* Re2133 plasmid–free cells do not fluoresce in the FL1-A detection channel of the flow cytometer (Fig. 1b, c). All cells presenting fluorescence intensity above a threshold of 8×10^2 in the FL1-A channel were considered eGFP-positive based on fluorescence intensity of the reference strain Re2133.

All fluorescence intensity distributions presented a normal distribution according to boxplot representation and did not vary during growth (Fig. 1c, d); the means and medians were equal and the whiskers were symmetric compared with the median. Promoter strength can be established by ranking plasmid-bearing strains from lowest to highest fluorescence intensity distribution at the single-cell level (Fig. 1b, c): P_{lac}, P_{tac}, P_{n25}, and P_{j5}. The increase in fluorescence intensity was equal to a half decade between P_{lac} and P_{tac}, one decade between P_{tac} and P_{n25}, and a tenth of a decade between P_{n25} and P_{j5}. No significant differences were observed between the promoters P_{n25} and P_{j5}, reaching the maximum of fluorescent protein accumulation in the cell.

Cell permeabilization and eGFP excretion

Membrane permeability and extracellular fluorescence intensity were evaluated during flask cultures. The impact of the metabolic burden due to different levels of eGFP production was also evaluated through cell permeability. At inoculation, the percentage of permeabilization was low under 5% for P_{lac}, P_{tac}, and P_{n25} but up to 25% for P_{j5}. For P_{lac}, P_{tac}, and P_{n25} promoters, the percentage of PI-positive cells (i.e., propidium iodide–stained cells) increased over time to reach up to 15% for P_{lac}, 13% for P_{tac}, and 22% for P_{n25} whereas for P_{j5}, the percentage did not vary (25%) (Fig. 2a).

The strain Re2133/pKRSF1010-P_{lac}-egfp maintained the lowest extracellular fluorescence intensity over time (Fig. 2b). The same kinetic was observed for pKRSF1010-P_{tac}-egfp except for the last point, which was significantly higher. The strains Re2133/pKRSF1010-P_{n25}-egfp and Re2133/pKRSF1010-P_{j5}-egfp presented with the highest extracellular fluorescence intensity levels. Even for the medium-strength promoter P_{n25}, there was a notable increase in eGFP excretion in the medium.

Although the relative amount of permeabilized cells was equal for Re2133/pKRSF1010-P_{lac}-egfp and Re2133/pKRSF1010-P_{tac}-egfp, the extracellular fluorescence intensity for the promoter P_{tac} was higher than that for P_{lac}. Increased permeabilization percentages for stronger constitutive promoters led to higher extracellular fluorescence intensity.

Plasmid monitoring during batch cultures in the bioreactor

A scale up from flask cultures to 5-L bioreactors was carried out to increase the number of cell generations and to amplify the phenomena described above. Therefore, the impact of the eGFP expression on *C. necator* physiology was further investigated for the two extreme plasmid constructions detailed above: pKRSF1010-P_{lac}-egfp and pKRSF1010-P_{j5}-egfp.

Impact of promoter strength on the growth kinetics

Re2133/pKRSF1010-P_{lac}-egfp reached a mean specific growth rate of 0.23 ± 0.01 h^{-1} as obtained previously in flasks (Fig. 3a). The Re2133/ pKRSF1010-P_{j5}-egfp strain reached a mean growth rate of 0.13 ± 0.01 h^{-1}. This value was slightly higher than the results obtained in flasks, likely due to a better control of cell environment (i.e., pH regulation, dissolved O_2 level). However, this growth rate could not be maintained for P_{j5} and decreased from 25 h until the end of the culture.

Impact of promoter strength on the fluorescence intensity distribution

For Re2133/pKRSF1010-P_{lac}-egfp, according to the boxplot representation, the fluorescent cell population presented all along the culture, a Gaussian distribution that did not vary (Fig. 3b); means and medians were equal and the boxes as well as the whiskers were symmetric. For Re2133/pKRSF1010-P_{j5}-egfp, the distribution range started to increase at 5 cell generations. On the last sample, the distribution could not be considered Gaussian anymore; a non-fluorescent subpopulation appeared and increased during the last hours of culture.

Cell permeabilization and eGFP excretion

For Re2133/pKRSF1010-Pl_{ac}-egfp, the percentage of permeabilized cells remained low, under 2% (Fig. 3c). However, this

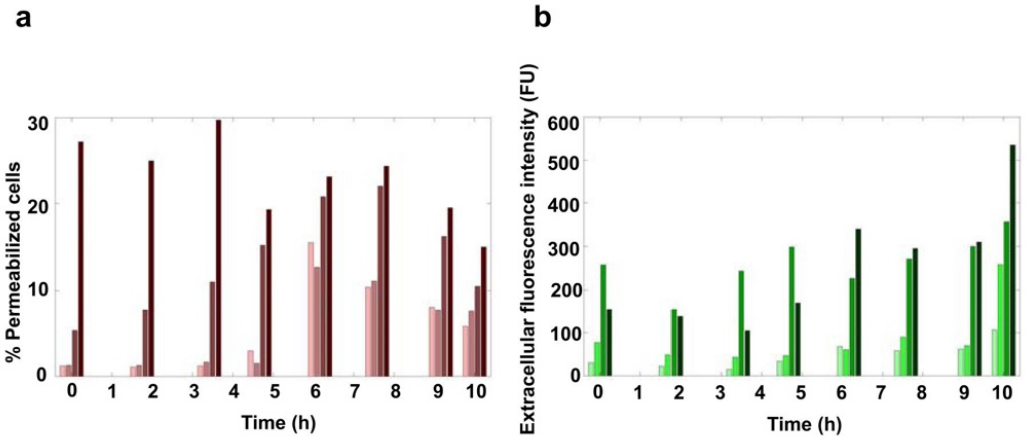

Fig. 2 **a** Percentage of permeabilized cells from broth cultures of *Cupriavidus necator* Re2133 strains during growth in flasks, harboring plasmids encoding for eGFP production with different constitutive promoters: Re2133/pKRSF1010-P_{j5}-eGFP (■), Re2133/pKRSF1010-P_{n25}-eGFP (■), Re2133/pKRSF1010-P_{tac}-eGFP (■), and Re2133/pKRSF1010-P_{lac}-eGFP (■). Data obtained by propidium iodide staining and flow cytometry (FL3 channel). **b** Extracellular fluorescence intensity from broth cultures of *Cupriavidus necator* Re2133 strains, harboring plasmids encoding for eGFP production with different constitutive: Re2133/pKRSF1010-P_{j5}-eGFP (■), Re2133/pKRSF1010-P_{n25}-eGFP (■), Re2133/pKRSF1010-P_{tac}-eGFP (■), and Re2133/pKRSF1010-P_{lac}-eGFP (■). Data obtained from fluorescence intensity measurements performed by a multiplate reader on broth sample supernatants

percentage increased all along the culture for Re2133/pKRSF1010-P_{j5}-egfp (Fig. 3d) and eventually reached 23% of permeabilized cells at 51 h.

Even if the extracellular fluorescence intensity increased for both strains, the levels reached by pKRSF1010-P_{j5}-egfp were 14-fold higher than those reached by pKRSF1010-P_{lac}-

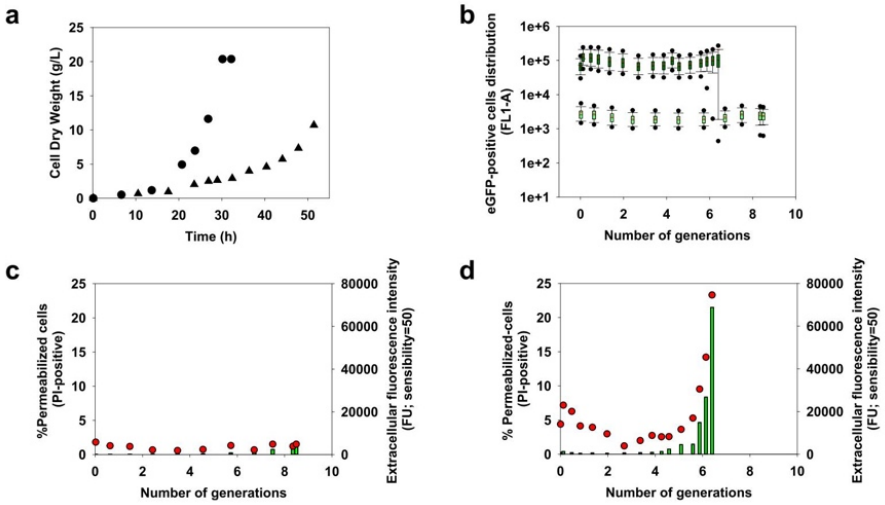

Fig. 3 **a** Growth kinetic in batch bioreactor of *Cupriavidus necator* Re2133 strains, harboring plasmids encoding for eGFP production with different constitutive promoters: Re2133/pKRSF1010-P_{lac}-eGFP (black-filled circle) and pKRSF1010-P_{j5}-eGFP (black-filled up-pointing triangle). Data obtained by optical density measurements at 600 nm. **b** Boxplot comparing the fluorescence intensity distribution depending on the cell generation number during batch bioreactor fermentations of the strains Re2133/pKRSF1010-P_{lac}-egfp (■) and pKRSF1010-P_{j5}-egfp (■). Data obtained by flow cytometry in FL1 channel. **c** Percentage of PI-positive cells (●) and extracellular fluorescence intensity (■), depending on the cell generation number, from batch cultures of *Cupriavidus necator* Re2133/pKRSF1010-P_{lac}-eGFP. Data obtained by flow cytometry (FL3 channel) and fluorescence measurements by a multiplate reader on supernatants. **d** Percentage of PI-positive cells (●) and extracellular fluorescence intensity (■), depending on the cell generation number, from batch cultures of *Cupriavidus necator* Re2133/pKRSF1010-P_{j5}-eGFP. Data obtained by flow cytometry (FL3 channel) and fluorescence measurements by a multiplate reader on supernatants

egfp, with a twofold lower biomass concentration.

Plasmid monitoring during batch culture: confrontation of fluorescence measurements with the traditional plate count method

To verify the validity of our plasmid expression level monitoring method, we confirmed our results with our reference method: parallel plate count.

For Re2133/pKRSF1010-P_{lac}-egfp, the results given by flow cytometry and plate count were comparable (Fig. 4a, c). The concentrations of eGFP-positive and gentamycin + kanamycin-resistant cells presented the same order of magnitude and the same evolution through time. The same observation can be made with the whole cell population and the gentamycin-resistant population concentration.

For Re2133/pKRSF1010-P_{j5}-egfp (Fig. 4b, d), cell concentrations given by plate count and flow cytometry seemed to evolve following the same dynamics. However, in the case of total cells and plasmid-bearing cell concentration, plate count gave lower results than fluorescence measurements all along the culture. So, plate count results were underestimated probably due to cultivability issues.

Fluorescence-activated cell sorting in conditions of plasmid curing by temperature

From the previous experiments, P_{lac} was chosen as the constitutive promoter to induce eGFP expression for the design of the plasmid expression level monitoring method; it was a good compromise between minimizing metabolic load on host cells and ensuring significant fluorescence intensity of single cells. So, the fluorescent cassette P_{lac}-egfp was cloned on a pBBad plasmid, and this backbone was used to encode recombinant molecule production (e.g., isopropanol (Crepin et al. 2016; Grousseau et al. 2014; Marc et al. 2017)) in our research team.

Our expression monitoring method was subjected to population heterogeneity in order to ensure that our eGFP biosensor would allow detecting it. So, the easiest approach was to induce population heterogeneity artificially. Plasmid-curing methods (Buckner et al. 2018; di Mauro et al. 1969; Trevors 1986) were reported in the literature to induce plasmid loss and population heterogeneity. In the present study, a plasmid-curing method based on temperature increase was set up to show the evolution of eGFP fluorescence intensity distribution within single cells in conditions of population heterogeneity. This experiment was based on successive subcultures of

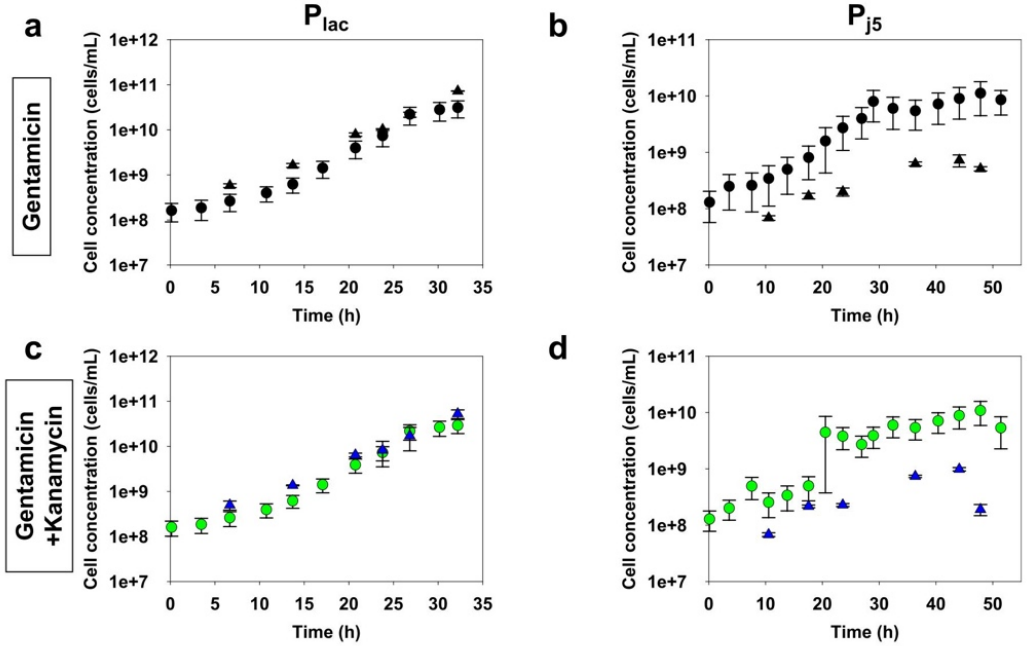

Fig. 4 **a** Comparison of the whole cell population concentration measured by flow cytometry (black-filled circle) and by plate count (black-filled up-pointing triangle) for Re2133/pKRSF1010-P_{lac}-eGFP during batch cultures. **b** Comparison of the amount of fluorescent cell concentration (green-filled circle) and the amount of kanamycin resistant cell concentration (blue-filled up-pointing triangle) for Re2133/pKRSF1010-P_{lac}-eGFP during batch cultures. **c** Comparison of the whole cell population concentration measured by flow cytometry (black-filled circle) and by plate count (black-filled up-pointing triangle) for Re2133/pKRSF1010-P_{j5}-eGFP during batch cultures. **d** Comparison of the amount of fluorescent cell concentration (green-filled circle) and the amount of kanamycin-resistant cell concentration (blue-filled up-pointing triangle) for Re2133/pKRSF1010-P_{j5}-eGFP during batch cultures

Re2133/pCB1 at 37 °C to maximize the number of cell generations exposed to plasmid-curing conditions.

Intensity fluorescence distribution during subcultures

After 6 successive subcultures (corresponding to 19 cell generations), only one subpopulation was observed. The fluorescence intensity distribution of eGFP-positive cells remained around a median of 3.6×10^3 in FL1-A, corresponding to the reference value for this strain under optimum culture conditions. The related population (2.1×10^3; 9.9×10^3) in the FL1-A channel was called "subpopulation P_2" (Fig. 5a). However, starting from 19 cell generations, three distinct subpopulations could be detected. Subpopulation P_2 remained visible. Another fluorescent subpopulation with a lower median value of 1.2×10^3 in FL1-A emerged; this corresponding population (4.9×10^2; 2.1×10^3) in the FL1-A channel was called "subpopulation P_1." A non-fluorescent subpopulation with a median of 2×10^2 in FL1-A appeared too; this related population (4.0×10^1; 4.9×10^2) in the FL1-A channel was named "subpopulation P_0."

Fluorescence-activated cell sorting was used to separate cells isolated from these three subpopulations according to their fluorescence intensity. The aim was to compare growth and fluorescent characteristics of the three subpopulations to better understand the loss of fluorescence intensity.

Cultivability and growth kinetics

During fluorescence-activated cell sorting (FACS), a single cell was deposited in each well of a 96-well plate. Six conditions were tested: subpopulations P_0, P_1, and P_2 were cultivated on TSB with 5 $mg \cdot L^{-1}$ gentamicin (total *C. necator* cells) and with 5 $mg \cdot L^{-1}$ gentamicin and 50 $mg \cdot L^{-1}$ kanamycin as a selection pressure (*C. necator* plasmid–bearing cells). The same antibiotic conditions were tested on solid medium for the subpopulations P_0, P_1, and P_2. All plates were incubated at 30 °C and multiplate reader measurements were performed regularly during cell growth on plates containing liquid medium.

No growth was detected for the population P_0, neither by absorbance measurements nor by fluorescence intensity measurements. Two hypotheses could explain this phenomenon: either cells or events were not cultivable or no cell was added to the plate because of too stringent selection conditions during cell sorting. The target criteria for cell selection before sorting based on fluorescence intensity were the same for all three subpopulations regarding the size (FSC) and the granulometry (SSC) of the cells. So, the absence of growth cannot be explained by a failure in the well inoculation.

However, cells grew on the plates containing subpopulations P_1 and P_2. On the plates containing subpopulation P_1 with gentamicin, growth was observed in 83% of the wells on liquid and 65% of the wells on solid medium. On the plates containing subpopulation P_1 with gentamicin + kanamycin, 80% of the wells on liquid and 70% of the wells on solid medium have grown. So, cells from the subpopulation P_1 were still resistant to kanamycin, as the percentages of growth were similar with and without selection pressure. On the plates containing subpopulation P_2 with gentamicin, 74% of the wells on liquid and 53% of the wells on solid medium presented growth. On the plates containing subpopulation P_2 with gentamicin + kanamycin, 71% of the wells on liquid and 58% of the wells on solid medium presented growth. So, cultivability was higher for the P_1 subpopulation compared with the P_2 subpopulation, both on liquid and on solid medium. For both subpopulations, cultivability was higher on liquid medium than on solid medium.

The mean growth rate was calculated for every well (Fig. 5b). On the one hand, P_1 cells tended to grow faster on average both on gentamicin at 0.07 ± 0.02 h^{-1} and on gentamicin + kanamycin at 0.09 ± 0.03 h^{-1}. On the other hand, P_2 cells grew slightly slower on average at 0.05 ± 0.01 h^{-1} on both antibiotic conditions.

Endpoint measurements of fluorescence intensity distribution in cell populations grown from single cells

In order to evaluate the fluorescent behavior of the progenies from the specific cell-sorted subpopulations (P_0, P_1, and P_2), the endpoint for each well was also analyzed by flow cytometry. Fluorescence intensity distribution regarding P_0, P_1, and P_2 subpopulations was determined based on the gates previously described (Fig. 5a). 3D scatter plots (Fig. 5c) were drawn in order to highlight sample variability according to the repartition of percentage of each subpopulation within a sample (i.e., well). The (x, y, z) coordinates of a point correspond to the percentage of fluorescent cells in P_0, P_1, or P_2 gates.

Three distinct clusters were identified and reported on 3D scatter plots. Thresholds of the red cluster (P_0 [0–10%]; P_1 [0–10%]; P_2 [80–100%]) corresponded to distributions composed of the highest P_2 cell contents. Thresholds of the purple cluster (P_0 [10–40%]; P_1 [25–35%]; P_2 [40–70%]) corresponded to distributions composed of the highest P_1 cell contents. The thresholds of the blue cluster (P_0 [10–40%]; P_1 [10–20%]; P_2 [40–70%]) corresponded to an intermediate cluster between the red and blue clusters.

According to each 3D scatter plot, one can clearly observe higher heterogeneity in the P_1 subpopulation progeny samples, in terms of endpoint fluorescence intensity distribution, compared with the subpopulation P_2 in both antibiotic conditions. Nevertheless, there was less heterogeneity for both subpopulations in the double antibiotic condition, which was more stringent.

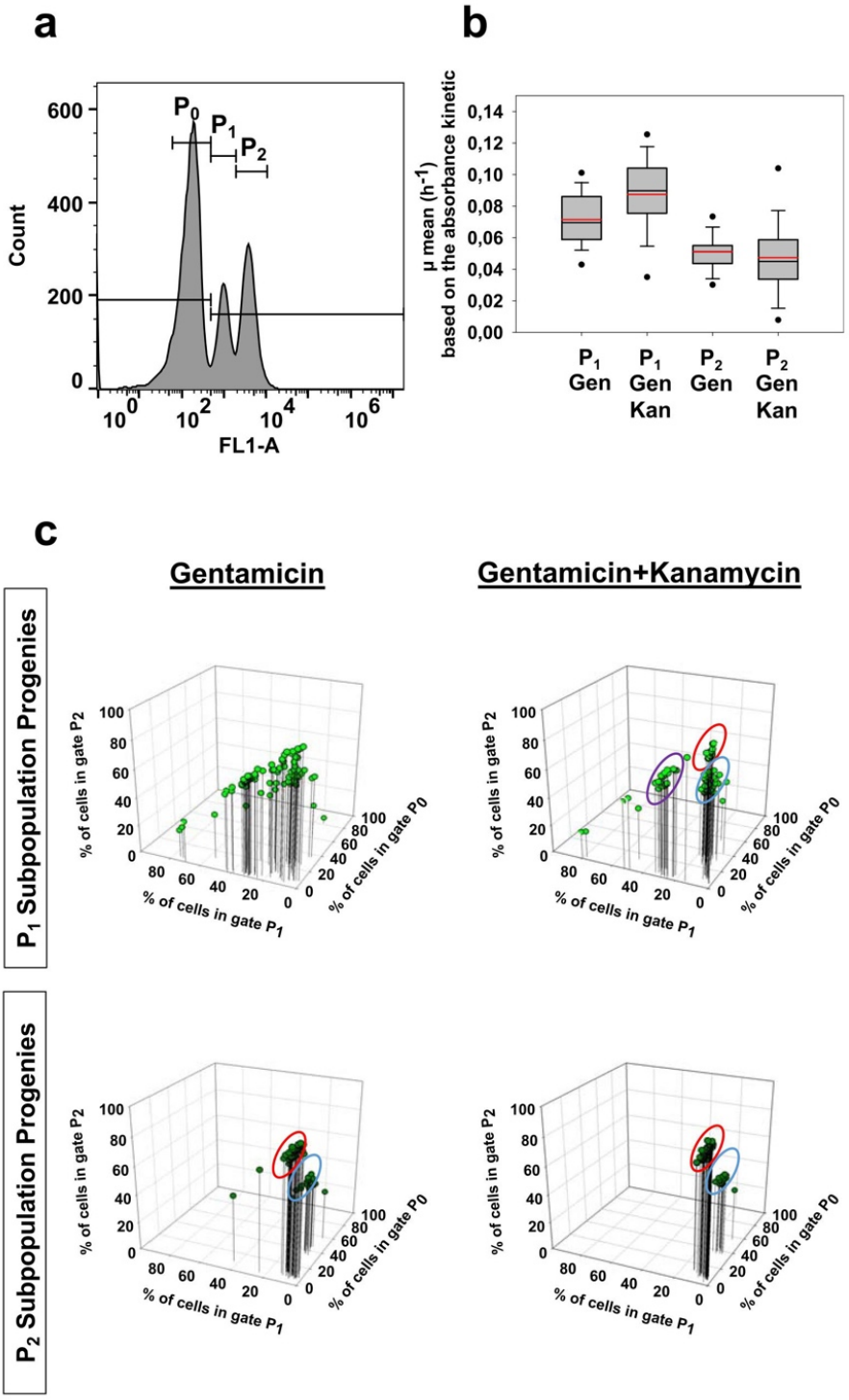

Fig. 5 **a** Fluorescence intensity distribution of the three subpopulations (P_0, P_1, and P_2) of *Cupriavidus necator* Re2133/pCB1 under plasmid-curing conditions. Data obtained by flow cytometry in channel FL1. **b** Boxplot comparing growth rates on the 96-well plates for the subpopulations P_1 and P_2, both on gentamicin and on gentamicin + kanamycin. Data obtained from optical density measurements at 600 nm. **c** Upper left: 3D scatter plot for fluorescence intensity distribution in the gates P_0, P_1, and P_2 for every well grown from a single cell from the subpopulation P_1 on gentamicin. Upper right: 3D scatter plot for fluorescence intensity distribution in the gates P_0, P_1, and P_2 for every well grown from a single cell from the subpopulation P_1 on gentamicin + kanamycin. Lower left: 3D scatter plot for fluorescence intensity distribution in the gates P_0, P_1, and P_2 for every well grown from a single cell from the subpopulation P_2 on gentamicin. Lower right: 3D scatter plot for fluorescence intensity distribution in the gates P_0, P_1, and P_2 for every well grown from a single cell from the subpopulation P_2 on gentamicin + kanamycin

The progenies of the cell-sorted subpopulation P_1, on selective medium, gave fluorescence distribution endpoints mostly composed of P_2 cells, like those shown in the blue (45% of sample distributions) and red (20% of sample distributions) clusters. However, the amount of P_1 cells in their fluorescence intensity distribution was the highest reached, like that shown by the purple cluster (25% of sample distributions).

Cells grown from the subpopulation P_2 on both antibiotic conditions gave fluorescence distribution endpoints mostly composed of P_2 cells, like those shown in the blue (30% of sample distributions) and red (70% of sample distributions) clusters.

Discussion

The goal of this study was to develop a quick and reliable method for monitoring variations in the constitutive expression level of reporter protein under dynamic bioprocesses. Because this technique was based on the expression of a recombinant eGFP by plasmid-bearing cells, a reporter system had to be chosen with the minimum impact on the physiology of host cells while allowing detectable cell fluorescence. As amply demonstrated in the literature (Bentley et al. 1990; De Gelder et al. 2007; Glick 1995; Million-Weaver and Camps 2014; Silva et al. 2012), the expression of a recombinant plasmid forces a metabolic burden on the host. In those publications, metabolic burden was quantified at the whole population scale by expression of plasmid-borne products, by the plasmid copy number in cells, and by plate count on selective medium. In the present study, the relative importance of the metabolic burden was evaluated indirectly from growth kinetics and cell physiology based on single-cell analyses in order to get access to the subpopulation distributions.

Flow cytometry had already been used to monitor plasmid stability within a pure culture of fluorescent *E. coli* strain in the work of Bahl et al. (2004). GFP expression was induced by a lac-promoter and encoded on the chromosome of *E. coli*. A functional *lacI* gene, encoding for a repressor protein, was integrated on the recombinant plasmid, thus preventing GFP expression initiation when plasmid is present in the cell. Inversely, GFP biosynthesis is induced after plasmid loss and plasmid-free cells were fluorescent. Our methods might be seen as complementary because of the two aims to detect expression heterogeneities: on the one hand, GFP production was a reporter for plasmid loss in Bahl et al. and on the other hand, eGFP production was a biosensor of plasmid expression level stability in our work. The accuracy of both methods was confronted to traditional plate count measurements. As for all biosensor-based approaches, bias has to be considered for both methods: (i) Half-life time of the molecules involved (i.e., eGFP and LacI) may lead to an underestimation of population heterogeneity; (ii) metabolic burden put on the host by the recombinant plasmid and/or the chromosomal insertion needs to be considered carefully in order to prevent phenotypic instability; metabolic burden might be the cause of plasmid instability or methylation of recombinant gene on the host's chromosome (Heller et al. 1995). Biosensors are precious tools for in vivo and/or in situ monitoring; however, it is crucial to be aware of the drawbacks.

In the work of Gruber et al. (2014), promoter strength has been evaluated at the whole population scale in the plasmids pKRSF1010/P_{lac}-egfp, pKRSF1010/P_{tac}-egfp, pKRSF1010/P_{n25}-egfp, and pKRSF1010/P_{j5}-egfp. The ranking of these promoters from the weakest to the strongest was P_{lac}, P_{tac}, P_{n25}, to P_{j5}. At the whole population level, the increase in fluorescence intensity was equal to 23% between P_{lac} and P_{tac}, 133% between P_{tac} and P_{n25}, and 100% between P_{n25} and P_{j5}. At the single-cell level, the ranking of these promoters according to their strength was confirmed; however, the increase in fluorescence intensity between promoters was more important when evaluated at the whole population level than at the single-cell level. Furthermore, for strong promoters like P_{j5}, the increase in the fluorescence intensity compared with medium strength promoters like P_{n25} was not as high as expected; over a critical threshold, there was no significant difference between medium and strong promoters at the single-cell level. This all suggested that the eGFP intensity measured at the whole population level might not entirely be due to intracellular eGFP. Most likely, eGFP molecules might be leaking outside the cells. This was confirmed by the fact that with increasing promoter strength, the percentage of permeabilized cells raised faster and higher, leading to higher eGFP excretion levels and lower fluorescence intensity of single cells. In that sense, after 5 cell generations in batch, the strain Re2133/pKRSF1010-P_{j5}-egfp presented a strong fluorescence intensity loss due to high permeabilization percentage and a high extracellular fluorescence. Promoter evaluation is usually done based on total fluorescence absorbance measurements using a spectrophotometer and a multiplate reader; this work demonstrates that an analysis at the single-cell level brings new insight into promoter evaluation.

The major effect in enhancing the promoter force was observed on growth kinetics, specifically through a decrease in the host maximal growth rate. For weak promoters as P_{lac} and P_{tac}, growth kinetic reduction was less drastic than for medium and strong promoters, P_{n25} and P_{j5}.

Furthermore, the results given by the two plasmid monitoring techniques were compared: parallel plate count and recombinant protein expression. By comparing these two methods, plasmid expression level stability was measured by detection of the expression of two different recombinant gene sets (eGFP and kanamycin resistance) encoded on the plasmid. For Re2133/pKRSF1010-P_{lac}-egfp cultures in batch, the two methods gave comparable results. However, for Re2133/

pKRSF1010-P_{j5}-egfp, plate count gave lower concentration than flow cytometry. This could be explained by the fact that plate counting depends on the cell's cultivability, which decreased drastically because of the metabolic load put on the host by P_{j5}. However, with both plate count and flow cytometry, no significant plasmid expression level fluctuations were observed during the tested culture conditions. To our knowledge, the drastic negative impact of the promoter P_{j5} on cell growth and physiology in the case of recombinant molecule production has never been highlighted before, and to our knowledge, indeed the very high strength of the constitutive promoter P_{j5} has always been presented as a positive productivity aspect like in the works of Gruber et al. (2014) and Lee et al. (2019), regarding eGFP and isoprene production, respectively. The use of stronger promoters leads to increased recombinant molecule production and so higher plasmid-related metabolic load. This increased protein production level might become toxic for the cells, as shown in the case of red fluorescent protein (Shemiakina et al. 2012).

So, in the present case study, the promoter P_{lac} has been chosen to constitutively induce the production of eGFP by plasmid-bearing cells, due to its significant fluorescence at the single-cell level and its low metabolic load on host cell metabolism.

When working with reporter molecules, the half-life time of the reporter protein must be considered. In this work, the ex vivo half-life time of eGFP was determined at 36 h (data not shown). Evidence was found in the literature that *Cupriavidus necator* has a particular segregation mechanism responsible for proper segregation of polyhydroxyalkanoate (PHA) granules during cell division and ensured, under balanced conditions, equal distribution of granules between daughter cells (Slaninova et al. 2018). It would be worth considering that the same mechanism would apply to eGFP and that after plasmid loss or expression cessation in the host cell, eGFP molecules in the mother cell should be equally segregated in daughter cells during cell division (Huh and Paulsson 2011). So, in the case where the signal is not saturated, fluorescence intensity eGFP should decrease exponentially in plasmid-free cells from generations to generations. Depending on their growth rate, cells may be counted as non-fluorescent in less than three cell generations (Alhumaizi et al. 2006). In conclusion, the non-eGFP-producing fluorescent cell population would present lower fluorescence intensity than eGFP-producing fluorescent cell population and consequently would lead to a significant decrease in fluorescence intensity distribution median after a single generation.

The eGFP biosensor needed to be subjected to population heterogeneity induced by plasmid-curing methods, to verify its accuracy in stringent conditions. After cell sorting, cells originated from the P_1 subpopulation were able to grow on kanamycin selection pressure, meaning that even after successive subcultures at 37 °C, cells of the P_1 subpopulation kept their plasmid. Plus, it had been shown that cells originated from the P_1 subpopulation grew faster and had a better cultivability both on liquid and solid medium than cells originated from the P_2 subpopulation. The favored hypothesis coming from these observations was that the reduced fluorescence intensity of P_1 subpopulation might be due to a lower eGFP expression in the cells compared to the P_2 subpopulation; indeed, a decrease in metabolic burden favored an increased growth rate of cell populations.

Like expected, cells from the P_2 subpopulation gave P_2 daughter cells after growth from a single cell. However, for cells from the P_1 subpopulation, only a small portion of wells (< 4%) were composed of 100% cells in the P_1 gate. Even if 25% of the wells gave cell populations with more than 25% of cells in the P_1 gate, it seemed like daughter cells from the subpopulation P_1 regained the ability to fluoresce higher (in the P_2 gate) after growth at optimal temperature of 30 °C; indeed 20% of wells gave cell population with more than 80% of cells in the P_2 gate.

In conclusion, the gene encoding for eGFP expression was inserted into different strains in order to analyze the fluorescence emitted at the single-cell level. This method offers the clear advantage of measuring the fluorescence emitted by eGFP molecules within single cells, thus giving access to the heterogeneity distribution within cell populations, whereas techniques at the whole population scale only measure the mean fluorescence emitted by cell populations. In this approach for plasmid expression level monitoring, it is crucial to minimize the effects of metabolic load on host.

We showed that increased promoter strength led to increased fluorescence intensity at the single-cell level up to a max and had a significant negative impact on growth kinetics and cell permeability. The use of the promoter P_{j5} led to strong fluorescence intensity loss, increased cell permeability, and important cultivability issues. Among all the promoters tested, P_{lac} presented with the lowest metabolic load on the host and ensured sufficient and significant fluorescence intensity of single cells; its use to control *egfp* transcription was found to be a good compromise. Batch cultivations showed that plasmid expression level monitoring by eGFP fluorescence measurement was a time-saving and relevant method, compared with the more traditional method of plate counting, when the weakest promoter P_{lac} was used. Plasmid-curing experiments on the strain Re2133/pCB1 showed the apparition of three subpopulations of P_0, P_1, and P_2 characterized by different fluorescence intensities at the single-cell level. The subpopulation P_0 was the non-fluorescent population

and the subpopulation P_2 was the reference fluorescent population. The decreased fluorescence intensity of the subpopulation P_1 compared with the subpopulation P_2 was due to an adaptation of eGFP expression levels in single cells in response to thermal stress. For the population P_1, the decrease in eGFP expression level was correlated with a decrease in metabolic load and so increased growth rate and cultivability when cells grown again at 30 °C. So, our plasmid expression level reporter system based on an eGFP biosensor allowed detecting population heterogeneity in plasmid-curing-like conditions with different plasmid expression levels.

Further steps would be testing our expression monitoring technique under "toxic" recombinant molecule–producing conditions in order to better understand the causes of plasmid expression level heterogeneity.

Acknowledgments We thank Petra Heidinger for the generous gift of the pKRSF1010 plasmids and fruitful discussions. We thank Delphine Lestrade from TWB for her assistance and expertise during the cell sorting experiments.

Authors' contributions statement CB, JL, SA, NG, and SG conceived and designed research. CB conducted experiments and analyzed data. CB wrote the manuscript and JL, SA, NG, and SG reviewed it. All authors read and approved the manuscript.

Availability of data and material All data generated or analyzed during this study are included in the present work.
Code availability Not applicable.

Funding information Funding was obtained from Doctoral Research Assignments from the French Ministry of Research.

Compliance with ethical standards

Competing interests The authors declare that they have no competing interests.

Ethical approval Not applicable, since the work does not involve any study with human participants or animals.

Consent to participate Not applicable.

References

Alhumaizi K, Alwan A, Ajbar A (2006) Competition of plasmid-bearing and plasmid-free organisms in a chemostat: a study of bifurcation phenomena. Math Comput Model 44(3–4):342–367. https://doi.org/10.1016/j.mcm.2006.01.021

Bahl ML, Sorensen SJ, Hansen LH (2004) Quantification of plasmid loss in *Escherichia coli* cells by use of flow cytometry. FEMS Microbiol Lett 232(1):45–49. https://doi.org/10.1016/s0378-1097(04)00015-1

Bentley WE, Quiroga OE (1993) Investigation of subpopulation heterogeneity and plasmid stability in recombinant *Escherichia coli* via simple segregated model. Biotechnol Bioeng 42(2):222–234. https://doi.org/10.1002/bit.260420210

Bentley WE, Mirjalili N, Andersen DC, Davis RH, Kompala DS (1990) Plasmid-encoded protein: the principal factor in the "metabolic burden" associated with recombinant bacteria. Biotechnol Bioeng 35(7):668–681. https://doi.org/10.1002/bit.260350704

Bi CH, Su P, Muller J, Yeh YC, Chhabra SR, Beller HR, Singer SW, Hillson NJ (2013) Development of a broad-host synthetic biology toolbox for *Ralstonia eutropha* and its application to engineering hydrocarbon biofuel production. Microb Cell Factories 12:1–10. https://doi.org/10.1186/1475-2859-12-107

Binder D, Drepper T, Jaeger KE, Delvigne F, Wiechert W, Kohlheyer D, Grunberger A (2017) Homogenizing bacterial cell factories: analysis and engineering of phenotypic heterogeneity. Metab Eng 42:145–156. https://doi.org/10.1016/j.ymben.2017.06.009

Brehm-Stecher BF, Johnson EA (2004) Single-cell microbiology: tools, technologies, and applications. Microbiol Mol Biol R 68(3):538. https://doi.org/10.1128/mmbr.68.3.538-559.2004

Buckner MMC, Ciusa ML, Piddock LJV (2018) Strategies to combat antimicrobial resistance: anti-plasmid and plasmid curing. Fems Microbiol R 42(6):781–804. https://doi.org/10.1093/femsre/fuy031

Budde CF, Riedel SL, Willis LB, Rha C, Sinskey AJ (2011) Production of poly(3-hydroxybutyrate-co-3-hydroxyhexanoate) from plant oil by engineered *Ralstonia eutropha* strains. Appl Environ Microbiol 77(9):2847–2854. https://doi.org/10.1128/aem.02429-10

Carlquist M, Fernandes RL, Helmark S, Heins AL, Lundin L, Sorensen SJ, Gernaey KV, Lantz AE (2012) Physiological heterogeneities in microbial populations and implications for physical stress tolerance. Microb Cell Factories 11. https://doi.org/10.1186/1475-2859-11-94

Ceroni F, Boo A, Furini S, Gorochowski TE, Borkowski O, Ladak YN, Awan AR, Gilbert C, Stan GB, Ellis T (2018) Burden-driven feedback control of gene expression. Nat Methods 15(5):387. https://doi.org/10.1038/nmeth.4635

Cinelli RAG, Ferrari A, Pellegrini V, Tyagi M, Giacca M, Beltram F (2000) The enhanced green fluorescent protein as a tool for the analysis of protein dynamics and localization: local fluorescence study at the single-molecule level. Photochem Photobiol 71(6):771–776. https://doi.org/10.1562/0031-8655(2000)071<0771:tegfpa>2.0.co;2

Crepin L, Lombard E, Guillouet SE (2016) Metabolic engineering of *Cupriavidus necator* for heterotrophic and autotrophic alka(e)ne production. Metab Eng 37:92–101. https://doi.org/10.1016/j.ymben.2016.05.002

De Gelder L, Ponciano JM, Joyce P, Top EM (2007) Stability of a promiscuous plasmid in different hosts: no guarantee for a long-term relationship. Microbiol-Sgm 153:452–463. https://doi.org/10.1099/mic.0.2006/001784-0

Delvigne F, Goffin P (2014) Microbial heterogeneity affects bioprocess robustness: dynamic single-cell analysis contributes to understanding of microbial populations. Biotechnol J 9(1):61–72. https://doi.org/10.1002/biot.201300119

Elowitz MB, Levine AJ, Siggia ED, Swain PS (2002) Stochastic gene expression in a single cell. Science 297(5584):1183–1186. https://doi.org/10.1126/science.1070919

Ewering C, Heuser F, Benolken JK, Bramer C, Steinbuchel A (2006) Metabolic engineering of strains of *Ralstonia eutropha* and *Pseudomonas putida* for biotechnological production of 2-methylcitric acid. Metab Eng 8(6):587–602. https://doi.org/10.1016/j.ymben.2006.05.007

Friedrich CG, Bowien B, Friedrich B (1979) Formate and oxalate metabolism in *Alcaligenes eutrophus*. J Gen Microbiol 115(NOV):185–192. https://doi.org/10.1099/00221287-115-1-185

Fukui T, Suzuki M, Tsuge T, Nakamura S (2009) Microbial synthesis of poly((R)-3-hydroxybutyrate-co-3-hydroxypropionate) from unrelated carbon sources by engineered *Cupriavidus necator*. Biomacromolecules 10(4):700–706. https://doi.org/10.1021/bm801391j

Fukui T, Ohsawa K, Mifune J, Orita I, Nakamura S (2011) Evaluation of promoters for gene expression in polyhydroxyalkanoate-producing *Cupriavidus necator* H16. Appl Microbiol Biotechnol 89(5):1527–1536. https://doi.org/10.1007/s00253-011-3100-2

Glick BR (1995) Metabolic load and heterologous gene-expression. Biotechnol Adv 13(2):247–261. https://doi.org/10.1016/0734-9750(95)00004-a

Gonzalez-Cabaleiro R, Mitchell AM, Smith W, Wipat A, Ofiteru ID (2017) Heterogeneity in pure microbial systems: experimental measurements and modeling. Front Microbiol 8. https://doi.org/10.3389/fmicb.2017.01813

Grousseau E, Lu JN, Gorret N, Guillouet SE, Sinskey AJ (2014) Isopropanol production with engineered *Cupriavidus necator* as bioproduction platform. Appl Microbiol Biotechnol 98(9):4277–4290. https://doi.org/10.1007/s00253-014-5591-0

Gruber S, Hagen J, Schwab H, Koefinger P (2014) Versatile and stable vectors for efficient gene expression in *Ralstonia eutropha* H16. J Biotechnol 186:74–82. https://doi.org/10.1016/j.jbiotec.2014.06.030

Gruber S, Schwab H, Koefinger P (2015) Versatile plasmid-based expression systems for Gram-negative bacteria-general essentials exemplified with the bacterium *Ralstonia eutropha* H16. New Biotechnol 32(6):552–558. https://doi.org/10.1016/j.nbt.2015.03.015

Gruber S, Schwendenwein D, Magomedova Z, Thaler E, Hagen J, Schwab H, Heidinger P (2016) Design of inducible expression vectors for improved protein production in *Ralstonia eutropha* H16 derived host strains. J Biotechnol 235:92–99. https://doi.org/10.1016/j.jbiotec.2016.04.026

Grunwald S, Mottet A, Grousseau E, Plassmeier JK, Popovic MK, Uribelarrea JL, Gorret N, Guillouet SE, Sinskey A (2015) Kinetic and stoichiometric characterization of organoautotrophic growth of *Ralstonia eutropha* on formic acid in fed-batch and continuous cultures. Microb Biotechnol 8(1):155–163. https://doi.org/10.1111/1751-7915.12149

Haroon MF, Skennerton CT, Steen JA, Lachner N, Hugenholtz P, Tyson GW (2013) In-solution fluorescence in situ hybridization and fluorescence-activated cell sorting for single cell and population genome recovery. In: DeLong EF (ed) Microbial metagenomics, metatranscriptomics, and metaproteomics, Methods in enzymology, vol 531. Elsevier Academic Press Inc, San Diego, pp 3–19

Heller H, Kammer C, Wilgenbus P, Doerfler W (1995) Chromosomal insertion of foreign (Adenovirus-type-12, plasmid, or bacteriophage-lambda) DNA is associated with enhanced methylation of cellular DNA segments. Proc Natl Acad Sci USA 92(12):5515–5519. https://doi.org/10.1073/pnas.92.12.5515

Hoefel T, Wittmann E, Reinecke L, Weuster-Botz D (2010) Reaction engineering studies for the production of 2-hydroxyisobutyric acid with recombinant *Cupriavidus necator* H 16. Appl Microbiol Biotechnol 88(2):477–484. https://doi.org/10.1007/s00253-010-2739-4

Huh D, Paulsson J (2011) Random partitioning of molecules at cell division. Proc Natl Acad Sci USA 108(36):15004–15009. https://doi.org/10.1073/pnas.1013171108

Johnson BFRYS (1971) Dissimilation of aromatic compounds by *Alcaligenes eutrophus*. J Bacteriol 107(2):468–475

Lee CL, Ow DSW, Oh SKW (2006) Quantitative real-time polymerase chain reaction for determination of plasmid copy number in bacteria. J Microbiol Methods 65(2):258–267. https://doi.org/10.1016/j.mimet.2005.07.019

Lee HW, Park JH, Lee HS, Choi W, Seo SH, Anggraini ID, Choi ES, Lee HW (2019) Production of bio-based isoprene by the mevalonate pathway cassette in *Ralstonia eutropha*. J Microbiol Biotechnol 29(10):1656–1664. https://doi.org/10.4014/jmb.1909.09002

Loftie-Eaton W, Tucker A, Norton A, Top EM (2014) Flow cytometry and real-time quantitative PCR as tools for assessing plasmid persistence. Appl Environ Microbiol 80(17):5439–5446. https://doi.org/10.1128/aem.00793-14

Lu JN, Brigham CJ, Rha C, Sinskey AJ (2013) Characterization of an extracellular lipase and its chaperone from *Ralstonia eutropha* H16. Appl Microbiol Biotechnol 97(6):2443–2454. https://doi.org/10.1007/s00253-012-4115-z

Marc J, Grousseau E, Lombard E, Sinskey AJ, Gorret N, Guillouet SE (2017) Over expression of GroESL in *Cupriavidus necator* for heterotrophic and autotrophic isopropanol production. Metab Eng 42:74–84. https://doi.org/10.1016/j.ymben.2017.05.007

Martins BMC, Locke JOW (2015) Microbial individuality: how single-cell heterogeneity enables population level strategies. Curr Opin Microbiol 24:104–112. https://doi.org/10.1016/j.mib.2015.01.003

di Mauro E, Synder L, Marino P, Lamberti A, Coppo A, Tocchini-Valentini GP (1969) Rifampicin sensitivity of the components of DNA-dependent RNA polymerase. Nature 222(5193):533–537. https://doi.org/10.1038/222533a0

Mifune J, Nakamura S, Fukui T (2010) Engineering of pha operon on *Cupriavidus necator* chromosome for efficient biosynthesis of poly(3-hydroxybutyrate-co-3-hydroxyhexanoate) from vegetable oil. Poly Degrad Stabil 95(8):1305–1312. https://doi.org/10.1016/j.polymdegradstab.2010.02.026

Million-Weaver S, Camps M (2014) Mechanisms of plasmid segregation: have multicopy plasmids been overlooked? Plasmid 75:27–36. https://doi.org/10.1016/j.plasmid.2014.07.002

Mortier J, Tadesse W, Govers SK, Aertsen A (2019) Stress-induced protein aggregates shape population heterogeneity in bacteria. Curr Genet 65(4):865–869. https://doi.org/10.1007/s00294-019-00947-1

Muller S, Nebe-von-Caron G (2010) Functional single-cell analyses: flow cytometry and cell sorting of microbial populations and communities. Fems Microbiol R 34(4):554–587. https://doi.org/10.1111/j.1574-6976.2010.00214.x

Muller S, Harms H, Bley T (2010) Origin and analysis of microbial population heterogeneity in bioprocesses. Curr Opin Biotechnol 21(1):100–113. https://doi.org/10.1016/j.copbio.2010.01.002

Muller J, MacEachran D, Burd H, Sathitsuksanoh N, Bi CH, Yeh YC, Lee TS, Hillson NJ, Chhabra SR, Singer SW, Beller HR (2013) Engineering of *Ralstonia eutropha* H16 for autotrophic and heterotrophic production of methyl ketones. Appl Environ Microbiol 79(14):4433–4439. https://doi.org/10.1128/aem.00973-13

Nana GYG, Ripoll C, Cabin-Flaman A, Gibouin D, Delaune A, Janniere L, Grancher G, Chagny G, Loutelier-Bourhis C, Lentzen E, Grysan P, Audinot JN, Norris V (2018) Division-based, growth rate diversity in bacteria. Front Microbiol 9. https://doi.org/10.3389/fmicb.2018.00849

Rakotomalala R (2011) Tests de normalité - Techniques empiriques et tests statistiques. Université Lumière, Lyon, p 2

Sato S, Fujiki T, Matsumoto K (2013) Construction of a stable plasmid vector for industrial production of poly(3-hydroxybutyrate-co-3-hydroxyhexanoate) by a recombinant *Cupriavidus necator* H16 strain. J Biosci Bioeng 116(6):677–681. https://doi.org/10.1016/j.jbiosc.2013.05.026

Shaner NC, Steinbach PA, Tsien RY (2005) A guide to choosing fluorescent proteins. Nat Methods 2(12):905–909. https://doi.org/10.1038/nmeth819

Shemiakina II, Ermakova GV, Cranfill PJ, Baird MA, Evans RA, Souslova EA, Staroverov DB, Gorokhovatsky AY, Putintseva EV, Gorodnicheva TV, Chepurnykh TV, Strukova L, Lukyanov S, Zaraisky AG, Davidson MW, Chudakov DM, Shcherbo D (2012) A monomeric red fluorescent protein with low cytotoxicity. Nat Commun:3. https://doi.org/10.1038/ncomms2208

Silva F, Queiroz JA, Domingues FC (2012) Evaluating metabolic stress and plasmid stability in plasmid DNA production by *Escherichia coli*. Biotechnol Adv 30(3):691–708. https://doi.org/10.1016/j.biotechadv.2011.12.005

Skulj M, Okrslar V, Jalen S, Jevsevar S, Slanc P, Strukelj B, Menart V (2008) Improved determination of plasmid copy number using quantitative real-time PCR for monitoring fermentation processes. Microb Cell Factories:7. https://doi.org/10.1186/1475-2859-7-6

Slaninova E, Sedlacek P, Mravec F, Mullerova L, Samek O, Koller M, Hesko O, Kucera D, Marova I, Obruca S (2018) Light scattering on PHA granules protects bacterial cells against the harmful effects of UV radiation. Appl Microbiol Biotechnol 102(4):1923–1931. https://doi.org/10.1007/s00253-018-8760-8

Slater S, Houmiel KL, Tran M, Mitsky TA, Taylor NB, Padgette SR, Gruys KJ (1998) Multiple beta-ketothiolases mediate poly(beta-hydroxyalkanoate) copolymer synthesis in *Ralstonia eutropha*. J Bacteriol 180(8):1979–1987

Sydow A, Pannek A, Krieg T, Huth I, Guillouet SE, Holtmann D (2017) Expanding the genetic tool box for *Cupriavidus necator* by a stabilized L-rhamnose inducible plasmid system. J Biotechnol 263:1–10. https://doi.org/10.1016/j.jbiotec.2017.10.002

Tal S, Paulsson J (2012) Evaluating quantitative methods for measuring plasmid copy numbers in single cells. Plasmid 67(2):167–173. https://doi.org/10.1016/j.plasmid.2012.01.004

Tracy BP, Gaida SM, Papoutsakis ET (2010) Flow cytometry for bacteria: enabling metabolic engineering, synthetic biology and the elucidation of complex phenotypes. Curr Opin Biotechnol 21(1):85–99. https://doi.org/10.1016/j.copbio.2010.02.008

Trevors JT (1986) Plasmid curing in bacteria. FEMS Microbiol Lett 32(3–4):149–157

Wegrzyn G, Wegrzyn A (2002) Stress responses and replication of plasmids in bacterial cells. Microb Cell Factories 1. https://doi.org/10.1186/1475-2859-1-2

Wong YM, Brigham CJ, Rha C, Sinskey AJ, Sudesh K (2012) Biosynthesis and characterization of polyhydroxyalkanoate containing high 3-hydroxyhexanoate monomer fraction from crude palm kernel oil by recombinant *Cupriavidus necator*. Bioresour Technol 121:320–327. https://doi.org/10.1016/j.biortech.2012.07.015

Zielenkiewicz U, Ceglowski P (2001) Mechanisms of plasmid stable maintenance with special focus on plasmid addiction systems. Acta Biochim Pol 48(4):1003–1023

Part 3 : Results and discussion

Chapter 2: Identification of heterologous subpopulations from a pure culture in a bioreactor

Subchapter 2: Study of plasmid expression level heterogeneity under plasmid-curing like conditions

2.2.1 Abstract

Plasmid expression level was studied in response to stringent culture conditions, supposed to enhance plasmid instability, through plasmid curing strategies. The aim of this work was to study the response of the plasmid expression biosensor under various cultivation modes (*i.e.* batch, chemostat) and to investigate the impact of growth rate on the plasmid expression level heterogeneity. Two plasmid curing strategies were first tested for their efficiency at generating heterogeneity in batch: rifampicin addition and temperature increase. We observed that temperature increase from 30 to 37°C was the most efficient plasmid curing strategy. Too high temperature of 42°C was found to be inhibitory of cell growth and therefore, did not allow dynamic analysis during growth. The impact of the dilution rate in chemostat (*i.e.* specific growth rate) on plasmid expression under plasmid curing-like conditions was studied. To generate a heterogeneous population in terms of plasmid expression levels, successive batches at 37°C were initially conducted. Three distinct fluorescent subpopulations P_0 (not fluorescent), P_1 (low fluorescence, median = $1 \cdot 10^3$) and P_2 (high fluorescence, median = $6 \cdot 10^3$) were obtained. From there, the chemostat culture was implemented to study the long-term stress response under well-controlled environment at defined dilution rates and supra-optimal culture temperature. It was shown that for dilution rates comprised between 0.05 and 0.1 h^{-1}, the subpopulation P_2 (62 % *vs.* 90 %) was favored compared to P_1 cells (54 % *vs.* 1 %), especially when growth rate increased. Our biosensor was efficient at discriminating subpopulation presenting different expression levels under stringent heterogeneous culture conditions. Plus, we showed that controlling growth kinetics had a stabilizing impact on plasmid expression levels, even under heterogeneous expression conditions.

KEYWORDS:

Plasmid curing, chemostat, plasmid stability, expression level, flow cytometry, Single-cell analysis, *Cupriavidus necator* H16

2.2.2 Introduction

Historically, microbial populations cultivated in assumed homogeneous environments are by extension also considered homogeneous in terms of its individuals. Nowadays, this postulate is being discussed and more and more studies showing that population heterogeneity can be observed among monoclonal cultures in homogeneous environments are being published (Carlquist *et al.* 2012, Delvigne *et al.* 2014, Gonzalez-Cabaleiro *et al.* 2017, Heins *et al.* 2018). In recombinant bioprocesses, population heterogeneity contributes to enhance process instability (Binder *et al.* 2017). Therefore, a better understanding of the mechanisms leading to phenotypic homogeneity of engineered strains is mandatory to ensure bioprocess robustness. In previous work (Boy et *al.*, 2020), a plasmid expression level monitoring method based on the expression of a plasmid-encoded eGFP biosensor has been designed, in order to identify subpopulations presenting different phenotypic behaviors. At first, this method was used in homogeneous cell populations. Then, its single-cell response to artificially induce plasmid expression level heterogeneity was studied in flasks through serial subcultures at increased temperature and cell sorting through FACS (*i.e.* Fluorescence Activated Cell Sorting) technology. FACS allowed investigating each subpopulation physiological characteristics separately (*i.e.* growth rate) (Boy *et al.* 2020). As these experiments were performed in flasks with less than 20 cell generations, it would be interesting to increase the cell generation number submitted to plasmid curing-like conditions to amplify the heterogeneity in plasmid expression levels. In this work, the response of our plasmid expression level monitoring method in plasmid-curing like conditions is studied.

Plasmid curing strategies are developed to favor the removal of plasmids from bacterial cells, generally to obtain plasmid-free cells to study specific plasmid-encoded metabolisms (Andersen *et al.* 1981, Hughes *et al.* 1984, Monchy *et al.* 2006); or as a strategy to combat plasmid-encoded antimicrobial resistance (Zaman 2010, Buckner *et al.* 2018). The choice of the most fitting curing agent for a plasmid vector is hardly predictable. Plasmids significantly differ in their ability to be cured depending on their own properties. So, no universally effective curing agent has been identified yet. Some curing agents have been found to damage and stress out cells in a non-specific way, while some seems to act in a more specific manner (Trevors 1986, Zaman 2010). Many strategies have been developed over the years and are generally based on temperature increase (Andersen *et al.* 1981, Hughes *et al.* 1984, Buckner *et al.* 2018), plasmid incompatibility (Trevors *et al.* 1986, Buckner *et al.* 2018), antibiotic addition (*such as*. mitomycin C (Andersen *et al.* 1981, Hughes *et al.* 1984, Trevors *et al.* 1986), novobiocin (Trevors *et al.* 1986), rifampicin (di Mauro *et al.* 1969, Andersen *et al.* 1981, Hughes *et al.* 1984, Trevors *et al.* 1986)), addition of DNA intercalating agents (*such as.* acridine orange (Andersen *et al.* 1981, Zaman *et al.* 2010)), acriflavine (Trevors *et al.* 1986), ethidium bromide (Andersen *et al.* 1981, Zaman *et al.* 2010)), or detergent additions (*such as.* sodium dodecyl sulphate (Andersen *et al.*

1981, Zaman *et al.* 2010)). In most protocols, plasmid curing techniques are coupled with successive subcultures under these stringent conditions. *Cupriavidus sp.* homologous plasmids have already been removed by some of these methods: acridine orange, ethidium bromide, sodium dodecyl sulfate (Andersen *et al.* 1981), benzoate (Hughes *et al.* 1984), rifampicin, mitomycin C and higher growth temperature (Andersen *et al.* 1981, Hughes *et al.* 1984). In this work, attention was drawn to rifampicin addition and temperature increase.

Rifampicin addition as plasmid curing strategy was interesting in our case of study, as it causes variations in the plasmid expression level through disruption in plasmid DNA transcription. Rifampicin was shown to bind to RNA polymerase molecule, the enzyme responsible for DNA transcription by forming a stable drug-enzyme complex (Wehrli *et al.* 1983). In Bazzicalupo et *al.* (1972), rifampicin specifically inhibited the initiation step in the reaction catalyzed by RNA polymerase, therefore eliminating the F'-lac plasmid from *E. coli*. Studies showed that plasmids seemed to have been completely evacuated from *Escherichia coli* (Haemolysin and F'-lac plasmids (Buckner *et al.* 2018)), *Staphylococcus aureus* (Penicillinase plasmids (Trevors *et al.* 1986, Buckner *et al.* 2018)) and *Cupriavidus necator* (100 $mg \cdot L^{-1}$ for Hydrogenase plasmids (Andersen *et al.* 1981)). Nevertheless, rifampicin did not allow curing plasmid from *E. coli* strains whose RNA polymerases were rifampicin-resistant (di Mauro *et al.* 1969, Bazzicalupo *et al.* 1972, Trevors *et al.* 1986, Buckner *et al.* 2018).

Increasing growth temperature from 5 to 7°C up to the optimal growth temperature was used as an effective curing strategy. Mechanisms of plasmid curing by temperature are not well known, but hypothesis have been suggested to propose that such strategy might directly interfere with plasmid replication mechanisms by applying temperatures higher than the optimal working temperature of RNA polymerases. This curing strategy was coupled with series of subcultures using successive inoculations when log phase has been reached (Trevors *et al.* 1986). Several cell generations have to be generated in order to be efficient. In *C. necator*, a growth temperature of 42°C (12 degree above optimal growth temperature) was successfully applied for curing plasmids (Hughes *et al.* 1984).

Cupriavidus necator has regain a lot of interest those past years, based on its natural metabolic potentialities such as both autotrophic and heterotrophic growth (Johnson *et al.* 1971, Friedrich *et al.* 1979, Budde *et al.* 2011, Grousseau *et al.* 2014, Grunwald *et al.* 2015, Crepin *et al.* 2016, Marc *et al.* 2017), and as its poly-β-hydroxybutyrate (*abbr.* PHB) biosynthesis pathways (Pohlmann *et al.* 2006, Koller *et al.* 2010, Cruz *et al.* 2019, Nangle *et al.* 2020, Tang *et al.* 2020). Especially, synthetic biology and metabolic engineering have been implemented in order to build heterologous metabolic pathways for synthon biosynthesis (Ewering *et al.* 2006, Hoefel *et al.* 2010, Muller *et al.* 2013, Grousseau *et al.* 2014, Crepin *et al.* 2016, Marc *et al.* 2017, Black *et al.* 2018, Krieg *et al.* 2018, Garrigues *et al.* 2020). In

that context, it is crucial to develop and validate tools to be able to evaluate the robustness of strain within a bioprocess.

In order to further evaluate our capacity to monitor the heterogeneity of plasmid expression level at the single-cell level, *C. necator* strains bearing an engineered eGFP-biosensor plasmid were submitted to various plasmid curing conditions to artificially induce heterogeneity. Herein we aimed at studying more precisely the response of the biosensor under various cultivation modes (batch and chemostat) and investigating the impact of growth rate on plasmid expression level heterogeneity. First, the two plasmid curing strategies were led in batch mode to evaluate their impact on cell physiology (subpopulations) and cell macroscopic behavior. Then, the most efficient plasmid curing strategy was applied in chemostat

2.2.3 Material and Methods

2.2.3.1 Strains

C. necator Re2133 (Budde *et al.* 2011) was used as expression strain. This strain was obtained by deleting genes encoding for acetoacetyl-CoA reductases (*phaB1B2B3*) and for PHA synthase (*phaC1*) from the wildtype strain *C. necator* H16 / ATCC17699 which was gentamicin resistant (Gen^R). The strains *Escherichia coli* S17-1 and Top10 were used during plasmid construction.

2.2.3.2 Plasmids

The plasmid used in this work was the plasmid pCB1. This plasmid encodes for an eGFP through the insertion of the P_{lac}-*egfp* cassette (Gruber *et al.* 2014) on the pBBad (Fukui *et al.* 2009) backbone, derived from the pBBR1MCS-2 plasmid, (Kovach *et al.* 1995) which bears kanamycin resistance (Kan^R). Its design and associated molecular biology protocols were described in more details in Boy et *al*. (2020).

2.2.3.3 Media

The rich medium for precultures was composed of 27.5 $g \cdot L^{-1}$ Tryptic Soy Broth (TSB, Becton Dickinson, Sparks, MD, USA) with addition of 10 $mg \cdot L^{-1}$ gentamicin and 200 $mg \cdot L^{-1}$ kanamycin as final concentration. For Tryptic Soy Agar (*abbr.* TSA) plates, 20 $g \cdot L^{-1}$ agar was added to the TSB medium.

For molecular biology, the rich Lysogeny broth medium (*abbr.* LB) was used and composed of 10 $g \cdot L^{-1}$ of peptone, 5 $g \cdot L^{-1}$ of yeast extract and 10 $g \cdot L^{-1}$ of NaCl (*i.e.* sodium chloride). For LB agar plates, 20 $g \cdot L^{-1}$ agar was added to the LB medium.

The mineral medium used for flasks cultivation was previously described in Lu et *al.* (Lu *et al.* 2013). Gentamicin (10 mg·L^{-1}) and kanamycin (200 mg·L^{-1}) were added to this medium. Fructose (20 g·L^{-1}) and NH_4Cl (0.5 g·L^{-1}) were respectively used as carbon and nitrogen sources.

The mineral medium used for bioreactor cultivation was composed as follows (per liter): $(NH_4)_2SO_4$, 2.8 g; $MgSO_4$-$7H_2O$, 0.75 g; phosphorus (Na_2HPO_4-$12H_2O$, 1.5 g; KH_2PO_4, 0.25 g); nitrilotriacetic acid, 0.285 g; ammonium iron(III) citrate (28%), 0.09 g; $CaCl_2$, 0.015 g; trace elements (H_3BO_3, 0.45 mg; $CoCl_2$-$6H_2O$, 0.3 mg; $ZnSO_4$,$7H_2O$, 0.15 mg; $MnCl_2$-$4H_2O$, 0.045 mg; Na_2MoO4-$2H_2O$, 0.045 mg; $NiCl_2$-$6H_2O$, 0.03 mg; $CuSO_4$, 0.015 mg). Fructose (30 g·L^{-1}) was used as carbon source.

2.2.3.4 Precultures on fructose

One glycerol stock was plated on TSA plates containing 10 mg·L^{-1} gentamicin and 200 mg·L^{-1} kanamycin. The plates were incubated for 72 h at 30 °C. One colony was used to inoculate a rich medium flask culture (3 mL), which was grown for 48 h at 30 °C and 110 rpm. Then, the whole broth volume was used to inoculate a 30 mL mineral medium culture flask, which was incubated at 30 °C and 110 rpm during 24 h. Finally, the whole broth volume was used to inoculate a 300 mL mineral medium culture flask. The baffled flasks were incubated at 30 °C and 110 rpm during 10 h. This flask was used to inoculate the bioreactor culture.

2.2.3.5 Plasmid curing during batch cultivations on fructose

Batch cultivations consisted in non-limited growth on fructose. The cultures were led in a 5 L bioreactor Biostat®B-DCU (Sartorius, Germany) with a working volume of 3 L. Regulation and monitoring were done using MFCS/win 2.1 software package (Sartorius, Germany). Partial pressure of dioxygen (pO2) in the medium was measured with the optical oxygen sensor InPro 6860i (Mettler Toledo, USA) and pH was measured with a pressurized gel-filled pH electrode (Mettler Toledo, USA).

Temperature was regulated at 30 °C and pH at 7.0 by addition of a 4 M KOH solution. Fermentation was carried out in aerobic conditions (*i.e.* air flow and stirring rates were regulated to maintain pO2 above 30 %). The initial fructose concentration in medium was 50 g·L^{-1}. To prevent nutrient limitation, pulses of rich phosphorus solution (7 mL·L^{-1}) and trace elements solution (2 mL·L^{-1}) were carried out every 10 g·L^{-1} of biomass produced.

After reaching a concentration of 7.5 g_{CDW}·L^{-1} of biomass in the bioreactor, plasmid curing strategies were applied: either by an addition of 50 mg·L^{-1} of rifampicin or an increase of the temperature of culture up to 42°C.

2.2.3.6 Successive batch subcultures from 30 to 37°C

To generate population heterogeneity prior the start of the continuous culture, successive batch subcultures were made. Batch cultivations were performed as detailed above with an initial fructose concentration of 10 $g \cdot L^{-1}$. The first batch was carried out at 30°C until fructose was completely consumed, 900 mL fermentation broth was then withdrawn through a peristaltic pump and 900 mL of fresh bioreactor mineral medium were added in the bioreactor. Temperature was increased at 37°C. For the seven next batches at 37°C, the protocol was the same. After the eighth batch at 37°C, the chemostat cultivation was started.

2.2.3.7 Plasmid curing during continuous cultivation on fructose

Fructose-limited continuous culture was established by feeding the bioreactor with fresh medium (Bioreactor mineral medium supplemented with 10 $g \cdot L^{-1}$ fructose). In chemostat-modes, dilution rates were steady at 0.05 and 0.1 h^{-1} respectively.

Steady state conditions were reached after at least five residence times (*i.e.* 0.05 h^{-1}, 100 h and 7.21 cell generations; 0.1 h^{-1}, 50 h and 7.21 cell generations). The steady state phase was assessed through constant measurements of biomass and residual fructose concentrations, as well as stable composition of the exhaust gases. Temperature was set at 37°C, and pH was regulated at 7. The partial pressure of dioxygen was maintained at 30 % of the saturation through aeration and stirring regulation.

2.2.3.8 Analytical procedures

Biomass characterization

Biomass concentration was measured by optical density (OD) at 600 nm using a visible spectrophotometer (DR3900, Hachlange, Loveland, Colorado, USA) with a 0.2 cm path length absorption cell (Hellma). OD was correlated to cell dry weight (CDW) measurements (*i.e.* 2 $g_{CDW} \cdot L^{-1}$ = 1 OD unit). For cell dry weight measurements, 0.2 µm pore-size polyamide membranes (Sartorius, Göttingen, Germany), were beforehand dried (60°C, 200mmHg, 72 h) and weighted. Culture medium was sampled and filtrated on dried membranes which were dried again in the same conditions.

Metabolite quantification

Cells samples were centrifuged, and supernatants were filtrated (0.2 µm PTFE syringe filters, VWR) before being used for substrate and products determination. The residual fructose and organic acids concentrations were quantified by high-performance liquid chromatography (HPLC). The HPLC instrument (Series 1100, Agilent) was equipped with an ion-exchange column (Aminex HPX-87H, 300×7.8 mm, Bio-Rad, Hercules, CA, USA) protected with a guard column (Cation H+ cartridge, 30×4.6 mm, Bio-Rad) and coupled to a RI detector and an UV detector (λ=210 nm). The column was eluted

with 2.5 mM H_2SO_4 as a mobile phase at 50 °C at a flow rate of 0.5 mL·min^{-1}. Residual nitrogen was quantified by higher-pressure ionic chromatography (HPIC). The HPIC instrument (ICS-2100 RFIC, Dionex) was equipped with an IonPac™ CS16 column (RFIC™, 3x50mm, BioRad) and an ion suppressor CERS 500 (2 mm, Thermo Scientific). The column was eluted with 30 mM metanesulfonic acid as a mobile phase at 40 °C and a 40 mA ion suppressor current, at a flow rate of 0.36 mL·min^{-1}.

Plate count

C. necator is naturally resistant to gentamycin and plasmid-bearing cells are resistant to kanamycin. Plasmid stability was quantified by parallel plate count on antibiotic selective TSB Petri dishes (10 mg·L^{-1} Gentamicin and 10 mg·L^{-1} Gentamicin + 200 mg·L^{-1} Kanamycin). Serial dilutions were performed in physiological water (0.85 % NaCl) tubes (BioMérieux, Marcy-l'Étoile, France). For every sample, three dilutions were tested, between 10^{-5} and 10^{-9}. The diluted sample were plated in triplicate with the Whitley Automated Spiral Plater (Don Whitley Scientific, Shipley, UK). From these data, the decimal reduction rate of plasmid-expressing cells was calculated as the ratio of the concentration of total cells (Gen^R) on the concentration of plasmid-expressing cells (Gen^RKan^R); this ratio was converted to logarithm.

Flow Cytometry

Cell permeability (FL3 channel) and eGFP-fluorescence (FL1 channel) were measured at single-cell level with the BD Accuri C6® flow cytometer (BD Biosciences, Franklin Lakes, NJ, USA). Propidium iodide (*abbr.* PI) (Molecular probes, Invitrogen, USA) was used for the quantification of permeable cells. After dilution in physiological water at 10^6 cells·mL^{-1}, cell samples were stained with 20 µL of a solution at 20 µM PI and incubated 20 minutes at room temperature in the dark. A 100 % dead–cell control was prepared by incubating cells in 70 % isopropanol for 1 h at room temperature. Samples were run until 20, 000 events were counted at 14 µL·min^{-1} using milli-Q water as sheath fluid. The Forward Scatter Signal (threshold: 12, 000) and Side Scatter Signal (threshold: 2, 000) were used as trigger channels. Data acquisition was performed with BD Accuri CFlow® software. Data processing was achieved with FlowJo software (Becton Dickinson, Sparks, MD, USA). Decimal reduction rate was calculated as described above from plasmid-expressing cells (eGFP-positive cells; FL1-A > $8{\cdot}10^2$) and total cells (Single cells; cells situated on the bisectors of both FSC-A *vs* FSC-H and SSC-A *vs* SSC-H).

Fluorescence measurements in the medium

Samples were centrifuged 3 min at 13, 000 rpm with a MiniSpin® table-top microcentrifuge (Eppendorf, Germany). The extracellular fluorescence intensity in the supernatant was measured with the Synergy™ HT (Biotek®, USA) multiplate reader at excitation wavelength 485 ± 20 nm and emission

wavelength 525 ± 20 nm at sensitivity of 50. Black Nunclon® 96-well plates (ThermoFisher, USA) were used.

2.2.3.9 Statistical analysis: Normality of distribution functions by BoxPlot representation

Boxplots are graphical tools used to represent distributions through graphical localization parameters: the median (50th percentile, red line), the first (25th percentile) and third quartile (75th percentile). The first and third quartiles respectively represent the bottom and top of the boxplot. The median was represented by the line inside the box. The interquartile range (IQR) was situated between the first and third quartile and represents the length of the box. The whiskers represent the minimum and maximum values when they are within 1.5 x IQR from both extremities of the box. Values above 1.5 x IQR were considered as outliers and are represented by points. A symmetric boxplot with its median in the middle of the box and same length whiskers might be expected to be normally distributed (Rakotomalala *et al.* 2011).

2.2.3.10 Data analysis

The error on the specific growth rate (determined as being the slope of $\ln[g_{CDW} \cdot L^{-1}] = f(t)$ for batch on dry mass) was calculated as the standard deviation (SD) of the slope. For the yield determination, the state variables (concentrations for batch or weights for fed-batch) were plotted pairwise in a scatter plot within the considered period of the culture. A linear regression was applied to determine the yield (as the slope) and the error (as the SD of the slope).

2.2.4 Results

In order to evaluate our capacity to monitor heterogeneity in plasmid expression level at the single cell level, the *C. necator* strain Re2133 was transformed with the plasmid biosensor (pCB1). It was based on the insertion of a constitutive eGFP into the pBBad plasmid (Fukui *et al.* 2009), usually used for the expression of specific synthetic metabolic pathways (Grousseau *et al.* 2014, Marc *et al.* 2017). Cell population was analyzed through flow cytometry throughout the cultivation in order to get access to single-cells analysis. Therefore, the distribution of the level of plasmid expression could be confronted to fluorescence intensity distribution within the entire population. As it was previously demonstrated that the plasmid pCB1 presented a low metabolic burden on *C. necator* Re2133 host cells (Boy *et al.* 2020), any variations detected in the plasmid expression could be attributed to external factors, like plasmid curing strategy, or variations in dilution rate.

For all the experiments, data were presented depending on cell generations, in order to compare experiments regardless of growth dynamics.

2.2.4.1 Plasmid curing strategy suitable with expression level monitoring during batch cultures

Two different plasmid curing strategies, temperature increase and rifampicin addition, were carried out in batch mode with the strain Re2133/pCB1 in order to define the most efficient method to enhance heterogeneity in plasmid expression. Analyses were supported by macroscopic data (*e.g.* growth kinetics, yields) and population heterogeneity description.

Impact of rifampicin addition and temperature increase on the growth of C. necator Re2133/pCB1 in batch

For the rifampicin-based strategy, preliminary cultures in flasks were achieved beforehand in order to evaluate the concentration of rifampicin needed in the bioreactor to induce plasmid curing (*data not shown*), concentrations from 50 to 150 $mg \cdot L^{-1}$ were tested. A concentration of 50 $mg \cdot L^{-1}$ rifampicin allowed the highest reduction in the number of plasmid-expressing cells without completely inhibiting growth. For the temperature-based strategy, temperature regulation was set at 42°C, based on previous experiments described in the literature (Andersen *et al.* 1981, Trevors *et al.* 1986).

For both strategies, cultivations in bioreactors were achieved under optimal culture conditions up to 7.5 $g_{CDW} \cdot L^{-1}$ of biomass in the bioreactor. Then, plasmid curing was induced in both bioreactors.

The specific growth rates during the different phases were determined from the biomass concentration evolution (**Table 1**). In both conditions, before plasmid curing induction the specific growth rate was equal to 0.21 ± 0.04 h^{-1} and 0.22 ± 0.03 h^{-1}, for rifampicin and temperature respectively, which was consistent with optimal culture conditions. After rifampicin addition, the specific growth rate dropped to 0.09 ± 0.01 h^{-1}. After temperature increase, growth rate was drastically reduced to 0.009 ± 0.001 h^{-1}. Once biomass reached a concentration of 10 $g_{CDW} \cdot L^{-1}$ (6.6 cell generations), temperature was set back at 30°C to verify the reversibility of the phenomenon. Growth rate remained greatly diminished and only reached 0.04 ± 0.01 h^{-1} after 13 h (about 1 generation).

Biomass production yields (**Table 1**) were evaluated from fructose consumption concentrations and compared to theoretical data 0.53 $g.g^{-1}$ (Aragao *et al.* 1996). As expected, before plasmid curing induction, the overall biomass production yields were comparable for both cultures, within 0.47 ± 0.02 $g_X \cdot g_S^{-1}$, and rather close to the theoretical yield. However, after plasmid curing induction, yield values decreased for both strategies. The reduction rate was more important after temperature increase (- 62 %) than after rifampicin addition (- 27 %). After switching temperature back to 30°C, yield seemed to be recovered close to the theoretical reference value, even when the growth rate was still affected.

Table 1: Growth rate evolution and biomass production yields from fructose under plasmid curing conditions in batch cultivations in bioreactors

	μ (h^{-1})		$Y_{s,x}$ ($g_X \cdot g_S^{-1}$)	
	Optimal growth	**Plasmid curing**	**Optimal growth**	**Plasmid curing**
Rifampicin	0.21 ± 0.04 (0-11h)	0.09± 0.01 (19-25h)	0.48 ± 0.01	0.35 ± 0.01
Temperature	0.22 ± 0.02 (0-11h)	*42°C* : 0.009 ± 0.001 (19-45h) *30°C:* 0.04 ± 0.01 (49-62h)	0.47 ± 0.02	0.19 ± 0.02 *(42°C)* 0.45 ± 0.03 *(30°C)*

Subpopulation characterization

Plasmid expression level monitoring

The fluorescence intensity distribution of eGFP fluorescent cells was measured by flow cytometry in order to quantify different expression levels. Boxplots have been chosen to represent fluorescence intensity distributions. Distributions of population are represented versus both the generation number and the time course of the culture; indeed, even if the generation number is similar, the contact time with the stress is different (about 10 h for rifampicin and 55 h for the temperature).

Under optimal culture conditions, fluorescence intensity distribution was Gaussian for both cultures, as the first and third quartile had equal lengths, and as the mean and median value were equal (**Figure 1**). Plasmid curing conditions were induced after 5.9 generations. For plasmid curing by rifampicin addition (**Figures 1a & b**), the first quartile widened showing a slight sliding of the fluorescence intensity distribution toward lesser fluorescent cells. For plasmid curing by temperature increase at 42°C (**Figures 1c & d**), fluorescence intensity distribution widened globally and the median slipped toward lower fluorescence intensity distribution. This phenomenon seemed to be partly reversible as median increased again when temperature was set back to 30°C. This was not due to a change in the quantum yield of eGFP at 42 and 30°C, as we checked that eGFP was not impact by temperature increase at 42 °C. Supernatant was incubated at 42 °C for 24 h, and no variation in the value of fluorescence intensity was detected compared to 37°C (*data not shown*). For an equal generation number between both plasmid curing conditions, the associated culture length is way longer for temperature increase (70 h), as growth rate was significantly diminished, compared to rifampicin addition (25 h).

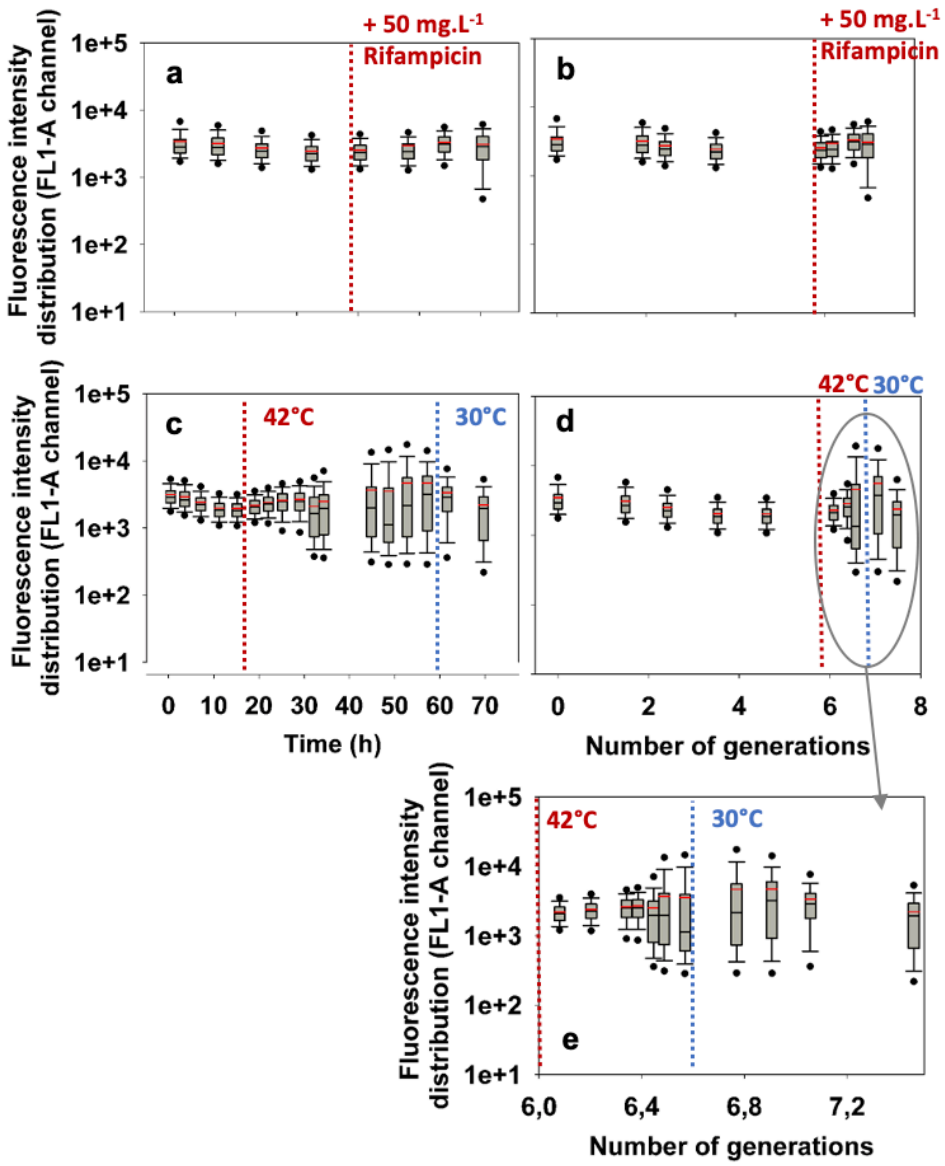

Figure 1 : Box plot representation of fluorescence intensity distribution of eGFP-positive cells in the FL1-A channel throughout fermentation for the strain Re2133/pCB1 under plasmid curing conditions with rifampicin addition (time (a) and generations (b)) and temperature increase (time (c), generations (d), magnification between 6 and 7.5 generations (e))

Plasmid stability

Plasmid expression stability was evaluated through flow cytometry and plate count. A gap in cell concentrations between plate count and flow cytometry might reveal a cultivability loss, due to the side effects of plasmid curing on the physiology of host cells. In addition, the dynamic of plasmid expression was evaluated through decimal reduction rates.

In the rifampicin experiment (**Figure 2a),** concentrations of total cells and of cells expressing the plasmid were consistent both by plate count and flow cytometry throughout the culture; meaning gentamicin resistant cell concentration (Gen^R) was equal to single-cell concentration, and that

gentamicin and kanamycin resistant cell concentration (Gen^RKan^R) was equal to eGFP-positive cell concentration. The cultivability was not reduced by rifampicin addition. The specific growth rate calculated from the single-cells concentration by flow cytometry was compared to the one determined from the cell dry weight, described beforehand. Growth rate by flow cytometry was evaluated at 0.24 ± 0.03 h^{-1} under optimal growth conditions, and at 0.06 ± 0.05 h^{-1} after plasmid curing induction. Even if growth rate evaluation was noisier by flow cytometry, the orders of magnitude reached was once again equivalent. Thus, flow cytometry and cell dry weight measurements gave comparable growth dynamics. The decimal reduction rate (**Figure 2c**) remained lower than 0.05 for both counting methods confirming that there was no significant decrease in the plasmid expression due to rifampicin addition.

In the temperature experiment (**Figure 2b**), total and plasmid-expressing cell concentrations were consistent both by plate count and flow cytometry under optimal growth conditions. After plasmid curing induction, the gap between the two counting methods increased reaching a one-decade difference for both plasmid-expressing cell and total cell populations. Growth considerably slowed down and cell concentration even decreased for Gen^R and Gen^RKan^R populations, which might confirm that cell cultivability decreased. For some samples, no growth was observed on gentamicin + kanamycin plates at the tested dilutions. When temperature was set back to 30°C after 6.6 cell generations, cell concentration increased slightly for both counting methods and both cell populations. Returning to optimal temperature conditions has prevented further decrease in the cell cultivability but did not allow a complete recovery of cells, as they were not able to grow at their original rate. Like for rifampicin above, the growth rate from flow cytometry was compared to growth rate from cell dry weight. Growth rate by flow cytometry was evaluated at 0.23 ± 0.04 h^{-1} under optimal growth conditions, at 0.004 ± 0.004 h^{-1} after plasmid curing induction and at 0.03 ± 0.05 h^{-1} after temperature was set back to 30°C, consistent with the ones calculated from biomass concentrations.

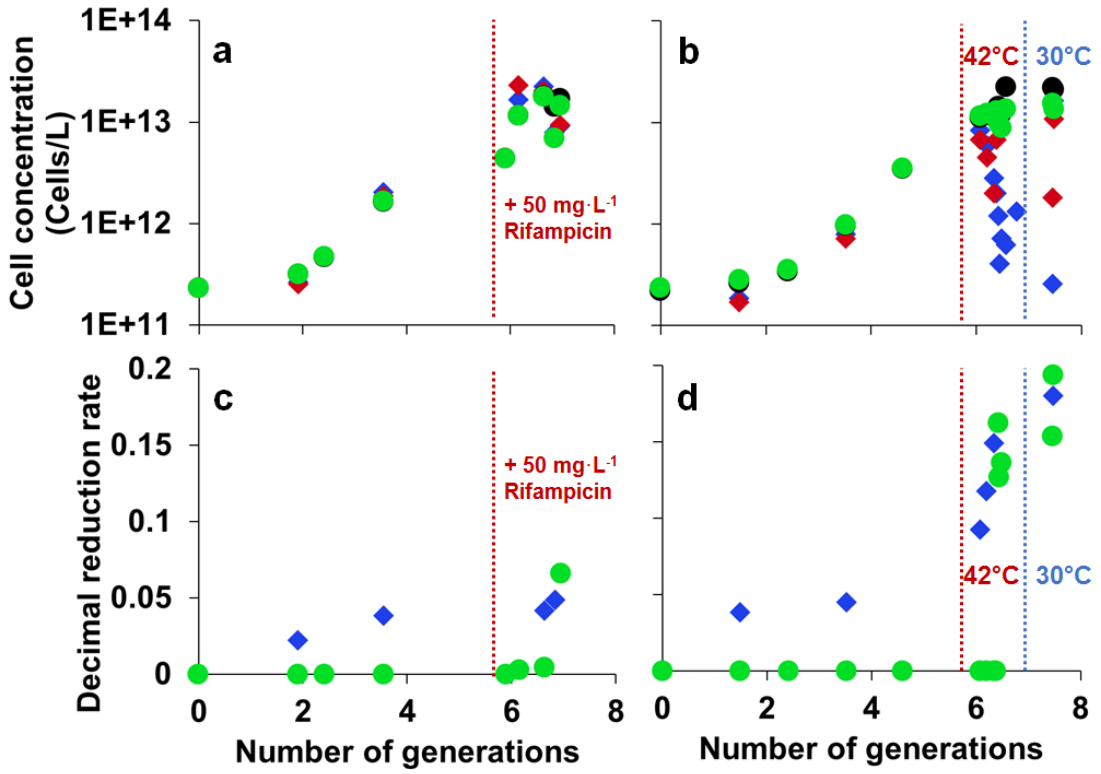

Figure 2 : Cell concentration in cells·L^{-1} for the rifampicin experiment, *vs.* cell generations by plate count (◆ Gen^R and ◆ Gen^R+Kan^R) and flow cytometry (● Single cells and ● eGFP-positive cells) (a). Cell concentration in cells·L^{-1} for the temperature experiment, vs cell generations by plate count (◆ Gen^R and ◆ Gen^R+Kan^R) and flow cytometry (● Single cells and ● eGFP-positive cells) (b). Decimal reduction rate for the rifampicin (c) and temperature (d) experiments, vs cell generations by plate count (◆) and flow cytometry (●)

Decimal reduction rate (**Figure 2d**) reached a maximum value of 0.18 for plasmid curing by temperature increase and 0.06 by rifampicin. Batch conditions were identical as both precultures were led exactly in the same manner; permeability as well as fluorescence levels were also verified to be identical before bioreactor inoculation. A low decimal reduction rate was measured before plasmid curing induction, either by temperature or rifampicin, by both counting methods: flow cytometry and plate count. After thermal plasmid curing induction, decimal reduction rate increased from 0 to 0.16 by flow cytometry, and from 0.2 to 0.15 by plate count. This value stabilized around 0.18 by both counting methods after temperature decrease. No significant increase was detected after rifampicin addition, by both counting methods.

Plasmid expression loss increased significantly after plasmid curing induction. When comparing plasmid curing strategies, it appears obvious that temperature increase presented the most negative effect on the cell concentration for plasmid-expressing and total cell populations, and consequently on the decimal reduction rate. This negative impact was more notable on plate count measurements, certainly due to cultivability loss.

Cell permeability and eGFP leakage

To further investigate cell physiology, cell permeability and eGFP leakage in the medium were investigated (**Figure 3**). Under optimal culture conditions, the percentage of permeabilized cells was low (% PI-positive cells < 5 %) for both experiments. The higher RFU value at the beginning of the batches might be due to a higher eGFP leakage in flasks precultures. Relative extracellular fluorescence intensity (*i.e.* extracellular fluorescence intensity normalized by optical density at 600 nm) decreased, because optical density increased significantly faster than extracellular fluorescence intensity. This was consistent with low cell permeabilization and the stable normal fluorescence intensity distribution showed above (**Figure 1**). Therefore, eGFP excretion in the medium was low under optimum culture conditions. Initial optical density and fluorescence intensity in the supernatant were taken as reference to calculate relative fluorescence intensity in the medium.

After rifampicin addition (**Figure 3a**), the percentage of permeabilized cells remained low. The relative extracellular fluorescence intensity was constant, meaning that the amount eGFP excreted by cells became constant and stable.

After temperature increase (**Figure 3b**), the percentage of permeabilized cells increased quickly up to 10 %. The relative extracellular fluorescence intensity increased abruptly. Since cell growth had stopped, the increase in relative extracellular fluorescence was only due to enhanced cell permeabilization. As a result, the fluorescence intensity distribution decreased in single-cells (**Figure 1**). Thus, single-cells excreted more eGFP as the percentage of permeabilized cells increased. When temperature was set back to 30°C, cell permeabilization percentage decreased, because the newly formed cell population was not permeable and so, overthrown the cell population permeabilized by temperature. Meanwhile, relative extracellular fluorescence intensity decreased. Temperature increase led to an enhanced eGFP leakage outside of cells, but this phenomenon could be slowed down by returning to optimal temperature.

The most appropriate approach to generate population heterogeneity had to be selected for further experiments. Plasmid curing by temperature led to a significant decrease in the plasmid expression levels, which was not the case with rifampicin addition. It might partially be due to a too stringent culture conditions as shown by high cell permeabilization percentage and cultivability loss by plate count. Both strategies led to decreased growth rate. However, temperature increase at 42°C almost completely inhibited growth. Therefore, the temperature increase was the most promising method to induce population heterogeneity. However, to avoid too high cell permeabilization and cultivability loss which might disrupt our further study, the setpoint temperature had to be slightly decreased at 37°C.

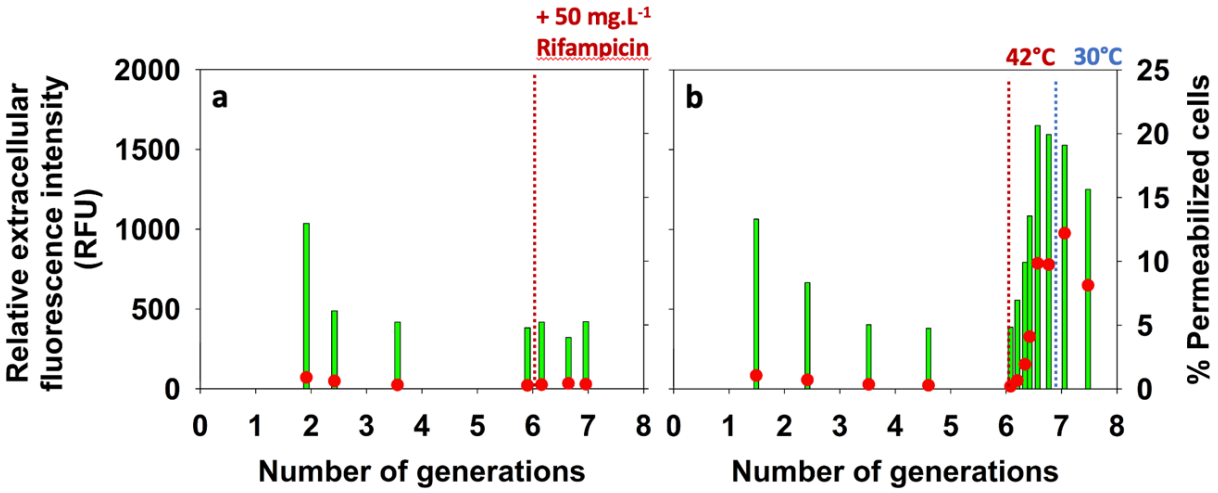

Figure 3: Comparison of extracellular fluorescence intensity and the percentage of permeabilized cells throughout fermentation with addition of rifampicin (a) and temperature increase at 37°C (b). Legend: (●) % PI-positive cells; (■) extracellular fluorescence intensity

2.2.4.2 Plasmid expression level monitoring during continuous culture at sub-optimal temperature

In order to study the impact of the dilution rate (*i.e.* growth rate) on the stability of the plasmid expression, we measured the eGFP fluorescence in cells cultivated in chemostat under fructose limitation and under plasmid-curing like conditions. It has been reported that the plasmid replication rate and/or plasmid copy number could be regulated by the dilution rate in chemostat (Koizumi *et al.* 1985, Reinikainen *et al.* 1989, Klumpp *et al.* 2011).

The combination of plasmid curing and chemostat mode should allow creating more cell generations, amplifying the phenomenon observed in batch mode and studying the impact of the dilution rate (*i.e.* growth rate) on plasmid stability.

Our study showed that a temperature of 42°C (as previously reported on *C. necator* in (Andersen *et al.* 1981)) completely inhibit cell growth and negatively impact cell cultivability. This growth inhibition by too high culture temperature was consistent with other previous studies with different microorganisms (Andersen *et al.* 1981, Hughes *et al.* 1984). Therefore the chemostat temperature was set at 37°C instead, a 7°C-increase from the optimal temperature, which was advised for plasmid-curing experiments (Trevors *et al.* 1986). This temperature condition had already been applied in our previous work for plasmid curing during successive subcultures in flasks (Boy *et al.* 2020). In such condition, three different subpopulations could be discriminated based on their fluorescence intensity distribution after 19 cell generations: P_0 (not fluorescence), P_1 (low fluorescence intensity, median value in FL1-H = $1 \cdot 10^3$) and P_2 (high fluorescence intensity, median value in FL1-H = $6 \cdot 10^3$). Subpopulations P_1 and P_2 presented a slight difference in their specific growth rates in 96-well plates

in double selective medium (*i.e.* gentamicin + kanamycin) with 0.09 ± 0.03 h^{-1} and 0.05 ± 0.01 h^{-1}, respectively.

Successive batches

First, a batch culture was led at 30°C in order to set the reference condition. This reference condition was characterized by 100 % eGFP-positive cells whose fluorescence intensity distribution was centered on the median of the subpopulation P_2 (= $6 \cdot 10^3$). Then, successive batch cultures were carried out in the same bioreactor at 37°C until the three subpopulations P_0, P_1 and P_2 appeared. Then, chemostat was started at a dilution rate of 0.05 h^{-1}.

Growth rate during successive batches varied significantly depending on the culture conditions applied (**Table 2**). At 30°C, growth rate was maintained at 0.25 ± 0.01 h^{-1}, which was consistent with optimal culture conditions for this strain. Then, during the first batch at 37°C, the specific growth rate dropped to 0.06 ± 0.01 h^{-1}. This was the lowest specific growth rate observed, since it increased in the next batches from 0.15 ± 0.01 to 0.22 ± 0.01 h^{-1}. So, in the last 37°C-batch, the specific growth rate was only 20 % lower to its value at 30°C.

Table 2: Specific growth rates and fluorescence intensity repartition (P_0, P_1, P_2) during successive batches at 30 and 37°C

Successive batches	μ (h^{-1})	final %P_0	final %P_1	final %P_2
Batch 30°C	0.25 ± 0.01	5	14	81
Batch 37°C: n°1	0.06 ± 0.01	5	14	81
Batch 37°C: n°2	0.18 ± 0.01	2	11	87
Batch 37°C: n°3	0.16 ± 0.01	1	11	88
Batch 37°C: n°4	0.15 ± 0.01	3	10	87
Batch 37°C: n°5	0.17 ± 0.01	5	22	73
Batch 37°C: n°6	0.22 ± 0.01	9	32	59
Batch 37°C: n°7	0.20 ± 0.01	5	32	63
Batch 37°C: n°8	0.20 ± 0.01	7	46	47

At the end of the batch at 30°C, the whole cell population remained stable mainly in the subpopulation P_2 gate (**Figures 4a & 5**), corresponding to the fluorescence intensity distribution under optimal culture conditions. The fluorescence intensity distribution remained symmetric and narrow around the median until the end of the 30°C batch (**Figure 5**).

At the beginning of the first 37°C batch, the median of the fluorescence intensity distribution quickly reached $4 \cdot 10^3$ again in the FL1-H channel. The distribution range was wider than during the 30°C batch. Between 0 and 15 cell generations, the fluorescence intensity distribution remained mostly in the P_2 subpopulation gate (**Figure 5**), but its distribution range increased throughout this time-period (**Figure 4a**). After 15 cell generations, the distribution range increased drastically towards the lower

fluorescence intensity, which was confirmed by the increase in the percentage of P_1 fluorescent cells (**Figure 6**). After 30 cell generations, subpopulations P_1 and P_2 were clearly obtained, each one representing approximately 50 % of the eGFP-positive cell population. At that stage, it was decided to switch to chemostat mode.

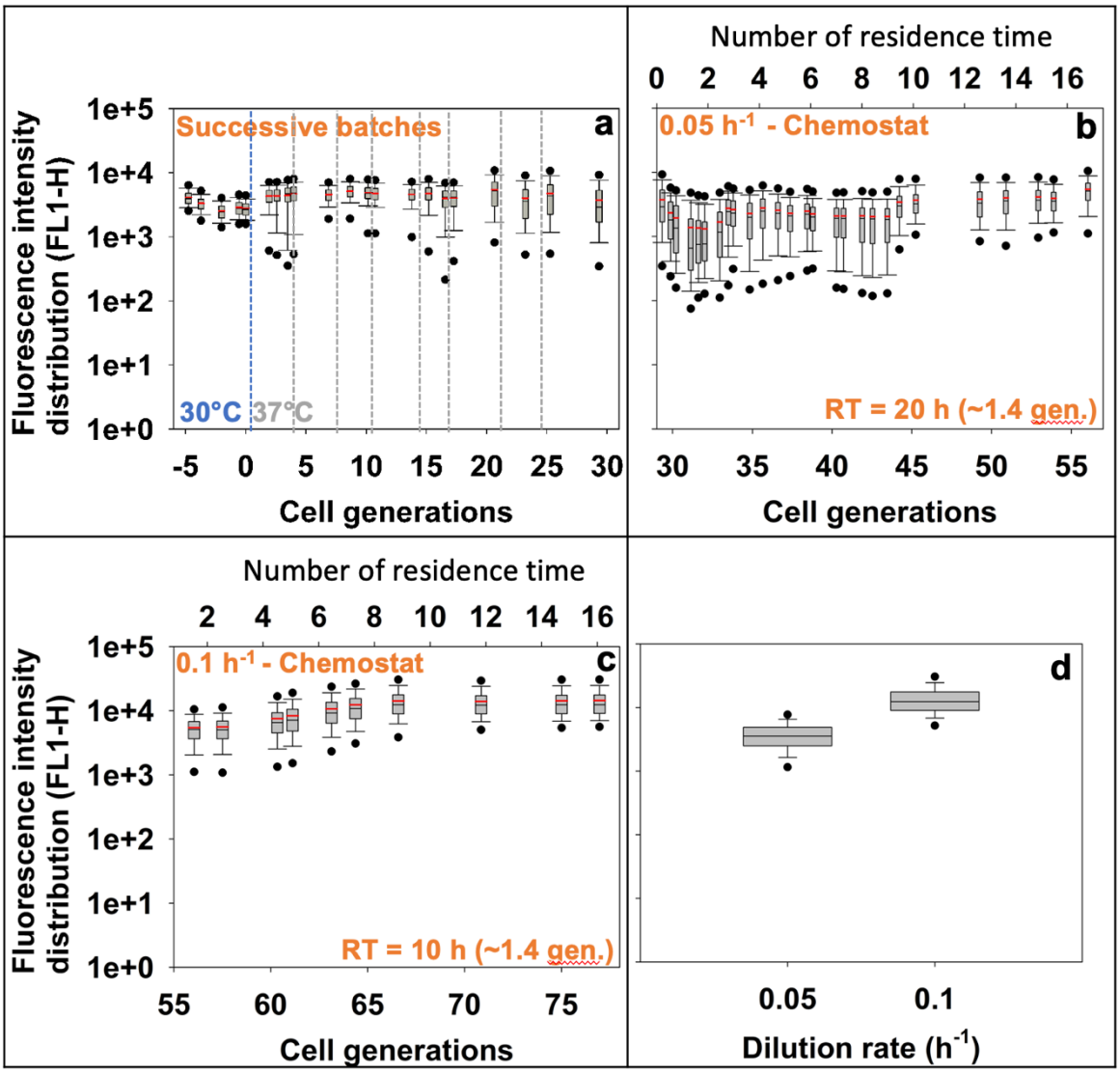

Figure 4 : Plasmid expression levels represented through fluorescence intensity distribution in the FL1-H channel by boxplots during successive batches at 30 and 37°C (a), chemostat at 37°C and 0.05 h^{-1} (b) and chemostat at 37°C and 0.10 h^{-1} (c). Comparison of plasmid expression level distribution on the last point of the 0.05 and 0.1 h^{-1} chemostats, at respectively, 53 and 75 generations (d); Delimitation between successive batches were shown by blue and grey vertical lines

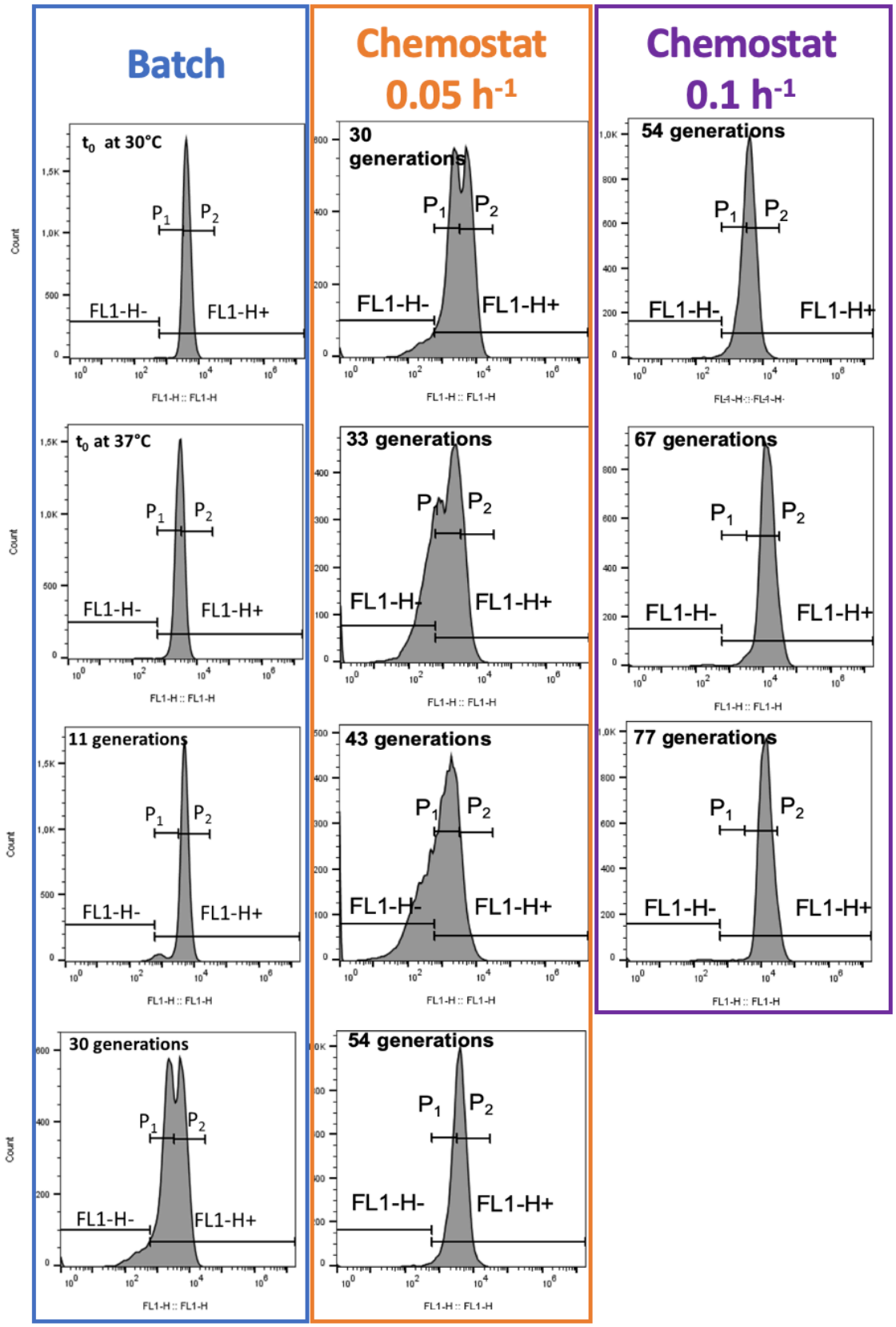

Figure 5 : Evolution of fluorescence intensity distribution in the FL1-H channel at different time of culture

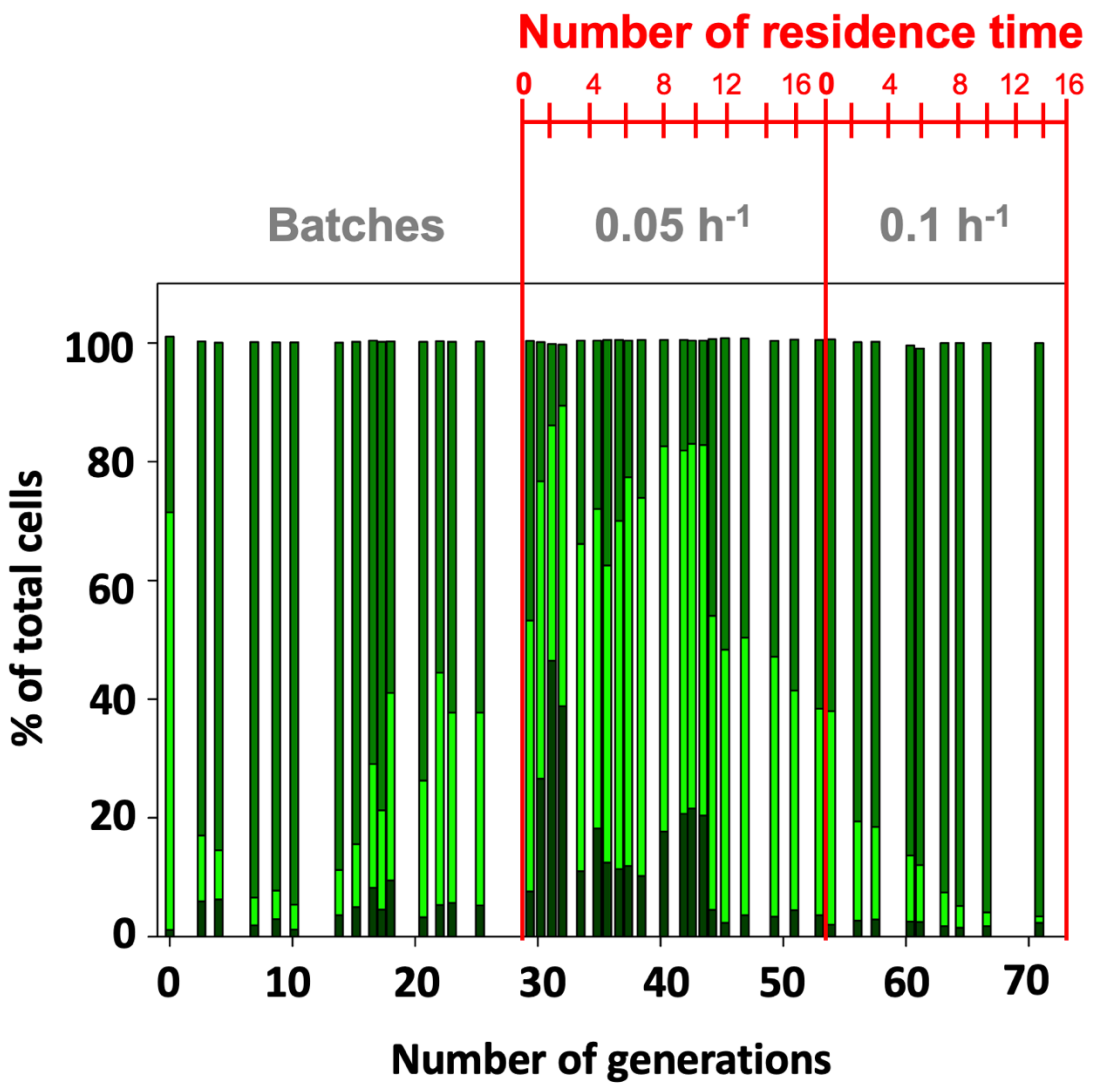

Figure 6 : Percentage of P_2-cells (■) and P_1-cells (■) and P_0-cells (■) by flow cytometry through the number of cell generations, and the number of residence time. Red vertical lines represent the delimitation between fermentation conducts (batch, chemostat)

Plate count was performed at the end of each successive batch (**Figure 7a & b**). For flow cytometry measurements, only endpoints of each batches were shown. The results for flow cytometry and plate count analysis gave cell concentrations comprised in the same order of magnitude. During successive batches, cell concentration reached around 10^{10} cells·mL^{-1} both by plate count and flow cytometry.

During the successive batches (until 30 generations), the decimal reduction rate (**Figure 7c**) obtained for Gen^RKan^R cells remained close to zero, meaning that all cells present in the bioreactor were expressing the plasmid phenotype, even without selection pressure in the bioreactor. Decimal reduction rate for P_2-cells also remained close to zero, but this value started increasing after 15 cell generations up to 0.25. This corresponded to the decrease of the decimal reduction rate for P_1 and P_0-

cells. During the first 15 generations, the decimal reduction rate for P_1 and P_0-cells was higher, around 1 and 1.25 respectively.

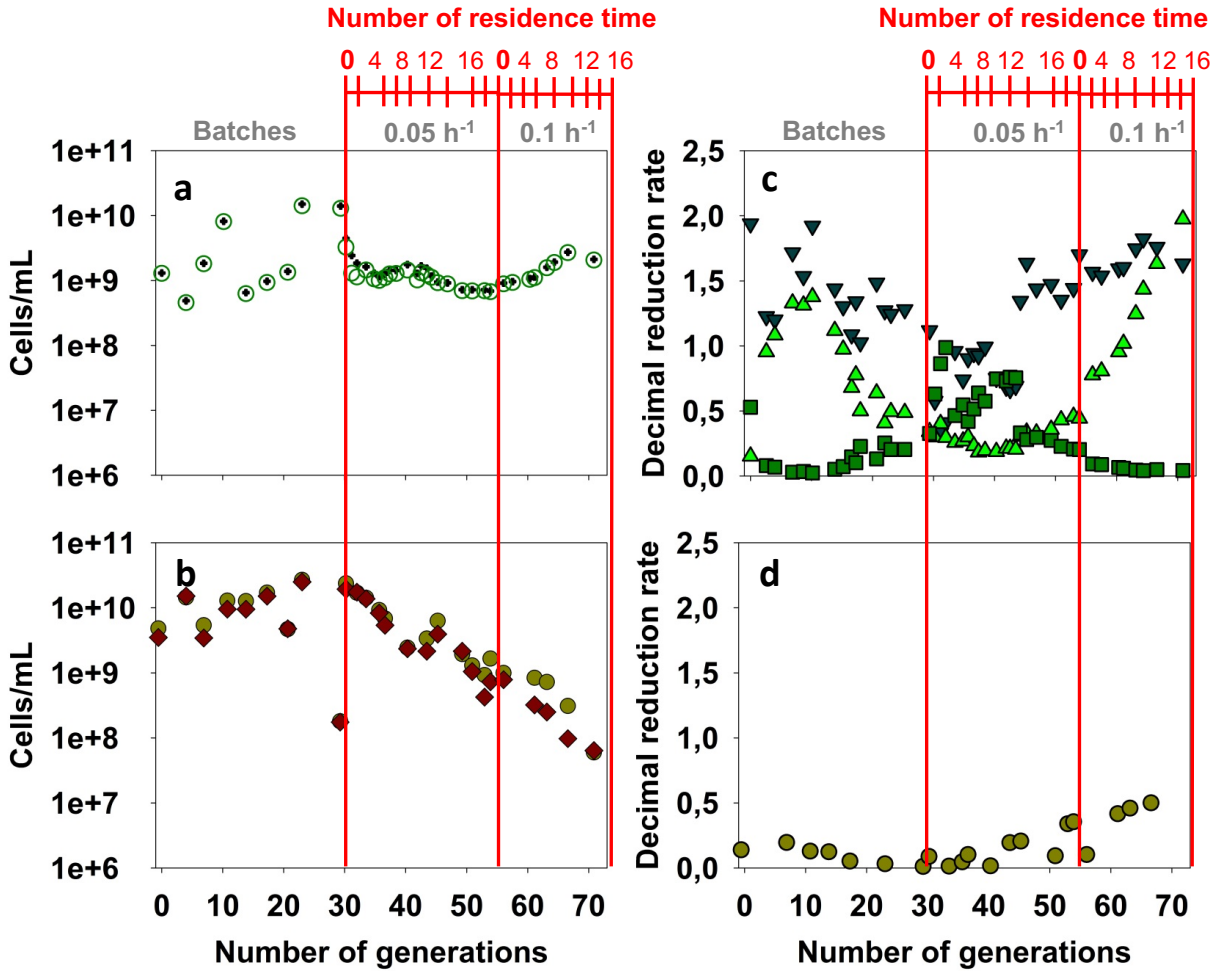

Figure 7 : Cell concentrations *vs.* the number of generations for (a) fluorescent cells (○) and total cells (✚) determined by flow cytometry as well as (b) Gen^R cells (●) and Gen^RKan^R cells (◆). (c) Decimal reduction rate *vs.* the number of generations for P_2-cells (■), P_1-cells (▲), P_0-cells (▼) and for (d) Gen^RKan^R cells (●)

Chemostat at 0.05 h^{-1}

Chemostat in plasmid curing-like conditions was led to study the impact of dilution rate on plasmid expression levels. First, a low dilution rate of 0.05 h^{-1} was set, which was close to the lowest specific growth rate obtained during successive batches at 37°C and close to the specific growth rate of P_2-cells (0.07 ± 0.02 h^{-1}) determined on selective medium (gentamicin + kanamycin) in 96-well plates (Boy *et al.* 2020). The 0.05 h^{-1}-chemostat was carried out at 37°C for 340 h, corresponding to 27 cell generations. At the macroscopic level, the total biomass concentration expressed as dry cell weight and OD_{600nm} was maintained constant at 5 $g_{CDW}·L^{-1}$ (*i.e.* 2.5 OD_{600nm}). In addition, no significant changes of metabolism were identified based on extracellular metabolites (no production of organic acids) and exhausted gas analyses. Based on those macroscopic analyses, the steady state was reached after 35

generations (7.2 generations after beginning of 0.05 h^{-1}-chemostat) and still settled after 20 generations.

Nevertheless, based on single cell level analysis, it was possible to show an evolution of the distribution of the different subpopulations within the culture stabilized at a stable total biomass concentration.

Two phases could be observed concerning the evolution of fluorescence intensity distribution. First, between 30 and 45 cell generations, fluorescence intensity distribution was maintained at the proportion 20 % P_2, 60 % P_1 and 20 % P_0 (**Figure 6**). At the beginning of the 0.05 h^{-1}-chemostat (*i.e.* between 30 and 33 generations), an over-increase of the subpopulation P_0 (40 %) had been observed at the expense of the subpopulations P_2 (10 %) and P_1 (50%) (**Figures 5 & 6**) as shown on boxplots on fluorescence intensity distribution (**Figure 4b**). On the same time period (*i.e.* 30 to 45 cell generations), P_1–cells decimal reduction rate remained low (under 0.2) whereas it increased transitory for P_2 -cells up to 0.75 (**Figure 7c**). Meanwhile, the decimal reduction rate for kanamycin-resistant cells remained rather low, under 0.2 (**Figure 7d**). Second, between 45 and 55 cell generations, the proportion of the P_2 subpopulation increased from 40 to 60 %, whereas the proportion of the subpopulations P_0 (5 %) and P_1 (35 %) decreased (**Figure 6**). The fluorescence intensity distribution was centered on the P_2 cell gate with a shouldering in the P_1 cell gate (**Figure 5**; cytogram at 54 generations), and boxplot median ($2{\cdot}10^3$) and mean values ($2.5{\cdot}10^3$) stabilized in the FL1-H channel. The overall plasmid-expressing population (eGFP-positive and kanamycin resistant) presented a low decimal reduction rate (**Figures 7 c & d**), and plasmid phenotype remained expressed in most cells. This was consistent with the high stable fluorescence intensity distribution in single-cells (**Figure 4b**).

Cell concentration (**Figure 7a**) decreased and stabilized around $7{\cdot}10^8$ cells·mL^{-1} in steady state by flow cytometry. By plate count, cell concentration decreased regularly all along fermentation until reaching $1{\cdot}10^9$ cells·mL^{-1} at the end of the first chemostat cultivation.

Therefore, by decreasing the dilution rate to 0.05 h^{-1}, chemostat mode favored the apparition of the subpopulation P_2, which presented the highest fluorescence intensity distribution, after 10 numbers of residence time corresponding to 15 generation growing in such condition.

Chemostat at 0.1 h^{-1}

To pursue our study of the impact of dilution rate on plasmid expression levels, a higher dilution rate of 0.1 h^{-1} was applied in this experiment. Chemostat was carried out at 37°C and 0.1 h^{-1} for 160 h, corresponding to 23 cell generations (16 hydraulic residence time). As exposed beforehand on macroscopic data, the total biomass concentration was maintained constant at 5 $g_{CDW}{\cdot}L^{-1}$. Likewise, no significant changes in metabolism were identified based on extracellular metabolites and exhausted

gas analyses. Based on those macroscopic analyses, steady state was reached at 62 generations (7.2 generations after beginning of 0.1 h^{-1}-chemostat) and maintained for 23 cell generations.

Between 55 and 62 cell generations (*i.e.* 5 residence times), boxplots showed that the distribution range remained the same width (**Figure 4c**). However, the boxplots themselves were symmetrically transposed by following median/mean increase. This was consistent with the observation that fluorescence intensity distribution slided symmetrically through higher median value in the P_2 cells gate (**Figure 5**) and that the proportion of P_0 and P_1-cells kept on decreasing while the proportion of P_2 cells increased (**Figures 5 & 7a**)). Once steady state was reached at 62 generations (*i.e.* 7.2 residence time), boxplots were reproducibly centered on the P_2-subpopulation (**Figures 4c & 5**). It was interesting to notice that fluorescence intensity distributions median was significantly higher at the end of the 0.1 h^{-1} - chemostat ($1{\cdot}10^4$ in FL1-H) compared to the 0.05 h^{-1}-chemostat ($5{\cdot}10^3$ in FL1-H) (**Figure 4d**) even if they were both mainly comprised in the P_2-gate.

On the one hand, at steady state, cell concentration measured by flow cytometry slightly increased and stabilized at the steady state at $4{\cdot}10^9$ cells·mL^{-1} (**Figure 7a**). On the other hand, cell concentration measured by plate count decreased significantly from 1.10^9 to 8.10^7 cells·mL^{-1}. The main reason might lie in cell cultivability loss due to the extended amount of time at 37°C (620 hours from batches to chemostat) and to the higher intracellular eGFP concentration for the P_2 population at 0.1 h^{-1} dilution rate (FL1 median $1{\cdot}10^4$) compared to FL1 median $5{\cdot}10^3$ for P_2 population at 0.05 h^{-1}, as a too important eGFP intracellular concentration might be toxic to cells.

Therefore, increasing the dilution rate from 0.05 to 0.1 h^{-1} favored the maintain of the subpopulation P_2 compared to P_1 with an increase in intracellular eGFP concentration for the P_2 population reaching the value of the reference culture at 30°C.

2.2.5 Discussion

Plasmid curing in *Cupriavidus necator* has been used to study the impact of plasmid-encoded mechanisms (*e.g.* hydrogen utilization (Andersen *et al.* 1981) and toluene metabolism (Hughes *et al.* 1984)) on both plasmid-bearing and -free cells, by removing the involved plasmid from host cells. Several plasmid curing strategies have been used, presenting with different efficiency levels and ease of use. Here we used plasmid curing method to generate heterogeneity in a cell population in terms of plasmid expression level. Therefore, a mild plasmid curing strategy inducing this heterogeneity was searched without completely inhibiting cell growth. Temperature increase and rifampicin addition were selected as curing agents in batch. Despite its lower reported efficiency, rifampicin was chosen as a disruptor of plasmid transcription in bacteria (Wehrli *et al.* 1983, Buckner *et al.* 2018), with the expectation of obtaining an average efficiency on plasmid curing without drastic growth inhibition.

Population heterogeneity was studied by flow cytometry based on eGFP-fluorescence and by plate count based on kanamycin resistance.

The heterogeneity was found more pronounced after a temperature increase (30 to 42°C) whereas almost none was observed after rifampicin addition (50 $mg \cdot L^{-1}$). This result confirmed the low efficiency of rifampicin as a curing agent (Buckner *et al.* 2018). On the contrary, temperature increase allowed inducing higher levels of plasmid heterogeneity as the percentage of plasmid-expressing cells decreased to maximum 60 %. The plasmid expression level distribution widened after plasmid curing, especially after temperature increase. This expression level heterogeneity at a single-cell level in response to plasmid curing was not observed in previous works, as plasmid stability measurements were mainly based on mean analysis within the overall population (Andersen *et al.* 1981, Hughes *et al.* 1984, Monchy *et al.* 2006, Zaman *et al.* 2010, Buckner *et al.* 2018).

For temperature increase, cell concentrations calculated by plate count were lower than by flow cytometry. For rifampicin addition, there was no difference. Therefore, there was a cultivability loss during plasmid curing by temperature. These observations were supported by propidium iodide staining of cells. After temperature increase, the percentage of permeabilized cells increased up to 15 %, while it remained null with rifampicin. Cells previously grown at 42 °C were not able to completely recover when grown again at 30°C.

Although plate count data presented higher heterogeneity than flow cytometry data (certainly because of cultivability), its level achieved by both counting methods was still quite low. This might be explained by the fact that cell growth drastically slowed down (- 57 %, rifampicin, - 95 %, temperature 42°C) after plasmid curing induction. An insufficient amount of cell generations may have been generated to observe the plasmid curing phenomenon because of the negative impact of both curing agents on cell replication mechanisms.

So, a temperature of 42 °C might have been too stringent for cells. Therefore, in the following experiments temperature was set to 37°C instead allowing inducing heterogeneity and not drastically inhibiting the growth rate. This was confirmed during successive batches grown at 37°C where a heterogeneity of plasmid expression was still obtained but with a higher growth. The three fluorescent subpopulations P_0 (low/no fluorescence), P_1 (medium fluorescence) and P_2 (high fluorescence), observed in our previous work during successive flasks subcultures (Boy *et al.* 2020) have been reproduced. Therefore, successive batches at 37°C were proved to be an effective strategy to obtain a heterogeneous plasmid expression level distribution. The three distinct fluorescent subpopulations P_0, P_1, P_2 were obtained after 30 cell generations. It took way more cell generations to obtain the three distinct subpopulations in successive batches compared to successive flasks subcultures (*i.e.* 19 cell

generations (Boy et al. 2020)). This is most probably due to the fact that flask cultures presented more stringent growth conditions that the conditions for bioreactor cultures where the environment is better controlled. (*i.e.* dissolved oxygen concentration and pH).

The continuous cultivation mode is particularly suitable to analyze stress responses of cell subpopulations in a defined physiological state, at a controlled specific growth rate. Here, chemostat was applied to study the impact of the dilution rate on the plasmid expression level by measuring the eGFP fluorescence, under plasmid-curing like conditions. This mode of cultivation had already been used in previous works to show that plasmid expression level (*i.e.* plasmid replication rate, plasmid copy number) could be regulated by the dilution rate (*i.e*. growth rate) (Koizumi *et al.* 1985, Lin-Chao *et al.* 1986, Dupoet *et al.* 1987, Klotsky *et al.* 1987, Reinikainen *et al.* 1989, Ryan *et al.* 1991, Klumpp *et al.* 2011). These studies were based on overall measurement of plasmid DNA content, plasmid copy number, etc. There are different opinions in the literature concerning the impact of dilution rate on plasmid expression level, as it highly depends on the "plasmid vector - host cell" association (Chew *et al.* 1988, D'Angio *et al.* 1994). For instance, different behavior could be observed even depending on the limiting substrate (glucose, ammonium, phosphate or sulphate) or the medium used for the same association (Chew *et al.* 1988). On one hand, increased dilution rates led to decreased plasmid copy number. This is the most common trend as lower plasmid copy number leads to lower metabolic load and therefore higher growth rates (Patnaik *et al.* 2000). This is the case for *Escherichia coli* K12 with plasmid R1 (Light *et al.* 1982), for *E. coli* Br/A with plasmid pBR322 (Lin-Chao *et al.* 1986) and for *E. coli* JM13 with plasmid pUC8 (Ryan *et al.* 1991). On the other hand, plasmids that confer a growth advantage to host cells are less common but might change physiological state of the cell to favor growth (Patnaik *et al.* 2000). It is the case of the association of *E. coli* K12 with the plasmid pBR322 (Noack *et al.* 1981, Reinikainen *et al.* 1989, Klumpp *et al.* 2011) and also *Bacillus stearothermophilus* CU21 with the plasmid pLP11 (Koizumi *et al.* 1985), where plasmid copy number increases with growth rate. There is no definitive explanation for this phenomenon yet, but this behavior usually concerns low copy number plasmids and plasmid whose replication is cell-cycle specific (Patnaik *et al.* 2000). It has been reported that the plasmid copy number might increase with increasing dilution rates in bacteria, for plasmids presenting low to medium copy number. The plasmid used here, pBBR1MCS-2, is known to be a medium copy plasmid at around 30 copies per cell (Buch *et al.* 2010).

In most cases, increased expression level lead to increased metabolic load in host cells (Patnaik *et al.* 1994). So, plasmid curing strategy by temperature increase was applied in chemostat in order to amplify the phenomenon observed in flasks and batch mode, over an increased number of cell generations, and to analyze the impact of the dilution rate (*i.e.* growth rate). Chemostat was set at 2 dilution rates (0.05 and 0.1 h^{-1}) at 37°C and analyzed in terms of subpopulations. Those dilution rates

were chosen because they covered the range of the specific growth rates of the P_1 and P_2 sub-populations determined in 96 - well plates in selective medium (Boy *et al.* 2020). Moreover, 0.05 h^{-1} was close to the lowest specific growth rate observed in the second successive batch at 37°C (where P_2-cell were still majority). Even when macroscopic steady states were reached after 5 residence times, variations in the fluorescence intensity distribution could be observed. At 0.05 h^{-1}, the steady state favored the settlement of the subpopulation P_1 (80 %) within 10 cell generations, corresponding to 7 residence times. The cell population in the bioreactor was completely renewed and subsisting P_2-cells from the batches were progressively washed out. However, after 10 new cell generations, a progressive sliding was observed toward the increase in the subpopulation P_2. This might be explained by the fact that cells were able to adapt to this increased temperature conditions within a certain amount of cell generations at this controlled dilution rate. Therefore, at subpopulation level, the steady state at dilution rate of 0.05 h^{-1} led to a 60 % - 35 % repartition between subpopulations P_2 and P_1, respectively. The fluorescence intensity median reached at the end of the 0.1 h^{-1}-chemostat ($1 \cdot 10^4$ in FL1-H) was significantly higher than the one reached at the end of the 0.05 h^{-1}- chemostat ($5 \cdot 10^3$ in FL1-H), even if still maintained in the P_2-gate. So, switching the chemostat dilution rate up to 0.1 h^{-1} resulted in the increase of the subpopulation P_2 over the subpopulation P_1. This suggests that the maximal specific growth rates previously estimated for P_1 and P_2 have been largely underestimated in 96 - wells plate, otherwise P_2 would have been washed out of the bioreactor. The near-homogeneous population (90 % P_2) reached at steady state 0.1 h^{-1} could be the result of a growth-rate dependent increase in the plasmid copy number of P_1 subpopulation to match the maximal number possible in the strain for this dilution rate (subpopulation P_2). The subpopulation P_2 was maintained and the fluorescence intensity distribution was very stable over time. Cells managed to cope with this higher dilution without the need to decrease the protein production performance in supra-optimal temperature conditions, as it was also the case under optimal growth conditions.

In conclusion, the plasmid curing strategy selected for chemostat was based on successive batches at 37°C, as we showed that (1) rifampicin was not an efficient strategy to generate population heterogeneity and that (2) temperature increase at 42°C completely inhibited cell growth. Successive batch subcultures at 37°C were the most efficient strategy to generate the three fluorescent subpopulations P_0, P_1 and P_2. It took 30 cell generations, from a 100 % P_2 population to obtain a 50 – 50 % repartition between P_1 and P_2. Then, chemostat showed that plasmid expression level could be increased (P_2 gate) through higher dilution rates (0.05 – 0.1 h^{-1}) for *C. necator* Re2133/pCB1 at 37°C. This study provided new insight in subpopulation dynamics, whereas previous works about the impact of dilution rate on plasmid expression were based on mean population measurements and overall plasmid stability.

2.2.6 Results synthesis

Plasmid expression levels in *C. necator* strains bearing an engineered eGFP-biosensor plasmid were evaluated in response to stressful culture conditions, enhancing plasmid instability through plasmid curing strategies: temperature increase and rifampicin addition. The response of our eGFP - plasmid expression biosensor was studied under batch and chemostat cultivation modes, and the influence growth rate on the plasmid expression level heterogeneity was investigated.

➔ **Temperature increase was a more efficient plasmid curing strategy than rifampicin addition.** However, a too high temperature of 42°C was found to be inhibitory of cell growth and therefore, did not allow dynamic analysis during growth.

➔ Fluorescence intensity distribution after plasmid curing induction was way more heterogeneous during temperature increase than after rifampicin addition. When temperature was set back at 30°C, this was partially reversible. So, decimal reduction rate reached was higher for temperature (0.18), than for rifampicin (< 0.05). A significant decrease in cultivability was detected at a temperature of 42°C, which was not the case after rifampicin addition.

➔ Percentage of permeabilized cells after rifampicin addition remained low and the amount eGFP excreted by cells was constant and stable. After temperature increase, the percentage of permeabilized cells and relative extracellular fluorescence intensity increased quickly. The increase in relative extracellular fluorescence was only due to enhanced cell permeabilization, because there was no growth after plasmid curing by temperature.

➔ **At the end of the successive batches at 37°C, expression level heterogeneity was efficiently generated and three distinct fluorescent subpopulations P_0 (not fluorescent), P_1 (low fluorescence, median = $1 \cdot 10^3$) and P_2 (high fluorescence, median = $6 \cdot 10^3$) were obtained.**

➔ At 30°C, growth rate was comparable to its value in optimal culture conditions for this strain and fluorescence intensity distribution remained Gaussian. During the first batch at 37°C, the specific growth rate dropped, but increased again in the next batches, close to its maximum value. Fluorescence intensity distribution range increased towards less fluorescent cells and the percentage of P_1 fluorescent cells increased too. After 30 cell generations, subpopulations P_1 and P_2 were clearly obtained. Decimal reduction rate for Gen^RKan^R cells was low and cells expressed plasmid phenotype without selection pressure. Decimal reduction rate for P_2-cells increased up to 0.25.

➔ **Chemostat mode between 0.05 and 0.1 h^{-1} favored the apparition of P_2-cells.** Nevertheless, fluorescence intensity distributions median was significantly higher in the P_2-gate at the end of the 0.1 h^{-1} - chemostat ($1 \cdot 10^4$ in FL1-H) compared to the 0.05 h^{-1}- chemostat ($5 \cdot 10^3$ in FL1-H).

➔ Even when steady state was reached (>5 residence times) and that macroscopic measurement showed stability in biomass concentration, outlet gas composition or null fructose concentration, variations in the fluorescence intensity distribution could be observed.

➔ At 0.05 h^{-1} - chemostat, during the first 3 cell generations, subpopulation P_2 drastically decreased in favor of the subpopulation P_0 and P_1. The fluorescence intensity distribution was centered on the P_1 cell gate with a shouldering in the P_0 cell gate. From 45 to 55 cell generations, the proportion of P_2-cells increased, leading to a decrease in the proportion of P_1-cells (P_0, 2%; P_1, 36%; P_2, 62%). Fluorescence intensity distribution's median increased and was centered at the limit between the P_1 and P_2 cell gates.

➔ At 0.1 h^{-1} - chemostat, fluorescence intensity distribution slided symmetrically through a higher median value in the P_2 cells gate, and the proportion of P_2 cells increased. Once steady state was reached, fluorescence intensity distribution was centered on the P_2-subpopulation.

Part 3 : Results and discussion

Chapter 2: Identification of heterologous subpopulations from a pure culture in a bioreactor

Subchapter 3: Investigation of the robustness of *Cupriavidus necator* engineered strains during fed-batch cultures

2.3.1 Abstract

It is of major interest to ensure stable and performant microbial bioprocesses, therefore maintaining high strain robustness is one of the major future challenges in industrial microbiology. Strain robustness can be defined as the persistence of genotypic and / or phenotypic traits in a system. In this work, robustness of an engineered strain was assessed in response to implementations of sugar feeding strategies (pulses and continuous) and plasmid stabilization systems (kanamycin resistance and Post-Segregational Killing *hok/sok*). Strain robustness of *C. necator* engineered strains was investigated in fed-batch bioreactor cultures which is a relevant mode to reach high cell densities. Host cells bore a recombinant plasmid encoding for a plasmid expression level monitoring system, based on eGFP fluorescence quantified by flow cytometry. Plasmid expression stability has been quantified by plate count of antibiotic resistant cells. We showed that a sugar fluctuating environment increased cell permeability (10 % *vs.* 20 %, end of culture) and relative extracellular fluorescence intensity (300 *vs.* 619 RFU, end of culture), thus disrupting plasmid expression levels at single-cell level. On the contrary, a continuous sugar feeding strategy allows keeping cells in a better robustness. Moreover, the plasmid stabilization system Post-Segregational Killing *hok/sok* maintained strain robustness efficiently at the level of its macroscopic behavior and in its single-cell characteristics. Surprisingly, the kanamycin resistance system led to a detrimental impact on both cell permeability and plasmid expression level.

KEYWORDS

Cupriavidus necator H16, Post-Segregational Killing, eGFP reporter protein, fed-batch, plasmid stability, cell permeability, single-cell analysis

2.3.2 Introduction

Ensuring phenotypic homogeneity in engineered microorganisms is of major interest to enable maintaining production yields and avoiding process instability (Binder *et al.* 2017). However, the insertion of a recombinant plasmid generally leads to a metabolic load on host cells due to heterogeneous gene expression, plasmid maintenance and recombinant molecule production (Bentley *et al.* 1993, Glick *et al.* 1995, Silva *et al.* 2012, Million-Weaver *et al.* 2014, Ceroni *et al.* 2018, Park *et al.* 2018, Lv *et al.* 2019). This means that two major biological mechanisms are competing within plasmid-bearing cells: plasmid maintenance and cell growth (Silva *et al.* 2012). It is generally admitted that plasmid-free cells grow faster than plasmid-bearing cells, resulting in a growth rate difference that intensifies segregational instability (Bentley *et al.* 1990, Glick *et al.* 1995, De Gelder *et al.* 2007). Consequently, recombinant protein expression decreases globally and leads to the reduction of process performance.

Green Fluorescence Protein (*abbr*. GFP) and some of its derivatives such as enhanced GFP (*abbr.* eGFP), have been shown to be useful biosensors for the detection of variations in gene expression both in single-cells and in total populations (Morschhäuser *et al.* 1998, Blokpoel *et al.* 2003, Carroll *et al.* 2003, Argueta *et al.* 2004, Chudakov *et al.* 2010, Utratna *et al.* 2014, Cao *et al.* 2018, Wons *et al.* 2018). In our previous work (Boy *et al.* 2020), a plasmid expression level monitoring method based on the expression of a plasmid-encoded eGFP biosensor has been designed. Our system was tested in culture conditions allowing validating its relevance to quantify both homogeneous and induced-heterogeneous cell populations. The results showed that this specific eGFP biosensor could be valuable to study both plasmid expression level variations under recombinant production of a molecule of interest in *Cupriavidus necator* and strain robustness under intensive production conditions.

Cupriavidus necator H16 is a chemolithoautotrophic bacterium, well-known for its capacity to produce and store up to 80 % of its dry cell weight of Poly-β-hydroxybutyrate (*abbr.* PHB) (Ryu *et al.* 1997, Pohlmann *et al.* 2006). Its genome was entirely sequenced and mainly annotated (Schwartz *et al.* 2003, Pohlmann *et al.* 2006, Cramm *et al.* 2009). *C. necator* has a versatile metabolism and is naturally able to consume organic carbon sources (fructose (Budde *et al.* 2011, Grousseau *et al.* 2014), oils (Budde *et al.* 2011), formic acid (Grunwald *et al.* 2015), fatty acids (Johnson *et al.* 1971, Wang *et al.* 2010), organic acids (Doi *et al.* 1988)) and inorganic ones (CO_2 (Repaske *et al.* 1976, Tanaka *et al.* 1995)). So, developing and improving tools for the genetic engineering of *C. necator* would open up to new possibilities in terms of synthetic biology of the strain. The interest in developing a complete genetic toolbox for *C. necator* has intensified in recent years, especially for plasmid construction (Bi *et al.* 2013, Sato *et al.* 2013, Gruber *et al.* 2014, Sydow *et al.* 2017). To increase strain robustness, examples of stabilizing mechanisms have already been efficiently transposed to recombinant plasmids in *C. necator*

through stabilizing cassette insertion. They are classified in three main stabilizing categories. First, plasmid addiction systems consist in the killing of plasmid-free cells, or the reduction of their growth rate (Friehs *et al.* 2004). Three of them have already been adapted to *C. necator*: antibiotic resistance (*e.g.* kanamycin (Grousseau *et al.* 2014, Gruber *et al.* 2014), chloramphenicol (Sydow *et al.* 2017)), chromosomal mutation complementation (*e.g.* single-cell auxotrophy through KDPG-aldolase (Voss *et al.* 2006), proline (Budde *et al.* 2011)) and Post-Segregational Killing (*e.g. parDE* operon from the RP4 plasmid (Gruber *et al.* 2014)). Second, site-specific recombination systems ensure that plasmid multimers formed during replication and / or recombination can be resolved by a site-specific recombination system. Each monomer is transmitted independently to daughter cells. This system can also be referred as plasmid multimer resolution system (Zielenkiewicz *et al.* 2001). The *parCBA* operon encoding for the multimer resolution system of the plasmid RK2 (or RP4) (Easter *et al.* 1998) from *Escherichia coli* has been tested in *C. necator* (Gruber *et al.* 2014). Third, active partitioning systems ensure that the plasmid copies are vertically transmitted efficiently to every daughter cell (Zielenkiewicz *et al.* 2001, Schwartz *et al.* 2003, Million-Weaver *et al.* 2014). The partition locus of the megaplasmid pMOL28 from *C. metallidurans* CH34 has been successfully applied in *C. necator* H16 (Sato *et al.* 2013).

Hereinafter, attention was drawn to two plasmid addiction systems: kanamycin resistance and *hok/sok* Post-Segregational Killing system. On one hand, kanamycin resistance is rather commonly used with plasmids of *C. necator* (Grousseau *et al.* 2014, Gruber *et al.* 2014, Marc *et al.* 2017). On the other hand, to our knowledge, the *hok/sok* PSK system has never been used in *C. necator* before. First, the mode of action of kanamycin consists in interfering with protein synthesis by binding to bacterial ribosome. This leads to an incorrect alignment with mRNA and consequently to an amino acid misreading during protein synthesis. Non-functional peptide chains are synthesized. The kanamycin resistance system used here is neomycin phosphotransferase II (*abbr.* NPTII) from the *neo* gene (*i.e.* neomycin-resistance) of the transposon Tn5, which is part of the aminoglycoside 3'-phosphotransferase APH(3')-II subclass (Yenofsky *et al.* 1990). Its mode of action consists in catalyzing the ATP-dependent phosphorylation of kanamycin on its 3'-hydroxyl group and thus, making the antibiotic chemically unstable (Haas *et al.* 1975, Yenofsky *et al.* 1990, Wright *et al.* 1999, Ramirez *et al.* 2010). Second, the Post-Segregational Killing system *hok/sok* from the R1 plasmid of *E. coli* ensures plasmid stabilization by the killing of plasmid-free cells. It encodes for two RNAs: *hok* mRNA and *sok* antisense RNA. The *hok* gene encodes for the toxin protein Hok. The *sok* antisense RNA indirectly regulates *hok* translation (Thisted *et al.* 1994). Plasmid stabilization mechanism of the PSK system *hok/sok* is based on the differential decay rate between *sok* antisense RNA, who has the highest, and the Hok toxin (Thisted *et al.* 1994). During cell division, if the plasmid is transmitted only to one of the two daughter cells,

plasmid-bearing cells will express the *sok* antisense RNA to block Hok toxin actions and remain viable. Plasmid-free cells die from the toxin because the unstable antisense *sok* RNA antitoxin has been degraded (Cooper *et al.* 2000, Friehs *et al.* 2004).

In addition, fluctuating environments are known to generate and / or amplify population heterogeneities and a loss of strain robustness (Barkai *et al.* 2007, Masel *et al.* 2009, Delvigne *et al.* 2015, Limberg *et al.* 2017). In Nature, cell populations have to adapt to fluctuating growth conditions (*e.g.* temperature, pH, nutrients, toxin concentrations). To do so, cell populations may improve their fitness thanks to individuals that evolve stochastically between several different phenotypes. Therefore, some cells might always be prepared to face sudden environmental fluctuations (Kussell *et al.* 2005, Acar *et al.* 2008). In industrial bioprocesses, the apparition of such transitory fluctuations (*e.g.* temperature, pH, nutrient concentrations) might greatly disrupt process performances: reduction of production and biomass yield, decreased growth and production rates (Lara *et al.* 2006, Hewitt *et al.* 2007, Limberg *et al.* 2017).

The aim of this work was to study robustness of a plasmid-expressing *C. necator* strain in fed-batch cultures under nitrogen-limited conditions. More specifically, the impact of plasmid expression levels of the recombinant protein through eGFP single-cell fluorescence was investigated. To do so, strain robustness was first investigated in conditions of different sugar feeding strategies (pulses and continuous) in order to determine the least disruptive strategy. Then, strain robustness was investigated through two plasmid stabilization systems (Kanamycin resistance and Post-Segregational Killing *hok/sok*) in order to evaluate their impact on cell growth and single-cell characteristics.

2.3.3 Material and methods

2.3.3.1 Strains

Cupriavidus necator Re2133 (Budde *et al.* 2011) was used as expression strain. This strain was obtained by deleting genes from the PHB production pathway, encoding for acetoacetyl-CoA reductases (*phaB1B2B3*) and for PHA synthase (*phaC1*) from the wildtype strain *C. necator* H16 / ATCC17699 which was gentamicin resistant (Gen^R). The strains *Escherichia coli* S17-1 and Top10 were used for plasmid construction.

2.3.3.2 Plasmids

The plasmids pCB1 and pCB3 were used in this work. The design and associated molecular biology protocols for the construction of the plasmid pCB1 were explained in more details in Boy et *al*. (2020). The plasmid pCB3 was constructed following the same methodology, from the plasmid backbone

pBBAD-Par. The plasmid pCB3 encodes for the Post-Segregational Killing (*abbr.* PSK) system *hok/sok*. Both plasmids encode for the P_{lac}-*eGFP* cassette and for kanamycin resistance (Kan^R).

2.3.3.3 Media

The rich medium for precultures was composed of 27.5 $g \cdot L^{-1}$ Tryptic Soy Broth (TSB, Becton Dickinson, Sparks, MD, USA) with addition of 10 $mg \cdot L^{-1}$ gentamicin and 200 $mg \cdot L^{-1}$ kanamycin as final concentration. For Tryptic Soy Agar (*abbr.* TSA) plates, 20 $g \cdot L^{-1}$ agar was added to the TSB medium.

For molecular biology, the rich Lysogeny broth medium (*abbr.* LB) was used and composed of 10 $g \cdot L^{-1}$ of peptone, 5 $g \cdot L^{-1}$ of yeast extract and 10 $g \cdot L^{-1}$ of NaCl. For LB agar plates, 20 $g \cdot L^{-1}$ agar was added to the LB medium.

The mineral medium used for flasks cultivation was previously described in Lu et *al.* (Lu *et al.* 2013). Gentamicin (10 $mg \cdot L^{-1}$) and kanamycin (200 $mg \cdot L^{-1}$) were added to this medium. Fructose (20 $g \cdot L^{-1}$) and NH_4Cl (0.5 $g \cdot L^{-1}$) were respectively used as carbon and nitrogen sources.

The mineral medium used for bioreactor cultivation was composed as follows (per liter): $(NH_4)_2SO_4$, 2.8 g; $MgSO_4$-$7H_2O$, 0.75 g; phosphorus (Na_2HPO_4-$12H_2O$, 1.5 g; KH_2PO_4, 0.25 g); nitrilotriacetic acid, 0.285 g; ammonium iron(III) citrate (28%), 0.09 g; $CaCl_2$, 0.015 g; trace elements (H_3BO_3, 0.45 mg; $CoCl_2$-$6H_2O$, 0.3 mg; $ZnSO_4$,$7H_2O$, 0.15 mg; $MnCl_2$-$4H_2O$, 0.045 mg; Na_2MoO4-$2H_2O$, 0.045 mg; $NiCl_2$-$6H_2O$, 0.03 mg; $CuSO_4$, 0.015 mg). Fructose was used as sole carbon source with an initial concentration of 50 $g \cdot L^{-1}$ for the culture with pulses and 30 $g \cdot L^{-1}$ for the culture with continuous feeding. For experiments containing kanamycin as selection pressure, 100 $mg \cdot L^{-1}$ of kanamycin was added in the medium at inoculation and every 10 $g_{CDW} \cdot L^{-1}$ of biomass produced.

2.3.3.4 Precultures on fructose

One glycerol stock was plated on TSA plates containing 10 $mg \cdot L^{-1}$ gentamicin and 200 $mg \cdot L^{-1}$ kanamycin. The plates were incubated for 72 h at 30 °C. One colony was used to inoculate a rich medium flask culture (3 mL), which was grown for 48 h at 30 °C and 110 rpm. Then, the whole broth volume was used to inoculate a 30 mL mineral medium culture flask, which was incubated at 30 °C and 110 rpm during 24 h. Finally, the whole broth volume was used to inoculate a 300 mL mineral medium culture flask. The baffled flasks were incubated at 30 °C and 110 rpm during 10 h. This flask was used to inoculate the bioreactor culture.

2.3.3.5 Fed-batch cultivations on fructose

Batch cultivations consisted in non-limited growth on fructose. The cultures were led in a 5 L bioreactor Biostat®B-DCU (Sartorius, Germany) with a working volume of 3 L. Regulation and monitoring were done using MFCS/win 2.1 software package (Sartorius, Germany). Partial pressure of dioxygen (pO2)

in the medium was measured with the optical oxygen sensor InPro 6860i (Mettler Toledo, USA) and pH was measured with a pressurized gel-filled pH electrode (Mettler Toledo, USA).

Temperature was regulated at 30 °C and pH at 7.0 by addition of a 4 M KOH solution. Fermentation was carried out in aerobic conditions (*i.e.* air flow and stirring rates were regulated to maintain pO_2 above 30 %).

Fed-batch phases were initiated when nitrogen exhaustion was reached in the bioreactor mineral medium (*i.e.* corresponding to 5 $g_{CDW}·L^{-1}$ biomass). Nitrogen (ammonium, NH_4^+) was the limiting substrate and was fed in the bioreactor through calibrated peristaltic pumps with an exponential flow rate set at 0.04 h^{-1}. This growth rate was chosen based on previous works to investigate isopropanol producing conditions, with fructose pulse feeding strategy (Marc *et al.* 2017). Initial fructose concentration was equal to 50 $g·L^{-1}$ for the culture with pulses and 30 $g·L^{-1}$ for the culture with continuous feeding.

Two strategies were developed for fructose feeding during the fed-batch cultures:

3) **Fructose pulse strategy**: when fructose concentration reached 20 $g·L^{-1}$ in the bioreactor, a pulse was performed to reach 50 $g·L^{-1}$ of fructose.
4) **Controlled feeding strategy**: when fructose concentration reached 20 $g·L^{-1}$, fructose was fed exponentially in the bioreactor to maintain a constant residual concentration of 20 $g·L^{-1}$.

To prevent nutrient limitation, a phosphorus solution (7 $mL·L^{-1}$) and a trace elements solution (2 $mL·L^{-1}$) were added every 10 $g_{CDW}·L^{-1}$ of biomass produced. Plus, to maintain selection pressure, a kanamycin solution at 50 $g·L^{-1}$ was also added (2 $mL·L^{-1}$) every 10 $g_{CDW}·L^{-1}$.

2.3.3.6 Analytical procedures

Biomass characterization

Biomass concentration was measured by optical density (OD) at 600 nm using a visible spectrophotometer (DR3900, Hachlange, Loveland, Colorado, USA) with a 0.2 cm path length absorption cell (Hellma). OD was correlated to cell dry weight (CDW) measurements (*i.e.* 2 $g_{CDW}·L^{-1}$ = 1 OD unit). For cell dry weight measurements, 0.2 µm pore-size polyamide membranes (Sartorius, Göttingen, Germany), were beforehand dried (60°C, 200mmHg, 72 h) and weighted. Culture medium was sampled and filtrated on dried membranes which were dried again in the same conditions.

Metabolite quantification

Cells samples were centrifuged, and supernatants were filtrated (0.2 µm PTFE syringe filters, VWR) before being used for substrate and products determination. The residual fructose and organic acids concentrations were quantified by high-performance liquid chromatography (HPLC). The HPLC instrument (Series 1100, Agilent) was equipped with an ion-exchange column (Aminex HPX-87H, 300×7.8 mm, Bio-Rad, Hercules, CA, USA) protected with a guard column (Cation H+ cartridge, 30×4.6 mm, Bio-Rad) and coupled to a RI detector and an UV detector (λ=210 nm). The column was eluted with 2.5 mM H_2SO_4 as a mobile phase at 50 °C at a flow rate of 0.5 mL·min^{-1}. Residual nitrogen was quantified by higher-pressure ionic chromatography (HPIC). The HPIC instrument (ICS-2100 RFIC, Dionex) was equipped with an IonPac™ CS16 column (RFIC™, 3x50mm, BioRad) and an ion suppressor CERS 500 (2 mm, Thermo Scientific). The column was eluted with 30 mM metanesulfonic acid as a mobile phase at 40 °C and a 40 mA ion suppressor current, at a flow rate of 0.36 mL·min^{-1}.

Plate count

Plasmid stability was quantified by parallel plate count on antibiotic selective TSB Petri dishes (10 mg·L^{-1} Gentamicin and 10 mg·L^{-1} Gentamicin + 200 mg·L^{-1} Kanamycin). Serial dilutions were performed in physiological water (0.85 % NaCl) tubes (BioMérieux, Marcy-l'Étoile, France). For every sample, three dilutions were tested, between 10^{-5} and 10^{-9}. The diluted sample were plated in triplicate with the Whitley Automated Spiral Plater (Don Whitley Scientific, Shipley, UK). Decimal reduction rate from plate count measurements was calculated as: $N = log\left(\frac{Gen^R cells}{Gen^R Kan^r cells}\right)$.

Flow Cytometry

Cell permeability was accessed with propidium iodide staining (FL3 channel) and eGFP-fluorescence of plasmid-expressing cells (FL1 channel) by the BD Accuri C6® flow cytometer (BD Biosciences, Franklin Lakes, NJ, USA). Cell samples were diluted in physiological solution at 10^6 cells·mL^{-1} and then, were stained with 20 µL of a solution at 20 µM propidium iodide (*abbr.* PI) (Molecular Probes, Invitrogen, USA) and incubated 20 min at room temperature in the dark. A 100 % dead–cell control was prepared by incubating cells in 70 % isopropanol for 1 h at room temperature. Samples were run until 20, 000 events were counted at 14 µL·min^{-1} using milli-Q water as sheath fluid. The Forward Scatter Signal (threshold: 12, 000) and Side Scatter Signal (threshold: 2, 000) were used as trigger channels. Data acquisition was performed with BD Accuri CFlow® software and data processing was achieved with FlowJo software (Becton Dickinson, Sparks, MD, USA). Decimal reduction rate was calculated as described above from plasmid-expressing cells (eGFP-positive cells, FL1-A > $8 \cdot 10^2$) and total cells (Single cells, bisectors of both FCS-A *vs* FSC-H and SSC-A *vs* SSC-H): $N = log\left(\frac{Single-cells}{eGFP-cells}\right)$.

Extracellular fluorescence measurement

Samples were centrifuged 3 min at 13, 000 rpm with a MiniSpin® table-top microcentrifuge (Eppendorf, Germany). The extracellular fluorescence intensity in the supernatant was measured with the Synergy™ HT (Biotek®, USA) multiplate reader at excitation wavelength 485 ± 20 nm and emission wavelength 525 ± 20 nm at sensitivity of 50. Black Nunclon® 96-well plates (ThermoFisher, USA) were used. Relative extracellular fluorescence intensity was calculated as: $RFU = \frac{FU_t - FU_{t_0}}{OD_t - OD_{t_0}}$.

2.3.3.7 *Data analysis*

Specific substrate consumption (fructose q_S, ammonium q_N) and biomass production (μ) rates were calculated from experimental data and mass balances (carbon, nitrogen and elemental). Specific growth rate was determined as $ln(X\ in\ g_{CDW} \cdot L^{-1}) = f(t)$ and its error was calculated as the standard deviation of the slope. Determination of specific oxygen consumption (q_{O_2}) and carbon dioxide production (q_{CO_2}) was based on mass balance calculations in both liquid and gaseous phase, from inlet/outlet gas composition, temperature, pH, stirring, oxygen partial pressure (pO_2), and liquid volume. For overall production/consumption yield calculation, masses were plotted pairwise in a scatter plot. A linear regression was used to determine the considered yields and the error was calculated by the standard deviation of the slope.

2.3.3.8 *Statistical analysis: Normality of distribution functions by BoxPlot representation*

Boxplots are graphical tools used to represent distributions through graphical localization parameters: the median (50th percentile, red line), the first (25th percentile) and third quartile (75th percentile). The first and third quartiles respectively represent the bottom and top of the boxplot. The median was represented by the line inside the box. The interquartile range (IQR) was situated between the first and third quartile and represents the length of the box. The whiskers represent the minimum and maximum values when they are within 1.5 x IQR from both extremities of the box. Values above 1.5 x IQR were considered as outliers and are represented by points. A symmetric boxplot with its median in the middle of the box and same length whiskers might be expected to be normally distributed (Rakotomalala *et al.* 2011).

2.3.4 Results

2.3.4.1 *Impact of fructose feeding strategy*

In order to evaluate whether fluctuating nutrient environment may impact the strain robustness, two different sugar feeding strategies were carried out. Nitrogen-limited fed batch cultures were performed by implementing either a pulse-based fructose feeding or a continuous fructose feeding. The plasmid monitoring system developed in Boy et *al.* (2020), based on the expression of eGFP by

plasmid-bearing cells was used. The pCB1 strain was grown under selection pressure (*i.e.* 100 $mg \cdot L^{-1}$ kanamycin addition at inoculation and every 10 $g_{CDW} \cdot L^{-1}$ of biomass produced).

Growth kinetics characteristics

Carbon, nitrogen and elemental balances were checked and completed at least at 90 % for both cultures. A final biomass production (**Figures 1a & b**) of 137 g for pulses and 210 g for continuous feeding was obtained. The global biomass production yields from fructose were equal to 0.28 ± 0.01 $g_X \cdot g_S^{-1}$ and 0.32 ± 0.01 $g_X \cdot g_S^{-1}$ for pulse and continuous feeding, respectively (**Table 1**). No organic acid, other than pyruvate, was produced during culture with continuous fructose feeding. A slight transient peak of pyruvate was detected after the initiation of the fed-bath phase once nitrogen was exhausted for both conditions, at 4.96 g for continuous feeding and 4.86 g for pulses. However, other organic acids were produced only during the culture with fructose pulses (**Figure 2**): citrate, acetate, aceto-acetate and succinate to a lesser extent. This production represented 15 % of the carbon flow during fed-batch culture. For acetate and succinate, the mass produced increased continuously from the beginning of the fed-batch phase; but, for acetate only until biomass started slowing down. For aceto-acetate, production was very noisy and started at the beginning of the fed-batch phase. For citrate, three peaks of production could be observed, after the beginning of the nitrogen–limited phase and after the first two fructose pulses. However, it was re-consumed after each pulse and represented less than 1 % of the carbon flow.

During batch phase, the specific growth rates for both conditions were equal to 0.25 ± 0.01 h^{-1} and 0.22 ± 0.01 h^{-1}, respectively with the initial fructose concentration at 30 and 50 $g \cdot L^{-1}$ (**Figure 1c & d**). Then, the growth rate was maintained around 0.04 ± 0.02 h^{-1} by the controlled nitrogen feeding for both fructose feeding strategies during fed-batch. The number of cell generations produced was 7 with fructose pulse and 8 with continuous feeding. With fructose pulses, growth slowed down after 65 h, just after the third fructose pulse, and stopped at 7.25 generations (80 h) (**Figure 1a & c**). During fed-batch phase for continuous feeding, fructose consumption rate was close to 0.14 ± 0.03 $g_S \cdot g_X^{-1} \cdot h^{-1}$. For pulse feeding, fructose consumption rate increased in response to every fructose addition and then stabilized around 0.15 $g_S \cdot g_X^{-1} \cdot h^{-1}$ in-between pulses. Meanwhile, ammonium consumption rate was close to 0.006 ± 0.001 $g_{NH3} \cdot g_X^{-1} \cdot h^{-1}$ with fructose pulse and to 0.008 ± 0.004 $g_{NH3} \cdot g_X^{-1} \cdot h^{-1}$ for continuous feeding (**Figures 1c & d**). During the pulse experiment, ammonium consumption rate dropped just after the third fructose pulse (**Figure 1c**), way sooner than with a continuous fructose feeding (**Figure 1d**).

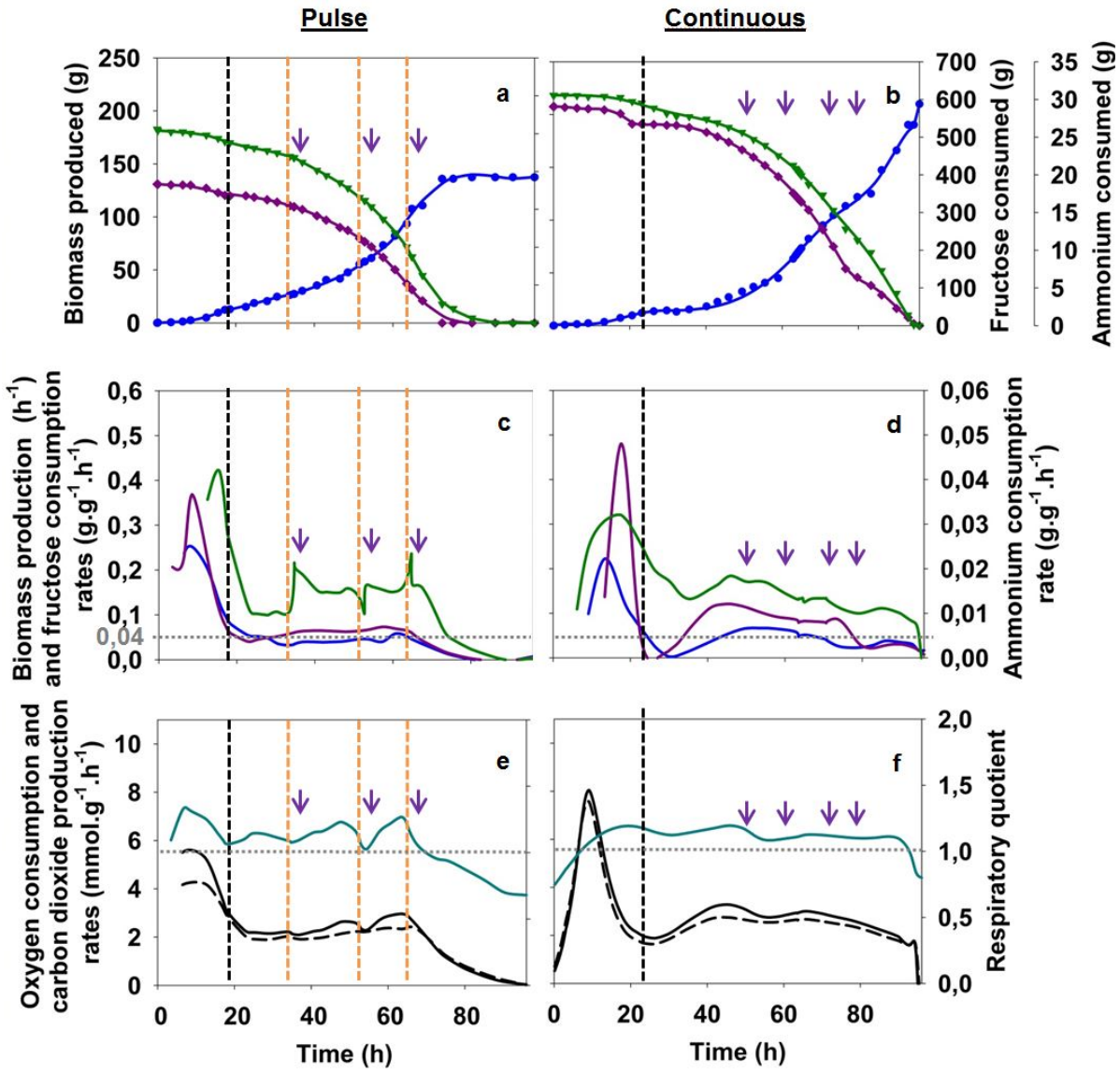

Figure 1 : Cumulated biomass production (●), fructose (▼) and ammonium (◆) consumption during culture of the strain Re2133/pCB1 with kanamycin: with fructose pulses (a) and continuous feeding (b). Growth rate (➡), fructose (➡) and ammonium (➡) consumption rates during Re2133/pCB1 culture of the strain Re2133/pCB1 with kanamycin: with fructose pulse (c) and continuous feeding (d). Respiratory quotient (➡), oxygen consumption (➡➡➡) and carbon dioxide (➡) production rates during culture of the strain Re2133/pCB1 with kanamycin: with fructose pulse (e) and continuous feeding (f). Black vertical lines represent the beginning of the fed-batch phase and orange vertical lines represent fructose pulses. Purple arrows represent additions (kanamycin, 100 mg·L^{-1}; elements and phosphorus solutions)

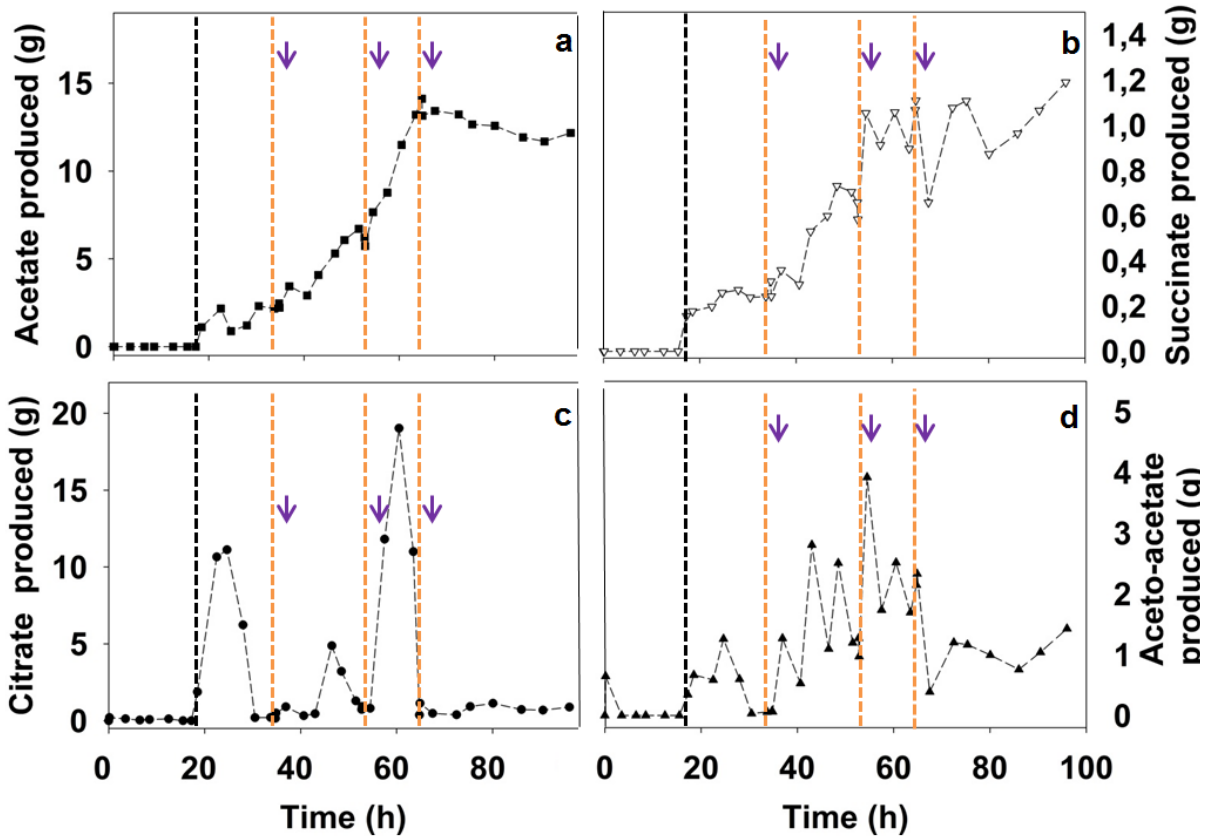

Figure 2: Organic acids production during fructose pulses: acetate (a:■), succinate (b:▽), citrate (c:●), and aceto-acetate (d:▲). Black vertical lines represent the beginning of the fed-batch phase and orange vertical lines represent fructose pulses. Purple arrows represent additions (kanamycin, 100 mg·L^{-1}; elements and phosphorus solutions)

The respiratory quotient (*abbr.* RQ) was stable around 1.13 ± 0.03 during fed-batch phase (20 - 90h) for continuous feeding (**Figure 1f & Table 1**). Specific CO_2 production and O_2 consumption rates were comprised around 2.81 ± 0.57 and 2.48 ± 0.49 mmol·g^{-1}·h^{-1}, respectively. For fructose pulses during fed-batch, respiratory quotient seemed to transiently decrease in response to fructose pulses, until the third fructose pulse where it constantly decreased to 0.7 (**Figure 1e & Table 1**). On this time period, such a decrease in the RQ might be explained by the production of organic acids due to their more oxidized nature (*i.e.* degrees of reduction of 3 for citric and acetoacetic acids, 3.33 for pyruvic and 3.5 for succinic compared to 4.2 for biomass) when growth had stopped (theoretical RQ at 1.06 for growth only). CO_2 specific production rate and O_2 specific consumption rate were comprised around 2.41 ± 0.30 and 2.14 ± 0.22 mmol·g^{-1}·h^{-1}, respectively; a slight increase in carbon dioxide production rate was detected after the two first pulses.

Single-cell analysis of plasmid expression levels

Single-cell analysis was supported by flow cytometry data, and plasmid expression levels analysis by both plate count and flow cytometry measurements. All these data were studied in light of physiological measurements (*i.e.* cell permeability).

During batch phase, the cell permeability percentage (**Figures 3a & b**) was low (below 5 %) for both conducts. Meanwhile, relative extracellular fluorescence intensities were weak between 100-200 RFU, in all tested conditions. An increase was observed at nitrogen depletion for both experiments (6 and 8%). In fed-batch phase, the percentage of permeabilized cells was overall higher when driving by pulse (10 - 20 %) than by continuous feeding (5 - 10 %). Nevertheless, a clear difference was observed after the third addition of sugar when the percentage of permeabilized cells rose to 20 % while it remained below 10 % on the continuously fed batch. Thus, linked to permeability increase, the relative extracellular fluorescence intensity was higher in the pulse mode and increased all along the culture, up to 619 RFU. In the continuously fed reactor, relative extracellular fluorescence intensity was kept more stable compared to fructose pulses, as the percentage of permeabilized cells remained closer to a constant, suggesting equilibrium between new formed cells by growth and permeabilized ones.

Boxplots representing fluorescence intensity distribution were globally wider in the pulse mode during fructose addition (**Figure 3c**), especially in the direction of the first quartile. The fluorescence intensity distribution was close to normal (*i.e.* median = mean and first quartile length = third quartile length) for continuous fructose feeding (until 60 h) and during pulses (until 30 h); even if there was a slight heterogeneity at the outliers (*i.e.* extreme values, 5 and 95 % of the distribution) in continuous feeding (**Figures 3c & d**). After that, distribution range increased for both feeding strategies. After 60h of culture, boxplots presented a wider and non-Gaussian distribution range for all culture conditions. Distribution ranges were noisier for continuous feeding compared to pulse feeding when growth had stopped.

The decimal reduction rates (**Figure 3e**) increased significantly at 55 h (by flow cytometry) and 70 h (by plate count). With continuous fructose feeding (**Figure 3f**), decimal reduction rates (for flow cytometry and plate count) were low and not significant (< 0.2) throughout the culture.

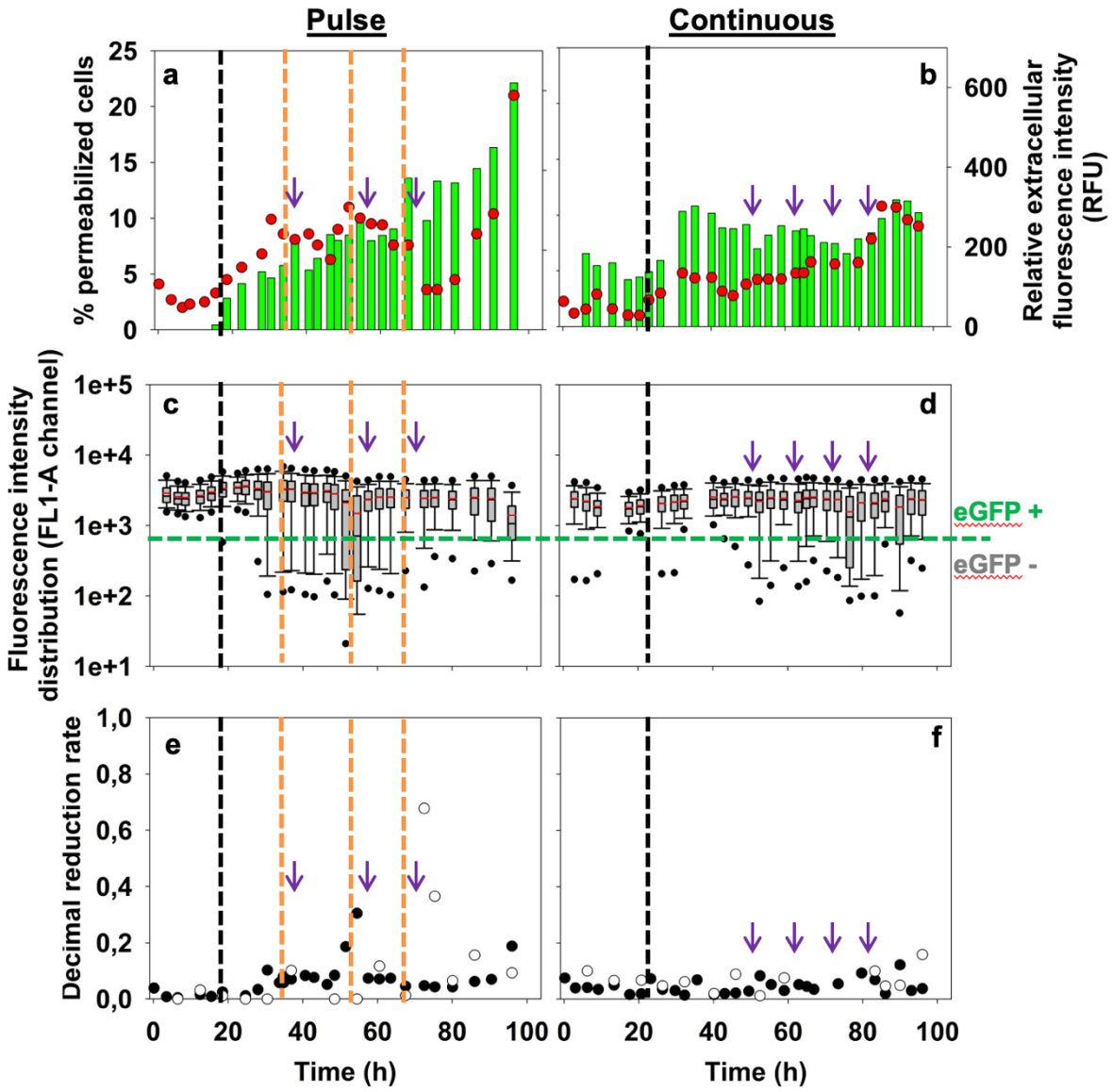

Figure 3 : Relative extracellular fluorescence intensity (FU/OD) (■) and percentage of permeabilized cells (●) in the FL3-A channel for Re2133/pCB1 with kanamycin: with fructose pulse (a) and continuous feeding (b). Boxplot comparison on fluorescence intensity distribution in the FL1-A channel for Re2133/pCB1 with kanamycin: with fructose pulse (c) and continuous feeding (d). Evolution of the decimal reduction rate for Re2133/pCB1 with kanamycin: with fructose pulses (e) and continuous feeding (f) based on plate count (○) and flow cytometry (●) measurements. Black vertical lines represent the beginning of the fed-batch phase and orange vertical lines represent fructose pulses. Purple arrows represent additions (kanamycin, 100 mg·L^{-1}; elements and phosphorus solutions)

The continuous fructose feeding strategy allowed both slightly more stable plasmid expression levels and more efficient macroscopic behavior in terms of cell permeability and overall production yields, compared to pulse fructose feeding. Thus, the continuous strategy was retained in fed-batch bioreactor to pursue our experiments.

2.3.4.2 Impact of plasmid stabilization systems

In order to assess the efficiency of plasmid stabilization systems in maintaining strain robustness, fed-batch experiments were carried out with strains expressing two different plasmid stabilization systems. Kanamycin resistance (strain Re2133/pCB1) and Post-Segregational Killing system *hok/sok* (strain Re2133/pCB3) were evaluated based on their contribution to strain robustness: macroscopic, physiological behavior and expression stability. Fed-batch experiments were carried out following the strategy described above with continuous fructose feeding.

Systems based on plasmid-encoded antibiotic resistance

The plasmid stabilization system based on kanamycin resistance was expressed in a constitutive manner on the strain Re2133/pCB1. Kanamycin (100 $mg \cdot L^{-1}$) was added at inoculation and every 10 $g_{CDW} \cdot L^{-1}$ of biomass produced.

Growth kinetics characteristics

For both fermentation conditions, carbon, nitrogen and elemental balances closed above 95 %. Final biomass production reached for both strains was 178 g without antibiotic and 210 g with kanamycin after 8 cell generations (**Figures 4a & b**). In order to evaluate differences in terms of carbon, nitrogen and oxygen repartition according to the plasmid management, overall yields were calculated and compared to the theoretical values. There was no difference in the values of overall yields measured between the batch phase and the fed-batch phase in both culture conditions. Both overall growth yields were equal to 0.32 ± 0.01 $g_X \cdot g_S^{-1}$ (0.40 ± 0.01 $Cmol_X \cdot Cmol_S^{-1}$), a 40 % decrease compared to the theoretical biomass production yield from fructose (0.53 $g_X \cdot g_S^{-1}$ (Aragao *et al.* 1996)) (**Table 1**). This decrease in biomass overall yield from fructose was due to diversion of the carbon flow toward CO_2 production in our culture conditions. Its overall yield from fructose was always comprised in the same order of magnitude at 0.89 ± 0.02 $g_{CO2} \cdot g_S^{-1}$ and 0.85 ± 0.02 for $g_{CO2} \cdot g_S^{-1}$ without and with kanamycin, respectively (**Table 1**). No organic acids were produced during both cultures, except pyruvate produced transiently after the beginning of the fed-batch phase when nitrogen was exhausted then quickly consumed. For nitrogen, overall biomass production from ammonium was equal to 5.60 ± 0.08 $g_X \cdot g_{NH3}^{-1}$ without antibiotic and 5.40 ± 0.20 $g_X \cdot g_{NH3}^{-1}$ with kanamycin (**Table 1**). This difference appears non-significant based on the value of the standard deviation between the two culture conditions. Nevertheless, these yields were 6 to 9 % lower than the theoretical one (5.96 $g_X \cdot g_{NH3}^{-1}$).

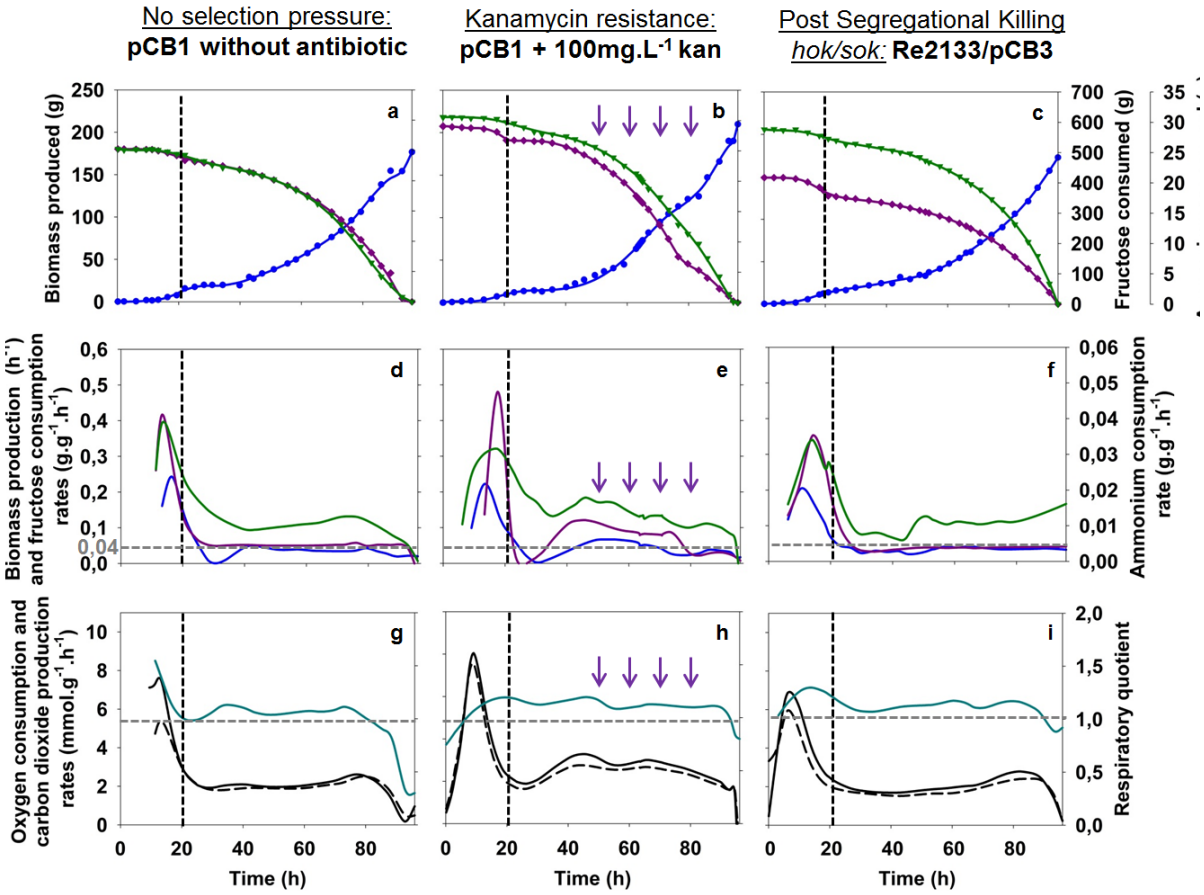

Figure 4: Biomass production (●), fructose (▼) and ammonium (◆) consumption during culture of the strains Re2133/pCB1 (without (a) and with kanamycin (b) and pCB3 (c)). Growth rate (▰), fructose (▰) and ammonium (▰) consumption rates during Re2133/pCB1 culture of the strains Re2133/pCB1 (without (d) and with kanamycin (e)) and pCB3 (f)). Respiratory quotient (▰), oxygen consumption (▰▰▰) and carbon dioxide (▰) production rates during culture of the strains Re2133/pCB1 (without (g) and with kanamycin (h) and pCB3 (i)). Black vertical lines represent the beginning of the fed-batch phase and purple arrows represent additions (kanamycin, 100 mg·L^{-1}; elements and phosphorus solutions)

During batch phase (**Figures 4d & e**), nitrogen limitation occurred when the biomass concentration reached 4 g_{CDW}·L^{-1}. For the strain *C. necator* Re2133/pCB1, the specific growth rate reached 0.22 ± 0.01 h^{-1} and 0.24 ± 0.01 h^{-1}, with and without kanamycin respectively. During fed-batch phase, growth dynamics were imposed by the nitrogen feeding rates, the specific growth rates of the pCB1 strain was maintained around 0.05 ± 0.01 h^{-1} (between 45 and 80 h) in presence of kanamycin and 0.04 ± 0.01 h^{-1} (between 45 and 70 h) without kanamycin. Specific consumption rates of fructose and ammonium during fed-batch phase were overall slightly higher with kanamycin addition; but, decreased all along fed-batch phase.

The respiratory quotient was stable around 1.05 ± 0.06 during fed-batch phase (20 - 90h) without antibiotic (**Figure 4g & Table 1**). Meanwhile, the respiratory quotient with kanamycin was stable around 1.13 ± 0.03 during fed-batch phase (20 - 90h). (**Figure 4h & Table 1**).

Single-cell analysis

In all culture conditions, an increase in the permeabilized cells percentage was observed just after the beginning of the fed-batch phases; slight with kanamycin addition (2 to 5 %) and more important without it (2 to 10 %) (**Figures 5a & b**). This could be explained as a direct answer to the transient nitrogen depletion that cells face at the end of the batch phase. For the strain Re2133/pCB1 without kanamycin, the value of permeabilized cells was higher, because a slightly longer starvation phase (*i.e.* 3 h instead of less than 1 h) before nitrogen was fed exponentially in the medium. At the end of the fed-batch phase, the maximum percentage of permeabilized cells was higher in presence of kanamycin, with 15 % instead of 5 % without selection pressure, both at 170 g of biomass produced. Relative extracellular fluorescence intensity increased mainly after the beginning of the fed-batch phase for both culture conditions and remained quite constant along the cultures. During fed-batch phase, its value was close to 175 RFU and 200 RFU with and without kanamycin addition, respectively and its evolution roughly followed the curve of the percentage of permeabilized cells for both culture conditions.

Intracellular eGFP distribution was represented by boxplots to highlight fluorescence intensity distribution at the single-cell level throughout fermentation. Boxplot distribution was close to normal during most of the batch phase for both culture conditions (**Figures 5d & e**). There was a slight heterogeneity at the level of the outliers (*i.e.* extreme values, under 5 and above 95 % of the total distribution) for kanamycin addition (**Figure 5e**). After the beginning of the fed-batch phase, boxplot distribution range increased. Without antibiotic, the distribution range returned to a normal configuration after 55 hours and until the end of the culture. With kanamycin, the boxplot distribution range was close to normal until 40 h, even if extreme values were rather low. After 60 h, the distribution profile increased and boxplots were not normal anymore.

To evaluate plasmid expression loss, decimal reduction rate was calculated from two counting methods: traditional plate count method based on expression of kanamycin resistance encoded on the plasmid, and eGFP biosensor monitoring method (**Figures 5g & h**). Only data from flow cytometry were shown here, as they were similar to results from plate count. Decimal reduction rate was low for all strains and culture conditions tested, and plasmid stability loss was very slight.

So, the widening in plasmid expression level distribution might be due to two phenomena: (1) the increase in the percentage of permeabilized cells and eGFP leakage (*i.e.* PI-positive cells; either eGFP-positive or -negative) compared to the non-selective condition, and (2) a very slight plasmid expression loss (*i.e.* eGFP-negative and PI-negative cells).

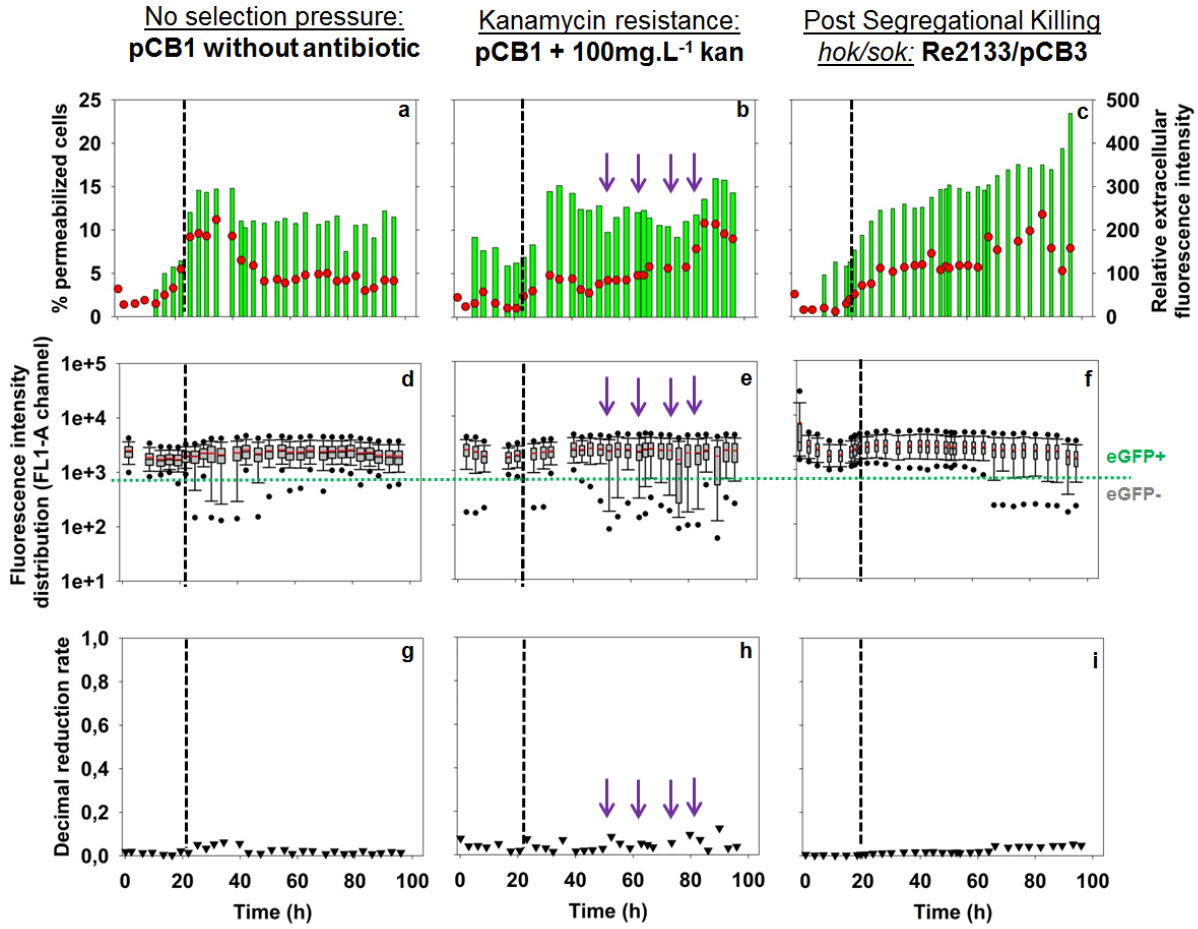

Figure 5 : Relative extracellular fluorescence intensity (FU/OD) (●) and percentage of permeabilized cells (●) in the FL3-A channel for Re2133/pCB1 without (a) and with (b) kanamycin and pCB3 (c). Boxplot comparison on fluorescence intensity distribution in the FL1-A channel for Re2133/pCB1 without (d) and with (e) kanamycin and pCB3 (f). Evolution of the decimal reduction rate N (▼) during pCB1 without (g) and with (h) kanamycin and pCB3 (i). Black horizontal lines represent the beginning of the fed-batch phase. Purple arrows represent additions (kanamycin, 100 mg·L^{-1}; elements and phosphorus solutions)

Plasmid stabilization system based on kanamycin resistance was accompanied by variations in the plasmid expression level, as seen through boxplots, and induced higher permeabilization percentage of cells. Plasmid stability was maintained during 8 cells generations but, it was not due to kanamycin resistance as plasmid stability was maintained also without selection pressure.

System based on plasmid-encoded Post Segregational Killing System

The second plasmid stabilization system tested was based on the expression of a toxin / antitoxin system (*hok / sok*) which was expressed in a constitutive manner on the pCB3 plasmid.

Growth kinetics characteristics

Carbon, nitrogen and elemental balances were recovered (> 95 %). Final biomass production reached for pCB3 with 173 g over 8.16 generations was close to those obtained for pCB1 without kanamycin addition, considered as reference culture (**Figures 4 a & c & Table 1**). Like stated beforehand, there was no difference between the values of overall yields measured between the batch phase and the fed-batch phase. Concerning biomass production from fructose, the overall yield for pCB3 was equal to 0.32 ± 0.01 $g_X \cdot g_S^{-1}$ (0.40 ± 0.01 $Cmol_X \cdot Cmol_S^{-1}$) similar to the one obtained for pCB1. CO_2 production from biomass was equal to 0.87 ± 0.02 $g_{CO2} \cdot g_S^{-1}$ for pCB3. Like for pCB1, biomass overall yield was decreased in the benefit of CO_2 production.

No organic acids were produced during the experiment. There was a transient pyruvate production after the beginning of the fed-batch phase with 9 g for pCB3, which was quickly consumed. The overall biomass production from nitrogen yield 5.21 ± 0.41 $g_X \cdot g_{NH3}^{-1}$ for pCB3 was comparable to pCB1. This difference appears non-significant based on the value of the standard deviation. Experimental data presented a 6 to 12.5 % decrease compared to the theoretical biomass production yield from ammonium (5.96 ± 0.41 $g_X \cdot g_{NH3}^{-1}$).

During batch phase, the maximum growth rate reached was 0.20 ± 0.01 h^{-1} for Re2133/pCB3 and 0.24 ± 0.01 h^{-1} for Re2133/pCB1 (**Figures 4d & f & Table 1**). During the fed-batch phase, the specific growth rate applied was 0.04 ± 0.01 h^{-1} for pCB1 and 0.03 ± 0.01 h^{-1} for pCB3. There was no significant difference in the fed-batch monitoring strategy based on the growth rate imposed by the nitrogen feeding. For both strains, fructose and ammonium consumption rates were close during fed-batch phases. For pCB3, the respiratory quotient was stable around 1.14 ± 0.02, all along the fed-batch phase (**Figure 4g & i & Table 1**). Specific CO_2 production and O_2 consumption rates were stable around 2.10 ± 0.40 and 1.84 ± 0.30 $mmol \cdot g_X^{-1} \cdot h^{-1}$, respectively.

Single-cell analysis

In all culture conditions, an increase in permeabilized cells percentage was observed just after the beginning of the fed-batch phase (**Figures 5 a & c**). This could be explained by the transient nitrogen depletion at the end of the batch phase. During the fed-batch phase, the percentage of permeabilized cells kept on increasing for pCB3 up to 13 %, while the value remained stable around 3 % for pCB1.

During fed-batch phase, relative extracellular fluorescence in the supernatant was stable around 200 RFU for pCB1 and it increased continuously from 200 to 470 RFU for pCB3 and seemed to be correlated to permeability increase. However, the last two points for Re2133/pCB3 have to be considered with caution as optical density decreased because of cell lysis, as confirmed in cytograms (*data not shown*).

A comparison of plasmid expression level between our reference strain Re2133/pCB1 and Re2133/pCB3 strain carrying the PSK system was carried out. Regarding flow cytometry distributions (**Figures 5d & f**), both strains presented a similar fluorescence intensity distribution that was normal and stable through batch phase. At the beginning of the fed-batch, boxplots distribution ranges for pCB1 were significantly more disrupted than with pCB3. After 60 h culture up to the end, boxplot distribution ranges for pCB3 were wider in direction of the first quartile. This was consistent with the increased relative extracellular fluorescence intensity observed for pCB3 beforehand, as permeable cells presented lower fluorescence intensity (*data not shown*). Therefore, higher permeabilization percentage led to increased eGFP leakage, to higher relative extracellular fluorescence intensity, and to wider boxplots distribution ranges.

The decimal reduction rates measured by plate count and flow cytometry data (**Figures 5g & i)** for both pCB1 and for pCB3 through time were not significant and no plasmid loss was detected.

Table 1: Summary of macroscopic data for the strains Re2133/pCB1 (with or without kanamycin; with pulse or continuous fructose feeding) and pCB3

Strains	μ	$R_{S/X}$	$R_{NH3/X}$	$R_{S/CO2}$	**By-products**	**RQ**	q_{CO2}	q_{O2}
	h^{-1}	$g_X \cdot g_S^{-1}$	$g_X \cdot g_{NH3}^{-1}$	$g_{CO2} \cdot g_S^{-1}$			$mmol \cdot g_X^{-1} \cdot h^{-1}$	$mmol \cdot g_X^{-1} \cdot h^{-1}$
Re2133/pCB1 *Continuous feeding*	0.24	0.32 ± 0.01	5.60 ± 0.08	0.89 ± 0.02	none	1.05 ± 0.06	2.14 ± 0.23	2.05 ± 0.24
Re2133/pCB1 + Kan *Pulse feeding*	0.25	0.28 ± 0.01	6.6 ± 0.2	0.74± 0.01	acetate, succinate, aceto-acetate, citrate	1.12 ± 0.08	2.41 ± 0.30	2.14 ± 0.22
Re2133/pCB1 + Kan *Continuous feeding*	0.22	0.32 ± 0.01	5.4 ± 0.2	0.85 ± 0.02	none	1.13 ± 0.03	2.81 ± 0.57	2.48 ± 0.49
Re2133/pCB3 *Continuous feeding*	0.2	0.32 ± 0.01	5.21 ± 0.41	0.87 ± 0.02	none	1.14 ± 0.02	2.10 ± 0.4	1.84 ± 0.3
Reference (Aragao et *al.* 1996)		0.53	5.96	0.51				

2.3.5 Discussion

The aim of this work was to assess robustness of engineered strains under nitrogen-limited fed-batch cultures with *C. necator*. Strain robustness was studied under two sugar feeding strategies (pulses and continuous) and with two plasmid stabilization systems (kanamycin resistance and Post-Segregational Killing *hok/sok*). Strain robustness was defined as the ability of cells to maintain homogenous growth, production performances and plasmid expression levels, among individuals over a long period of culture.

Traditionally, substrate feeding strategy for fed-batches can be carried out either by continuous feeding necessitating programmable pumps or more simply by pulse addition. In previous works, the two strategies were applied with *C. necator*, the pulse-based strategy for fructose feeding was applied for the production of isopropanol (Marc *et al.* 2017) and the continuous strategy (maintain at 20 $g \cdot L^{-1}$) was led during alka(e)ne production (Crepin *et al.* 2016); both in nitrogen limited fed-batch mode. It is well-known that sugar pulsed strategy led to fluctuating environments, which may reduce process performance and strain robustness, as reported in some studies (Lara *et al.* 2006, Hewitt *et al.* 2007, Limberg *et al.* 2017). In *E. coli*, high glucose pulses might be accompanied by an overflow metabolism in strict aerobic conditions, which might lead to acetate production (Lara *et al.* 2009, Neubauer *et al.* 2010). High substrate concentrations in the feeding zone during pulses might also lead to enhanced respiratory activity and so, to dissolved oxygen depletion (Lara *et al.* 2006). In this case, under oxygen limitation, a fermentative metabolism might occur and divert carbon flow toward acetate, formate and ethanol productions (Lara *et al.* 2009, Neubauer *et al.* 2010). If organic acids are produced in high enough concentrations, pH decrease might also occur locally in the feeding zone. All these phenomena might lead to strain robustness disruption. Thus, a continuous feeding strategy was applied during the culture of the strain Re2133/pCB1 under selective pressure and results were compared to pulse-feeding strategy, in terms of strain robustness.

No significant impact was observed on the specific growth rate or on overall production yields, as a result of the difference in the initial fructose concentration (30 *vs* 50 $g \cdot L^{-1}$) during the batch phase (0.25 ± 0.01 h^{-1} for pulse feeding and 0.22 ± 0.01 h^{-1} for continuous feeding). During the fed-batch phase, the growth was dictated by the dynamics of the nitrogen-feeding conduct and was equal for both feeding strategies. The global biomass production yields on fructose were found higher in the continuously fed reactor. No organic acid was detected with continuous feeding, whereas organic acid production occurred in the pulse experiment, representing up to 15 % of the consumed carbon. Therefore, organic acids and growth competed for the carbon. Pyruvate was transiently produced after nitrogen depletion and re-consumed for both fructose feeding strategies. This transient phenomenon might likely be due to a carbon overflow at the onset of nitrogen limitation as previously reported in engineered *C. necator*

strains (Crepin *et al.* 2016, Marc *et al.* 2017). The explanations for the production of citrate, acetoacetate and acetate are given as follows. First, the production of citric acid was reported during fed-batch cultures with alka(e)ne engineered *C. necator* strains (Crepin *et al.* 2016). However, quantities measured during alka(e)ne production were lower (1 $g \cdot L^{-1}$ on fructose; 2 $g \cdot L^{-1}$ on CO_2) than the ones determined in this work with pulse feeding (max. 20 g, corresponding to 6.7 $g \cdot L^{-1}$). The accumulation of citrate could be explained by a disruption in the TCA cycle via the inhibition of aconitase. Nitrogen limitation is known to inhibit aconitase's activity in some oleaginous microorganisms, leading to citrate excretion (Evans *et al.* 1984, Ratledge 2002). As a natural producer of PHB, *C. necator* could, to some extent, follow the patterns of metabolic regulation of oleaginous microorganisms, which might be favored under alka(e)ne production or with fructose excess under nitrogen-limited culture conditions. Second, the accumulation of acetoacetate during fed-batch phase might be due to the redirection of the carbon flow from acetyl-CoA toward the biosynthesis of PHB. As this pathway has been deleted in the *C. necator* Re2133 strain downstream of the acetoacetyl-coA, aceto-acetate was likely produced by the acetoacetyl-CoA transferase that is naturally present in *C. necator* (Grousseau *et al.* 2014). Third, the accumulation of acetate coming from the conversion of the acetyl-CoA *via* phosphate acetyltransferase - acetate kinase pathway has already been reported in the PHB –deleted strains and engineered strains (Crepin *et al.* 2016) or in response to oxygen limitation (Tang *et al.* 2020).

C. necator presents a natural carbon overflow metabolism toward the production of PHB in conditions of nutritional limitation (*e.g.* nitrogen, phosphate), which can represent up to 80 % of its dry cell mass (Ryu et al. 1997). However, as said above, the PHB biosynthesis pathway was deleted in our strain. One might hypothesize that with fructose pulses under sugar fluctuating conditions, the transitory excess carbon flow was re-directed toward the production of organic acids. In Marc et *al*. (2017), no organic acids were produced during the same nitrogen-limited phase with fructose pulses. Therefore, in isopropanol engineered strains, the redirection of this carbon overflow was probably totally drawn by the isopropanol biosynthetic pathway. This was not the case for alka(e)ne production in *C. necator*, where the amount of organic acids produced during fed-batch increased with continuous fructose feeding (Crepin *et al.* 2016). The efficiency of the carbon flow redirection logically depends on the design of the synthetic pathway.

The percentage of permeabilized cells was globally higher during fructose pulse feeding. This increase in cell permeability was correlated with higher relative extracellular fluorescence intensity, due to higher eGFP leakage outside the cells. The main effect of higher sugar concentrations on microbes is osmotic shock. Since water diffuses through membranes as a response of increased osmotic pressure. Therefore, water activity decreases in cells (Lengeler *et al.* 1998, Parish *et al.* 2006). As a result, enzyme

activity might be disrupted, which could lead to a weakening of DNA structure, growth inhibition or cell permeabilization (Parish *et al.* 2006). The response toward high sugar concentrations highly depends on the microorganism (Kushner *et al.* 1964). A promoter inducible by carbon starvation (*csiE*) has been used to control GFP expression in *E.coli* (Delvigne *et al.* 2011, Delvigne *et al.* 2011) to study the impact of sugar-mixing imperfections on protein expression and/or excretion. Three cultivation modes were investigated: chemostat, fed-batch and scale down reactor (*abbr.* SDR, that mimics heterogeneity in large scale bioreactors through a recycle loop). GFP excretion in the medium was dependent on the nature of stress encountered by cells in a given bioreactor conduct. During strict sugar limitation under prolonged culture conditions in chemostat and fed-batch modes, permeabilized cell percentage was higher and was correlated to higher GFP leakage intensity. Under sugar fluctuating environments, in chemostat (switch from batch to chemostat, or abrupt changes in dilution rate) and in SDR (glucose gradient in recycle loop), GFP excretion was slowed down. Indeed, such complex extracellular fluctuations (*i.e.* transitory glucose non-limiting conditions) might have induced an overflow metabolism and inactivated the carbon-limitation promoter (*csiE*). In this case, membrane was in a better state (*i.e.* low permeability) and this could be due to an adaptation of cells to constantly fluctuating environments in SDR. GFP leakage was shown to be correlated with higher permeabilization percentages, and so, was lower for SDR compared to fed-batch mode. However, our results were different concerning the impact of environmental fluctuations on cell permeability, as cells tended to be more permeable under pulse feeding compared to continuous feeding. First, the intensity of sugar concentration fluctuations was different, as fructose concentrations varied from 20 to 50 $g \cdot L^{-1}$ in our work, and glucose concentrations from 0 to about 1 $g \cdot L^{-1}$ in Delvigne et *al*. (2011). Then, fluctuations occurred more regularly in the SDR (every 8 min) than in our fed-batch culture (12 – 18 h in between pulses), which might favor the adaptation of cells to fluctuating environments in SDR. Finally, cultures conditions were glucose-limited in Delvigne et *al.* (2011), which was not the case in our work ([fructose] > 20 $g \cdot L^{-1}$). Glucose-limitation led to a drop of cell viability (*i.e*. increase in cell permeability, by PI-staining) in chemostat, whereas cells adapted to fluctuating culture conditions in SDR.

The decimal reduction rate was considered not significant for continuous feeding when calculated by plate count and flow cytometry. For pulse feeding, decimal reduction rates were low (< 0.2), except after the second fructose pulse (0.3 at 55 h by flow cytometry) and the third one (0.7 at 70 h by plate count), indicating a slight plasmid stability loss. In both culture conditions, the majority of cells were plasmid-expressing cells. But they presented heterogeneous plasmid expression levels either after fructose pulses or after extended culture durations under selection pressure. Until 30 h for pulses and 60 h for continuous feeding, plasmid expression level distribution could be considered close to normal, according to boxplot representation. However, after these moments, expression level distributions

were noisy until the end of fed-batch phase, because of two phenomena. Firstly, in both cultures, increased cell permeability was correlated with increased eGFP leakage, which contributed to widen fluorescence intensity distribution, as permeabilized cells presented globally a lower fluorescence intensity. Secondly, during pulse feeding a slight increase in decimal reduction rate was detected (at 55 and 70 h) and might reveal a slight loss in plasmid expression level (*i.e.* widening of the first quartile) that could impact fluorescence intensity distribution.

The continuous fructose feeding strategy which allowed homogeneous and stable culture conditions during fed-batch phase was selected to pursue strain robustness evaluation. The impact of two plasmid stabilization mechanisms on strain robustness was studied: kanamycin resistance and Post-Segregational Killing (PSK) *hok/sok*. The reference culture (*i.e.* Re2133/pCB1 without kanamycin addition) and the cultures led under plasmid stabilization conditions (*i.e.* Re2133/pCB1 with kanamycin and pCB3 with PSK system) were compared on their impact on macroscopic behavior, plasmid expression levels and cell physiology.

Both plasmid stabilization systems presented close biomass and CO_2 production yields from fructose between the two stabilization systems. However, there was a significant reduction in the biomass production yield from fructose compared to the theoretical value. Indeed, overall biomass production yield from fructose was 40 % lower compared to reference value (0.53 $g_X \cdot g_S^{-1}$, Aragao et *al.* 1996) and the missing carbon was deviated toward the production of CO_2. It is likely due to the presence of the plasmid in host cells and to the production of eGFP by plasmid-expressing cells.

During fed-batch phase, the permeabilized cell percentage decreased and stabilized around 5 % for pCB1 without antibiotic. However, it increased up to 10 % for pCB1 with kanamycin and up to 15 % for pCB3. As a result, the strains reached different relative extracellular fluorescence intensity, from lowest to highest: pCB1, pCB1 with kanamycin and pCB3. It appears that stabilization systems (kanamycin resistance and PSK system) led to an increase in eGFP leakage outside of cells. The distribution profiles of fluorescence at the single-cell level widen at the end of culture (*i.e.* stably for pCB3 and noisy for pCB1 + kanamycin), when relative extracellular fluorescence intensity and percentage of permeabilization increased, for plasmid stabilization systems. Plasmid expression levels were more stable throughout culture for the strain Re2133/pCB3, especially at the beginning of the fed-batch phase compared to the strain Re2133 with and without kanamycin. Therefore, Re2133/pCB3 presented an advantage in terms of strain robustness compared to the strain Re2133/pCB1 all along the culture, based on more homogeneous plasmid expression levels at nitrogen depletion and until 60 h of culture. Maintaining plasmid expression levels without the use of antibiotics (with PSK *hok/sok*) might be interesting to avoid their addition in cultures at industrial scale, to decrease the economic

cost of the bioprocess and the risk of multidrug resistance issue. We can precise that the intracellular fluorescence intensity distribution and the levels of extracellular fluorescence intensity in the medium (eGFP leakage) reached in this study were far lower than the values reached in our previous work (Boy et *al.*, 2020) with the strain Re2133/pKRSF1010-P_{j5}-eGFP in flasks (*i.e.* eGFP constitutively induced by the strong promoter P_{j5}). Thus, eGFP leakage in this work was not due to a too high intracellular fluorescence intensity that the host cells would not be able to cope with.

For all fermentation conditions, plate count and flow cytometry measurements gave comparable cell number for the total cell population and the plasmid expressing cells population. So, neither of the plasmid stabilization system studied impacted cell cultivability. The decimal reduction rates calculated from flow cytometry and plate count data were not significant for both plasmid stabilization strategies, as it was already the case without selection pressure for Re2133/pCB1.

Due to its stability under well-controlled intensive culture condition, the plasmid pCB3 would be a valuable backbone to evaluate plasmid expression levels in new recombinant protein production conditions or for expressing novel biosynthetic pathways. Therefore, any modification in plasmid expression levels might be attributed to the recombinant protein production.

In conclusion, we demonstrated that the sugar feeding mode is as important as expressing stabilization systems for maintaining strain robustness. In nitrogen limited fed batch cultures, a continuously sugar feeding allowed a better carbon use for protein synthesis (avoiding organic acid excretion), a lower heterogeneity of the plasmid expression and a lower cell permeabilization. Among the stabilization systems tested here, the PSK system showed the best ability to maintain plasmid expression level stability. Surprisingly, the kanamycin resistance system showed negative impact on plasmid expression level, growth and cell permeability. Therefore, the PSK system *hok/sok* in a stable environment allowed improving strain robustness during growth of engineered *C. necator* strain in fed-batch cultures. The so-designed plasmid pCB3 would be an interesting tool to study plasmid expression levels for the production of other recombinant proteins or for expressing biosynthetic pathways.

2.3.6 Results synthesis

The robustness of *C. necator* plasmid-expressing strains during fed-batch cultures under nitrogen-limited conditions was studied. The impact of plasmid expression levels of the recombinant protein through eGFP single-cell fluorescence was investigated with two sugar feeding strategies (pulses and continuous) and two plasmid stabilization systems (Kanamycin resistance and Post-Segregational Killing *hok/sok*).

Impact of fructose feeding

➔ **The continuous fructose feeding strategy allowed both slightly more stable plasmid expression levels and more efficient macroscopic behavior (cell permeability, overall production yields).**

➔ Organic acids production during culture (15 % of the carbon flow at the end of the fed-batch) with fructose pulses: citrate, acetate, aceto-acetate and succinate. This was consistent with the 15 % increase observed for global biomass production yield measured with the fructose continuous feeding (where no organic acids were produced). RQ and specific consumption rates varied in response to fructose pulses.

➔ In fed-batch phase, the percentage of permeabilized cells was overall higher by pulse (10 - 20 %) than by continuous feeding (5 - 10 %). Permeability increase was linked to RFU intensity, and was higher in the pulse mode. With continuous feeding, RFU intensity was kept more stable compared to fructose pulses, as the percentage of permeabilized cells remained closer to a constant. This suggested equilibrium between new formed cells by growth and permeabilized ones.

➔ The fluorescence intensity distribution was close to normal (*i.e.* Gaussian) for continuous fructose feeding (until 60 h) and during pulses (until 30 h). After that, distribution range increased for both feeding strategies and could not be considered normal anymore. Decimal reduction rates were more heterogeneous (peaks at 0.4 and 0.7) with pulse feeding than with continuous fructose where they were low and not significant (< 0.2) throughout the culture.

Impact of plasmid stabilization system

➔ **PSK system *hok/sok* allowed improving strain robustness by showing the best ability to maintain plasmid expression level stability. Kanamycin resistance system showed negative impact on plasmid expression level, growth and cell permeability.**

➔ No difference of growth rate during batch with and without kanamycin or with PSK (0.22 ± 0.01 h^{-1};0.24 ± 0.01 h^{-1}; 0.20 ± 0.01 h^{-1}, respectively), or on overall production yields.

➔ Higher percentage of permeabilized cells in presence of kanamycin or PSK (15 and 13 %, respectively) instead of 5 % without selection pressure. Relative extracellular fluorescence intensity increased mainly after the beginning of the fed-batch phase with and without kanamycin and remained quite constant along the cultures. With PSK, RFU intensity increased continuously from 200 to 470 RFU. In all cultures, its evolution roughly followed the curve of the percentage of permeabilized cells.

➔ Fluorescence intensity distribution increased during fed-batch phase: without antibiotic, the distribution range returned to a normal configuration after a few hours and with kanamycin, distribution ranges were close to normal before increasing again in a non-Gaussian manner. For the PSK system, fluorescence intensity distribution ranges were tighter and close to normal, before increasing at the end of culture. Decimal reduction rate was low with all plasmid construction designs, all along culture.

Part 3 : Results and discussion

Chapter 3: Plasmid expression level heterogeneity during heterogeneous isopropanol production studied by an eGFP monitoring system in fed-batch bioreactor

3.1 Abstract

Phenotypic heterogeneity in recombinant bioprocesses for the production of molecules of economic interest have been suspected to lower production yields and rates, even in the case of monoclonal cultures in homogeneous environments. In this work, we studied plasmid expression level heterogeneity during isopropanol production by a *Cupriavidus necator* fluorescent strain in fed-batch mode. In a previous work, eGFP was identified as a promising plasmid expression reporter for *C. necator* either in optimal culture conditions or plasmid curing-like ones. *C. necator* was engineered as a bioproduction platform toward isopropanol. So, this strain was engineered to combine both isopropanol and eGFP productions, to use expression levels of the plasmid-encoded eGFP to report isopropanol efficiency variations at the single-cell level. Production yields and rates have been shown to be dependent on isopropanol tolerance. So, the aim of this work was to understand the mechanisms behind plasmid instability during isopropanol production. Single-cell analysis was achieved by flow cytometry, to get access to plasmid expression level distribution, as well as cell permeabilization percentage. We showed that coupled isopropanol and eGFP production by *C. necator* presented a cumulative metabolic load compared to only isopropanol or eGFP producing strains. The expression of eGFP during isopropanol production led to a lower isopropanol tolerance (15 % permeability at 6 $g \cdot L^{-1}$ with eGFP production, at 12 $g \cdot L^{-1}$ without), and the fluorescent strain reached a 65 % lower isopropanol maximum titer than the reference strain. It was determined that when isopropanol concentration increased, cell permeabilization increased as well, leading to protein leakage and plasmid expression level reduction for the fluorescent strain. It was shown that plasmid expression stability decreased because of increasing isopropanol concentrations, which impacted negatively isopropanol production dynamics. The strain, Re2133/pEG7c was more tolerant toward isopropanol than the strain Re2133/pJLCB2. So, even if isopropanol titer reached by the fluorescent strain Re2133/pJLCB2 (5.3 $g \cdot L^{-1}$) was significantly lower than the reference strain Re2133/pEG7c (15.1 $g \cdot L^{-1}$), this study gave hints on how to improve recombinant protein performances.

KEYWORDS

Cupriavidus necator, eGFP, isopropanol, fed-batch cultivations, flow cytometry, plasmid expression levels, Single cells

3.2 Introduction

Phenotypic heterogeneity occurs when a clonal population presents several distinct phenotypes even in homogeneous environments. Even monoclonal cultures grown in homogeneous environments might experience cellular heterogeneity. So, in other words, the amount of protein produced from a particular gene will vary among cells in a population and also through time for a single cell. Most of the time, this is due to heterogeneous gene expression (Swain *et al.* 2002, Brehm-Stecher *et al.* 2004, Cao *et al.* 2018, Heins *et al.* 2018, Calabrese *et al.* 2019). Noise in the gene expression is a natural phenomenon arising in two ways: "intrinsic" and "extrinsic" noises (Elowitz *et al.* 2002, Nana *et al.* 2018, Mortier *et al.* 2019). "Intrinsic" noise is caused by the gene expression itself. Indeed, reactions leading to transcription and translation do not necessary occur simultaneously nor in the same order, among cells. A gene might be expressed at different levels even within cells in the same state. Such stochastic behavior is defined locally by the particular gene sequence and the inherent properties of the encoded protein (Swain *et al.* 2002, Cao *et al.* 2018). "Extrinsic" noise is due to fluctuations in the amount of crucial cellular components like regulatory proteins, ribosomes, RNA polymerase or even stage in the cell cycle. Indeed, these molecules are also gene products and therefore vary through time and within cells. So, extrinsic noise appears independently of the expression of the gene of interest, but nevertheless has an effect on it (Swain *et al.* 2002, Cao *et al.* 2018).

In engineered strains, heterologous gene insertion is a supplementary source of cell-to-cell variability. Indeed, both maintenance and expression of those heterologous genes induce a metabolic load on host cells. In most cases, metabolic load is due to extracellular transcriptional resource consumption during recombinant gene expression (Ceroni *et al.* 2018). Therefore, two biological phenomena are competing within engineered strains: recombinant gene maintenance and host cell growth (Silva *et al.* 2012). Resource redistribution might significantly disrupt translation, especially if mRNAs expressed from the heterologous gene sequence encode for strong RBS (*i.e.* Ribosome Binding Sites). In this case, a significant proportion of ribosomes should no longer be available for expression of host genes. Metabolic load leads to growth rate decrease and global physiological modifications. Therefore, the performance of engineered microorganisms toward the production of the recombinant molecules of interest decreases. Finally, the production of a recombinant molecule might be toxic for host cells, which might eventually cause plasmid expression loss (Ceroni *et al.* 2018).

Whether it is due to stochastic gene expression or metabolic load, population heterogeneity is believed to lessen production yields and enhance process instability. Thus, securing phenotypic homogeneity in engineered microbial populations is of major interest for synthetic biology and bioprocess optimization (Delvigne *et al.* 2014, Binder *et al.* 2017, Gonzalez-Cabaleiro *et al.* 2017).

Bioprocesses are traditionally characterized through bulk-scale measurements based on average values of cell populations. However, such methods are not suitable to study the behavior of individual cells especially within heterogeneous cell populations. Single-cell techniques have been intensively investigated these past years in order to trigger key biological mechanisms in living single cells, like the stochasticity of gene expression (Zielenkiewicz *et al.* 2001, Longo *et al.* 2006, Muller *et al.* 2010, Carlquist *et al.* 2012, Delvigne *et al.* 2014, Boy *et al.* 2020). A significant variety of proteins have been investigated as gene expression reporters. Among them the most used are: *lacZ* encoding for *E. coli* beta-galactosidase, *luxAB* encoding for *Vibrio harveyi* luciferase and *gfp* encoding for *Aequorea Victoria* green fluorescent protein (Cao *et al.* 2018). GFP reporter proteins have often been coupled to flow cytometry. Nowadays, gene reporters based on GFP and its derivatives are the most widely used biological tools for dynamic gene expression analysis in living cells (Morschhäuser *et al.* 1998, Blokpoel *et al.* 2003, Carroll *et al.* 2003, Argueta *et al.* 2004, Longo *et al.* 2006, Utratna *et al.* 2014, Wons *et al.* 2018).

Cupriavidus necator H16 has a versatile metabolism and is naturally able to consume both organic (Johnson *et al.* 1971, Friedrich *et al.* 1979, Budde *et al.* 2011, Grunwald *et al.* 2015, Marc *et al.* 2017) and inorganic carbon sources (Tanaka *et al.* 1995, Crepin *et al.* 2016, Marc *et al.* 2017, Garrigues *et al.* 2020). *C. necator* is able to store up to 80 % of its dry cell weight in poly-β-hydroxybutyrate (*abbr.* PHB) (Ryu *et al.* 1997, Pohlmann *et al.* 2006), by diverting carbon flow toward PHB biosynthesis under nutrient limitation conditions and with excess carbon (Koller *et al.* 2010). Like for PHB, several biosynthesis pathways for chemicals of economic interest comprise acetyl-coA as pathway precursor. Thus, lighter genetic modifications are necessary to divert carbon flow after acetyl-coA toward a recombinant molecule biosynthesis (Crepin *et al.* 2016, Marc *et al.* 2017, Garrigues *et al.* 2020). In recent works, *C. necator* has been engineered to produce of isopropanol (Grousseau *et al.* 2014, Marc *et al.* 2017, Sydow *et al.* 2017, Garrigues *et al.* 2020), isobutanol (Black *et al.* 2018), alka(e)ne (Crepin *et al.* 2016), carboxylic acids (Ewering *et al.* 2006, Hoefel *et al.* 2010), alpha-humulene (Krieg *et al.* 2018) and methyl ketones (Muller *et al.* 2013), both heterotrophically and autotrophically.

In the present work, heterologous production of isopropanol by *C. necator* Re2133 was chosen as a study case to evaluate plasmid expression levels during the production of isopropanol. The strain *C. necator* Re2133 was unable to synthesize PHB. The recombinant plasmid used, contained an arabinose

induced-isopropanol operon composed of genes encoding for acetoacetyl-CoA transferase (*ctf*) acetoacetate decarboxylase (*adc*) and alcohol dehydrogenase (*adh*) from *Clostridium* species (Grousseau *et al.* 2014).

Production titers reached by engineered strains might be limited by alcohol toxicity in host strains (Chakravarty *et al.* 2018). High solvent hydrophobicity increases its toxic impact on host cells, indeed, leading to solvent accumulation in the cytoplasmic membrane, causing higher cell permeability (ATP, ions, phospholipids, RNA, proteins leaking), higher membrane fluidity (cell membrane stability, structure disruption) and membrane protein function disruption (nutrient transport disruption) (Nicolaou *et al.* 2010, Dunlop *et al.* 2011, Mukhopadhyay *et al.* 2015). Solvents might also denature biological molecules and lead to protein unfolding, DNA and lipid damages, RNA unfolding or degradation (Nicolaou *et al.* 2010). Consequently, cell growth is inhibited which might lead to cell death. The isopropanol titer produced by *Cupriavidus necator* could be increased up to 9.1 $g \cdot L^{-1}$ (+ 7 %) by overexpressing chaperon *GroESL* genes in the isopropanol production cassette (Marc *et al.* 2017). The expression of *GroESL* in solvent-producing microorganisms has been shown to increase cell tolerance (Mukhopadhyay *et al.* 2015). Marc et *al.* (2017) showed that increased isopropanol tolerance was due to (1) higher specific activity of the heterologous enzymes of the isopropanol production pathway, leading to a maintain of the carbon flow toward isopropanol production; and (2) decreased cell permeability toward higher isopropanol concentrations.

Previously we designed an eGFP based plasmid expression level monitoring system for *Cupriavidus necator* (Boy *et al.* 2020). In this work, the corresponding P_{lac}-*eGFP* cassette was inserted into the isopropanol producing plasmid pEG7c (Grousseau *et al.* 2014). The global aim of this work was to study the impact of the production of a toxic recombinant molecule on the plasmid expression levels. The present study was supported by macroscopic data (metabolite concentrations, production/consumption yields and rates) as well as single-cell analysis (flow cytometry).

3.3 Material and method

3.3.1 Strains

C. necator Re2133 (Budde *et al.* 2011) was used as expression strain. This strain was obtained by deleting genes encoding for acetoacetyl-CoA reductases (*phaB1B2B3*) and for PHA synthase (*phaC1*) from the wildtype strain *C. necator* H16 / ATCC17699 which was gentamicin resistant (Gen^R). The strains *Escherichia coli* S17-1 and Top10 were used during plasmid construction.

3.3.2 Plasmids

The plasmids pEG7c, pCB1 and pJLCB2 were used in this work (**Table 1**). The design and associated molecular biology protocols for the construction of these plasmids were explained in more details in Grousseau et *al.* (2014), Marc et *al.* (2017) and Boy et *al.* (2020).

Table 1: Plasmids used in this work

Strains	Relevant characteristics	References
Re2133	*Cupriavidus necator* H16 *ΔphaB$_1$B$_2$B$_3$C$_1$* (Gen^R)	(Budde *et al.* 2011)
Plasmids		
pBBAD	pBBR1MCS-2 derivative (Kan^R), P$_{Bad}$ (L-Arabinose inducible promoter)	(Fukui *et al.* 2009)
pEG7c	pBBad (Kan^R), isopropanol operon *phaA* – RBS – *ctfAB* – RBS – *adc* – RBS - *adh* inserted into the multiple cloning site (MCS), P$_{Bad}$	(Grousseau *et al.* 2014)
pCB1	pBBad (Kan^R), P$_{lac}$-*egfp*	(Boy *et al.* 2020)
pJLCB2	pEG7c (Kan^R), P$_{lac}$-*egfp* (on the opposite strand, compared to pCB1)	This work

3.3.3 Media

The rich medium for precultures was composed of 27.5 g·L^{-1} Tryptic Soy Broth (TSB, Becton Dickinson, Sparks, MD, USA) with addition of 10 mg·L^{-1} gentamicin and 200 mg·L^{-1} kanamycin as final concentration. For Tryptic Soy Agar (*abbr.* TSA) plates, 20 g·L^{-1} agar was added to the TSB medium.

For molecular biology, the rich Lysogeny broth medium (*abbr.* LB) was used and composed of 10 g·L^{-1} of peptone, 5 g·L^{-1} of yeast extract and 10 g·L^{-1} of NaCl. For LB agar plates, 20 g·L^{-1} agar was added to the LB medium.

The mineral medium used for flasks cultivation was previously described in Lu et *al.* (Lu *et al.* 2013). Gentamicin (10 mg·L^{-1}) and kanamycin (200 mg·L^{-1}) were added to this medium. Fructose (20 g·L^{-1}) and NH_4Cl (0.5 g·L^{-1}) were respectively used as carbon and nitrogen sources. The mineral medium used for bioreactor cultivation was composed as follows (per liter): $(NH_4)_2SO_4$, 2.8 g; $MgSO_4$-$7H_2O$, 0.75 g; phosphorus (Na_2HPO_4-$12H_2O$, 1.5 g; KH_2PO_4, 0.25 g); nitrilotriacetic acid, 0.285 g; ammonium iron(III) citrate (28%), 0.09 g; $CaCl_2$, 0.015 g; trace elements (H_3BO_3, 0.45 mg; $CoCl_2$-$6H_2O$, 0.3 mg; $ZnSO_4$,$7H_2O$, 0.15 mg; $MnCl_2$-$4H_2O$, 0.045 mg; Na_2MoO4-$2H_2O$, 0.045 mg; $NiCl_2$-$6H_2O$, 0.03 mg; $CuSO_4$, 0.015 mg). Fructose was used as sole carbon source with an initial concentration of 30 g·L^{-1}. No antibiotics (*i.e.* gentamicin and kanamycin) were added in bioreactor cultures.

3.3.4 Fed-batch cultivations on fructose

Precultures and batch phases were achieved according to the protocol detailed in Boy et *al*. (2020) to avoid any limitation for cell growth. Fed-batch phases were initiated when nitrogen depletion was reached in the bioreactor mineral medium (corresponding to 4 $g_{CDW}·L^{-1}$ biomass). Nitrogen (using ammonium, NH_4^+) was the limiting substrate and was fed in the bioreactor through calibrated peristaltic pumps with an exponential flow rate set at 0.04 h^{-1}. This growth rate was chosen based on previous works to investigate isopropanol producing conditions (Marc *et al.* 2017). Initial fructose concentration was equal to 30 $g·L^{-1}$. After the beginning of the fed-batch phase, when fructose concentration reached 20 $g·L^{-1}$, fructose was fed exponentially in the bioreactor to maintain a constant residual concentration of 20 $g·L^{-1}$. Two guard flasks, kept in ice, allow the re-solubilization of gaseous acetone and isopropanol fractions in order to quantify their total production both in liquid and gas phases.

To prevent nutrient limitation, a phosphorus solution (7 $mL·L^{-1}$) and a trace element solution (2 $mL·L^{-1}$) were added every 10 $g_{CDW}·L^{-1}$ of biomass produced.

3.3.5 Analytical procedure

Biomass characterization

Biomass quantification was achieved through optical density (600nm) and cell dry weight measurements. These techniques were described in Boy et *al*. (2020).

Metabolite quantification

Cells samples were centrifuged, and supernatants were filtrated (0.2 µm PTFE syringe filters, VWR) before being used for substrate and products determination. The residual fructose and organic acids concentrations were quantified by high-performance liquid chromatography (HPLC). The HPLC instrument (Series 1100, Agilent) was equipped with an ion-exchange column (Aminex HPX-87H, 300×7.8 mm, Bio-Rad, Hercules, CA, USA) protected with a guard column (Cation H+ cartridge, 30×4.6 mm, Bio-Rad) and coupled to a RI detector and an UV detector (λ=210 nm). The column was eluted with 2.5 mM H_2SO_4 as a mobile phase at 50 °C at a flow rate of 0.5 $mL·min^{-1}$. Residual nitrogen was quantified by higher-pressure ionic chromatography (HPIC). The HPIC instrument (ICS-2100 RFIC, Dionex) was equipped with an IonPac™ CS16 column (RFIC™, 3x50mm, BioRad) and an ion suppressor CERS 500 (2 mm, Thermo Scientific). The column was eluted with 30 mM metanesulfonic acid as a mobile phase at 40 °C and a 40 mA ion suppressor current, at a flow rate of 0.36 $mL·min^{-1}$. Isopropanol and acetone concentrations were also determined by gas chromatography (GC), with a GC system

6890A Series (Hewlett Packard®, USA) and a column SupelQ-Plot 30 x 0.53mm (ID). Internal standard was 1 g·L^{-1} propionic acid.

Plate count

Plasmid stability was quantified by parallel plate count on antibiotic selective TSB Petri dishes (10 mg·L^{-1} gentamicin and 10 mg·L^{-1} gentamicin + 200 mg·L^{-1} kanamycin), as described in Boy et *al*. (2020). Decimal reduction rate from plate count measurements was calculated as: $N = log\left(\frac{Gen^R cells}{Gen^R Kan^r cells}\right)$.

Flow Cytometry

Cell permeability was accessed with propidium iodide staining (FL3 channel) and eGFP-fluorescence of plasmid-expressing cells (FL1 channel) by the BD Accuri C6® flow cytometer (BD Biosciences, Franklin Lakes, NJ, USA). Cell samples were diluted in physiological solution at 10^6 cells·mL^{-1} and then, were stained with 20 µL of a solution at 20 µM propidium iodide (*abbr.* PI) (Molecular Probes, Invitrogen, USA) and incubated 20 min at room temperature in the dark. A 100 % dead–cell control was prepared by incubating cells in 70 % isopropanol for 1 h at room temperature. Samples were run until 20, 000 events were counted at 14 µL·min^{-1} using milli-Q water as sheath fluid. The Forward Scatter Signal (threshold: 12, 000) and Side Scatter Signal (threshold: 2, 000) were used as trigger channels. Data acquisition was performed with BD Accuri CFlow® software and data processing was achieved with FlowJo software (Becton Dickinson, Sparks, MD, USA). Decimal reduction rate was calculated as described above from plasmid-expressing cells (eGFP-positive cells, FL1-A > 8·10^2) and total cells (Single cells, bisectors of both FCS-A *vs* FSC-H and SSC-A *vs* SSC-H): $N = log\left(\frac{Single-cells}{eGFP-cells}\right)$.

Fluorescence measurement in the medium

Extracellular fluorescence intensity in the supernatant was measured using a multiplate reader as described in Boy et *al*. (2020). Relative extracellular fluorescence intensity was calculated as: $RFU = \frac{FU_t - FU_{t_0}}{OD_t - OD_{t_0}}$. The optical density considered was corrected with the percentage of intact cells (*i.e.* not stained by propidium iodide).

3.3.6 Data analysis

Specific substrate consumption (fructose q_S, ammonium q_N) and biomass production (μ) rates were calculated from experimental data and mass balances (carbon, nitrogen and elemental). Specific growth rate was determined as $ln(X\ g_{CDW} \cdot L^{-1}) = f(t)$ and its error was calculated as the standard deviation of the slope. Determination of specific oxygen consumption (q_{O_2}) and carbon dioxide production (q_{CO_2}) was based on mass balance calculations in both liquid and gaseous phase, from

inlet/outlet gas composition, temperature, pH, stirring, oxygen partial pressure (pO_2), and liquid volume. For overall production/consumption yield calculation, masses were plotted pairwise in a scatter plot. A linear regression was used to determine the considered yields and the error was calculated by the standard deviation of the slope. The total mass of isopropanol and acetone produced were calculated on the sum of solvents in the bioreactor (liquid phase) and in both guard flasks (evaporation).

3.3.7 Statistical analysis: Normality of distribution functions by BoxPlot representation

Boxplot representation used to represent fluorescence intensity distribution in single-cells was described in Boy et *al*. (2020).

3.4 Results

Our aim was to study plasmid expression level variations during isopropanol production by an engineered *C. necator* strain. The strain Re2133/pJLCB2 was designed to express *egfp* and to synthesis isopropanol upon arabinose induction. This strain's behavior was compared to the non-isopropanol producing - fluorescent strain Re2133/pCB1 and the non-fluorescing - isopropanol producing strain Re2133/pEG7c. Strain characterization was achieved during fed-batch cultivation where fructose was fed continuously as the sole carbon source and under controlled nitrogen limitation.

3.4.1 Growth kinetics and isopropanol production

During batch phases, maximum growth rates were close for all three strains, with 0.23 ± 0.02 h^{-1} for Re2133/pEG7c (isopropanol operon), 0.21 ± 0.03 h^{-1} for Re2133/pJLCB2 (isopropanol operon + *egfp* cassette) and 0.24 ± 0.01 h^{-1} for Re2133/pCB1 (*egfp* cassette) (**Table 2 & Figure 1b**). During nitrogen limited fed-batch, after arabinose induction, Re2133/pEG7c and Re2133/pJLCB2 started producing isopropanol. Growth rates were maintained at a controlled growth rate of 0.03 ± 0.01 h^{-1} for Re2133/pEG7c, 0.04 ± 0.01 h^{-1} for pJLCB2 and 0.04 ± 0.01 h^{-1} for pCB1 by the controlled nitrogen limitation (**Figures 1b**).

Substrate consumption and metabolite production were quantified. In all cases, carbon, nitrogen and elemental balances were satisfied above 90 %. In fed-batch mode, maximum isopropanol concentration reached was 5.3 $g{\cdot}L^{-1}$ (38 h after induction) for the strain Re2133/pJLCB2 and 15.1 $g{\cdot}L^{-1}$ (76 h after induction) for Re2133/pEG7c (**Table 2**). Isopropanol was produced at a maximum production yield of 0.27 ± 0.01 $g_{IPA}{\cdot}g_S^{-1}$ for Re2133/pEG7c and 0.11 ± 0.02 $g_{IPA}{\cdot}g_S^{-1}$ for Re2133/pJLCB2, at the beginning of the fed-batch phase, before decreasing for all strains (**Table 2**). Profiles of isopropanol specific production rates presented the same dynamics for both strains (**Figure 1e**). First, after arabinose induction, isopropanol specific production rate increased up to a maximum, which was

equal to 0.09 $g_{IPA} \cdot g_S^{-1} \cdot h^{-1}$ (30 h) for Re2133/pEG7c, and 0.04 $g_{IPA} \cdot g_S^{-1} \cdot h^{-1}$ (20 h) for pJLCB2, before decreasing. The maximum isopropanol yield was reached on this time period. Then, isopropanol specific production rate was low until the end of culture.

Acetone was an intermediate in the isopropanol production pathway. It was produced simultaneously with isopropanol all along the fed-batch cultures (**Figures 1 d & e**). Maximum acetone production yields from fructose reached 0.024 ± 0.001 $g_{Ac} \cdot g_S^{-1}$ for Re2133/pEG7c and 0.011 ± 0.001 $g_{Ac} \cdot g_S^{-1}$ for pJLCB2 respectively (**Table 2**). Profiles of the acetone specific production rate followed the same behavior as for the isopropanol ones, confirming that both productions were coupled. The maximal acetone production rates were equal to 0.009 $g_{Ac} \cdot g_S^{-1} \cdot h^{-1}$ for Re2133/pEG7c and 0.003 $g_{Ac} \cdot g_S^{-1} \cdot h^{-1}$ for pJLCB2 (**Figure 1e**).

No significant organic acid production was detected during the culture for all strains. However, after induction by arabinose, a slight peak of pyruvic acid production was observed for the strain Re2133/pEG7c but was re-consumed shortly after; this was not the case for Re2133/pCB1 or pJLCB2 as no pyruvate was detected at all.

The respiratory quotient (*abbr.* RQ) reached a maximum value a few hours after arabinose induction (**Figure 1c**), at 1.96 (30h) for pEG7c and 1.90 (29h) for pJLCB2, approaching the theoretical value for isopropanol only (= 1.96). For the strain Re2133/pCB1 it remained stable around 1.05 ± 0.06 in the range of the theoretical RQ for growth (= 1.06), before decreasing in the last hours of culture. For Re2133/pEG7c and pJLCB2, its value stabilized until the end of culture at respectively 1.30 ± 0.07 and 1.19 ± 0.06.

Oxygen consumption rate was rather stable during fed-batch for all strains, at 2.2 ± 0.2 $mmol \cdot g \cdot h^{-1}$ for Re2133/pEG7c, 1.9 ± 0.3 $mmol \cdot g \cdot h^{-1}$ for pJLCB2 and 2.05 ± 0.24 $mmol \cdot g \cdot h^{-1}$ for pCB1 (**Figure 1c**). Its value decreased for Re2133/pJLCB2 and pCB1 at the end of culture. Likewise, carbon dioxide production rate was comprised around 2.9 ± 0.2 $mmol \cdot g \cdot h^{-1}$ for Re2133/pEG7c, 2.3 ± 0.4 $mmol \cdot g \cdot h^{-1}$ for pJLCB2 and 2.1 ± 0.2 $mmol \cdot g \cdot h^{-1}$ for pCB1 (**Figure 1c**).

It was interesting to consider the variation in the ratio between isopropanol and acetone production (**Figure 1d**). For the reference strain Re2133/pEG7c, this ratio remained stable at 13 ± 1 $Cmol_{isopropanol}/Cmol_{acetone}$ from arabinose induction until the stop in isopropanol production. For the strain Re2133/pJLCB2, the evolution of this ratio was drastically different. Just after arabinose induction, its value reached 13 ± 1 $Cmol_{isopropanol}/Cmol_{acetone,}$ which was equal to the behavior in Re2133/pEG7c. However, this value decreased continuously throughout fermentation until reaching 4

$Cmol_{isopropanol}/Cmol_{acetone}$ at the end of culture. This meant that there was an accumulation of acetone at the expense of isopropanol production at the end of culture.

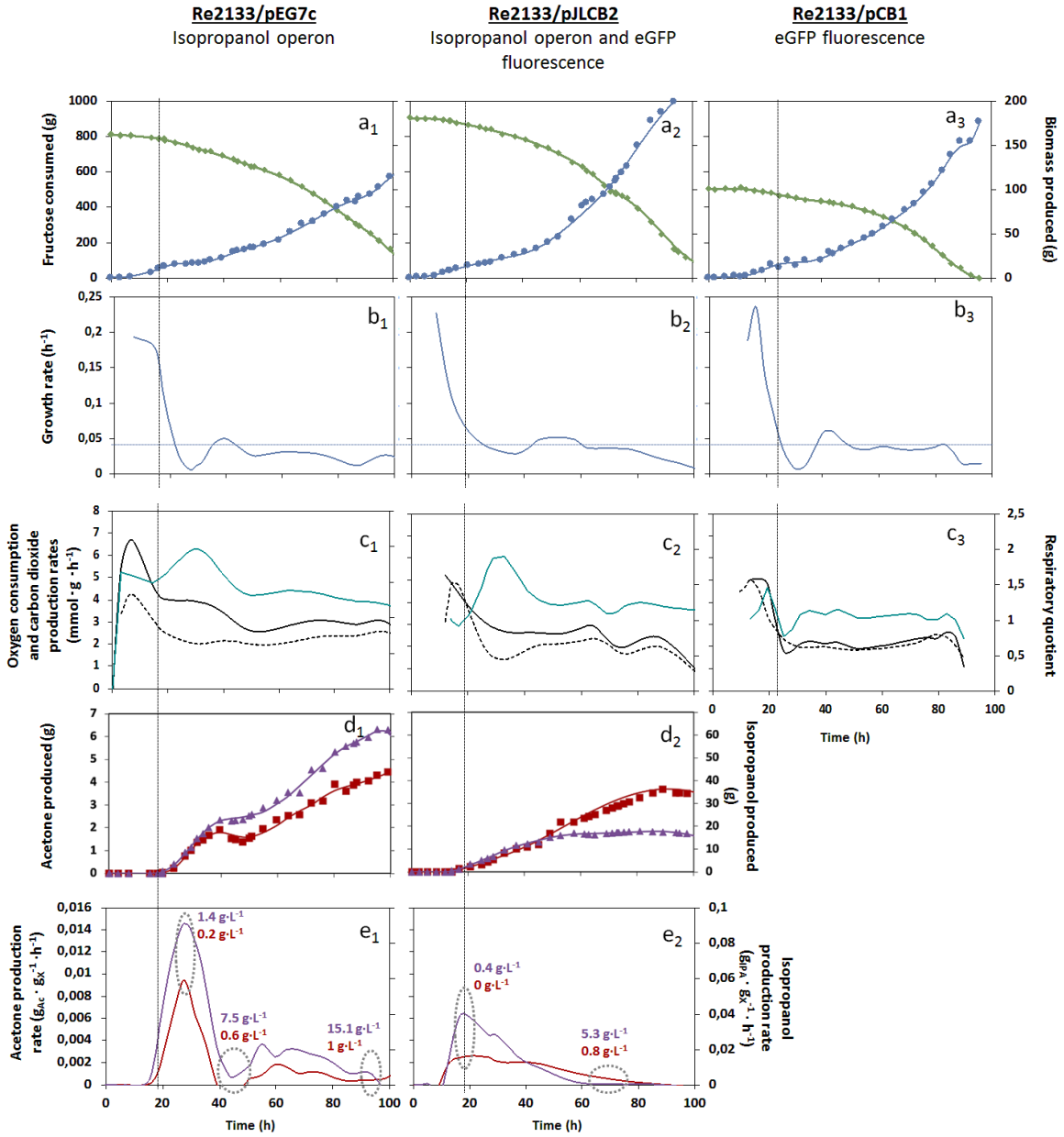

Figure 1: a. Cumulated biomass produced (●) and fructose consumed (◆). b. Growth rate evolution through time (▰). c. oxygen consumption (▰▰) and carbon dioxide (▰) production rates, and respiratory quotient (▰). d. Cumulated acetone (■) and isopropanol (▲) produced during fed-batch. e. Evolution of isopropanol (▰) and acetone (▰) production rates. Cultures in fed-batch of the strains Re2133/pEG7c (1), pJLCB2 (2) and pCB1 (3). The horizontal dotted black line represented the time limit between the batch phase and the fed-batch phase. The doted circles (e1 & 2) represent the moments when specific production rate was either maximum or minimum, and the corresponding isopropanol / acetone concentrations reached

During the batch phase (**Figure 2**), the carbon repartition between biomass and carbon dioxide were comparable for Re2133/pEG7c (60 : 40 %) and pJLCB2 (57 : 43 %). However, for Re2133/pCB1 the

proportions were inverted between biomass and carbon dioxide (40 : 60%), and stable all along the culture.

The highest isopropanol production yield was reached when the specific isopropanol production rate was at its maximum for all strains. The percentage of the carbon flow dedicated to isopropanol reached 41 % for Re2133/pEG7c and 20 % for pJLCB2; both isopropanol and acetone proportions were divided by two in Re2133/pJLCB2. The lower proportion of isopropanol in Re2133/pJLCB2 compared to pEG7c was mainly due to a higher carbon flow toward biomass synthesis (+ 17 %), and carbon dioxide (+ 6 %) to a lesser extent.

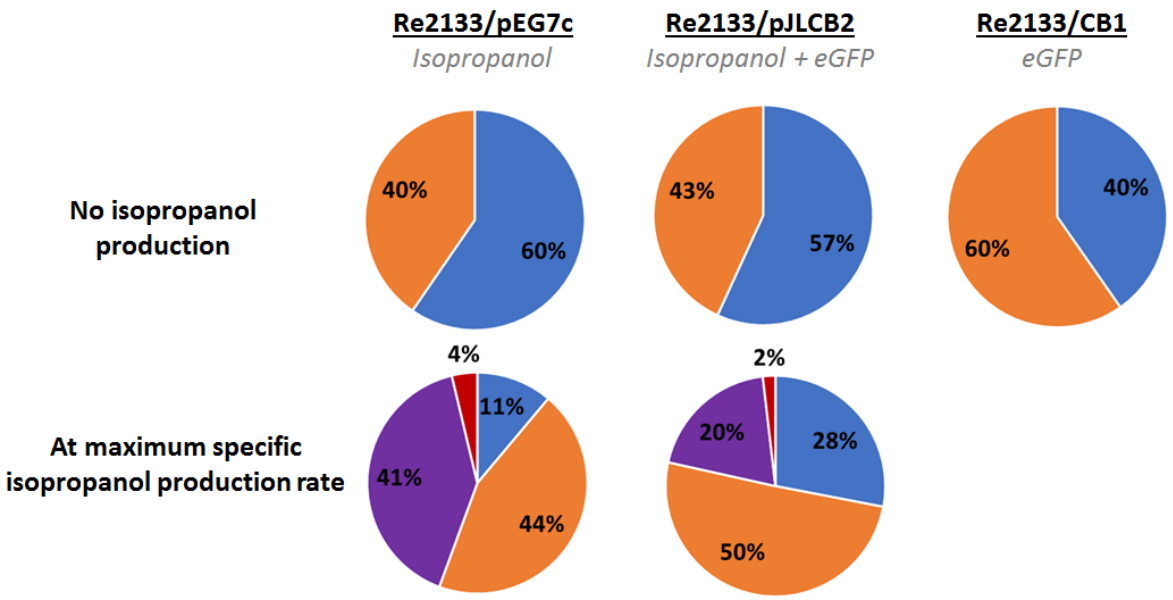

Figure 2 : Overall carbon repartition (% Cmol) between biomass (■), carbon dioxide (■), acetone (■) and isopropanol (■), based on global yields during culture of Re2133/pEG7c, pJLCB2 and pCB1

3.4.2 Inhibition by isopropanol production

After the induction, the isopropanol specific production rate increased up to a maximum ($q_{IPA, max}$) at a concentration of 1.4 $g \cdot L^{-1}$ of isopropanol produced for Re2133/pEG7c, and 0.4 $g \cdot L^{-1}$ for pJLCB2 (**Figures 1e**). For Re2133/pEG7c, isopropanol production rate decreased (- 96 %) until 7.5 $g \cdot L^{-1}$ of isopropanol were produced, and then remained low and constant until becoming null at 15.1 $g \cdot L^{-1}$ of isopropanol. For Re2133/pJLCB2, isopropanol specific production rate decreased until 5.3 $g \cdot L^{-1}$ of isopropanol were produced, and became null. For Re2133/pJLCB2, even when isopropanol concentration decreased in the medium because of higher evaporated quantities compared to produced quantities, isopropanol production rate remained null. So, critical isopropanol concentrations were equal to 15.1 $g \cdot L^{-1}$ for Re2133/pEG7c and 5.3 $g \cdot L^{-1}$ for pJLCB2.

3.4.3 Plasmid expression levels variations during isopropanol production

Plasmid expression levels were studied all along the fermentation, with and without isopropanol production. Flow cytometry was used as a fast and reliable method for fluorescence intensity measurements in single-cells (*i.e.* eGFP and IP). Plasmid stability was also evaluated by the more classical plate count method. The strains Re2133/pEG7c and pCB1 were used as reference, respectively for isopropanol production only and eGFP single-cell fluorescence only, to compare plasmid expression level variations in the strain Re2133/pJLCB2.

Plasmid expression levels analysis

Fluorescence intensity distribution among single cells was studied for the strains Re2133/pCB1 and pJLCB2, with a boxplot representation (**Figure 3**). The first observation was that fluorescence intensity in single cells was higher for Re2133/pJLCB2 than for Re2133/pCB1 during the batch phase. This was due to a change in plasmid construction because of construction challenges. The fluorescent cassette P_{lac}-*eGFP* had to be inserted on the opposite strand of DNA in pJLCB2, compared to the localization applied in the plasmid pCB1. Indeed, during plasmid construction it appeared like there was an incompatibility for the fluorescent cassette and isopropanol operon to be localized on the same DNA strand in our plasmid. No convincing explanation for this phenomenon has been found yet. A higher fluorescent intensity of single cells for Re2133/pJLCB2 compared to pCB1 might be due to a higher induction of the promoter P_{lac} when situated on the opposite DNA strand. Nevertheless, the threshold between fluorescent and non-fluorescent cells was still met at 8.10^2 in the FL1-A channel.

For the strain Re2133/pCB1, fluorescence intensity distribution of the total cell population was noisier during the first 30 h after nitrogen limitation (**Figure 3a**). During batch phase and after 60 h in fed-batch, fluorescence intensity distribution was considered close to Gaussian and reproducible through time. For the specific eGFP-positive cell population, fluorescence intensity distribution was Gaussian and reproducible all along culture (**Figure 3c**).

For the strain Re2133/pJLCB2, fluorescence intensity distribution was Gaussian and reproducible all along batch phase, both for total and eGFP-positive cell populations. After arabinose induction, median quickly dropped for the total cell population (**Figure 3b**), distribution range increased drastically between 30 and 40 h, and then more slowly until the end of culture. After 30 h, distribution could not be considered Gaussian anymore. For the eGFP-positive cell population, distribution range increased significantly between 20 and 30 h and then, remained stable (**Figure 3d**). After that, fluorescence intensity distribution was reproducible. Median and mean values slightly decreased and the first quartile became longer than the third quartile, as the number of “less “fluorescent cells increased.

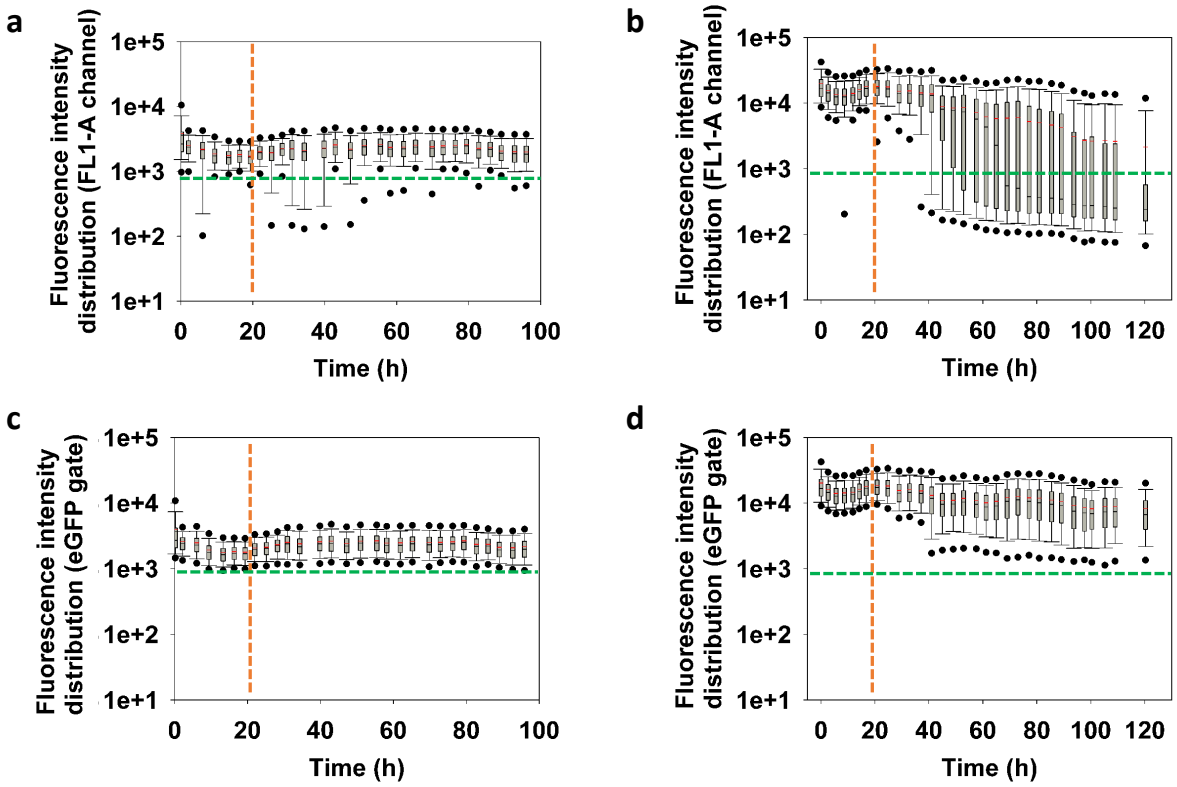

Figure 3 : Boxplot representation through time of fluorescence intensity distribution in the FL1-A channel for the total cell population of Re2133/pCB1 (a**) and pJLCB2 (**b**), and for the eGFP-positive population of Re2133/pCB1 (**c**) and pJLCB2 (**d**). The vertical dotted orange line represented the limit between the batch and fed-batch phases and the horizontal dotted green line represented the eGFP-positive gate**

Plasmid expression stability: flow cytometry vs. plate count

Decimal reduction rate (**Figure 4**) was used to compare plasmid expression stability by two reporters: eGFP biosensor (flow cytometry) and kanamycin resistance (plate count).

For Re2133/pEG7c, up to 9 $g.L^{-1}$ of isopropanol (and 0.6 $g{\cdot}L^{-1}$ of acetone), the decimal reduction rate calculated from plate count remained low under 0.5 (**Figures 4a, 4d & 4f)**. From 9 to 14 $g{\cdot}L^{-1}$ of isopropanol, the decimal reduction rate was maintained at 0.7. After 14 $g{\cdot}L^{-1}$ of isopropanol, the decimal reduction rate increased up to 1.6 at the end of culture.

For Re2133/pJLCB2, decimal reduction rate measured by plate count was significantly higher than the one measured by flow cytometry (**Figures 4b, 4e & 4g**) and it started increasing when 3.6 $g{\cdot}L^{-1}$ of isopropanol were produced in the liquid phase (21 h after induction, corresponding 0.5 $g{\cdot}L^{-1}$ of acetone). After 5.3 $g{\cdot}L^{-1}$ of isopropanol produced in the liquid phase, the quantity of isopropanol evaporated was more important than the quantity of isopropanol produced in the liquid phase, so isopropanol concentration in the liquid phase decreased. However, decimal reduction rate calculated by plate count kept on increasing until reaching 2.6 were reached at 1.7 $g{\cdot}L^{-1}$ of isopropanol in the

medium, because acetone concentration had kept on increasing at 0.8 $g \cdot L^{-1}$ on this time period. After that point, decimal reduction rate by plate count decreased slightly down to 1.5, as acetone concentration in the medium decreased as well, because of enhanced evaporation at the expense of production. By flow cytometry, decimal reduction rate was low all along the culture. When calculated by flow cytometry, decimal reduction rate was low, even if a slight heterogeneity was measured around 2 $g \cdot L^{-1}$, at the end of culture.

For Re2133/pCB1, decimal reduction rate was low all along culture, for both counting methods (**Figure 4c**).

Decimal reduction rate for Re2133/pJLCB2 was significantly higher, both by plate count and flow cytometry measurements, compared to Re133/pCB1 and pEG7c. So, the production of both eGFP and isopropanol by the same strain decreased plasmid stability expression, monitored by plate count and flow cytometry. This negative impact was more important on plate count.

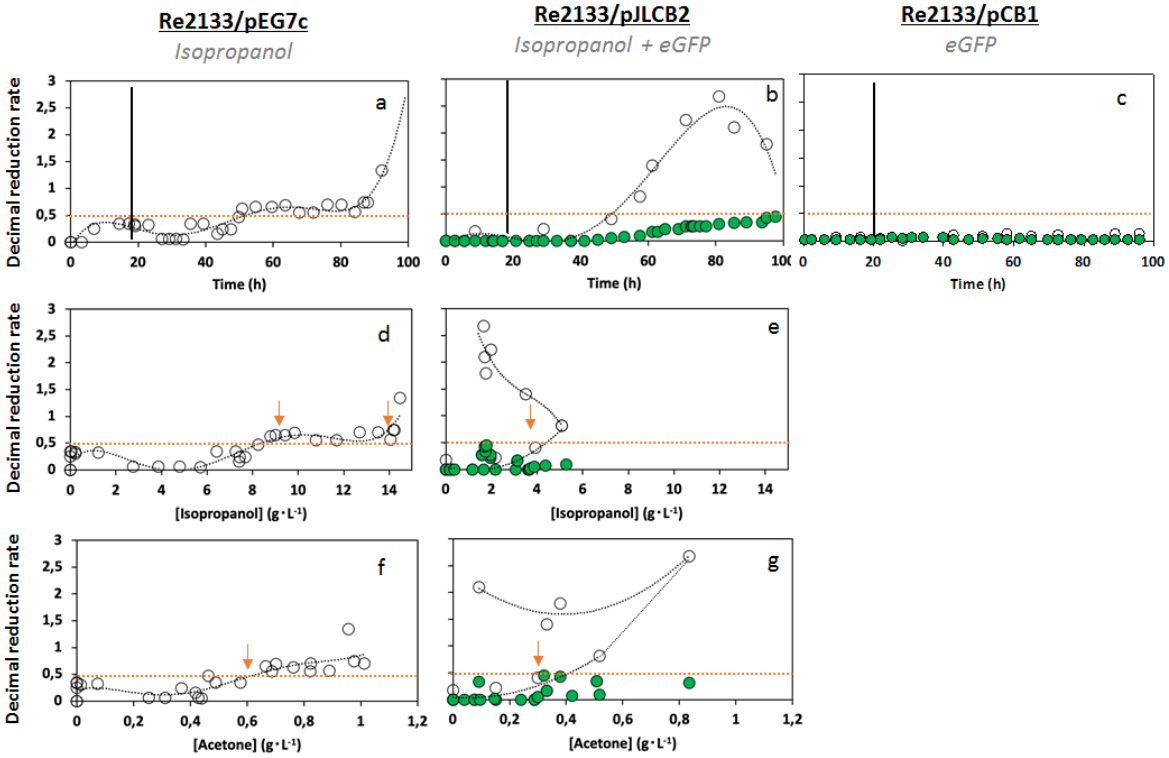

Figure 4 : Decimal reduction rate for the strains Re2133/pEG7c, pJLCB2 and pCB1 through time isopropanol and acetone concentrations, by plate count (○) and flow cytometry (●). The vertical black line represented the time limit between the batch phase and the fed-batch phase. Orange horizontal dotted lines represented the limit of a low decimal reduction level and orange arrows marked when this limit was crossed

3.4.4 Cell permeability and eGFP leakage

To study the impact of isopropanol production and / or eGFP expression on cell physiology, permeability and extracellular fluorescence were studied during culture.

During batch phase, all strains presented cell permeabilization percentage close to zero (**Figure 5**). For the strain Re2133/pEG7c, permeabilization percentage remained low until 55 h of culture, corresponding to 9 $g \cdot L^{-1}$ of isopropanol and 0.6 $g \cdot L^{-1}$ acetone (**Figures 5a & 5d**). Then, it increased regularly until reaching 25 % at the end of culture.

For Re2133/pJLCB2, after the beginning of the fed-batch phase, cell permeability increased regularly through time, as soon as isopropanol and acetone started being produced, until 5 % (**Figures 5b & 5e**). As explained above, isopropanol concentration decreased after reaching 5.3 $g \cdot L^{-1}$. Nevertheless, cell permeabilization kept on increasing because acetone concentration was still increasing in the medium. Cell permeabilization reached 20 % at the end of culture. For the same concentration of isopropanol produced, cell permeabilization percentage was significantly lower for Re2133/pEG7c than for pJLCB2. So, the strain Re2133/pJLCB2 appears clearly less tolerant to acetone and / or isopropanol than Re2133/pEG7c.

For the strain Re2133/pCB1, a slight transient peak at 8 % was measured just after the beginning of the fed-batch phase (**Figure 5c**). This was due to a nitrogen depletion phase that was longer (3h) for this strain compared to Re2133/pEG7c and pJLCB2 (less than 1h), due to technical problems at the initiation of nitrogen feeding. Then, cell permeabilization percentage was low, under 5 %, all along fermentation. Therefore, cell permeabilization percentage was higher for Re2133/pJLCB2 than for pCB1 all along culture.

Relative extracellular fluorescence intensity in the supernatant was largely higher for Re2133/pJLCB2 than for Re2133/pCB1 all along the culture (**Figures 5b, 5e & 5d**). This was consistent with the fact that the permeabilization percentage was significantly higher for Re2133/pJLCB2 all along the culture and that the fluorescence intensity of single-cells was higher in Re2133/pJLCB2 than in Re2133/pCB1.

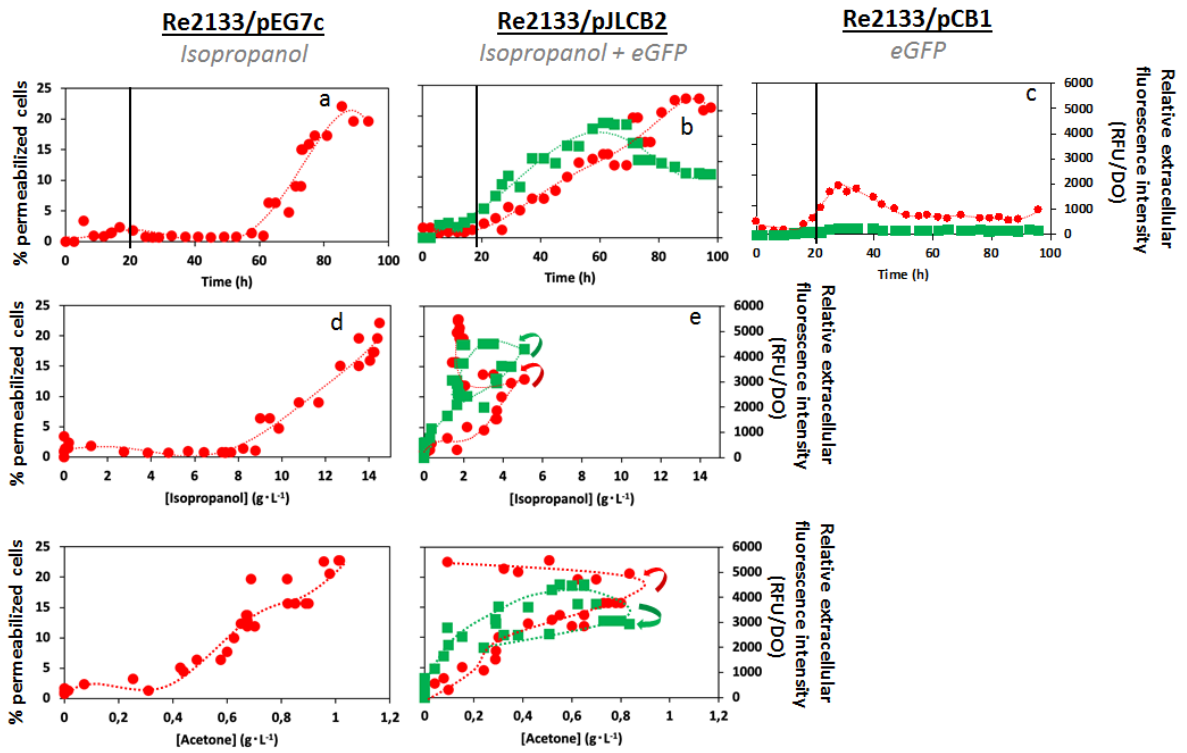

Figure 5: Cell permeabilization percentage (●) for the strains Re2133/pEG7c, pJLCB2 and pCB1 vs time, isopropanol and acetone concentrations and Relative extracellular fluorescence intensity (■) for Re2133/pJLCB2 and pCB1. The horizontal dotted black line represented the time limit between the batch phase and the fed-batch phase

Table 2 : Fed-batch cultivation parameters of the strains Re2133/pEG7c, pJLCB2 and pCB1. N/A; not applicable

	μ_{max}	μ_{prod}	$[isopropanol]_{max}$	Yield biomass	Yield CO_2	Yield isopropanol	Yield acetone	$[Isopropanol]_{Critical}$
	h^{-1}	h^{-1}	$g \cdot L^{-1}$	$g \cdot g^{-1}$	$g \cdot g^{-1}$	$g \cdot g^{-1}$	$g \cdot g^{-1}$	$g \cdot L^{-1}$
pEG7c	0.23 ± 0.02	0.03 ± 0.01	15.1	0.44 ± 0.02 (batch) 0.09 ± 0.01 (19-35h) 0.17± 0.01 (47-92h)	0.54 ± 0.03 (batch) 0.65 ± 0.01 (19-35h) 0.90± 0.01 (47-92h)	**0.27 ± 0.01** (19-35h) 0.098 ± 0.003 (47-92h)	**0.024 ± 0.001** (19-35h) 0.007 ± 0.003 (47-92h)	15.1
pJLCB2	0.21 ± 0.03	0.04 ± 0.01	5.3	0.48 ± 0.04 (batch) 0.19 ± 0.01 (14-45h) 0.30± 0.001 (48-77h)	0.66 ± 0.04 (batch) 0.62 ± 0.01 (14-45h) 0.86± 0.01 (48-77h)	**0.11 ± 0.01** (14-45h) 0.004± 0.001 (48-77h)	**0.011 ± 0.001** (14-45h) 0.006± 0.001 (48-77h)	5.3
pCB1	0.24 ± 0.01	0.04 ± 0.01	N/A	0.32 ± 0.01	0.89 ± 0.02	N/A	N/A	N/A

3.5 Discussion

Plasmid expression level heterogeneity might have a major negative impact on recombinant molecule production by decreasing production rates and yields (Delvigne *et al.* 2014, Binder *et al.* 2017, Gonzalez-Cabaleiro *et al.* 2017). A plasmid-encoded biosensor was used to quantify variations in plasmid expression levels, thereby identifying factors involved in plasmid instability mechanisms. This way, a better understanding of these phenomena might lead to bioprocess optimization. This study was led in the particular case of isopropanol production from fructose by *Cupriavidus necator*. Isopropanol production pathway and eGFP as protein reporter were both plasmid-encoded. The aim of this work was to study the impact of isopropanol and eGFP productions on both plasmid expression levels and isopropanol production.

In our study, the maximum titer reached was significantly higher for the reference strain Re2133/pEG7c (15.1 $g \cdot L^{-1}$) compared to Re2133/pJLCB2 (*eGFP*, 5.3 $g \cdot L^{-1}$, - 65 %). Plus, a higher maximum isopropanol production yield was measured for Re2133/pEG7c (+ 59 %) compared to Re2133/pJLCB2. So, the maximum production yield depended on whether eGFP was expressed or not. With the strain Re2133/pEG7c, we reached both higher maximum titer (+ 78 %) and yield (+ 70%) in comparison with results obtained by Marc et *al.* (2017) (*i.e.* 8.5 $g \cdot L^{-1}$ and 0.159 ± 0.005 $g_{IPA} \cdot g_S^{-1}$). In our study, 82 % of the theoretical isopropanol production yield was reached (0.33 $g \cdot g^{-1}$ calculated by metabolic modelling) which was the closest recorded yet.

When isopropanol concentration increased for Re2133/pEG7c and pJLCB2, membrane permeability increased, compared to Re2133/pCB1. Indeed, it was shown that cell permeability and membrane fluidity increased in response to higher alcohol concentration in producing strains (Jia *et al.* 2010). The strain Re2133/pEG7c presented a better tolerance toward isopropanol and acetone productions in terms of cell permeability (3% permeabilized cells) compared to Re2133/pJLCB2 (8 %). This might be explained by the fact that Re2133/pJLCB2 also produced eGFP. Depending on culture conditions, GFP has been shown to increase cell permeability (Ansari *et al.* 2016). So, in optimal growth conditions, cell permeability in fluorescent cells might remain low. However, under more challenging culture conditions, like isopropanol production or fluctuating environments (*i.e.* fructose pulses, see "Results and discussion", Chapter 2, Subchapter 3), eGFP might contribute to increase cell permeability.

As cell permeability increased during isopropanol production, eGFP molecules leaked outside of cells during fed-batch. Indeed, relative extracellular fluorescence intensity increased regularly until critical isopropanol concentration (5.3 $g \cdot L^{-1}$) was reached in the medium for Re2133/pJLCB2. Both isopropanol and acetone presented a negative impact on cell permeability. Indeed, acetone might have a more important impact on cell permeability as it is a more hydrophobic solvent, which might solubilize

phospholipidic membrane of cells (Nicolaou *et al.* 2010, Dunlop 2011, Mukhopadhyay *et al.* 2015). The relative extracellular intensity for the strain Re2133/pCB1 was non-significant compared to Re2133/pJLCB2. This might be due to two phenomena: intracellular fluorescence intensity of single-cells was shown to be higher for Re213/pJLCB2 because of strain construction and cell permeability was higher for this strain. These statements could be supported by fluorescence intensity distribution decrease on the same time period. So, plasmid expression levels widened and decreased all along isopropanol production because of recombinant proteins leaking outside of cells.

For Re2133/pJLCB2, decimal reduction rate (*i.e.* plasmid expression loss) started increasing by both counting methods when a concentration of 3.6 $g \cdot L^{-1}$ isopropanol was reached in the bioreactor, which was close to the critical isopropanol concentration ($q_{IPA,\,max}$ = 0 $g_{IPA} \cdot g_X \cdot h^{-1}$; at 5.3 $g \cdot L^{-1}$). When isopropanol concentration decreased, decimal reduction rate still increased in response to increasing acetone concentrations. Then, decimal reduction rate drastically increased up to 2.6 by plate count and up to 0.5 by flow cytometry. So, for Re2133/pJLCB2, it could be observed that both isopropanol and acetone had a negative impact on plasmid expression stability. A similar behavior could be observed for Re2133/pEG7c, but to a lesser extent. The additional increase in decimal reduction rate by plate count (compared to flow cytometry) was due to cell cultivability decrease because of increased isopropanol concentrations (Chakravarty *et al.* 2018) for Re2133/pEG7c and pJLCB2. Indeed, decimal reduction rate (by both counting methods) increased with cell permeability, when isopropanol and acetone were produced. When no isopropanol / acetone was produced, decimal reduction rate was low all along culture for Re2133/pCB1. On one hand, decimal reduction rate by plate count reflects both cell cultivability and plasmid expression stability, which were both lower for Re2133/pJLCB2 compared to pEG7c and pCB1. On the other, decimal reduction rate by flow cytometry only reflects plasmid expression stability, which was lower for Re2133/pJLCB2 compared to pCB1. So, the decrease in decimal reduction rate measured by plate count at the end of culture with Re2133/pJLCB2 might be due to the decrease in isopropanol concentration (*i.e.* evaporation > production) in the medium and so, to a lesser medium toxicity. Therefore, new-forming cells were subjected to lower isopropanol concentrations and presented a better cultivability, leading to a smaller gap between both counting methods. This might explain why decimal reduction rate by flow cytometry kept on increasing on the same time period, as it was not impacted by cell cultivability. So, isopropanol production had a negative impact on both cell cultivability and plasmid expression stability, as already shown by plasmid expression levels above (*i.e.* fluorescence intensity distribution). In addition, the production of both isopropanol and eGFP by the strain Re2133/pJLCB2 caused an increased in the loss of plasmid expression and cell cultivability compared to both pCB1 and pEG7c. Finally, a decrease in plasmid expression stability appeared to cause a decrease in specific isopropanol production rate. As plasmid

expression was destabilized sooner for Re2133/pJLCB2, it was consistent with the lower isopropanol producing performances of the strain.

Since plasmid expression stability was lower for the strain Re2133/pJLCB2, a higher proportion of the carbon flow was dedicated to CO_2 and biomass production (50 and 28 % respectively at $q_{IPA,\ max}$), compared to the strain Re2133/pEG7c (44 and 11 %, respectively at $q_{IPA,\ max}$). Consequently, carbon flux toward acetone (2% at $q_{IPA,\ max}$) and isopropanol (20% at $q_{IPA,\ max}$) was greatly diminished for this strain (4 and 44% respectively, for pEG7c at $q_{IPA,\ max}$). To overcome this phenomenon, it might be beneficial to decrease the production growth rate in order to favor isopropanol production.

Now, considering the carbon repartition between isopropanol and acetone, acetone was accumulated in the medium in higher proportions for the strain Re2133/pJLCB2 compared to pEG7c, at the expense of isopropanol biosynthesis. This less efficient re-direction of carbon toward isopropanol might be caused by a lower specific activity of ADH (*i.e.* alcohol dehydrogenase) compared to ADC (*i.e.* acetoacetate decarboxylase), leading to a bottleneck in acetone hydrogenation and so, acetone accumulation. The apparition of such a bottleneck might either be due to lower amounts of ADH compared to ADC in cells, or to a lower availability of NADPH, H^+ for the hydrogenation of acetone toward isopropanol (Grousseau *et al.* 2014). Plus, as the eGFP molecules were shown to be excreted during isopropanol production in response to higher cell permeabilization, one might imagine that it could be the case of all intracellular proteins, including enzymes of the isopropanol production pathway.

Marc and coworkers (2017) showed that an improvement of specific activity of heterologous enzymes from the isopropanol production pathway (*i.e.* ADC, ADH) contributed to enhance cell tolerance toward isopropanol and led to better carbon redirection toward isopropanol. Indeed, with increasing isopropanol concentrations, intracellular proteins are likely to be partially or completely denatured (Ingram *et al.* 1984). This might disrupt activity of enzymes from the isopropanol production pathway as well as transcription and translation. As we showed that fluorescence expression in Re2133/pJLCB2 increased permeability during isopropanol production, it might be profitable to add a chaperon protein expression system (*ex. GroELS*) on the plasmid in order to stabilize protein expression. Because eGFP was also produced in Re2133/pJLCB2 it might have disrupted enzymes expression by competing ribosomes, RNAt or amino acid availability compared to non-fluorescent strains (Ceroni *et al.* 2018).

However, at the isopropanol concentrations considered (maximum 15.1 $g \cdot L^{-1}$), eGFP fluorescence intensity should not be significantly disrupted, as a 235 $g \cdot L^{-1}$ (30 % v/v) isopropanol concentration has already successfully applied to purify eGFP by chromatography, without disruption of the fluorescence signal (McRae *et al.* 2005). So, a change in fluorescence intensity distributions was only due to the

specific fluorescence intensity of a certain amount of eGFP molecules present in cells, and not to a change in the fluorescence signal of eGFP molecules because of denaturation by isopropanol.

In conclusion, a link could be established between variations in fluorescence intensity distribution and isopropanol / acetone production rates using eGFP biosensor to study plasmid expression levels. Using eGFP allowed the obtention of complementary information to the more traditional plate count method, which was impacted by cell cultivability. However, the plasmid construction used in this work presented several limits especially in terms of isopropanol production. Indeed, coupled isopropanol and eGFP productions in Re2133/pJLCB2 led to enhance cell permeability when isopropanol and acetone concentrations increased, compared to pEG7c. Plasmid stability was disrupted and led to a decrease in main metabolite production rates, because carbon flux re-direction toward isopropanol synthesis was less efficient than in the reference strain. So, even if a complete understanding of the mechanisms leading to plasmid expression heterogeneity during isopropanol production has not been reached yet, this work allowed studying the conflicting interactions between two different processes (*i.e.* isopropanol and eGFP production).

3.6 Results synthesis

➔ During batch, maximum growth rates were close, with 0.23 ± 0.02 h^{-1} for Re2133/pEG7c (isopropanol operon), 0.21 ± 0.03 h^{-1} for Re2133/pJLCB2 (isopropanol operon + *egfp* cassette) and 0.24 ± 0.01 h^{-1} for Re2133/pCB1 (*egfp* cassette).

➔ Maximum isopropanol production yield of 0.27 ± 0.01 $g_{IPA}{\cdot}g_S^{-1}$ for Re2133/pEG7c and 0.11 ± 0.02 $g_{IPA}{\cdot}g_S^{-1}$ for Re2133/pJLCB2. Maximum isopropanol production rate was equal to 0.09 $g_{IPA}{\cdot}g_S^{-1}{\cdot}h^{-1}$ for Re2133/pEG7c, and 0.04 $g_{IPA}{\cdot}g_S^{-1}{\cdot}h^{-1}$ for pJLCB2. Maximum acetone production yield reached 0.024 ± 0.001 $g_{Ac}{\cdot}g_S^{-1}$ for Re2133/pEG7c and 0.011 ± 0.001 $g_{Ac}{\cdot}g_S^{-1}$ for pJLCB2. The maximal acetone production rates were equal to 0.009 $g_{Ac}{\cdot}g_S^{-1}{\cdot}h^{-1}$ for Re2133/pEG7c and 0.003 $g_{Ac}{\cdot}g_S^{-1}{\cdot}h^{-1}$ for pJLCB2. The critical isopropanol concentration for isopropanol production was 15.1 $g{\cdot}L^{-1}$ for Re2133/pEG7c and 5.3 $g{\cdot}L^{-1}$ for pJLCB2.

➔ No organic acid production during for both strains. Only a slight peak of pyruvic acid production was observed for the strain Re2133/pEG7c after induction by arabinose, but was re-consumed shortly afterwards. None was detected for the strains Re2133/pCB1 or pJLCB2.

➔ At maximum specific isopropanol production rates, the percentage of the carbon flux dedicated to isopropanol reached 41 % for Re2133/pEG7c and 20 % for pJLCB2. This was due to a higher carbon flow toward biomass synthesis (+ 17 %), and carbon dioxide (+ 6 %) to a lesser extent, for the strain Re2133/pJLCB2. Plus, in Re2133/pJLCB2, acetone was accumulated in higher amount at the expense of isopropanol compared to Re2133/pEG7c.

➔ For the strain Re2133/pJLCB2, median quickly dropped after arabinose induction, distribution range increased drastically and could not be considered Gaussian anymore. For the specific eGFP-positive cell population, fluorescence intensity distribution was Gaussian and reproducible all along culture for Re2133/pCB1. For Re2133/pJLCB2, distribution range increased significantly after arabinose induction, and a population of “less “fluorescent cells increased. For Re2133/pCB1, distribution remained close to Gaussian throughout culture.

➔ For Re2133/pEG7c, decimal reduction rate (by plate count) increased up to 1.6 at the end of culture. For Re2133/pJLCB2, decimal reduction rate measured by plate count was significantly higher than the one measured by flow cytometry. Decimal reduction rate (by plate count) started increasing when 3.6 $g{\cdot}L^{-1}$ of isopropanol were produced in the liquid phase. Even when isopropanol concentrations in the liquid phase decreased, decimal reduction rate kept on increasing, because acetone concentration kept on increasing and a maximum decimal reduction rate of 2.6 was reached

at 80 h of culture, corresponding to 1.7 $g \cdot L^{-1}$ of isopropanol in the medium. For Re2133/pCB1, decimal reduction rate was low all along culture, for both counting methods. Thus, coupled eGFP and isopropanol caused a decrease in plasmid stability expression, both by plate count and flow cytometry. This negative impact was more important on plate count due to cultivability loss.

➔ For the strain Re2133/pEG7c, permeabilization percentage increased until reaching 25 % at the end of culture. For Re2133/pJLCB2, after the beginning of the fed-batch phase, cell permeability increased regularly through time, as soon as isopropanol and acetone started being produced. Cell permeabilization kept on increasing, even when isopropanol concentration decreased (because of evaporation when production stopped), and reached 20 % at the end of culture. So, the strain Re2133/pJLCB2 appears clearly less tolerant to acetone and / or isopropanol than Re2133/pEG7c. For the strain Re2133/pCB1, cell permeabilization percentage was low, under 5 %, all along fermentation. As a result, relative extracellular fluorescence intensity in the supernatant was largely higher for Re2133/pJLCB2 than for Re2133/pCB1 all along the culture.

Part 4: General discussion, conclusions and perspectives

Part 4: General discussion, conclusions and perspectives

L'enjeu principal lors du développement d'un bioprocédé est sa viabilité économique, qui passe par l'obtention de rendements de production élevés. Cependant, la robustesse d'un procédé de production d'une molécule d'intérêt, peut être menacé par l'apparition de sous-populations, qui pourraient impacter négativement les rendements et taux de production obtenus. Une meilleure compréhension des conditions favorisant l'apparition de ces sous-populations pourrait permettre de sécuriser la viabilité économique du bioprocédé.

Ce travail se concentre sur l'étude de l'influence des conditions opératoires sur l'apparition de sous-populations au sein d'une culture monoclonale en bioréacteur. Ces différentes conditions opératoires peuvent être dues à des différences de construction de souche, d'homogénéité de l'environnement de culture, et de composition du milieu de culture. Le but de ce travail de thèse est d'identifier les sous-populations provenant d'une culture pure en bioréacteur, de comprendre leurs effecteurs et de contrôler leur distribution, de par le modèle choisi : la stabilité de l'expression plasmidique lors de la production d'isopropanol par une souche recombinante de *Cupriavidus necator*. Un intérêt croissant pour la bactérie *C. necator* a été observé depuis quelques années, en raison de son métabolisme versatile (Johnson *et al.* 1971, Friedrich *et al.* 1979, Budde *et al.* 2011, Grunwald *et al.* 2015, Marc *et al.* 2017), qui en fait une bio-plateforme intéressante pour la production de molécules recombinantes (Ewering *et al.* 2006, Hoefel *et al.* 2010, Muller *et al.* 2013, Grousseau *et al.* 2014, Crepin *et al.* 2016, Marc *et al.* 2017, Sydow *et al.* 2017, Black *et al.* 2018, Krieg *et al.* 2018, Garrigues *et al.* 2020). L'étude de la littérature a révélé que les hétérogénéités de populations qui apparaissent dans les bioprocédés, peuvent être liés à une instabilité d'expression du plasmide recombinant (Brehm-Stecher *et al.* 2004, De Gelder *et al.* 2007). Cependant, les comportements des populations monoclonales sont souvent étudiés par des méthodologies à l'échelle des populations totales et basées sur des valeurs moyennes (Carlquist *et al.* 2012, Delvigne *et al.* 2014, Gonzalez-Cabaleiro *et al.* 2017). Une méthode de suivi de l'expression plasmidique à l'échelle de la cellule unique en cours de fermentation pourrait être proposée pour étudier le lien de causalité entre les conditions opératoires et le mécanisme de réponse des sous-populations.

La stratégie de recherche choisie, les méthodes analytiques développées, et les résultats expérimentaux obtenus au cours de ce travail permettent de construire des réponses aux questions scientifiques suivantes :

- Comment identifier et discriminer, avec fiabilité, différentes sous-populations provenant d'une culture pure en bioréacteur, dynamiquement, en cours de fermentation ?
- Quels sont les effecteurs de l'apparition d'hétérogénéités dans des cultures monoclonales en bioréacteur ? Comment évolue le comportement des sous-populations en réponse à ces effecteurs ?
- Peut-on contrôler la distribution de sous-populations dans un bioprocédé en cours de fermentation ? A quel niveau ce contrôle peut-il être opéré, avec quel niveau d'efficacité ?

Développement d'une méthode de suivi de sous-population en cours de fermentation chez C. necator :

La première étape de ce travail consistait à développer une méthodologie permettant le suivi dynamique de la distribution de niveau d'expression plasmidique en cours de fermentation. D'après les connaissances issues de la littérature, l'utilisation d'un biocapteur eGFP comme rapporteur de l'expression plasmidique, couplé à la cytométrie en flux, a été privilégiée. La charge métabolique imposée par un gène recombinant sur les cellules hôtes peut impacter la stabilité de l'expression plasmidique. Donc, lors de la construction de ce biocapteur, il nous a semblé essentiel de confronter plusieurs promoteurs constitutifs de forces différentes (P_{lac}, P_{tac}, P_{n25} et P_{j5}) afin d'assurer une faible charge métabolique sur l'hôte (*i.e*. taux de croissance, perméabilité membranaire) et une intensité de fluorescence suffisante pour permettre une détection des cellules uniques par cytométrie en flux.

Nous avons montré que plus la force du promoteur augmente (P_{lac}, P_{tac}, P_{n25} et P_{j5} ; faible à fort), plus l'intensité de fluorescence des cellules uniques est élevée. Dans l'article Gruber et *al.* (2014), une étude à l'échelle de la population avait été faite, et le même classement avait pu être effectué. Cependant, l'ampleur de l'augmentation de l'intensité de fluorescence avec des promoteurs de force croissante était plus importante sur la population totale que ce que nous avons obtenu sur les cellules uniques. De plus, les intensités de fluorescence entre les deux promoteurs les plus forts (P_{n25} et P_{j5}) sont du même ordre au niveau de la cellule unique. Dans une étude à l'échelle de la population globale, l'intensité de fluorescence moyenne mesurée n'est pas entièrement due aux molécules d'eGFP intracellulaires. Cela peut être expliqué par le fait que le niveau de perméabilité membranaire augmente d'autant plus que le niveau de force du promoteur est élevé. Cette augmentation de la perméabilité membranaire entraîne une augmentation de l'intensité de fluorescence extracellulaire, qui correspond à la fuite d'eGFP des cellules perméabilisées. Le promoteur fort P_{j5} permet bien une

induction plus importante de la production d'eGFP. Néanmoins, dans ce cas, la concentration d'eGFP intracellulaire atteint un seuil critique au-delà duquel les molécules d'eGFP excédentaires sont excrétées dans le milieu.

L'instabilité de l'expression plasmidique a été évaluée par deux méthodes différentes mais complémentaires : la cytométrie en flux et le comptage sur boîte. En culture batch, il a été montré que le plasmide faible P_{lac} permettait un maintien de la stabilité de l'expression plasmidique par les deux méthodes tout au long de la culture. Néanmoins, avec le plasmide P_{j5}, les concentrations de cellules portant le plasmide par comptage sur boîte était beaucoup plus faible que par cytométrie en flux. Cette diminution de cultivabilité était également suggérée par une perméabilité membranaire beaucoup plus élevée provoquant probablement la fuite de composés intracellulaires. De plus, nous avons observé que lorsque la force du promoteur constitutif augmente, le taux de croissance diminue drastiquement par rapport à la souche de référence qui ne porte pas le plasmide.

Donc, l'impact négatif considérable du promoteur P_{j5} sur la croissance et la physiologie cellulaire est dû à une production accrue de molécules recombinantes et donc à une charge métabolique plasmidique plus importante imposé aux cellules hôtes Dans ces conditions, les mécanismes de croissance cellulaire et de maintien / expression du plasmide sont en concurrence pour les mêmes ressources moléculaires (*e.g.* ATP, ARNt, acides aminés).

Pour vérifier sa fiabilité dans des conditions de perte plasmidique, le système biocapteur *P_{lac}-eGFP* a été confronté à la méthodologie de « *plasmid-curing* » par la température (37 °C), pour induire l'apparition d'hétérogénéité d'expression plasmidique. Après culture en erlenmeyer et repiquages successifs pour atteindre 19 générations cellulaires, trois populations de niveau d'expressions différents ont été détectées : P_0 (non fluorescent), P_1 (fluorescence moyenne) et P_2 (fluorescence élevée). Des cellules uniques issues de ces trois populations ont été triées par FACS puis repiquées pour étudier leur comportement. La population avec le niveau d'expression le plus élevé (P_2) a montré un taux de croissance faible alors que la population non fluorescente (P_0) s'avère non cultivable dans les conditions étudiées. Les cellules de la population de fluorescence moyenne (P_1) ont un taux de croissance plus élevées que P_2 et ont été partiellement capables de fluorescer à une intensité de valeur maximale (P_2) une fois cultivées en conditions optimales. Les différences de niveau de fluorescence entre les populations P_2 et P_1 était donc sûrement dues à une différence de niveau d'expression plasmidique à 37°C.

L'évaluation des promoteurs se fait généralement sur la base de mesures de l'absorbance totale de la fluorescence à l'aide d'un spectrophotomètre et / ou d'un lecteur multiplaque. Ce travail démontre

qu'une analyse au niveau de la cellule unique apporte un nouvel éclairage sur l'évaluation des promoteurs. Notre méthode de suivi de l'instabilité de l'expression plasmidique, basée sur une détection par cytométrie en flux de l'expression d'un biocapteur eGFP, a pu être utilisé pour la suite de notre étude.

Étude des effecteurs de l'apparition d'hétérogénéités de niveau d'expression plasmidique en cours de fermentation chez C. necator*, avec et sans production d'isopropanol*

- *Impact de l'environnement de culture*

Nous avons évalué la robustesse des souches en réponse à deux stratégies d'alimentation en sucre (*i.e.* pulse, continu), afin d'étudier l'impact d'un environnement fluctuant sur l'instabilité de l'expression plasmidique dans notre souche de référence Re2133/pCB1 (*i.e.* pBBad, P_{lac}-eGFP, Kan^R) Nous avons choisi ces deux méthodes car la stratégie de pulse a déjà été employée pour la production d'isopropanol (Marc *et al.* 2017) et la stratégie d'alimentation continue pour la production d'alka(e)ne (Crepin *et al.* 2016); toutes deux en mode fed-batch.

La stratégie d'apport par pulse conduit à des environnements fluctuants, ce qui peut réduire les performances des procédés et la robustesse des souches (Lara *et al.* 2006, Hewitt *et al.* 2007, Limberg *et al.* 2017). Les rendements de production de biomasse étaient plus élevés avec un apport continue en fructose. En effet, des acides organiques (*e.g.* citrate, acéto-acétate, acétate, succinate) étaient produits lors de l'ajout par pulse, détournant jusqu'à 15 % du flux de carbone. L'accumulation d'acides organiques était concomitante à une augmentation brutale de la concentration de fructose, qui déclenche un métabolisme d'overflow chez la souche *C. necator* Re2133, délétée pour la production de PHB.

La perméabilité membranaire était plus élevée durant les pulses ce qui s'accompagne d'intensités de fluorescence extracellulaire plus élevées, montrant une fuite de l'eGFP plus importante vers le milieu. Il a été soupçonné que sa cause principale pourrait résider dans une perturbation de la pression osmotique, liée à des concentrations en fructose importantes brusquement, entrainant une diminution de l'activité de l'eau.

La stabilité de l'expression plasmidique (*i.e.* comptage sur boîte, cytométrie en flux) est assurée pour les deux stratégies d'alimentation durant la phase batch et le début du fed-batch, même si quelques hétérogénéités ont tout de même été observées après les pulses. En revanche, la stabilité des niveaux

de l'expression plasmidique diminue ponctuellement après les pulses, ou seulement en fin de culture lors de l'ajout continu, en raison de l'augmentation de la perméabilité et de l'excrétion d'eGFP.

Ainsi, en mode fed-batch limité en azote, une alimentation en sucre continue a permis une meilleure utilisation du carbone pour la synthèse de biomasse (en évitant l'excrétion d'acides organiques), une plus faible hétérogénéité de l'expression plasmidique et une perméabilisation cellulaire plus faible.

- *Impact de la production d'isopropanol*

Dans un premier temps, l'impact de la production d'isopropanol sur la stabilité de l'expression plasmidique a été évalué par comptage sur boîte sur des souches non fluorescentes. La souche exprimant le système PSK *hok/sok* (Re2133/pEG20) a été comparée à une souche de référence (Re2133/pEG7c) et à une souche exprimant les protéines chaperones *GroESL* (Re1122/pEG23), sur la base de leurs capacités de production d'isopropanol. Le système PSK repose sur l'expression d'une antitoxine (non stable) et d'une toxine (stable) par les cellules portant le plasmide, permettant ainsi d'éliminer les cellules ayant perdu celui-ci. Cette méthode permet d'apporter une pression de sélection sur les cellules portant le plasmide sans pour autant avoir recours à un antibiotique. Le système *GroESL* permet quant à lui de sécuriser et d'optimiser le repliement des protéines et même de réparer des séquences peptiques endommagées.

La souche de référence Re2133/pEG7c présentait les meilleures performances en termes de concentration maximale (15.1 $g \cdot L^{-1}$), rendement (0.27 ± 0.01 $g_{IPA} \cdot g_S^{-1}$) et vitesse spécifique de production en isopropanol (0.09 $g_{IPA} \cdot g_X^{-1} \cdot h^{-1}$). Les deux souches recombinantes montrent une amélioration de leur robustesse sur des phénomènes précis. La surexpression de *GroESL* a permis d'améliorer la tolérance des cellules à l'isopropanol (*i.e.* perméabilisation, croissance pendant production) et l'expression du système PSK *hok/sok* a permis de diminuer la production d'acétone. Les deux constructions ont permis de rediriger le flux de carbone vers la production d'isopropanol. Néanmoins, certains inconvénients ont limité leurs performances. La souche Re2133/pEG23 (*GroESL*) présentait une mauvaise stabilité plasmidique pendant la phase de production, et la souche Re2133/pEG20 (PSK *hok/sok)* avait une tolérance plus faible à l'isopropanol (*i.e.* perméabilité élevée).

Ces résultats ont été comparé à ceux obtenus par Marc et *al.* (2017), en conditions d'ajout de fructose par pulse et de kanamycine, pour les souches RE2133/pEG7c et pEG23. Les conditions opératoires appliquées dans notre étude, avec ajout continu de fructose et sans antibiotique, ont permis d'obtenir des titres en isopropanol plus élevés (+ 78 % pour pEG7c, + 36 % pour pEG23). En effet, nous avions montré (Boy et *al*., not published: "Results and discussion" - Chapter 2 - Subchapter 2) que l'ajout de

kanamycine dans le milieu dans les mêmes conditions de cultures que Marc et *al.* (2017), entraînait une augmentation de la perméabilisation cellulaire, même chez les cellules portant le plasmide, résistantes à la kanamycine. Dans le même sous-chapitre (Boy et *al*., not published: "Results and discussion" - Chapter 2 - Subchapter 2), nous avons montré qu'une alimentation continue en fructose à une concentration fixée (20 $g \cdot L^{-1}$) permettait de maintenir, pendant la phase fed-batch limitée en azote, un niveau de perméabilité cellulaire plus bas, que durant les ajouts par pulse de fructose (50 $g \cdot L^{-1}$). Donc, ces conditions opératoires ont permis de maintenir une perméabilité membranaire plus faible, notamment pour la souche Re2133/pEG7c en conditions de production d'isopropanol. Ainsi, l'alimentation continue en fructose et l'absence d'antibiotique ont contribué à un impact positif sur la tolérance de la souche Re2133/pEG7c à l'isopropanol. En revanche, pour la souche Re2133/pEG23, l'expression des protéines chaperonnes *GroESL* à elles seules semblent avoir un impact positif sur la tolérance à l'isopropanol indépendamment de l'environnement de culture dans les conditions étudiées (*i.e.* avec ou sans antibiotique, avec pulse ou alimentation continue de fructose).

Dans un second temps, l'impact de la production d'isopropanol sur la stabilité de niveau d'expression plasmidique a été évalué par comptage sur boîte et cytométrie en flux sur une souche (Re2133/pJLCB2) portant le système de suivi du niveau de l'expression plasmidique P_{lac}-*eGFP*. Cependant, cette méthode présentait plusieurs limites, notamment en termes de production d'isopropanol. En effet, les productions couplées d'isopropanol et d'eGFP dans la souche Re2133/pJLCB2 ont conduit à une perméabilité membranaire accrue lorsque les concentrations d'isopropanol augmentent, par rapport à la souche de référence Re2133/pEG7c (*e.g.* 15 % à 6 $g \cdot L^{-1}$ pour pJLCB2 et à 12 $g \cdot L^{-1}$ pour pEG7c). Avec l'augmentation de la concentration en isopropanol, les protéines intracellulaires sont susceptibles d'être partiellement ou complètement dénaturées. Cela pourrait perturber l'activité des enzymes de la voie de production de l'isopropanol, des protéines de choc thermique ainsi que celles des enzymes impliquées dans la transcription et la traduction. En revanche, il a été montré dans la littérature qu'aux concentrations en isopropanol étudiées, le signal de fluorescence des molécules d'eGFP ne devrait pas être perturbé.

En raison de cette perméabilité membranaire accrue, des molécules d'eGFP ont été excrétées à l'extérieur des cellules, entraînant une diminution des niveaux d'expression plasmidique dans les cellules (*i.e.* intensité de fluorescence extracellulaire, distribution de niveau d'expression plasmidique). On peut donc imaginer que cela pourrait être le cas de toutes les autres protéines intracellulaires, y compris les enzymes de la voie de production de l'isopropanol. Ainsi, la perturbation de la stabilité d'expression du plasmide a entraîné une diminution des taux de production d'isopropanol.

Dans la souche Re2133/pJLCB2, une accumulation d'acétone au dépend de l'isopropanol a été détectée, comparé à la souche Re2133/pEG7c. Cette ré-orientation moins efficace du flux de carbone vers l'isopropanol pourrait être due à une activité spécifique plus faible de l'ADH (alcool déshydrogénase) par rapport à l'ADC (acétoacétate décarboxylase). Cela ferait de l'hydrogénation de l'acétone l'étape limitante de la voie de biosynthèse de l'isopropanol et causerait une accumulation d'acétone. Les causes pourraient en être soit : des quantités plus faibles d'ADH par rapport à l'ADC dans les cellules, soit une disponibilité moindre de NADPH, H^+ pour l'hydrogénation de l'acétone vers l'isopropanol.

Ainsi, même si une compréhension complète des mécanismes conduisant à l'hétérogénéité de l'expression plasmidique pendant la production d'isopropanol n'a pas encore été atteinte, nous avons pu avoir un aperçu des stratégies de design de stabilité plasmidique qui pourraient permettre d'amplifier la production de molécules recombinantes dans des souches modifiées.

Contrôle des distributions de niveau d'expression plasmidique en cours de fermentation chez C. necator

- *Impact du contrôle du taux de croissance*

Nous avons mené des fermentations en modes batch et chémostat dans des conditions de culture non optimales de perte plasmidique (« plasmid curing ») afin d'évaluer notre capacité à contrôler le niveau de l'expression plasmidique par le taux de croissance, dans une population hétérogène. L'augmentation de la température et l'ajout de rifampicine ont été sélectionnés comme stratégies pour l'induction de l'hétérogénéité de niveau de l'expression plasmidique. La rifampicine a été choisie comme un perturbateur de la transcription plasmidique dans les bactéries, malgré son efficacité mitigée, dans l'espoir d'obtenir un « *plasmid curing »* d'efficacité moyenne, sans inhibition drastique de la croissance. L'hétérogénéité des populations a été étudiée par cytométrie de flux, basée sur la fluorescence de l'eGFP et par comptage sur plaque basé sur la résistance à la kanamycine.

L'hétérogénéité était plus prononcée après une augmentation de la température (30 à 42°C) alors qu'elle est faible après l'ajout de rifampicine (50 $mg \cdot L^{-1}$. Néanmoins, le niveau d'hétérogénéité atteint par augmentation de la température était encore assez faible, ce qui s'explique par une croissance considérablement ralentie après l'induction du « *plasmid curing »*. En effet, une perte de cultivabilité et des niveaux de perméabilisation plus élevés ont été mesurés. Il est donc possible qu'un nombre insuffisant de générations cellulaires ait été synthétisées en raison de l'impact négatif de l'augmentation de la température et de l'ajout de rifampicine sur les mécanismes de réplication cellulaire. Ainsi, une température de 42 °C pourrait avoir été trop stringente pour les cellules. Donc, la

température a donc été fixée à 37 °C dans les expériences suivantes, ce qui a permis d'induire une hétérogénéité de niveau d'expression et de ne pas inhiber radicalement le taux de croissance.

Les repiquages successifs en mode batch à 37 °C se sont avérés la stratégie la plus efficace pour générer les trois sous-populations fluorescentes P_0 (non fluorescent), P_1 (fluorescence moyenne) et P_2 (fluorescence élevée). Il a fallu 30 générations cellulaires, à partir d'une population P_2 à 100 %, pour obtenir une répartition de 60 à 40 % entre P_1 et P_2.

Une culture continue a été mené à 2 taux de dilution différents (0,05 et 0,1 h^{-1}) à 37°C. A un taux de dilution de 0,05 h^{-1}, l'état stationnaire a favorisé l'apparition de la sous-population P_1 (80 %) dans un premier temps, car la population cellulaire dans le bioréacteur a été complètement renouvelée et les cellules P_2 issues des batchs successifs ont été progressivement éliminées. Dans un second temps, une augmentation progressive de la sous-population P_2 a été observée, car les cellules ont été capables de s'adapter à cette augmentation de température après un certain nombre de générations, à ce taux de dilution contrôlé.

A un taux de dilution de 0,1 h^{-1}, l'intensité de fluorescence atteinte à la fin du chémostat était significativement plus élevée que celle atteinte à la fin du chémostat à 0,05 h^{-1}, même si elle était toujours maintenue au seuil P_2. Ainsi, un taux de dilution à 0,1 h^{-1} a entraîné l'augmentation de la sous-population P_2 par rapport à la sous-population P_1. A l'état stationnaire pour un taux de dilution de 0,1 h^{-1}, une population quasi-homogène en P_2 est atteinte. Elle pourrait être le résultat d'une augmentation du nombre de copies de plasmide de la sous-population P_1, dépendante du taux de croissance, pour atteindre le nombre maximal (sous-population P_2) pour cette souche à ce taux de dilution. Les cellules ont réussi à faire face à ce taux de dilution plus élevé sans avoir besoin de diminuer la performance de production de protéines dans des conditions de température supra-optimales, comme c'était également le cas dans des conditions de croissance optimales.

- *Impact du design plasmidique*

L'impact de deux mécanismes de stabilisation des plasmides sur la robustesse de la souche a été étudié : la résistance à la kanamycine (Re2133/pCB1 + kanamycine) et la PSK (Post-Segregational Killing) *hok/sok* (Re2133/pCB3).

Pendant la phase fed-batch, une augmentation du pourcentage de cellules perméabilisées a été observé pour Re2133/pCB1 avec ajout de kanamycine (10 %) et Re2133/pCB3 (15 %), par rapport à la souche de référence Re2133/pCB1 (5 %). Les systèmes de stabilisation ont entraîné une augmentation

de l'excrétion des molécules d'eGFP à l'extérieur des cellules. Les profils de distribution de la fluorescence s'élargissent en fin de culture, lorsque l'intensité relative de la fluorescence extracellulaire et le pourcentage de perméabilisation augmentent, pour les systèmes de stabilisation des plasmides. La souche exprimant le système PSK présentait un avantage en termes de robustesse, sur la base de niveaux d'expression plasmidique plus homogènes en phase fed-batch. Aucun des systèmes de stabilisation des plasmides étudiés n'a eu d'impact sur la cultivabilité des cellules.

En raison de sa stabilité dans des conditions de culture intensive bien contrôlées, le plasmide pCB3 constituerait un outil intéressant pour évaluer les niveaux d'expression plasmidique dans de nouvelles conditions de production de protéines recombinantes ou pour exprimer de nouvelles voies de biosynthèse. Par conséquent, toute modification des niveaux d'expression plasmidique pourrait être attribuée à la production de protéines recombinantes. De manière surprenante, la résistance à la kanamycine n'a pas permis d'améliorer la robustesse de procédé et on contraire a plutôt eu l'effet inverse.

Perspectives

Compte tenu des résultats obtenus lors de cette thèse, les suggestions suivantes peuvent être apportées quant à des futurs travaux :

Dans le cadre de la production d'isopropanol, nous avons observé une instabilité de l'expression plasmidique plus importante lorsque le biocapteur eGFP était codé sur le plasmide recombinant. Cette instabilité plasmidique accrue avait entraîné une diminution de la productivité en isopropanol. Il serait intéressant de développer une stratégie pour contrebalancer cet effet.

- Une première piste serait d'évaluer l'impact du taux de croissance en fed-batch sur la production d'isopropanol pour cette souche. En effet, nous avons observé que la synthèse de biomasse était favorisée au détriment de la production d'isopropanol pendant le fed-batch. Un taux de croissance plus bas (< 0.04 h^{-1}) pourrait permettre de rediriger plus efficacement le flux de carbone vers la production d'isopropanol.
- Une autre possibilité serait d'insérer le gène codant pour l'expression de protéines chaperones *GroESL*, déjà utilisé dans le chapitre 2-3. Ainsi, il serait peut-être possible de limiter l'augmentation de la perméabilité membranaire et la fuite d'eGFP observée lors de la production d'isopropanol, mais aussi de sécuriser le repliement des enzymes de la voie de biosynthèse de l'isopropanol.

Une accumulation d'acétone un peu plus importante a été observée durant la production d'isopropanol, dans nos conditions de cultures, par les souches Re2133/pEG23 (opéron isopropanol, chaperones *GroESL*) et pJLCB2 (opéron isopropanol, P_{lac}-eGFP). Cette accumulation est certainement due au fait que l'hydrogénation de l'acétone en isopropanol est la phase limitante de la voie de biosynthèse d'isopropanol pour ces souches, en raison d'une activité plus faible de l'alcool déshydrogénase (ADH) comparée à l'acétoacétate décarboxylase (ADC).

- Les dosages enzymatiques des activités spécifiques des enzymes de la voie de biosynthèse de l'isopropanol (*i.e.* THL, CTF, ADC, ADH) pour toutes les souches testées en cours de fermentation permettrait de déterminer si cette différence d'activité est en fait due à une quantité plus faible d'ADH comparée à ADC.
- Le NADPH, H^+ est un cofacteur de l'hydrogénation de l'acétone en isopropanol. Par conséquent, un problème dans l'approvisionnement en NADPH, H^+ pourrait causer une limitation de l'activité de l'ADH. Par conséquent, le dosage du NADPH, H^+ dans les cellules dans les différentes souches testées, en cours de fermentation, permettrait de mettre en évidence de potentielles différences de disponibilité de ce co-facteur.

La technique du Flow-FISH, décrite dans la partie bibliographique de cette thèse, serait aussi une approche intéressante pour suivre spécifiquement la stabilité plasmidique au niveau génétique en cours de fermentation. En effet, cette technique permet un marquage par un fluorochrome, à la fois de l'ARN plasmidique et de l'ARN génomique (ARN 16s) afin de discriminer au niveau génétique, les cellules portant le plasmide de celles l'ayant perdu ; permettant ainsi un suivi direct de stabilité plasmidique. Néanmoins, pour l'instant, cette méthodologie présente encore des limitations à son application dans le suivi dynamique de la perte plasmidique chez les bactéries en cours de fermentation. D'une part, sa durée très longue d'analyse d'échantillons est non compatible avec un suivi dynamique en cours de fermentations. D'autre part, cette méthode est appliquée en routine pour les cellules animales, ce qui n'est pas encore le cas avec les cellules bactériennes où elle est encore en voie de développement. Cet écart est notamment dû aux plus faibles quantités d'ARN 16s présent chez les bactéries, qui pourrait limiter la détection des cellules en raison d'un marquage trop faible par le fluorochrome. Le développement d'un protocole de Flow-FISH compatible avec notre cas d'étude permettrait une analyse approfondie, au niveau génétique, des phénomènes d'instabilité du niveau d'expression plasmidique déjà observés durant cette thèse.

Compte tenu de la versatilité du métabolisme de *Cupriavidus necator*, il serait intéressant d'appliquer notre système de suivi de l'instabilité plasmidique à l'échelle de la cellule unique à d'autres configurations de production de molécules recombinantes par ce microorganisme, avec d'autres

substrats. Il pourrait par exemple être imaginé d'étudier l'instabilité d'expression plasmidique par notre biocapteur eGFP en cours de production d'isopropanol à partir de CO_2 (Marc *et al.* 2017, Garrigues *et al.* 2020), ou de production d'alka(e)ne à partir de fructose et CO_2 (Crepin *et al.* 2016), avec *C. necator*.

References

References

References of the introduction about gasoline production and consumption:

[1] https://www.connaissancedesenergies.org/levolution-des-marches-petroliers-dici-2024-vue-par-laie-190311

[2] https://www.iea.org

[3] https://www.wri.org/blog/2020/02/greenhouse-gas-emissions-by-country-sector

[4] https://www.total.fr/mes-deplacements/tout-savoir-sur-les-carburants-total/differents-types-de-biocarburants

---

Acar, M., J. T. Mettetal and A. van Oudenaarden (2008). "Stochastic switching as a survival strategy in fluctuating environments." Nature Genetics **40**(4): 471-475.

Alhumaizi, K., A. Alwan and A. Ajbar (2006). "Competition of plasmid-bearing and plasmid-free organisms in a chemostat: A study of bifurcation phenomena." Mathematical and Computer Modelling **44**(3-4): 342-367.

Andersen, K., R. C. Tait and W. R. King (1981). "Plasmids required for utilization of molecular hydrogen by *Alcaligenes eutrophus*." Archives of Microbiology **129**(5): 384-390.

Anindyajati, A. A. Artarini, C. Riani and D. S. Retnoningrum (2016). "Plasmid Copy Number Determination by Quantitative Polymerase Chain Reaction." Scientia pharmaceutica **84**(1): 89-101.

Ansari, A. M., A. K. Ahmed, A. E. Matsangos, F. Lay, L. J. Born, G. Marti, J. W. Harmon and Z. Sun (2016). "Cellular GFP Toxicity and Immunogenicity: Potential Confounders in in Vivo Cell Tracking Experiments." Stem Cell Rev Rep **12**(5): 553-559.

Aragao, G. (1996). "Production de poly-beta-hydroxyalcanoates par *Alcaligenes eutrophus*: caractérisation cinétique et contribution à l'optimisation de la mise en oeuvre des cultures." Institut National des Sciences Appliquées de Toulouse, Thèse no d'ordre: 403.

Argueta, C., K. Yuksek and M. Summers (2004). "Construction and use of GFP reporter vectors for analysis of cell-type-specific gene expression in *Nostoc punctiforme*." J Microbiol Methods **59**(2): 181-188.

Arrigucci, R., Y. Bushkin, F. Radford, K. Lakehal, P. Vir, R. Pine, D. Martin, J. Sugarman, Y. Zhao, G. S. Yap, A. A. Lardizabal, S. Tyagi and M. L. Gennaro (2017). "FISH-Flow, a protocol for the concurrent detection of mRNA and protein in single cells using fluorescence in situ hybridization and flow cytometry." Nat Protoc **12**(6): 1245-1260.

Atkin-Smith, G. K., S. Paone, D. J. Zanker, M. Duan, T. K. Phan, W. Chen, M. D. Hulett and I. K. H. Poon (2017). "Isolation of cell type-specific apoptotic bodies by fluorescence-activated cell sorting." Scientific Reports **7**(1): 39846.

Avraham, R., N. Haseley, D. Brown, C. Penaranda, H. B. Jijon, J. J. Trombetta, R. Satija, A. K. Shalek, R. J. Xavier, A. Regev and D. T. Hung (2015). "Pathogen Cell-to-Cell Variability Drives Heterogeneity in Host Immune Responses." Cell **162**(6): 1309-1321.

Bahl, M. L., S. J. Sorensen and L. H. Hansen (2004). "Quantification of plasmid loss in *Escherichia coli* cells by use of flow cytometry." Fems Microbiology Letters **232**(1): 45-49.

Bailey, J. E. (1993). Host-vector interactions in *Escherichia coli*. Bioprocess Design and Control. Berlin, Heidelberg, Springer Berlin Heidelberg**:** 29-52.

Barkai, N. and B. Z. Shilo (2007). "Variability and robustness in biomolecular systems." Mol Cell **28**(5): 755-760.

Bazzicalupo, P. and G. P. Tocchini-Valentini (1972). "Curing of an *Escherichia coli* episome by rifampicin (acridine orange-F + -F - -Hfr-lac)." Proceedings of the National Academy of Sciences of the United States of America **69**(2): 298-300.

Bellani, M., C. Nudel and C. Sanchez Rivas (1997). "Site-specific recombination system from Tn1000(γδ) stabilises recombinant plasmids in *Escherichi coli*." Biotechnology Letters **19**(4): 331-334.

Bentley, W. E., N. Mirjalili, D. C. Andersen, R. H. Davis and D. S. Kompala (1990). "Plasmid-encoded protein : the principal factor in the "metabolic burden" associated with recombinant bacteria." Biotechnology and Bioengineering **35**(7): 668-681.

Bentley, W. E. and O. E. Quiroga (1993). "Investigation of subpopulation heterogeneity and plasmid stability in recombinant *Escherichia coli* via simple segregated model." Biotechnology and Bioengineering **42**(2): 222-234.

Bergquist, P. L., E. M. Hardiman, B. C. Ferrari and T. Winsley (2009). "Applications of flow cytometry in environmental microbiology and biotechnology." Extremophiles **13**(3): 389-401.

Bi, C. H., P. Su, J. Muller, Y. C. Yeh, S. R. Chhabra, H. R. Beller, S. W. Singer and N. J. Hillson (2013). "Development of a broad-host synthetic biology toolbox for *Ralstonia eutropha* and its application to engineering hydrocarbon biofuel production." Microbial Cell Factories **12**.

Binder, D., T. Drepper, K. E. Jaeger, F. Delvigne, W. Wiechert, D. Kohlheyer and A. Grunberger (2017). "Homogenizing bacterial cell factories: Analysis and engineering of phenotypic heterogeneity." Metabolic Engineering **42**: 145-156.

Black, W. B., L. Zhang, C. Kamoku, J. C. Liao and H. Li (2018). "Rearrangement of Coenzyme A-Acylated Carbon Chain Enables Synthesis of Isobutanol via a Novel Pathway in *Ralstonia eutropha*." ACS Synth Biol **7**(3): 794-800.

Blokpoel, M. C., R. O'Toole, M. J. Smeulders and H. D. Williams (2003). "Development and application of unstable GFP variants to kinetic studies of mycobacterial gene expression." J Microbiol Methods **54**(2): 203-211.

Boy, C., J. Lesage, S. Alfenore, N. Gorret and S. E. Guillouet (2020). "Plasmid expression level heterogeneity monitoring via heterologous eGFP production at the single-cell level in *Cupriavidus necator*." Applied Microbiology and Biotechnology.

Brehm-Stecher, B. F. and E. A. Johnson (2004). "Single-cell microbiology: Tools, technologies, and applications." Microbiology and Molecular Biology Reviews **68**(3): 538-+.

Bruland, N., I. Voss, C. Bramer and A. Steinbuchel (2010). "Unravelling the C3/C4 carbon metabolism in Ralstonia eutropha H16." J Appl Microbiol **109**(1): 79-90.

Bruno, T. J., A. Wolk and A. Naydich (2009). "Composition-Explicit Distillation Curves for Mixtures of Gasoline with Four-Carbon Alcohols (Butanols)." Energy & Fuels **23**(4): 2295-2306.

Buch, A. D., G. Archana and G. Naresh Kumar (2010). "Broad-host-range plasmid-mediated metabolic perturbations in *Pseudomonas fluorescens* 13525." Appl Microbiol Biotechnol **88**(1): 209-218.

Buckner, M. M. C., M. L. Ciusa and L. J. V. Piddock (2018). "Strategies to combat antimicrobial resistance: anti-plasmid and plasmid curing." Fems Microbiology Reviews **42**(6): 781-804.

Budde, C. F., S. L. Riedel, L. B. Willis, C. Rha and A. J. Sinskey (2011). "Production of Poly(3-Hydroxybutyrate-co-3-Hydroxyhexanoate) from Plant Oil by Engineered *Ralstonia eutropha* Strains." Applied and Environmental Microbiology **77**(9): 2847-2854.

Burgdorf, T., O. Lenz, T. Buhrke, E. van der Linden, A. K. Jones, S. P. J. Albracht and B. Friedrich (2005). "NiFe -hydrogenases of *Ralstonia eutropha* H16: Modular enzymes for oxygen-tolerant biological hydrogen oxidation." Journal of Molecular Microbiology and Biotechnology **10**(2-4): 181-196.

Burgos, J. S., C. Ramírez, R. Tenorio, I. Sastre and M. J. Bullido (2002). "Influence of reagents formulation on real-time PCR parameters." Mol Cell Probes **16**(4): 257-260.

Calabrese, F., I. Voloshynovska, F. Musat, M. Thullner, M. Schlömann, H. H. Richnow, J. Lambrecht, S. Müller, L. Y. Wick, N. Musat and H. Stryhanyuk (2019). "Quantitation and Comparison of Phenotypic Heterogeneity Among Single Cells of Monoclonal Microbial Populations." Frontiers in microbiology **10**: 2814-2814.

Cao, H. and O. P. Kuipers (2018). "Influence of global gene regulatory networks on single cell heterogeneity of green fluorescent protein production in *Bacillus subtilis*." Microb Cell Fact **17**(1): 134.

Carapuça, E., A. R. Azzoni, D. M. F. Prazeres, G. A. Monteiro and F. J. M. Mergulhão (2007). "Time-course determination of plasmid content in eukaryotic and prokaryotic cells using Real-Time PCR." Molecular Biotechnology **37**(2): 120-126.

Carlquist, M., R. L. Fernandes, S. Helmark, A. L. Heins, L. Lundin, S. J. Sorensen, K. V. Gernaey and A. E. Lantz (2012). "Physiological heterogeneities in microbial populations and implications for physical stress tolerance." Microbial Cell Factories **11**.

Carrier, T., K. L. Jones and J. D. Keasling (1998). "mRNA stability and plasmid copy number effects on gene expression from an inducible promoter system." Biotechnology and Bioengineering **59**(6): 666-672.

Carroll, J. A., P. E. Stewart, P. Rosa, A. F. Elias and C. F. Garon (2003). "An enhanced GFP reporter system to monitor gene expression in Borrelia burgdorferi." Microbiology **149**(Pt 7): 1819-1828.

Ceroni, F., A. Boo, S. Furini, T. E. Gorochowski, O. Borkowski, Y. N. Ladak, A. R. Awan, C. Gilbert, G. B. Stan and T. Ellis (2018). "Burden-driven feedback control of gene expression." Nature Methods **15**(5): 387-+.

Chakravarty, J. and C. J. Brigham (2018). "Solvent production by engineered *Ralstonia eutropha*: channeling carbon to biofuel." Appl Microbiol Biotechnol **102**(12): 5021-5031.

Chapman, G. V. (2000). "Instrumentation for flow cytometry." Journal of Immunological Methods **243**(1-2): 3-12.

Chew, L. C. K., W. C. A. Tacon and J. A. Cole (1988). "Effect of growth conditions on the rate of loss of the plasmid pAT153 from continuous cultures of *Escherichia coli* HB101." FEMS Microbiology Letters **56**(1): 101-104.

Choi, S.-J. P., Doo-Hong; Chung, Soo-Il ; Jung, Kyung-Hwan (2000). "Plasmid Stability in Long-Term hG-CSF Production Using L−Arbinose Promoter System of *Escherichia coli* " Journal of Microbiology and Biotechnology **10**(3): 321-326.

Chudakov, D. M., M. V. Matz, S. Lukyanov and K. A. Lukyanov (2010). "Fluorescent proteins and their applications in imaging living cells and tissues." Physiol Rev **90**(3): 1103-1163.

Collas, F., W. Kuit, B. Clément, R. Marchal, A. M. López-Contreras and F. Monot (2012). "Simultaneous production of isopropanol, butanol, ethanol and 2,3-butanediol by *Clostridium acetobutylicum* ATCC 824 engineered strains." AMB Express **2**(1): 45.

Connor, M. R., A. F. Cann and J. C. Liao (2010). "3-Methyl-1-butanol production in *Escherichia coli*: random mutagenesis and two-phase fermentation." Applied microbiology and biotechnology **86**(4): 1155-1164.

Cooper, T. F. and J. A. Heinemann (2000). "Postsegregational killing does not increase plasmid stability but acts to mediate the exclusion of competing plasmids " Proceedings of the National Academy of Sciences of the United States of America **97**(23): 12643-12648.

Cramm, R. (2009). "Genomic View of Energy Metabolism in *Ralstonia eutropha* H16." Journal of Molecular Microbiology and Biotechnology **16**(1-2): 38-52.

Crépin, L., M. Barthe, F. Leray and S;E. Guillouet (2018)."Alka(e)ne synthesis in *Cupriavidus necator* boosted by the expression of the endogenous and heterologous ferredoxin-ferredoxin reductase systems" Biotechnology and Bioengineering **115**(10): 2576-2584.

Crepin, L., E. Lombard and S. E. Guillouet (2016). "Metabolic engineering of *Cupriavidus necator* for heterotrophic and autotrophic alka(e)ne production." Metabolic Engineering **37**: 92-101.

Cruz, M. V., A. R. Gouveia, M. Dionísio, F. Freitas and M. A. M. Reis (2019). "A Process Engineering Approach to Improve Production of P(3HB) by *Cupriavidus necator* from Used Cooking Oil." International Journal of Polymer Science **2019**: 2191650.

Cunningham, D. S., Z. Liu, N. Domagalski, R. R. Koepsel, M. M. Ataai and M. M. Domach (2009). "Pyruvate kinase-deficient *Escherichia coli* exhibits increased plasmid copy number and cyclic AMP levels." Journal of bacteriology **191**(9): 3041-3049.

D'Angio, C., C. Béal, C.-Y. Boquien and G. Corrieu (1994). "Influence of dilution rate and cell immobilization on plasmid stability during continuous cultures of recombinant strains of *Lactococcus lactis subsp. lactis*." Journal of Biotechnology **34**(1): 87-95.

Davey, H. M. and P. Hexley (2011). "Red but not dead? Membranes of stressed *Saccharomyces cerevisiae* are permeable to propidium iodide." Environmental Microbiology **13**(1): 163-171.

Day, R. S., Fred (2008). "Fluorescent protein tools for studying protein dynamics in living cells: a review." Journal of Biomedical Optics **13**(3): 1-6.

De Gelder, L., J. M. Ponciano, P. Joyce and E. M. Top (2007). "Stability of a promiscuous plasmid in different hosts: no guarantee for a long-term relationship." Microbiology-Sgm **153**: 452-463.

Delobel, P., M. Pradal, B. Blondin and C. Tesniere (2012). "A 'fragile cell' sub-population revealed during cytometric assessment of *Saccharomyces cerevisiae* viability in lipid-limited alcoholic fermentation." Letters in Applied Microbiology **55**(5): 338-344.

Delvigne, F., J. Baert, S. Gofflot, A. Lejeune, S. Telek, T. Johanson and A. Lantz (2015). "Dynamic single-cell analysis of *Saccharomyces cerevisiae* under process perturbation: Comparison of different methods for monitoring the intensity of population heterogeneity." Journal of Chemical Technology and Biotechnology **90**.

Delvigne, F., A. Brognaux, F. Francis, J. C. Twizere, N. Gorret, S. J. Sorensen and P. Thonart (2011). "Green fluorescent protein (GFP) leakage from microbial biosensors provides useful information for the evaluation of the scale-down effect." Biotechnol J **6**(8): 968-978.

Delvigne, F., A. Brognaux, N. Gorret, P. Neubauer, A. Delafosse, M.-L. Collignon, D. Toye, M. Crine, M. Boxus and P. Thonart (2011). "Characterization of the response of GFP microbial biosensors sensitive to substrate limitation in scale-down bioreactors." Biochemical Engineering Journal **55**(2): 131-139.

Delvigne, F. and P. Goffin (2014). "Microbial heterogeneity affects bioprocess robustness: Dynamic single-cell analysis contributes to understanding of microbial populations." Biotechnology Journal **9**(1): 61-72.

Delvigne, F., H. Pêcheux and C. Tarayre (2015). "Fluorescent Reporter Libraries as Useful Tools for Optimizing Microbial Cell Factories: A Review of the Current Methods and Applications." Frontiers in Bioengineering and Biotechnology **3**(147).

Delvigne, F., Q. Zune, A. R. Lara, W. Al-Soud and S. J. Sørensen (2014). "Metabolic variability in bioprocessing: implications of microbial phenotypic heterogeneity." Trends in Biotechnology **32**(12): 608-616.

di Mauro, E., L. Synder, P. Marino, A. Lamberti, A. Coppo and G. P. Tocchini-Valentini (1969). "Rifampicin sensitivity of the components of DNA-dependent RNA polymerase." Nature **222**(5193): 533-537.

Diaz, M., M. Herrero, L. A. Garcia and C. Quiros (2010). "Application of flow cytometry to industrial microbial bioprocesses." Biochemical Engineering Journal **48**(3): 385-407.

Doi, Y., A. Tamaki, M. Kunioka and K. Soga (1988). "Production of copolyesters of 3-hydroxybutyrate and 3-hydroxyvalerate by Alcaligenes eutrophus from butyric and pentanoic acids." Applied Microbiology and Biotechnology **28**(4): 330-334.

Dunlop, M. J. (2011). "Engineering microbes for tolerance to next-generation biofuels." Biotechnology for Biofuels **4**(1): 32.

Dupoet, P. D., Y. Arcand, R. Bernier, J. N. Barbotin and D. Thomas (1987). "Plasmid stability in immobilized and free recombinant *Escherichia coli* JM105(pKK223-200) - Importance of oxygen diffusion, growth rate, and plasmid copy number." Applied and Environmental Microbiology **53**(7): 1548-1555.

Dürre, P. (1998). "New insights and novel developments in clostridial acetone/butanol/isopropanol fermentation." Applied Microbiology and Biotechnology **49**(6): 639-648.

Dürre, P. and H. Bahl (2008). Microbial production of Acetone/Butanol/Isopropanol. Biotechnology : Products of Primary Metabolism. G. R. H.-J. Rehm. **6:** 229-268.

Dusséaux, S., C. Croux, P. Soucaille and I. Meynial-Salles (2013). "Metabolic engineering of *Clostridium acetobutylicum* ATCC 824 for the high-yield production of a biofuel composed of an isopropanol/butanol/ethanol mixture." Metabolic Engineering **18**: 1-8.

Easter, C. L., H. Schwab and D. R. Helinski (1998). "Role of the parCBA operon of the broad-host-range plasmid RK2 in stable plasmid maintenance." Journal of Bacteriology **180**(22): 6023-6030.

Elowitz, M. B., A. J. Levine, E. D. Siggia and P. S. Swain (2002). "Stochastic gene expression in a single cell." Science **297**(5584): 1183-1186.

Evans, C. T. and C. Ratledge (1984). "Effect of Nitrogen Source on Lipid Accumulation in Oleaginous Yeasts." Microbiology **130**(7): 1693-1704.

Ewering, C., F. Heuser, J. K. Benolken, C. Bramer and A. Steinbuchel (2006). "Metabolic engineering of strains of *Ralstonia eutropha* and *Pseudomonas putida* for biotechnological production of 2-methylcitric acid." Metabolic Engineering **8**(6): 587-602.

Fernandes, R. L., M. Nierychlo, L. Lundin, A. E. Pedersen, P. E. P. Tellez, A. Dutta, M. Carlquist, A. Bolic, D. Schapper, A. C. Brunetti, S. Helmark, A. L. Heins, A. D. Jensen, I. Nopens, K. Rottwitt, N. Szita, J. D. van Elsas, P. H. Nielsen, J. Martinussen, S. J. Sorensen, A. E. Lantz and K. V. Gernaey (2011). "Experimental methods and modeling techniques for description of cell population heterogeneity." Biotechnology Advances **29**(6): 575-599.

Fiedler, M. and A. Skerra (2001). "proBA complementation of an auxotrophic *E. coli* strain improves plasmid stability and expression yield during fermenter production of a recombinant antibody fragment." Gene **274**(1): 111-118.

Friedrich, C. G., B. Bowien and B. Friedrich (1979). "Formate and oxalate metabolism in *Alcaligenes eutrophus*." Journal of General Microbiology **115**(NOV): 185-192.

Friehs, K. (2004). "Plasmid copy number and plasmid stability." Adv Biochem Eng Biotechnol **86**: 47-82.

Fukui, T., M. Suzuki, T. Tsuge and S. Nakamura (2009). "Microbial synthesis of poly((R)-3-hydroxybutyrate-co-3-hydroxypropionate) from unrelated carbon sources by engineered *Cupriavidus necator*." Biomacromolecules **10**(4): 700-706.

Gai, C. S., J. Lu, C. J. Brigham, A. C. Bernardi and A. J. Sinskey (2014). "Insights into bacterial CO_2 metabolism revealed by the characterization of four carbonic anhydrases in *Ralstonia eutropha* H16." AMB Express **4**(1): 2-2.

Garrigues, L., L. Maignien, E. Lombard, J. Singh and S. E. Guillouet (2020). "Isopropanol production from carbon dioxide in *Cupriavidus necator* in a pressurized bioreactor." New Biotechnology **56**: 16-20.

George, H. A., J. L. Johnson, W. E. Moore, L. V. Holdeman and J. S. Chen (1983). "Acetone, Isopropanol, and Butanol Production by *Clostridium beijerinckii* (syn. *Clostridium butylicum*) and *Clostridium aurantibutyricum*." Applied and environmental microbiology **45**(3): 1160-1163.

Gerdes, K., T. Thisted and J. Martinussen (1990). "Mechanism of post-segregational killing by the hok/sok system of plasmid R1: sok antisense RNA regulates formation of a hok mRNA species correlated with killing of plasmid-free cells." Mol Microbiol **4**(11): 1807-1818.

Gibson, D. G., L. Young, R. Y. Chuang, J. C. Venter, C. A. Hutchison and H. O. Smith (2009). "Enzymatic assembly of DNA molecules up to several hundred kilobases." Nature Methods **6**(5): 343-U341.

Givan, A. L. (2001). "Flow Cytometry: First Principles, Second Edition." 2nd Edition, John Wiley & Sons, Inc., New York.

Glick, B. R. (1995). "Metabolic load and heterologous gene-expression." Biotechnology Advances **13**(2): 247-261.

Gonzalez-Cabaleiro, R., A. M. Mitchell, W. Smith, A. Wipat and I. D. Ofiteru (2017). "Heterogeneity in Pure Microbial Systems: Experimental Measurements and Modeling." Frontiers in Microbiology **8**.

Grimbergen, A. J., J. Siebring, A. Solopova and O. P. Kuipers (2015). "Microbial bet-hedging: the power of being different." Current Opinion in Microbiology **25**: 67-72.

Grote, J., D. Krysciak and W. R. Streit (2015). "Phenotypic Heterogeneity, a Phenomenon That May Explain Why Quorum Sensing Does Not Always Result in Truly Homogenous Cell Behavior." Applied and environmental microbiology **81**(16): 5280-5289.

Grousseau, E., E. Blanchet, S. Déléris, M. G. E. Albuquerque, E. Paul and J.-L. Uribelarrea (2013). "Impact of sustaining a controlled residual growth on polyhydroxybutyrate yield and production kinetics in *Cupriavidus necator*." Bioresource Technology **148**: 30-38.

Grousseau, E., J. N. Lu, N. Gorret, S. E. Guillouet and A. J. Sinskey (2014). "Isopropanol production with engineered *Cupriavidus necator* as bioproduction platform." Applied Microbiology and Biotechnology **98**(9): 4277-4290.

Gruber, S., J. Hagen, H. Schwab and P. Koefinger (2014). "Versatile and stable vectors for efficient gene expression in *Ralstonia eutropha* H16." Journal of Biotechnology **186**: 74-82.

Gruber, S., H. Schwab and P. Koefinger (2015). "Versatile plasmid-based expression systems for Gram-negative bacteria-General essentials exemplified with the bacterium *Ralstonia eutropha* H16." New Biotechnology **32**(6): 552-558.

Grunwald, S., A. Mottet, E. Grousseau, J. K. Plassmeier, M. K. Popovic, J. L. Uribelarrea, N. Gorret, S. E. Guillouet and A. Sinskey (2015). "Kinetic and stoichiometric characterization of organoautotrophic growth of *Ralstonia eutropha* on formic acid in fed-batch and continuous cultures." Microbial Biotechnology **8**(1): 155-163.

Gupta, J. C., G. Pandey and K. J. Mukherjee (2001). "Two-stage cultivation of recombinant *Saccharomyces cerevisiae* to enhance plasmid stability under non-selective conditions: experimental study and modeling." Enzyme and Microbial Technology **28**(1): 89-99.

Haas, M. J. and J. E. Dowding (1975). "Aminoglycoside-modifying enzymes." Methods Enzymol **43**: 611-628.

Hägg, P., J. W. de Pohl, F. Abdulkarim and L. A. Isaksson (2004). "A host/plasmid system that is not dependent on antibiotics and antibiotic resistance genes for stable plasmid maintenance in *Escherichia coli*." Journal of Biotechnology **111**(1): 17-30.

Hanai, T., S. Atsumi and J. C. Liao (2007). "Engineered synthetic pathway for isopropanol production in *Escherichia coli*." Applied and environmental microbiology **73**(24): 7814-7818.

Haroon, M. F., C. T. Skennerton, J. A. Steen, N. Lachner, P. Hugenholtz and G. W. Tyson (2013). In-Solution Fluorescence In Situ Hybridization and Fluorescence-Activated Cell Sorting for Single Cell and Population Genome Recovery. Microbial Metagenomics, Metatranscriptomics, and Metaproteomics. E. F. DeLong. San Diego, Elsevier Academic Press Inc. **531:** 3-19.

Harrison, E. and M. A. Brockhurst (2012). "Plasmid-mediated horizontal gene transfer is a coevolutionary process." Trends in Microbiology **20**(6): 262-267.

Heins, A. L. and D. Weuster-Botz (2018). "Population heterogeneity in microbial bioprocesses: origin, analysis, mechanisms, and future perspectives." Bioprocess Biosyst Eng **41**(7): 889-916.

Heller, H., C. Kammer, P. Wilgenbus and W. Doerfler (1995). "Chromosomal insertion of foreign (Adenovirus-type-12, plasmid, or bacteriophage-lambda) DNA is associated with enhanced methylation of cellular DNA segments." Proceedings of the National Academy of Sciences of the United States of America **92**(12): 5515-5519.

Hernández-Ramírez, K. C., V. M. Chávez-Jacobo, M. I. Valle-Maldonado, J. A. Patiño-Medina, S. P. Díaz-Pérez, I. E. Jácome-Galarza, R. Ortiz-Alvarado, V. Meza-Carmen and M. I. Ramírez-Díaz (2017). "Plasmid pUM505 encodes a Toxin–Antitoxin system conferring plasmid stability and increased *Pseudomonas aeruginosa* virulence." Microbial Pathogenesis **112**: 259-268.

Hewitt, C. J., H. Onyeaka, G. Lewis, I. W. Taylor and A. W. Nienow (2007). "A comparison of high cell density fed-batch fermentations involving both induced and non-induced recombinant *Escherichia coli* under well-mixed small-scale and simulated poorly mixed large-scale conditions." Biotechnol Bioeng **96**(3): 495-505.

Hoefel, T., E. Wittmann, L. Reinecke and D. Weuster-Botz (2010). "Reaction engineering studies for the production of 2-hydroxyisobutyric acid with recombinant *Cupriavidus necator* H16." Applied Microbiology and Biotechnology **88**(2): 477-484.

Hughes, E. J., R. C. Bayly and R. A. Skurray (1984). "Characterization of a TOL-like plasmid from *Alcaligenes eutrophus* that controls expression of a chromosomally encoded p-cresol pathway." Journal of bacteriology **158**(1): 73-78.

Huguet, K. T., N. Rivard, D. Garneau, J. Palanee and V. Burrus (2020). "Replication of the Salmonella Genomic Island 1 (SGI1) triggered by helper IncC conjugative plasmids promotes incompatibility and plasmid loss." PLOS Genetics **16**(8): e1008965.

Ingram, L. O. and T. M. Buttke (1984). "Effects of alcohols on micro-organisms." Adv Microb Physiol **25**: 253-300.

Jang, Y.-S., A. Malaviya, J. Lee, J. A. Im, S. Y. Lee, J. Lee, M.-H. Eom, J.-H. Cho and D. Y. Seung (2013). "Metabolic engineering of *Clostridium acetobutylicum* for the enhanced production of isopropanol-butanol-ethanol fuel mixture." Biotechnology Progress **29**(4): 1083-1088.

Jensen, R. B. and K. Gerdes (1995). "Programmed cell-death in bacteria-proteic plasmid stabilization systems." Molecular Microbiology **17**(2): 205-210.

Jia, K., Y. Zhang and Y. Li (2010). "Systematic engineering of microorganisms to improve alcohol tolerance." Engineering in Life Sciences **10**: 422-429.

Johnson, B. F. R. Y. S. (1971). "Dissimilation of Aromatic Compounds by *Alcaligenes eutrophus* " Journal of Bacteriology **107**(2): 468–475.

Johnson, E. P., A. R. Strom and D. R. Helinski (1996). "Plasmid RK2 toxin protein ParE: Purification and interaction with the ParD antitoxin protein." Journal of Bacteriology **178**(5): 1420-1429.

Kim, C. H., J. Y. Lee, M. G. Kim, K. B. Song, J. W. Seo, B. H. Chung, S. J. Chang and S. K. Rhee (1998). "Fermentation strategy to enhance plasmid stability during the cultivation of *Escherichia coli* for the production of recombinant levansucrase." Journal of Fermentation and Bioengineering **86**(4): 391-394.

Klotsky, R. A. and I. Schwartz (1987). "Measurement of cat expression from growth-rate-regulated promoters employing beta-lactamase activity as an indicator of plasmid copy number." Gene **55**(1): 141-146.

Klumpp, S. (2011). "Growth-Rate Dependence Reveals Design Principles of Plasmid Copy Number Control." PLOS ONE **6**(5): e20403.

Koizumi, J., Y. Monden and S. Aiba (1985). "Effects of temperature and dilution rate on the copy number of recombinant plasmid in continuous culture of *Bacillus stearothermophilus* (pLP11)." Biotechnol Bioeng **27**(5): 721-728.

Koller, M., A. Atlić, M. Dias, A. Reiterer and G. Braunegg (2010). Microbial PHA Production from Waste Raw Materials. Plastics from Bacteria: Natural Functions and Applications. G. G.-Q. Chen. Berlin, Heidelberg, Springer Berlin Heidelberg**:** 85-119.

Kortmann, M., C. Mack, M. Baumgart and M. Bott (2019). "Pyruvate Carboxylase Variants Enabling Improved Lysine Production from Glucose Identified by Biosensor-Based High-Throughput Fluorescence-Activated Cell Sorting Screening." ACS Synth Biol **8**(2): 274-281.

Kovach, M. E., P. H. Elzer, D. S. Hill, G. T. Robertson, M. A. Farris, R. M. Roop and K. M. Peterson (1995). "Four new derivatives of the broad-host range cloning vector pBBR1MCS, carrying different antibiotic resistance cassettes." Gene **166**(1): 175-176.

Krieg, T., A. Sydow, S. Faust, I. Huth and D. Holtmann (2018). "CO(2) to Terpenes: Autotrophic and Electroautotrophic α-Humulene Production with *Cupriavidus necator*." Angew Chem Int Ed Engl **57**(7): 1879-1882.

Kushner, D. J. (1964). 4 - Microbial Resistance to Harsh and Destructive Environmental Conditions Issued as N.R.C. Contribution No. 7575. Chemotherapy of Bacterial Infections. R. J. Schnitzer and F. Hawking, Academic Press**:** 113-168.

Kussell, E. and S. Leibler (2005). "Phenotypic Diversity, Population Growth, and Information in Fluctuating Environments." Science **309**(5743): 2075.

Lara, A. R., E. Galindo, O. T. Ramírez and L. A. Palomares (2006). "Living with heterogeneities in bioreactors." Molecular Biotechnology **34**(3): 355-381.

Lara, A. R., E. Galindo, O. T. Ramírez and L. A. Palomares (2006). "Living with heterogeneities in bioreactors: understanding the effects of environmental gradients on cells." Mol Biotechnol **34**(3): 355-381.

Lara, A. R., H. Taymaz-Nikerel, M. R. Mashego, W. M. van Gulik, J. J. Heijnen, O. T. Ramírez and W. A. van Winden (2009). "Fast dynamic response of the fermentative metabolism of *Escherichia coli* to aerobic and anaerobic glucose pulses." Biotechnol Bioeng **104**(6): 1153-1161.

Lau, B. T. C., P. Malkus and J. Paulsson (2013). "New quantitative methods for measuring plasmid loss rates reveal unexpected stability." Plasmid **70**(3): 353-361.

Laurent, V. M., S. Henon, E. Planus, R. Fodil, M. Balland, D. Isabey and F. Gallet (2002). "Assessment of mechanical properties of adherent living cells by bead micromanipulation: Comparison of magnetic twisting cytometry vs optical tweezers." Journal of Biomechanical Engineering-Transactions of the Asme **124**(4): 408-421.

Lee, C., J. Kim, S. G. Shin and S. Hwang (2006). "Absolute and relative QPCR quantification of plasmid copy number in *Escherichia coli*." Journal of Biotechnology **123**(3): 273-280.

Lee, C. L., D. S. W. Ow and S. K. W. Oh (2006). "Quantitative real-time polymerase chain reaction for determination of plasmid copy number in bacteria." Journal of Microbiological Methods **65**(2): 258-267.

Lee, K., S. G. Kwon, S. H. Kim and Y. K. Kwak (2007). "Dielectrophoretic tweezers using sharp probe electrode." Sensors and Actuators A: Physical **136**(1): 154-160.

Lee, S. Y., J. H. Park, S. H. Jang, L. K. Nielsen, J. Kim and K. S. Jung (2008). "Fermentative butanol production by *Clostridia*." Biotechnology and Bioengineering **101**(2): 209-228.

Lemoine, A., F. Delvigne, A. Bockisch, P. Neubauer and S. Junne (2017). "Tools for the determination of population heterogeneity caused by inhomogeneous cultivation conditions." Journal of Biotechnology **251**: 84-93.

Lengeler, J. W. D., Gerhart ; Schlegel, Hans G. (1998). Growth and Nutrition. Biology of the Prokaryotes**:** 88-109.

Lessard, J. C. (2013). Chapter Eleven - Growth Media for E. coli. Methods in Enzymology. J. Lorsch, Academic Press. **533:** 181-189.

Light, J. and S. Molin (1982). "Expression of a copy number control gene (copB) of plasmid R1 is constitutive and growth rate dependent." Journal of bacteriology **151**(3): 1129-1135.

Limberg, M. H., M. Joachim, B. Klein, W. Wiechert and M. Oldiges (2017). "pH fluctuations imperil the robustness of *C. glutamicum* to short term oxygen limitation." J Biotechnol **259**: 248-260.

Lin-Chao, S. and H. Bremer (1986). "Effect of the bacterial growth rate on replication control of plasmid pBR322 in *Escherichia coli*." Molecular and General Genetics MGG **203**(1): 143-149.

Livak, K. J. and T. D. Schmittgen (2001). "Analysis of relative gene expression data using real-time quantitative PCR and the 2(-Delta Delta C(T)) Method." Methods **25**(4): 402-408.

Longo, D. and J. Hasty (2006). "Dynamics of single-cell gene expression." Molecular systems biology **2**: 64-64.

Lu, J. N., C. J. Brigham, C. Rha and A. J. Sinskey (2013). "Characterization of an extracellular lipase and its chaperone from *Ralstonia eutropha* H16." Applied Microbiology and Biotechnology **97**(6): 2443-2454.

Lv, Y., S. Qian, G. Du, J. Chen, J. Zhou and P. Xu (2019). "Coupling feedback genetic circuits with growth phenotype for dynamic population control and intelligent bioproduction." Metabolic Engineering **54**: 109-116.

Ma, Z., Y. Zhou, D. J. Collins and Y. Ai (2017). "Fluorescence activated cell sorting via a focused traveling surface acoustic beam." Lab Chip **17**(18): 3176-3185.

Mahr, R. and J. Frunzke (2016). "Transcription factor-based biosensors in biotechnology: current state and future prospects." Applied microbiology and biotechnology **100**(1): 79-90.

Marc, J., E. Grousseau, E. Lombard, A. J. Sinskey, N. Gorret and S. E. Guillouet (2017). "Over expression of GroESL in *Cupriavidus necator* for heterotrophic and autotrophic isopropanol production." Metabolic Engineering **42**: 74-84.

Martins, B. M. C. and J. O. W. Locke (2015). "Microbial individuality: how single-cell heterogeneity enables population level strategies." Current Opinion in Microbiology **24**: 104-112.

Masel, J. and M. L. Siegal (2009). "Robustness: mechanisms and consequences." Trends in Genetics **25**(9): 395-403.

Masters, M., G. Blakely, A. Coulson, N. McLennan, V. Yerko and J. Acord (2009). "Protein folding in *Escherichia coli*: the chaperonin GroE and its substrates." Research in Microbiology **160**(4): 267-277.

Mathur, A. and S. Chand (2009). "Model-based evaluation of plasmid segregational instability in repeated batch culture with recombinant *Escherichia coli*." Chemical Engineering Journal **153**(1-3): 227-230.

McRae, S. R., C. L. Brown and G. R. Bushell (2005). "Rapid purification of EGFP, EYFP, and ECFP with high yield and purity." Protein Expression and Purification **41**(1): 121-127.

Miao, F., P. Todd and D. S. Kompala (1993). "A single-cell assay of β-galactosidase in recombinant *Escherichia coli* using flow cytometry." Biotechnology and Bioengineering **42**(6): 708-715.

Millero, F. J. (1995). "Thermodynamics of the carbon dioxide system in the oceans." Geochimica et Cosmochimica Acta **59**(4): 661-677.

Million-Weaver, S. and M. Camps (2014). "Mechanisms of plasmid segregation: Have multicopy plasmids been overlooked?" Plasmid **75**: 27-36.

Monchy, S., M. A. Benotmane, R. Wattiez, S. van Aelst, V. Auquier, B. Borremans, M. Mergeay, S. Taghavi, D. van der Lelie and T. Vallaeys (2006). "Transcriptomic and proteomic analyses of the pMOL30-encoded copper resistance in *Cupriavidus metallidurans* strain CH34." Microbiology-Sgm **152**: 1765-1776.

Morschhäuser, J., S. Michel and J. Hacker (1998). "Expression of a chromosomally integrated, single-copy GFP gene in *Candida albicans*, and its use as a reporter of gene regulation." Mol Gen Genet **257**(4): 412-420.

Mortier, J., W. Tadesse, S. K. Govers and A. Aertsen (2019). "Stress-induced protein aggregates shape population heterogeneity in bacteria." Current Genetics **65**(4): 865-869.

Mukhopadhyay, A. (2015). "Tolerance engineering in bacteria for the production of advanced biofuels and chemicals." Trends in Microbiology **23**(8): 498-508.

Muller, J., D. MacEachran, H. Burd, N. Sathitsuksanoh, C. H. Bi, Y. C. Yeh, T. S. Lee, N. J. Hillson, S. R. Chhabra, S. W. Singer and H. R. Beller (2013). "Engineering of *Ralstonia eutropha* H16 for Autotrophic and Heterotrophic Production of Methyl Ketones." Applied and Environmental Microbiology **79**(14): 4433-4439.

Muller, S., H. Harms and T. Bley (2010). "Origin and analysis of microbial population heterogeneity in bioprocesses." Current Opinion in Biotechnology **21**(1): 100-113.

Nana, G. Y. G., C. Ripoll, A. Cabin-Flaman, D. Gibouin, A. Delaune, L. Janniere, G. Grancher, G. Chagny, C. Loutelier-Bourhis, E. Lentzen, P. Grysan, J. N. Audinot and V. Norris (2018). "Division-Based, Growth Rate Diversity in Bacteria." Frontiers in Microbiology **9**.

Nangle, S. N., M. Ziesack, S. Buckley, D. Trivedi, D. M. Loh, D. G. Nocera and P. A. Silver (2020). "Valorization of CO2; through lithoautotrophic production of sustainable chemicals in *Cupriavidus necator*." bioRxiv: 2020.2002.2008.940007.

Neubauer, P. and S. Junne (2010). "Scale-down simulators for metabolic analysis of large-scale bioprocesses." Current Opinion in Biotechnology **21**(1): 114-121.

Nicolaou, S. A., S. M. Gaida and E. T. Papoutsakis (2010). "A comparative view of metabolite and substrate stress and tolerance in microbial bioprocessing: From biofuels and chemicals, to biocatalysis and bioremediation." Metabolic Engineering **12**(4): 307-331.

Noack, D., M. Roth, R. Geuther, G. Müller, K. Undisz, C. Hoffmeier and S. Gáspár (1981). "Maintenance and genetic stability of vector plasmids pBR322 and pBR325 in *Escherichia coli* K12 strains grown in a chemostat." Molecular and General Genetics MGG **184**(1): 121-124.

Nyström, T. (2007). "A Bacterial Kind of Aging." PLoS Genetics **3**(12): e224.

Oberer, M., H. Lindner, O. Glatter, C. Kratky and W. Keller (1999). "Thermodynamic properties and DNA binding of the ParD protein from the broad host-range plasmid RK2/RP4 killing system." Biological Chemistry **380**(12): 1413-1420.

Papa, A. J. (2000). Propanols. Ullmann's Encyclopedia of Industrial Chemistry, Wiley-VCH Verlag GmbH & Co. KGaA.

Parish, M. (2006). "How do salt and sugar prevent microbial spoilage?" Scientific American **294**(5): 98.

Park, S. Y., R. M. Binkley, W. J. Kim, M. H. Lee and S. Y. Lee (2018). "Metabolic engineering of *Escherichia coli* for high-level astaxanthin production with high productivity." Metab Eng **49**: 105-115.

Patnaik, P. R. (1994). "Effect of feed cycling on plasmid stabilizationduring continuous fermentation - the case of variable plasmid loss probability." Canadian Journal of Chemical Engineering **72**(5): 929-934.

Patnaik, P. R. (2000). "An evaluation of models for the effect of plasmid copy number on bacterial growth rate." Biotechnology Letters **22**(21): 1719-1725.

Pecota, D. C., C. S. Kim, K. Wu, K. Gerdes and T. K. Wood (1997). "Combining the hok/sok, parDE, and pnd postsegregational killer loci to enhance plasmid stability." Applied and environmental microbiology **63**(5): 1917-1924.

Peralta-Yahya, P. P. and J. D. Keasling (2010). "Advanced biofuel production in microbes." Biotechnol J **5**(2): 147-162.

Persad, A. K., M. L. Williams and J. T. LeJeune (2017). "Rapid loss of a green fluorescent plasmid in *Escherichia coli* O157:H7." AIMS microbiology **3**(4): 872-884.

Pogliano, J. (2002). "Dynamic cellular location of bacterial plasmids." Current Opinion in Microbiology **5**(6): 586-590.

Pogliano, J., T. Q. Ho, Z. P. Zhong and D. R. Helinski (2001). "Multicopy plasmids are clustered and localized in *Escherichia coli*." Proceedings of the National Academy of Sciences of the United States of America **98**(8): 4486-4491.

Pohlmann, A., W. F. Fricke, F. Reinecke, B. Kusian, H. Liesegang, R. Cramm, T. Eitinger, C. Ewering, M. Potter, E. Schwartz, A. Strittmatter, I. Voss, G. Gottschalk, A. Steinbuchel, B. Friedrich and B. Bowien (2006). "Genome sequence of the bioplastic-producing "Knallgas" bacterium *Ralstonia eutropha* H16." Nature Biotechnology **24**(10): 1257-1262.

Polizzi, K. M. and C. Kontoravdi (2015). "Genetically-encoded biosensors for monitoring cellular stress in bioprocessing." Current Opinion in Biotechnology **31**: 50-56.

Ponciano, J. M., L. Gelder, E. M. Top and P. Joyce (2007). "The population biology of bacterial plasmids: A hidden Markov model approach." Genetics **176**(2): 957-968.

Pushnova, E. A., M. Geier and Y. S. Zhu (2000). "An Easy and Accurate Agarose Gel Assay for Quantitation of Bacterial Plasmid Copy Numbers." Analytical Biochemistry **284**(1): 70-76.

Raberg, M., K. Peplinski, S. Heiss, A. Ehrenreich, B. Voigt, C. Döring, M. Bömeke, M. Hecker and A. Steinbüchel (2011). "Proteomic and Transcriptomic Elucidation of the Mutant *Ralstonia eutropha* with Regard to Glucose Utilization." Applied and Environmental Microbiology **77**(6): 2058.

Rakotomalala, R. (2011). "Tests de normalité - Techniques empiriques et tests statistiques,." Université Lumière Lyon 2.

Ramirez, M. S. and M. E. Tolmasky (2010). "Aminoglycoside modifying enzymes." Drug resistance updates : reviews and commentaries in antimicrobial and anticancer chemotherapy **13**(6): 151-171.

Ratledge, C. (2002). "Regulation of lipid accumulation in oleaginous micro-organisms." Biochemical Society Transactions **30**(6): 1047-1050.

Reinikainen, P. and I. Virkajärvi (1989). "Escherichia coli growth and plasmid copy numbers in continuous cultures." Biotechnology Letters **11**: 225-230.

Repaske, R. and R. Mayer (1976). "Dense autotrophic cultures of *Alcaligenes eutrophus*." Applied and environmental microbiology **32**(4): 592-597.

Riber, L., M. Burmølle, M. Alm, S. M. Milani, P. Thomsen, L. H. Hansen and S. J. Sørensen (2016). "Enhanced plasmid loss in bacterial populations exposed to the antimicrobial compound irgasan delivered from interpenetrating polymer network silicone hydrogels." Plasmid **87-88**: 72-78.

Robinson, J. P. (2004). "Flow cytometry, in: G.L. Bowlin, G. Wnek (Eds.), Encyclopaedia of Biomaterials and Biomedical Engineering, Marcel Dekker, Inc., New York,." 630–640.

Rodriguez, E. A., R. E. Campbell, J. Y. Lin, M. Z. Lin, A. Miyawaki, A. E. Palmer, X. Shu, J. Zhang and R. Y. Tsien (2017). "The Growing and Glowing Toolbox of Fluorescent and Photoactive Proteins." Trends in Biochemical Sciences **42**(2): 111-129.

Rogers, J. K. and G. M. Church (2016). "Genetically encoded sensors enable real-time observation of metabolite production." Proceedings of the National Academy of Sciences **113**(9): 2388.

Ryan, W. and S. J. Parulekar (1991). "Recombinant protein synthesis and plasmid instability in continuous cultures of *Escherichia coli* JM103 harboring a high copy number plasmid." Biotechnology and Bioengineering **37**(5): 415-429.

Ryu, H. W., S. K. Hahn, Y. K. Chang and H. N. Chang (1997). "Production of poly(3-hydroxybutyrate) by high cell density fed-batch culture of *Alcaligenes eutrophus* with phospate limitation." Biotechnology and Bioengineering **55**(1): 28-32.

Sato, S., T. Fujiki and K. Matsumoto (2013). "Construction of a stable plasmid vector for industrial production of poly(3-hydroxybutyrate-co-3-hydroxyhexanoate) by a recombinant *Cupriavidus necator* H16 strain." Journal of Bioscience and Bioengineering **116**(6): 677-681.

Schendel, F. J., E. J. Baude and M. C. Flickinger (1989). "Determination of protein expression and plasmid copy number from cloned genes in Escherichia coli by flow injection analysis using an enzyme indicator vector." Biotechnology and Bioengineering **34**(8): 1023-1036.

Schobert, P. and B. Bowien (1984). "Unusual C-3 and C-4 Metabolism in the Chemoautotroph *Alcaligenes eutrophus*." Journal of Bacteriology **159**(1): 167-172.

Schwartz, E., A. Henne, R. Cramm, T. Eitinger, B. Friedrich and G. Gottschalk (2003). "Complete nucleotide sequence of pHG1: A *Ralstonia eutropha* H16 megaplasmid encoding key enzymes of H-2-based lithoautotrophy and anaerobiosis." Journal of Molecular Biology **332**(2): 369-383.

Shah, S. and V. Venkatramanan (2019). Advances in Microbial Technology for Upscaling Sustainable Biofuel Production**:** 69-76.

Shaner, N. C. (2014). "Fluorescent proteins for quantitative microscopy: important properties and practical evaluation." Methods Cell Biol **123**: 95-111.

Shaner, N. C., G. H. Patterson and M. W. Davidson (2007). "Advances in fluorescent protein technology." J Cell Sci **120**(Pt 24): 4247-4260.

Shaner, N. C., P. A. Steinbach and R. Y. Tsien (2005). "A guide to choosing fluorescent proteins." Nature Methods **2**(12): 905-909.

Shapiro, H. M. (2003). "Practical Flow Cytometry." 4th Edition, Wiley-Liss, New York.

Shimizu, R., K. Chou, I. Orita, Y. Suzuki, S. Nakamura and T. Fukui (2013). "Detection of phase-dependent transcriptomic changes and Rubisco-mediated CO2 fixation into poly (3-hydroxybutyrate) under heterotrophic condition in *Ralstonia eutropha* H16 based on RNA-seq and gene deletion analyses." BMC Microbiology **13**(1): 169.

Shintani, M. and H. Suzuki (2019). Plasmids and Their Hosts. DNA Traffic in the Environment. H. Nishida and T. Oshima. Singapore, Springer Singapore**:** 109-133.

Silva, F., J. A. Queiroz and F. C. Domingues (2012). "Evaluating metabolic stress and plasmid stability in plasmid DNA production by *Escherichia coli*." Biotechnology Advances **30**(3): 691-708.

Sjöback, R., J. Nygren and M. Kubista (1998). "Characterization of fluorescein–oligonucleotide conjugates and measurement of local electrostatic potential." Biopolymers **46**(7): 445-453.

Skulj, M., V. Okrslar, S. Jalen, S. Jevsevar, P. Slanc, B. Strukelj and V. Menart (2008). "Improved determination of plasmid copy number using quantitative real-time PCR for monitoring fermentation processes." Microbial Cell Factories **7**.

Smith, B. L. and T. J. Bruno (2007). "Improvements in the measurement of distillation curves: Part 3—Application to gasoline and gasoline + methanol mixtures." Ind. Eng. Chem. Res. **46**: 297.

Standley, M. S., S. Million-Weaver, D. L. Alexander, S. Hu and M. Camps (2019). "Genetic control of ColE1 plasmid stability that is independent of plasmid copy number regulation." Current genetics **65**(1): 179-192.

Strand, T. A., R. Lale, K. F. Degnes, M. Lando and S. Valla (2014). "A new and improved host-independent plasmid system for RK2-based conjugal transfer." PloS one **9**(3): e90372-e90372.

Sträuber, H. and S. Müller (2010). "Viability states of bacteria--specific mechanisms of selected probes." Cytometry A **77**(7): 623-634.

Swain, P. S., M. B. Elowitz and E. D. Siggia (2002). "Intrinsic and extrinsic contributions to stochasticity in gene expression." Proc Natl Acad Sci U S A **99**(20): 12795-12800.

Sydow, A., A. Pannek, T. Krieg, I. Huth, S. E. Guillouet and D. Holtmann (2017). "Expanding the genetic tool box for *Cupriavidus necator* by a stabilized L-rhamnose inducible plasmid system." Journal of Biotechnology **263**: 1-10.

Takahashi, Y., M. Shintani, L. Li, H. Yamane and H. Nojiri (2009). "Carbazole-degradative IncP-7 plasmid pCAR1.2 is structurally unstable in *Pseudomonas fluorescens* Pf0-1, which accumulates catechol, the intermediate of the carbazole degradation pathway." Applied and environmental microbiology **75**(12): 3920-3929.

Tamakawa, H., T. Mita, A. Yokoyama, S. Ikushima and S. Yoshida (2013). "Metabolic engineering of *Candida utilis* for isopropanol production." Applied Microbiology and Biotechnology **97**(14): 6231-6239.

Tanaka, K., A. Ishizaki, T. Kanamaru and T. Kawano (1995). "Production of poly(D-3-hydroxybutyrate) from CO_2, H_2, and O_2 by high cell density autotrophic cultivation of *Alcaligenes eutrophus*." Biotechnol Bioeng **45**(3): 268-275.

Tang, R., C. Weng, X. Peng and Y. Han (2020). "Metabolic engineering of *Cupriavidus necator* H16 for improved chemoautotrophic growth and PHB production under oxygen-limiting conditions." Metabolic Engineering **61**: 11-23.

Thisted, T., A. K. Nielsen and K. Gerdes (1994). "Mechanism of post-segregational killing - translation of Hok, SrnB and Pnd mRNAs of plasmids R1, F AND R483 is activated by 3'-end processing." Embo Journal **13**(8): 1950-1959.

Tiemeyer, A., H. Link and D. Weuster-Botz (2007). "Kinetic studies on autohydrogenotrophic growth of *Ralstonia eutropha* with nitrate as terminal electron acceptor." Applied Microbiology and Biotechnology **76**(1): 75-81.

Timoumi, A. (2017). Study of the dynamics of physiological and metabolic responses of *Yarrowia lipolytica* to environmental physico-chemical perturbations, INSA de Toulouse.

Tracy, B. P., S. M. Gaida and E. T. Papoutsakis (2010). "Flow cytometry for bacteria: enabling metabolic engineering, synthetic biology and the elucidation of complex phenotypes." Current Opinion in Biotechnology **21**(1): 85-99.

Trevors, J. T. (1986). "Plasmid curing in bacteria." Fems Microbiology Letters **32**(3-4): 149-157.

Tsien, R. Y. (1998). "The green fluorescent protein." Annual Review of Biochemistry **67**: 509-544.

Utratna, M. and C. P. O'Byrne (2014). "Using enhanced green fluorescent protein (EGFP) promoter fusions to study gene regulation at single cell and population levels." Methods Mol Biol **1157**: 233-247.

Vandamme, P. and T. Coenye (2004). "Taxonomy of the genus *Cupriavidus*: a tale of lost and found." International Journal of Systematic and Evolutionary Microbiology **54**: 2285-2289.

Voss, I. and A. Steinbuchel (2006). "Application of a KDPG-aldolase gene-dependent addiction system for enhanced production of cyanophycin in *Ralstonia eutropha* strain H16." Metabolic Engineering **8**(1): 66-78.

Wang, J., Z.-B. Yue, G.-P. Sheng and H.-Q. Yu (2010). "Kinetic analysis on the production of polyhydroxyalkanoates from volatile fatty acids by *Cupriavidus necator* with a consideration of substrate inhibition, cell growth, maintenance, and product formation." Biochemical Engineering Journal **49**(3): 422-428.

Weber, A. E. and K.-Y. San (1989). "A comparison of two plating techniques to estimate plasmid stability of a prolonged chemostat culture." Biotechnology Techniques **3**(6): 397-400.

Weber, A. E. and K. Y. San (1988). "Enhanced plasmid maintenance in a CSTR upon square-wave oscillatoins in the dilution rate." Biotechnology Letters **10**(8): 531-536.

Wehrli, W. (1983). "Rifampin: Mechanisms of Action and Resistance." Reviews of Infectious Diseases **5**(Supplement_3): S407-S411.

Wiacek, C., S. Müller and D. Benndorf (2006). "A cytomic approach reveals population heterogeneity of *Cupriavidus necator* in response to harmful phenol concentrations." Proteomics **6**(22): 5983-5994.

Wilde, E. (1962). "Untersuchungen über Wachstum und Speicherstoffsynthese von Hydrogenomonas." Archiv für Mikrobiologie **43**(2): 109-137.

Wons, E., D. Koscielniak, M. Szadkowska and M. Sektas (2018). "Evaluation of GFP reporter utility for analysis of transcriptional slippage during gene expression." Microbial Cell Factories **17**(1): 150.

Wright, G. D. (1999). "Aminoglycoside-modifying enzymes." Curr Opin Microbiol **2**(5): 499-503.

Wu, K. and T. K. Wood (1994). "Evaluation of the hok/sok killer locus for enhanced plasmid stability." Biotechnology and Bioengineering **44**(8): 912-921.

Wu, Y.-C. and S.-T. Liu (2010). "A sequence that affects the copy number and stability of pSW200 and ColE1." Journal of bacteriology **192**(14): 3654-3660.

Yamada, K., H. Suzuki, T. Takeuchi, Y. Kazama, S. Mitra, T. Abe, K. Goda, K. Suzuki and O. Iwata (2016). "Efficient selective breeding of live oil-rich Euglena gracilis with fluorescence-activated cell sorting." Scientific reports **6**: 26327-26327.

Yan, R. T., C. X. Zhu, C. Golemboski and J. S. Chen (1988). "Expression of solvent-forming enzymes and onset of solvent production in batch cultures of *Clostridium beijerinckii* ("*Clostridium butylicum*")." Applied and Environmental Microbiology **54**(3): 642-648.

Yenofsky, R. L., M. Fine and J. W. Pellow (1990). "A mutant neomycin phosphotransferase II gene reduces the resistance of transformants to antibiotic selection pressure." Proceedings of the National Academy of Sciences of the United States of America **87**(9): 3435-3439.

Zadran, S., S. Standley, K. Wong, E. Otiniano, A. Amighi and M. Baudry (2012). "Fluorescence resonance energy transfer (FRET)-based biosensors: visualizing cellular dynamics and bioenergetics." Applied Microbiology and Biotechnology **96**(4): 895-902.

Zaman, M. P., MH.; Akhter MZ. (2010). "Plasmid Curing of *Escherichia coli* Cells with Ethidium Bromide, Sodium, Dodecyl Sulfate and Acridine Orange." Bangladesh Journal of Microbiology **27**(1): 28-31.

Zhang, H., X. L. Cui, J. X. Bi, S. Dai and H. T. Ye (2015). "Single-cell analysis for bioprocessing." Engineering in Life Sciences **15**(6): 582-592.

Zhang, H. and K. K. Liu (2008). "Optical tweezers for single cells." Journal of the Royal Society Interface **5**(24): 671-690.

Zielenkiewicz, U. and P. Ceglowski (2001). "Mechanisms of plasmid stable maintenance with special focus on plasmid addiction systems." Acta Biochimica Polonica **48**(4): 1003-1023.

Zingaro, K. A. and E. Terry Papoutsakis (2013). "GroESL overexpression imparts *Escherichia coli* tolerance to i-, n-, and 2-butanol, 1,2,4-butanetriol and ethanol with complex and unpredictable patterns." Metab Eng **15**: 196-205.